CHARACTERISATION OF PORCELAIN ENAMEL COATINGS

A thesis submitted in partial fulfillment
of the requirements for the degree of

Doctor of Philosophy

in Materials and Process Engineering
by

MATTHEW NEIL HENDERSON

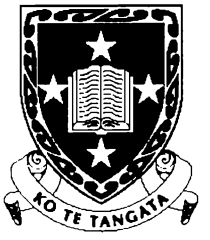

The
University
of Waikato
Te Whare Wānanga
o Waikato

April 2002

Abstract

This thesis focuses on the structural and compositional characterisation and corrosion performance of porcelain enamel coatings commonly used on metal substrates for protective and decorative purposes. These characteristics need to be better understood so the coatings remain competitive with alternative surface treatments/finishes. Raman and infrared spectroscopic techniques were used together, for the first time, to investigate porcelain enamel coatings. Five commercial porcelain coatings and their component raw materials were examined. In addition, the more conventional techniques for analysing porcelain enamels - EDS, ICP and XRD, were used. This complement of techniques makes this a unique and comprehensive study of enamel coatings. The effect of compositional changes on corrosion characteristics of porcelain enamels was then investigated using model formulations. Composition diagrams were constructed and used to explain acid and/or alkali attack on the commercial coatings.

Spectroscopic investigations showed that porcelain enamels are complex systems incorporating many different amorphous and crystalline phases. The main compounds in the frit samples investigated were silicates and borates. Si-O and Si-O-Si vibrations characteristic of SiO_4 tetrahedra were found both in the Raman and IR spectra. However, only the IR technique was capable of identifying the B-O bonds associated with B_2O_3. Amorphous silica was confirmed by XRD analysis. Amorphous phases and crystalline compounds were found within the fired glass enamel coatings. These were characterised by vibrational spectroscopy and XRD. The dominant compounds in the amorphous phase are borates and silicates as in the case of the frits. These compounds were identified through the presence of B-O-Si, Si-O-Si and B-O stretching modes in the Raman spectra. The ATR-IR spectrum of the coatings, which are surface specific, is dominated by B-O stretching modes suggesting that borates were at the coating surface. Many of the crystalline phases in the fired enamel coating detected by XRD and vibrational spectroscopic analysis including $FeCr_2O_4$, Cr_2O_3 and SiO_2 matched those in the colouring pigments.

Corrosion of the enamel coatings was examined in terms of their solid matter (destruction of glass network) as well as their heterogeneity (presence and nature

of bubbles in coatings). Composition diagrams developed for porcelain enamel coating systems were useful for correlating the phases in the glass matrix with specific properties to help explain coating corrosion performance. Varying the ratio of glass network formers and modifiers changed the structural properties of the coating and hence, its corrosion performance. Enamels with higher SiO_2 content, but similar modifier to R_2O_3 ratios were more resistant to corrosion because more compact silicate tetrahedra were formed. This decreased the number of non-bridging oxygen atoms in the structure, thereby reducing ion exchange between modifier ions in the coating and hydrogen ions in the solution.

There was a general trend for increased corrosion to be correlated with increased bubble area in the top 20 μm of coating. By contrast, there was no correlation between the bubble area over the entire depth of the coatings and weight loss after acid or alkali exposure. This is attributed to the formation of a barrier when the coating is exposed to acids, thus inhibiting further ion diffusion, which consequently retards further corrosion. This indicates that the upper bubble area rather than the total bubble area through the coating depth is an important factor in chemical resistance.

The information from EDS analyses of crystalline phases in the gloss green A coating, including spectra around pinhole defects, were expanded with Raman microscopy data. Raman spectra of a cross-section indicate α-Cr_2O_3 and α-quartz whereas the pinhole defect had only α-Cr_2O_3. Elemental mapping showed that elemental Cr clusters were in small discrete areas, with greater concentrations around the margin of the pinhole defect.

This study demonstrates the usefulness of Raman and IR in extending the understanding of porcelain enamel coatings. Using the set of techniques - Raman, IR, ICP, EDS and XRD - together, provided structural and compositional information, which can help improve the coating performance and the finish quality of enamel coatings. Composition diagrams developed from the ICP analytical information are very useful for developing coatings with better chemical resistance from optimised oxide ratios.

Acknowledgements

This work was funded through a New Zealand government research industrial fellowship (GRIF), contract no. AEL:501.

The Claude McCarthy Fellowship provided a scholarship to allow me present part of my research at the Porcelain Enamel Institute Technical Forum (1999), Nashville, USA.

There are many people I would like to acknowledge for their contributions to this thesis.

- My University supervisors; Assoc. Prof Janis Swan, Dr Kim Pickering and Dr Nigel Sammes. Many thanks to Janis Swan for her help and support.
- My external supervisors, Dr Diana Siew and Dr Jiangnan Yuan. Thankyou for your unlimited advice and support.
- Dr Geoff Tompsett, who spent many hours helping characterise the extensive amount of samples. Cheers G.T.
- Darry Faust and Charles Baldwin of Ferro Corp, Cleveland, USA
- Rod Hall, Todd, Graham, Joe, Kiri, Alex and Tilly from Ceratec, NZ Ltd
- My fellow students and staff, including Mike Phillips, Mike Brown, Conrad Lendrum, Wei Wang, Yanhai Du, Pieter Smilde, Bob Torrens, Clive Desouza, Garrett Butt, Jennie Davidson, Georges Adams, Tracey Murray, Yuanji Zhang, Lesley Falconer and Alf Harris.
- Dr Nick Kim and Rachel Bennett who helped me with the ICP analysis.
- All my colleagues at MPT.

I would like to thank my family for their unwavering support. Thanks Mum and Dad. Thanks Kim for helping with proof reading.

Finally, but most importantly, thanks to my wife Lisa, for all her positive encouragement and emotional support through the demanding times, which has enabled me to give my utmost effort to finish this work.

Contents

Chapter One - Introduction and Review

Chapter Two - Materials and Methodology

Chapter Three - Preliminary Characterisation and Coating Properties

Chapter Four - Phase Characterisation

Chapter Five - Chemical Resistance

Chapter Six - Study of Porcelain Enamel Coating and Pinhole Defect

Chapter Seven - Conclusions and Recommendations

List of Figures

Chapter One

Chapter Two

Chapter Three

Chapter Four

Chapter Five

Chapter Six

List of Tables

Chapter One

Chapter Two

Chapter Three

Chapter Four

Chapter Five

Chapter Six

Chapter One
Introduction and Review

Chapter One
Introduction and Review

1.1 General Introduction

Porcelain enamel coatings are complex alkali borosilicate glasses used to protect metal substrates and for their aesthetic qualities. They are often known as "vitreous enamels" because they are liquid in their original state. The glassy matrix is made from frits and additions, which have been milled and then fired onto a suitable metal substrate.

Technological advances in porcelain enamels in recent years have kept porcelain enamel coatings competitive with alternative finishes such as plastics and organic coatings. These advances include lower processing and material costs and improved coat finishes. Increased availability of decarburised steel has helped reduce coat defects and made durable single-coat finishes viable. Other developments include "clean only" (pickle free) pre-treatment for steel surfaces and electrostatic application of powder enamel.

This literature review addresses the general properties and requirements of porcelain enamel coatings and the substrate steel. Recent developments in product application and application processes are also covered. Manufacturing methods for the enamel coat including frits, milling, and mill additions are discussed in detail, as well as the application process and firing of the system. Techniques used to characterise properties of porcelain enamels are described along with the reasons for using particular methods. Finally the scope and objectives of the thesis are presented.

1.2 Porcelain Enamel Glass Structure

Porcelain enamel coatings are mainly amorphous and result when a molten solution cools. The atomic structure of amorphous material is short-range with no

long-range periodicity. The fired porcelain enamel matrix is very complex and contains some crystalline phases, which can be demonstrated using Raman spectroscopy[1] and X-ray diffraction.[2,3] These crystalline phases are often present to give opacity and colour.

The most generally accepted structural model for bulk amorphous silica (vitreous silica) is SiO_4 tetrahedral units connected together at bridging oxygens in a continuous random network.[4,5] The slight twisting in the bonding produces irregularities in of the structural pattern.[6]

Glass forming oxides exist independently in the glassy state but can combine with other added oxides. Consequently, structural properties change. Network formers such as SiO_2, B_2O_3, P_2O_5 Al_2O_3, Sb_2O_3, Sb_2O_5, GeO_2, As_2O_5 and P_2O_3[6,7] are covalent and have a tendency to form a network of bridging oxygen atoms.

Materials such as alkali metal and alkaline earth metal oxides and certain other oxides are called network modifiers because the can break up the network.[6] They are electrovalent materials that provide extra oxygen ions but do not participate in the network, thereby raising the O/Si ratio of the glass.[8] Typical network modifiers include oxides Li^+, Na^+, K^+, Ca^{2+} and Ba^{2+}.[7] In sodium silicates, each Na_2O molecule forms two non-bridging oxygen in SiO_2.[7,8] This is a very brittle structure. Thus, although alkaline oxides are very effective modifiers, the glasses produced may not be chemically durable.[8,9] Glass structure is further discussed in section 5.1.1.

1.3 General Requirements of Porcelain Enamel Coatings

Most vitreous coatings are designed to be homogenous, smooth, hard, easy to clean, and resistant to abrasion and scratching.[10,11] Many enamel coatings are also designed to be aesthetically pleasing. Other desirable properties include the ability to resist chemical attack from reagents including water, acids and atmospheric environment.

One requirement of a porcelain enamel coating is that it bonds with the substrate.[7,10,12] This bonding layer must have the correct thickness during and following the firing process.[10,12] Another requirement is that the porcelain enamel coating protects the metal substrate.

1.4 Porcelain Enamels Applications

Porcelain enamels are used for their protective and aesthetic properties. Applications include cookware, Architectural cladding, Chemical processing tanks, signs, stoves, gas barbecues, fire ranges, hot water tanks, heat exchangers and mechanical processing equipment. Some of these are shown in Figure 1.1.

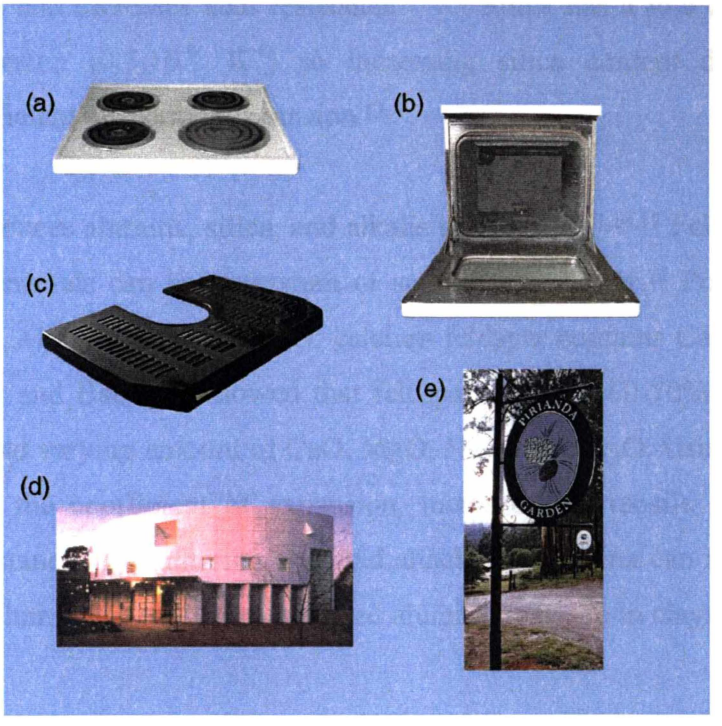

Figure 1.1 Examples of porcelain enamel applications; stovetop (a), stove interior (b), range top (c), architectural cladding (d), and signage (e).

Eppler and Gill[10] report that 85.4% of the USA porcelain enamel market in 1989 was ranges, water heaters, home laundry and dishwashers, 6.4% was cast iron sanitary-ware, and the rest was architectural, cookware and miscellaneous applications.

1.5 Porcelain Enamel Composition and Components

1.5.1 Frit Composition

The "frit" is the primary material for making a porcelain enamel coating. Frits are generally characterised as alkali borosilicates and have three main components: quartz, feldspar and borax. However, many other components can be used to obtain a specific frit (Table 1.1). Frits are made by smelting raw materials and additives into a predominately amorphous glassy matrix (see section 1.6.1).

Quartz or silica, the main constituent in glass, is the most common frit component and can comprise over 50 wt% of the ground coat for acid resistant enamels. The material is refractory and gives the enamel coating heat resistance, increases the melting point, and increases acid resistance.[7,13-16] Silica has a low coefficient of thermal expansion ($0.5.10^{-6}$. K^{-1}) so increasing silica content decreases the enamel's coefficient of thermal expansion.[13]

Feldspar introduces alumina, silica, and alkalis to the frit.[7,13,15,17] Feldspar used in ground coat enamels can be potassium or sodium based spar.[18] Potash feldspar contains K_2O, Al_2O_3, SiO_2, and Na_2O; calcium feldspar contains CaO, Al_2O_3 and $2SiO_2$.[7] Bauer and Bailey,[17] showed that feldspar contains 60-70% of SiO_2, 18-23% Al_2O_3, and varying amount of CaO, MgO, Na_2O, and K_2O. Using alumina in glass reduces the coefficient of expansion, increases the tensile strength, and increases resistance to weathering and acid attack.[7,17] Alumina can also be added to enamel as aluminium oxide and hydrated aluminium oxide in clays.[7]

Borax, is another major component and one of the most active of the fluxes used.[13] It ranges from 20-45 wt% of the frit batch for sheet steel ground coats, giving a typical glass coating 10-20% of B_2O_3 (boric oxide, or boron).[18] Borax has a low melting point and attacks other constituents, accelerating the rate an enamel coating reaches a uniform molten state.[13] It also shortens the firing temperature of enamels, improves strength and toughness of the enamel coating and helps give high lustre and deep brilliant colours.[13]

Table 1.1 Raw materials used in manufacture of frits.

Material	Typical Formulation	Purpose
Alumina	Al_2O_3	Refractory
Antimony oxide	Sb_2O_3	Opacifier
Borax	$Na_2B_4O_7$	Flux / electrolyte
Calcium carbonate	$CaCO_3$	Flux
Clay	$Al_2O_3.2SiO_2.2H_2O$	Refractory/ suspension agent
Cobalt oxide	Co_3O_4	Opacifier / adherence
Copper oxide	CuO	Opacifier
Feldspar	$K_2O.Al_2O_3.6SiO_2$	Refractory
Fluorspar	CaF_2	Flux
Iron oxide	Fe_2O_3	Flux / opacifier
Litharge	PbO	Flux
Lithium carbonate	Li_2CO_3	Flux
Manganese dioxide	MnO_2	Opacifier
Magnesium carbonate	$MgCO_3$	Electrolyte
Nickel oxide	NiO	Opacifier / adherence
Potassium carbonate	K_2CO_3	Flux
Silica (quartz)	SiO_2	Refractory
Sodium aluminate	Na_3AlO_3	Electrolyte
Sodium carbonate (soda ash)	Na_2CO_3	Flux
Sodium nitrite	$NaNO_3$	Electrolyte
Titanium dioxide	TiO_2	Opacifier
Zinc oxide	ZnO	Flux
Zirconium oxide	ZrO_2	Opacifier

Boric oxide gives important thermal properties and reduces surface tension,[7] assuring that the coating fits well to the steel substrate.[13] B_2O_3 is derived from dehydrated borax, hydrated borax, boric acid, or anhydrous boric acid.[13,18] However, using large amounts of flux (including boric acid) to reduce maturing temperature during firing has the disadvantage that it is difficult to achieve corrosion resistance.[7,12]

Cobalt provides darker colours such as black and blue (see section 1.5.4) and also acts as a bonding agent (see section 1.10). Cobalt contents range from 0.65 wt.% for regular blue-black enamel to 1.27 wt% for acid resistant enamel (Table 1.4).

Contents up to 5% do not affect the enamel and as little as 0.2% helps enamel adherence to the steel.[15]

Alkaline metal oxides such as sodium and potassium reduce the melting point of silica, allowing the enamel coat to fuse to the substrate at lower temperatures. Bauer[17] reports that sodium carbonate (Na_2CO_3) is the third major constituent of soda-lime silica glasses and acts as a flux, reducing the melting point. Adding alkali oxides increases the thermal expansion coefficient and reduces the enamel's durability to higher temperatures.[7] Sullivan[9] reports a high-alkali content tends to increase electrochemical corrosion and promote excessive boiling, which can cause large bubbles in the enamel.

Colouring oxides, opacifiers and pigments can either be added to the frit batch or as a mill addition (section 1.5.3).

1.5.2 Multiple-Frit Formulations

Porcelain enamel slips for ground coats are usually combinations of frits (called multiple frits) used to change the melting characteristics. Up to three different frit types are used. Multiple frit ground coats are often a blend of a soft (or low) melting temperature frit and one or two hard (or high) melting temperature frit.[14,15] The soft frits melt early in the firing cycle, wetting the steel surface and absorbing FeO as it is formed. Their "sealing effect" also prevents further oxygen uptake.[17] Andrews[15] reports that multiple frits involve differences in solubility in the mill liquor, which generally improve the stability of the slip. Medium to hard-frits raise the stability of ground coats.[17] This mixture extends the firing range (increase the melting point) of enamels,[15,17] and can improve the stress relationship between the substrate and the enamel coating during the firing and in the cooling stage.[15]

1.5.3 Mill Additions

Mill additions have the primary functions of keeping the frit in suspension, adjusting the set of slip, and determining the condition of the bisque and fired enamel. Mill additions are added to the frits and water before milling (wet

milling) and help produce the desired enamel slip for wet applications. The purpose of commonly used mill additions is given in Table 1.2.

Table 1.2 Mill additions.

Material	Formulation	Purpose / Function
Alumina (calcined)	Al_2O_3	Refractory – imparts heat resistance (increases alkali resistance)
Alumina (hydrate)	$Al_2O_3(3H_2O)$	Refractory – used to produce matt finish
Alginates (basic)	Organic - variable	Bisque adjuster - increases bisque hardness / reduce tearing / suspending agents
Ammonium carbonate	$(NH_4)_2CO_3H_2O$	Electrolyte, flocculating – set up agent in acid resisting enamels
Barium chloride	$BaCl_2.2H_2O$	Electrolyte, flocculating – set up agent in acid resisting and non acid resisting enamels
Barium sulphate	$BaSO_4$	Electrolyte, flocculating – may reduce dimpling / also used to improve workability of acid resisting enamels
Bentonite	$NaO_3(Al,Mg)_2Si_4O_{10}(OH)_2H_20$	Bisque adjuster / Suspending agent / hardens bisque – clay mineral
Borax (hydrated)	$Na_2B_4O_7.10H_2O$	Electrolyte, flocculating – improves set (stabiliser)/ reduces copper heading / rust preventative (used in ground coats)
Feldspar	$K_2O.Al_2O_3.6SiO_2$	Refractory – increase firing range / improve scratch resistance / reduce fish scaling
Gums	Organic - variable	Hardens bisque / suspending agent
Kaolinite	$Al_2O_3.2SiO_2.2H_2O$	Refractory / suspending agent
Magnesium carbonate	$MgCO_3$	Electrolyte - flocculating
Potassium chloride	KCl	Set up agent - used in titania opacified cover coats
Potassium carbonate	K_2CO_3	Bisque adjuster
Potassium nitrite	KNO_3	Bisque adjuster - increases set / reduces tearing
Silica (Quartz)	SiO_2	Refractory - increases chemical and heat resistance / prevents burn off during firing/ lowers gloss
Sodium aluminate	$NaAlO_2$	Electrolyte - flocculating
Sodium carbonate	Na_2CO_3	Electrolyte - flocculating / rust preventative
Sodium hydroxide	NaOH	Rust preventative
Sodium nitrite	$NaNO_2$	Electrolyte - flocculating / rust preventative
Titanium dioxide	TiO_2	Increases opacity
Urea	NH_2CONH_2	Bisque adjuster - reduce tearing
Water	H_2O	Used for wet enamels / possibly contain soluble salts
Zinc oxide	ZnO	Used as flux - lowers firing temperature
Zirconium oxide	ZrO_2	Opacifier / increases alkali resistance

Bentonite and kaolinite clays help suspend the enamel particles in the water. Clays containing silica also have refractory properties. Bentonite can strengthen the bisque (binder) and help reduce tearing (section 1.8.4). High bubble (HB) clay helps suspend the frit in the slip and also contributes to the bubble structure

because it has small amounts of organic matter.[19] Clay particles normally have a net negative surface charge and repel each other, which helps maintain a stable suspension.[20]

Silica is used as a mill addition to increase the firing range and prevent burn-off when firing the bisque.[16] Silica also increases chemical and heat resistance and decreases gloss of the coating.

Electrolytes, also known as "set up salts," help flocculate the clays and reduce the set (viscosity and flow).[14] Electrolytes, including potassium carbonate and sodium aluminate, are very alkaline and dissociate into electrically charged fragments in aqueous solution. The cations come from the metallic constituents and the anions from acidic constituents. Kyri[21] reports that the cations stiffen the clay suspension and the clay particle surfaces absorb the cations, which (because of their electrical charge) fix the surrounding water molecules. Currie[20] reports that adding certain electrolytes modifies the charge of the clays, reducing the interparticulate repulsion forces and lowering the degree of deflocculation.

Plastic clays such as the ball clays and fireclays often contain organic compounds.[19] These are mostly anionic and may act as protective colloids to help stabilise or lower the set of the enamel slip.[20]

Calcium carbonate or lithium carbonate is sometimes added to the mill of a ground coat charge to help give good bubble structure.[16] Adding up to 0.5 wt% borax improves the set and reduces the solubility of the frit.[19] Very small amounts (less than 0.25 %) of sodium nitrite can act as an electrolyte (set-up agent) when milling a ground coat slip, and also as a rust inhibitor.[16,19,21] Sodium nitrite in cover coat enamels can help prevent tearing.[16]

Water

Enamel slips applied to the steel will generally contain about 30 wt% water.[7,21] Kyri[21] considers that water can affect enamel quality and enamel defects can arise if unsuitable water is used. Water can contain dissolved salts. Bisqueing (the

drying process before firing) will deposit the salts from the water. Sulphate or chloride ions in the water can cause defects such as copper heads in ground coats.

1.5.4 Colorants and Pigments

Techniques for Colouring Vitreous Coatings

There are three common ways to add colour to a vitreous coating:[10,22]

- Having transition metal ions, which are coloured, in the coating material. This method is traditionally used for colouring glass.
- Precipitating a suitable crystalline phase.
- Dispersing a coloured crystalline phase (commonly called a pigment) in the coating, which is the most common method of obtaining colour.

The pigments should have high tinting strength, high refractive index, be free of greyness, and stable at high temperatures.[10]

Colourant Systems

Most materials used for colouring ceramics are oxide pigments (Table 1.3) because they are very stable in oxygen-containing ceramic systems[23] and resistant to high temperatures. These oxide pigments are introduced to the melt when the enamel frits are being wet milled.[7] The pigments do not dissolve when fired, but disperse throughout the enamel, acting as opacifiers and giving an appearance of colour because they have higher or lower refraction indices than other enamel material.[7,13,24] Although the appearance is classified as opaque, it usually is translucent.[13] Eppler[24] reports that the refractive index for the glass matrix is 1.5 - 1.6, which is lower than for commonly used opacifiers such as tin oxide (2.04), titanium oxide (2.52-2.76) and zirconium oxide (2.13-2.20).[7,13,24] Colouring oxides are often added to the system to counter the cobalt used as part of the adherence mechanism (but which imparts a blue colour to the system).

Opacity is developed in glass and glazes, using the same methods as for enamels.[13] If a pastel type colour is required, then an opacifier and pigment is added. The overall coating-pigment-opacifier compatibility must be considered when selecting materials.[24]

Table 1.3 Colouring oxides for vitreous coatings (Adapted from Eppler[10,22] and Burgyan and Eppler[23]).

Pigment system	Basic Chemical formula
Pink and Purple	
Chrome-alumina-pink spinel	$Zn(Al,Cr)_2O_4$
Chrome-alumina-pink corundum	$(Al,Cr)_2O_3$
Manganese-alumina-pink corundum	$(Al,Mn)_2O_3$
Zirconium-iron pink zircon	$(Zr,Fe)SiO_4$
Chrome-tin orchid cassiterite	$(Sn,Cr)O_2$
Chrome-tin pink sphene	$CaOSnO_2SiO_2$:Cr
Brown	
Zinc-iron-chromite brown spinel	$(Zn,Fe)(Fe,Cr)_2O_4$
Iron-chromite brown spinel	$Fe(Fe,Cr)_2O_4$
Iron-titanium brown spinel	Fe_2TiO_4
Nickel-ferrite brown spinel	$NiFeO_4$
Zinc ferrite brown spinel	$(Zn,Fe)Fe_2O_4$
Iron brown hematite	Fe_2O_3
Chrome-iron-manganese brown spinel	$(Fe,Mn)(Fe,Cr,Mn)_2O_4$
Chromium-manganese-zinc brown spinel	$(Zn,Mn)Cr_2O_4$
Yellow	
Zirconium-vanadium yellow baddeleyite	$(Zr,V)O_2$
Tin-vanadium yellow cassiterite	$(Sn,V)O_2$
Zirconium-praseodymium yellow zircon	$(Zr,Pr)SiO_4$
Lead-antimony yellow pyrochlore	$Pb2Sb_2O7$
Nickel-antimony-titanium yellow rutile	$(Ti,Ni,Sb)O_2$
Nickel-niobium-titanium yellow rutile	$(Ti,Ni,Nb)O_2$
Chrome-antimony-titanium buff rutile	$(Ti,Cr,Sb)O_2$
Chrome-niobium-titanium buff rutile	$(Ti,Cr,Nb)O_2$
Chrome-tungsten-titanium buff rutile	$(Ti,Cr,W)O_2$
Manganese-antimony-titanium buff rutile	$(Ti,Mn,Sb)O_2$
Green	
Chromium-green hematite	$(Cr,Fe)_2O_3$
Cobalt-chromite blue green spinel	$Co(Al_2Cr)_2O_4$
Cobalt-chromite green spinel	$CoCr_2O_4$
Cobalt-titanate green spinel	Co_2TiO_4
Victoria green garnet	$3CaOCr_2O_3SiO_2$
Nickel-silicate green olivine	$NiSiO_4$
Blue	
Cobalt-aluminate blue spinel	$CoAl_2O_4$
Cobalt-zinc aluminate blue spinel	$(Co,Zn)Al_2O_4$
Cobalt-silicate blue olovine	$CoSiO_4$
Cobalt-zinc silicate blue phenacite	$(Co,Zn)_2SiO_4$
Cobalt-tin blue-grey spinel	Co_2SnO_2
Cobalt-tin-alumina blue spinel	$CoAl_2O_4/Co_2SnO_4$
Zirconium-vanadium blue zircon	$(Zr,V)SiO_4$
Black	
Iron-cobalt black spinel	$(FeCo)Fe_2O_3$
Iron-cobalt-chromite black spinel	$(Co,Fe)(Fe,Cr)_2O_4$
Manganese-ferrite black spinel	$(Fe,Mn)(Fe,Mn)_2O_4$
Copper-chromite black spinel	$CuCr_2O_4$
Chromium-iron-nickel black spinel	$(Ni,Fe)(Cr,Fe)O_4$
Grey	
Cobalt-nickel grey periclase	$(Co,Ni)O$
Titanium-vandium-antimony grey rutile	$(Ti,V,Sb)O_2$
Tin-antimony grey cassiterite	$(Sn,Sb)O_2$

Common Colouring Oxides

Chromium oxide, Cr_2O_3 - a bright green crystalline powder added as a pigment to the melt. As it is insoluble, it does not dissolve during firing and remains suspended, giving opacification and colouration.[7,13] To reduce blistering, chromium oxide should not be used in coats applied directly to steel. Chromium is also commonly used in black enamels.[13,22]

Chromic oxide, CrO_3, - produces yellow but it dissociates and partly changes to Cr_2O_3 during melting, which result in a yellow green colour.

Cobalt oxide, CoO – only small amounts (<1%) can colour enamels.[13] It can be added as CoO, $CoO.Co_2O_3$ or Co_3O_4. Cobalt oxide gives a blue colour but cobalt oxide with other colouring oxides such as copper or chromium can produce different blues, ranging from pure cobalt blue, through greenish blue and blue-green to the green of chromium.[7,13] Cobalt oxide is also a constituent of black enamels.

Cobalt chromate, $CoCr_2O_4$ - is used with aluminium oxide. The colour is greener with higher concentrations of chromium and more blue at lower chromium oxide to cobalt ratios[7,22] Oxides of cobalt (blue) and nickel (black-brown) and iron (yellow-brown) impart darker shades to ground coat and direct on enamels.[25]

1.5.5 Ground Coat and Cover Coat Compositions

Porcelain enamels are classified as ground-coat or cover-coat enamels. Ground coats can sometimes be used as end-use coats rather than using the conventional two-coat systems. However, they are limited to the darker shades (or colours) given by the so-called adherence oxides, nickel and cobalt. As decarburised steels become more readily available, ground coats are more often being used as end-use coats. Fewer defects are produced because out-gassing during firing is decreased and a second (cover) coat is not needed to cover defects.

Direct-on coats can also be used on steel. In this process, a cover coat without the adherence oxides is applied directly to decarburised steel. The direct-on coat does, however, require that the steel surface be pickled and nickel dipped (see section 1.9.4) before enamelling so that enamel-steel adherence is successful.

The advantages of direct-on coats include:[26]

- The colour is not limited to the darker shades from adherence oxides cobalt and nickel.
- Less expensive because of simplified processing (one coat instead of two).
- Less damage during transportation and assembly.
- Better coverage of "difficult" areas (such as curved sections) because coating thickness is reduced.

Porcelain enamel coatings are characterised by their physical properties. For example, whether they are alkali resistant or regular blue/black enamel (Table 1.4). Opacity is another characterisation criterion. Examples include; Titania white or clear enamels (Table 1.5). Eppler and Gill[10] gives a detailed description of characterised enamel coatings.

Table 1.4 Melted oxide compositions of frits for ground-coat enamels for sheet steel.[14,27]

	Composition (wt %)			
Constituent	**Regular blue-black enamel**	**Alkali-resistant enamel**	**Acid-resistant enamel**	**Water-resistant enamel**
SiO_2	37.17	42.02	56.44	48.00
B_2O_3	22.21	18.41	14.90	12.82
Na_20	18.44	15.05	16.59	18.48
K_2O	0.99	2.71	0.51	...
Li_20	...	1.06	0.72	1.14
CaO	9.34	4.47	3.06	2.90
Al_20_3	4.53	4.38	0.27	...
ZrO_2	...	5.04	...	8.52
TiO_2	...	...	3.10	3.46
CuO	...	0.07	0.39	...
MnO_2	1.58	1.39	1.12	0.52
NiO	1.37	1.04	...	1.21
Co_3O_4	0.65	0.93	1.27	0.81
P_2O_5	1.15	0.68	...	0.20
F_2	2.57	2.75	1.63	1.94

Table 1.5 Melted oxide compositions of frits for cover-coat enamels for sheet steel.[14]

	Composition (wt %)		
Constituent	**Titania white enamel**	**Semi-opaque enamel**	**Clear enamel**
SiO_2	44.67	44.92	54.26
B_2O_3	14.28	16.40	12.38
Na_2O_3	8.27	8.67	6.55
K_2O	6.99	8.12	11.32
Li_2O	0.98	0.45	1.14
ZnO	...	0.74	...
ZrO_2	1.98	3.34	1.40
Al_2O_3	0.31	0.16	...
TiO_2	18.49	13.05	10.04
P_2O_5	1.32	0.88	...
MgO	0.5	...	...
F_2	2.21	3.27	2.91

Matte Coatings

Dispersing minerals such as aluminium oxide, willemite, zircon and titanium dioxide in selected frit combinations produces matte glazes.[28] The two methods most commonly used to produce lower gloss coating finishes are by adding high refractory oxides such as silica or alumina and by incorporating a specially formulated matting frit into the enamel frit blend.[29] However, adding too much alumina may reduce the coating's alkali resistance because the alumina may stop acting as a network forming oxide and acts as a network modifier, dramatically increasing the number of nonbridging oxygens (three nonbridging oxygens per Al).[30] Layne[29] reports that alumina also has a deleterious effect on the acid resistance of a coating. Matting frits are generally hard (high in refractories) or contain components that lower the gloss by causing incompatibility with other frits in the system. Adjusting particle size, firing temperature and time, and slip application technique can be used to control the matte and surface appearance.[28]

1.6 Enamel Manufacture

1.6.1 Smelting

Frits are made by smelting, which is a process where a mix of raw materials is melted then roll quenched into glassy type sheets. Usually the manufacturer then breaks the sheets into small pieces (frit). The smelting process is generally done between 1100°C and 1400°C.[31] Raw materials used in the "batch" composition are given in Table 1.1. This section does not give a detailed discussion of different

aspects of the smelting process such as batch preparation (weighing, mixing, and charging) and the smelters used.

Reactions During Smelting

At the high temperatures, the raw materials and additives react to produce a uniform glassy sheet. The chemical reaction (or rate of reaction), and hence the final composition, depends on factors such as raw materials mix, and temperatures used. A detailed description is given by Andrews.[15]

During the initial heating, fluxes melt and begin to react with the refractories.[19] Andrews[15] proposes, sodium nitrate evolves and melts to a mobile liquid (at ~308°C) in the initial smelting stages. The mobile liquid dissolves and reacts with other components in the batch. During this time, borax dehydrates and begins to melt, dissolving metal oxides and initiating chemical reaction in the batch.

As solution and decomposition occurs, carbon dioxide and nitrogen dioxide fluorine, water vapour and combustion products are produced.[19] Andrews[15] suggests that nitrogen oxides from the sodium nitrate, which has reacted with the other constituents, are also evolved (at temperatures up to 930°C). At this temperature, the molten soda ash (or sodium carbonate, Na_2CO_3) is an active flux and attacks the more acid constituents. Fluorides also help make the melt more mobile with increased attack on the feldspar and quartz grains.

Andrews[15] summarised reactions of smelting as:

- Room temperature - 260° C; Dehydration period.
- 260° C - 430° C; Developing the first liquid.
- 430° C - 700° C; Reaction period.
- 700° C - 900° C; Glass-forming period.

1.6.2 Milling

Enamellers mill (grind) the commercial frits, along with proprietary mill additions, to give the desired coat. The ball mills vary from 10 litres for test pots to 15,000 litres. However, the average in Europe is 2,000 litres.[21]

The frits can be wet or dry milled. Dry milling is used for dry enamel slips and wet milling is usually used for wet enamel application. If the milling method is not important, wet milling will usually be better. Suppliers grind dry electrostatic application frits without water then send the product to the enamellers.[27] As wet enamel slip application will be used in this research, the literature described concentrates mainly on wet milling.

The theory of milling, which is similar to milling ceramics, has been well investigated and documented.[7,11,15,19,21,31,32] The ball mill is a steel drum, usually internally lined with porcelain, high-density alumina or silica.[15,19] This drum usually has 50% to 55% by volume ceramic balls,[19,21,22,27] which can be made from porcelain, stealite or sintered corundum (high-density balls).[21] The mill lining and grinding balls should be made of the same material to reduce wear on either component. Often two different sizes of balls are used. The largest particles are broken by the large balls and then ground to their final size by the smaller balls.[32]

Grinding time will vary depending on slip fineness (or fines) required. Frit manufacturers usually specify a particular fineness range for each enamel type. If fineness does not meet specifications, the set may be inappropriate. For example, long milling times produce a large amount of fines, which give a high set (too soluble). If the particles are not ground sufficiently, coarse particles are produced and the set is very low.[31] Grinding time, rotation, mill size and type of mill charge determine how quickly the frit will be ground to the desired fineness. Milling temperature is affected by the mill charge size, which includes the balls, frit, mill additions and water. Bryant[31] reports that milling temperature affects solubility and fineness distribution of the mill charge. Fuller[32] proposes that solids content of the load will affect the fineness and particle size distribution.

Milling Actions

There are three actions in the mill:[32]

- Ball impact with the lining, with product in between.

- Ball-to-ball contact (which causes most of the grinding).
- Differential rotation of the balls, which causes shearing, dispersion and some size reduction.

Rotation speed affects ball movement in the drum, which determines grinding performance. If the drum rotates too quickly, balls and frit may move centrifugally, giving ineffective grinding (Figure 1.2a) and accelerated mill wear.[7,15,22] Inefficient milling and accelerated lining wear also occur if the drum rotates too slowly (Figure 1.2b). Correct drum rotation (Figure 1.2c) is a cascading effect, which produces efficient grinding with the least wear on the lining.

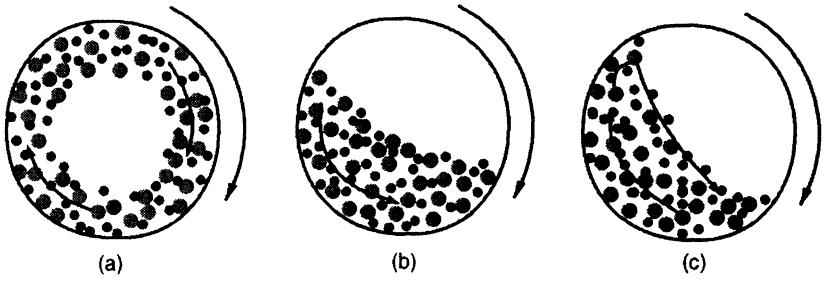

Figure 1.2 Schematic of ball milling speeds, (a) too fast, (b) too slow, (c) correct speed.

Mill-loading specifications are in Table 1.6. The correct rotation speed (rpm) must account for mill drum dimensions and charge (including frit, and ball weight and size). Each milling plant usually determines their final specifications by trial and error.

Table 1.6 Milling specifications (Adapted from Escol[16]).

Mill size (outside dimensions, m)		Frit charge (kg)	Weight of balls (kg)	Ball diameter (mm)	Mill speed (rpm)
Length	Diameter				
1.54	1.14	453.59	1088.62	76	32
1.37	0.91	226.80	498.95	64	40
1.12	0.91	181.44	408.23	64	42
0.91	0.91	90.72	217.72	51 - 38	48
0.76	0.61	45.40	113.40	38	60
0.25	0.25	2.72	5.90	25 - 13	85

Note – Millers often use a mixture of sizes of balls (up to three, usually two).

Fuller[32] reports that the critical speed occurs when an infinitely small particle centrifuges against the inner side of the mill drum and that the optimum speed is about 55% of the critical rpm. Fuller produced a formula for obtaining the critical speed (rpm) from the inside diameter (inches) of the mill For this thesis, the measurements have been converted to mm (Equation 1.1):

$$\frac{54.190}{\sqrt{I.D./60.961}} \qquad \textbf{Equ. 1.1}$$

where I.D. is the internal diameter in mm.

Eppler[11] suggests that a mill speed approximately 60% of the critical speed will give better results (Equation 1.2):

$$21D^{-\frac{1}{2}} \leq \text{critical speed} \leq 30D^{-\frac{1}{2}} \qquad \textbf{Equ. 1.2}$$

where critical speed is in rpm. and D is the mill diameter in metres. From equation 1.1, the optimum speed (55% of critical speed) for a 200 mm diameter mill drum is 18 rpm. From equation 1.2 with the same diameter mill drum the optimum speed (60% of critical speed) is between 28 and 40 rpm, which is a difference of between 56 to 122% from equation 1.1. For a 1 m diameter the difference between equations for the optimum speed is between 60 and 128%.

Slip Rheology

Phelps,[33, 34] showed that rheological properties of high solids, deflocculated slips, depend on particle size distribution of the solids. His helps findings can be summarised as:[34]

- Ceramic slips are liquid dispersions of polydisperse particulates with diameters of approximately 0.001 to 200 μm.

- All slips can be considered as non-colloidal particles (but with colloidal dimensions of less than 0.2 micron) supported and lubricated by a liquid sol.
- Extension of the size limits and deviation of the distribution from optimum packing produce variations in void space of packed systems of polydispersed particulates.
- The rheology distribution of non-colloidal particles in a liquid sol depends on the degree of subdivision and degree of deflocculation of the colloidal particles of the sol.

Currie[20] suggests that an enamel slip contains an aqueous suspension of glass particles, with about 50 vol% having an average diameter of 2 to 100 μm and up to 10 vol% having a diameter of less than 2 μm. The colloidal material consists of secondary glass particles, organic compounds and clays.

Milling fineness influences oxidation capacity of the steel during firing.[7] If the enamel is coarse, the material remains solid longer. The more infusible ground coats prevent free access of oxygen to the surface of the metal, which affects iron oxide diffusion and therefore the bond between the coating and steel. Frits with finer grain size usually have greater corrosion resistance, higher mechanical strength and lower firing temperatures.[35]

Specific Gravity of Slip

Specific gravity is controlled almost entirely as the ratio of water to solids.[14] The enamel frit manufacturer usually designs the enamel compositions for a specific application and assigns a specific gravity. The enameller uses this information to adjust the slip to get the required specific gravity. If the specific gravity is too low, drying the slip or blending it with a slip of higher specific gravity can increase it.[14]

Controlling Set

The thickness, viscosity and flow of an enamel slip are called the "set".[19] Viscosity will determine how the enamel drains down a panel.[20] Vargin[7] reports

that the flowability required is largely determined by the purpose of the enamel. This flow-ability is characterised by the viscosity required for the enamel to flow smoothly over the steel. Higher viscosity slips have higher specific gravity and a slower flow. If the slip is too thick, it does not flow or pour readily and is called high set. Low set slips are too thin and may not build up sufficiently when sprayed onto the substrate.[19]

1.7 Application and Firing Process

1.7.1 Methods of Coating the Substrate

The main methods for applying an enamel coating to a metal are wet spraying, dry powder coating (electrostatic), and dipping. The following factors determine whether the slip is applied manually or mechanically:[11,14]

- Type, shape and size of part
- Production output
- Energy and labour costs
- Space availability
- Environmental considerations

If there are many sizes and shapes, manual coating is best, whereas mechanised application is usually cheaper if higher production rates are required and similar shaped parts are being processed.

Wet Spraying Method

In wet spraying, the enamel slip is broken into a cloud of fine particles and transferred to the substrate pneumatically, mechanically or electrically. In manual spray applications, the porcelain enamel slip is forced from a pressure feed tank to the spray gun nozzle and atomised by clean compressed air regulated at 170 - 415 kPa.[14] This is the primary technique used for this research (Figure 1.3).

Dry Powder Coating (Electrostatic)

Dry powder coating involves electrostatic application of enamel powder to a conductive steel substrate. Individual coating particles are charged at a high voltage and then sprayed onto a conductive steel substrate surface.[11,36,37] This

process is suitable for high-volume production of parts requiring the same porcelain enamel coating type.[14]

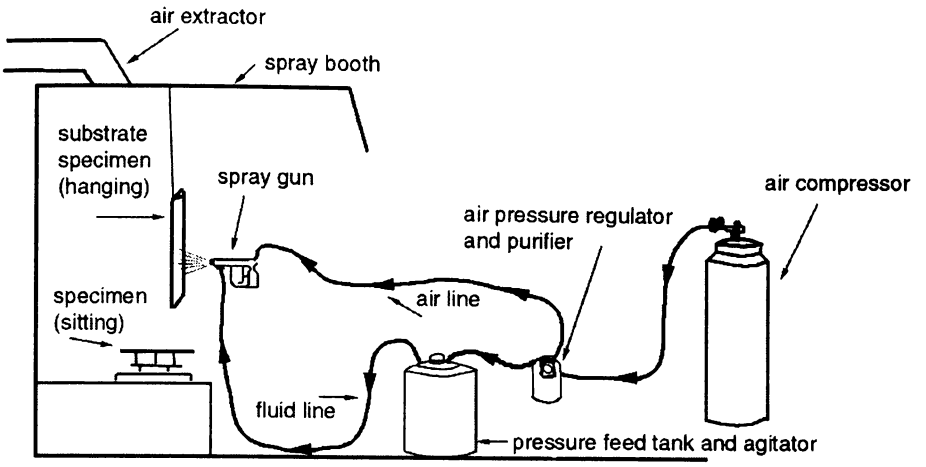

Figure 1.3 Schematic of manual wet spraying equipment.

The electrical charge holds the powdered glass on the steel while it proceeds to the firing furnace.[38] The enamels are dry milled along with additions that improve the resistivity of the enamel and impart the required powder flow characteristics.[19] The following are some advantages of electrostatic spraying:

- Less waste from over-spray than wet spraying (95 to 99% powder use).[11]
- Slip does not need to be dried before firing.
- Electrolytes or clays are not needed in the composition; therefore the coatings are more chemically resistant[19] (compared to wet spraying method).

Dipping

The steel article is immersed in the enamel coating slip, removed, and then drained to remove excess enamel slip.[11,14] The enamelled specimen is then dried at room temperature before firing. This method is commonly used for parts with difficult sections or where both sides must be coated.

1.7.2 Bisqueing

After the wet enamel slip has been applied to the article, it is dried before being fired. The dried enamel slip is called a bisque (or biscuit) and the drying process is

often known as bisqueing. During firing, water in the enamel slip can cause detrimental effects including breaking or cracking the enamel layer from the steel (known as tearing - section 1.8.4).[7,15,19,31] Moisture in the furnace can also cause blistering.

Most industrial enamellers use continuous dryers, which can be heated by convection, conduction, radiation and infrared. During the drying process, moisture initially evaporates from the enamel surface. Then, moisture containing dissolved salts diffuses from the lower layers of the enamel slip to the upper layers and migrates across the surface from the wetter to drier sections.[7,21]

In infrared drying, the water evaporates at the point where the heat is absorbed. Salt migration in the enamel layer is negligible,[21] which results in more even drying with fewer irregularities.

1.7.3 Firing Process

After the enamel coating is applied to the specimen, firing bonds the two materials. The firing process involves high temperature conversion of a viscous enamel slip (dried on substrate) to a consolidated coating. Firing also involves escape of gases through the coating before consolidation.

Firing can also be described as conversion of adhering particles to a continuous coating. The enamel coating must react with the substrate to form a firmly adherent glass enamel-to-substrate chemical bond.[7,10,13]

Firing Process - Ground Coat

Kyri[21] describes firing of ground-coat enamelled specimen in a U-type furnace (Figure 1.4). In the initial stages, any water remaining after drying evaporates.[7] At approximately 500°C, the surface of the steel oxidises[21] in the following way:[7]

$$2Fe + O_2 \rightarrow 2FeO \qquad \textbf{Equ. 1.3}$$

$$3Fe + 2O_2 \rightarrow Fe_3O_4 \qquad \textbf{Equ. 1.4}$$

As well as oxidation, there is a reaction between the sheet steel and water vapour. At approximately 710°C, the melting ground-coat enamel wets the steel surface and a sealed enamel film develops. The iron oxide reacts to form other complex compounds. There is a chemical exchange between iron and cobalt oxide and nickel oxide from the melted enamel on the steel surface. The iron oxide formed dissolves into the coating, developing the adhesive (or transition) zone (or layer).[9,12,39,40] Kyri[21], suggests that the adhesive layer forms at approximately 820°C. At approximately 750°C, mill additions including silica and clay begin to decompose. Vargin[7] suggests that the bound water in the kaolinite and other clay minerals begins to separate (due to decomposition) at 500°C. Kyri[21] suggests that the actual firing temperature is approximately 800°C starting about 3 minutes and ending at 5 minutes of the firing cycle (Figure 1.4).

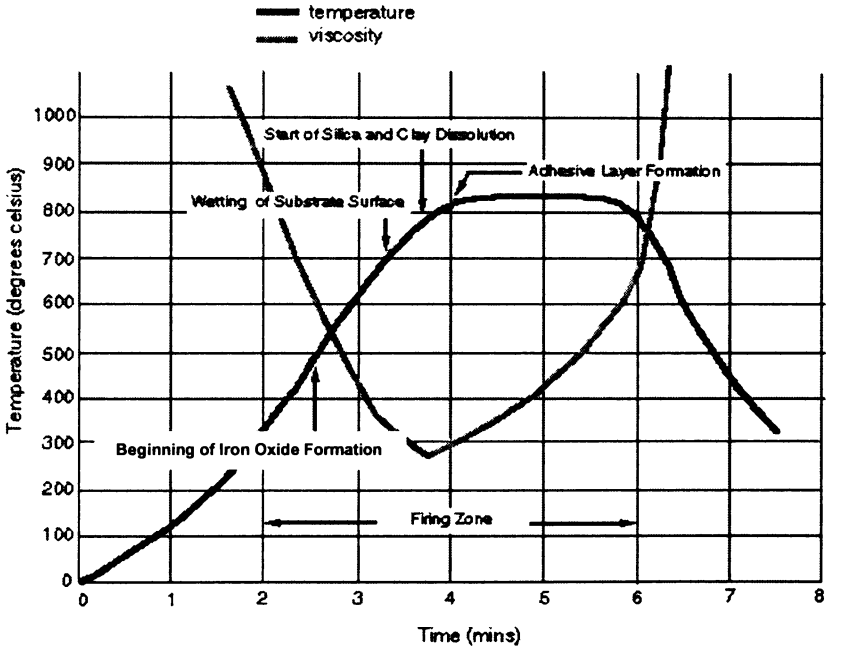

Figure 1.4 Typical firing of porcelain enamel ground coat in a U-type furnace. (adapted from Kyri[21] and *Bayer Technical Information*[41]).

Firing Cover-Coat Enamels

Cover-coat enamels are normally fired over a ground coat layer, and must bond to the ground coat. Cover coat firing temperatures are generally 30-50°C lower than for ground coats.[7]

Firing Time and Temperature

Because the total heat treatment is important, firing time and temperature can be varied (within limits) to obtain similar bonding and appearance.[14] However, there is a minimum practical temperature for producing a satisfactory enamel coating because complete fusion, acceptable adherence, and correct aesthetics must be achieved.[14] Increasing the firing time and temperature has the following effects:

- Colours in the surface of the coating change dramatically, especially the reds and yellow. White and colours generally shift toward yellow.[14]
- Gloss of the enamel coating increases.[14]
- Chemical resistance of the coating increases.[14,42]
- Gas bubbles are eliminated.[14]
- Enamel coating becomes denser and more brittle and less resistant to chipping.[14]
- Surface smoothness improves[42,43] and adherence is obtained at the optimum temperature.[14]

Coating Thickness

Coating thickness affects system properties such as; reflectance, stiffness, chip and impact resistance, hairline resistance, thermal shock resistance, corrosion resistance and electrical properties.[15] The optimum coating thickness depends on the substrate metal and the service requirements of the article. The minimum thickness of coating to achieve the desired appearance, functionality[14] and a smooth and uniform coverage should be used.[11] However, the coat must be sufficiently thick to heal over thin sections or to cover irregularities in the substrate.

Preventing Metal Distortion during Firing

Porcelain enamels must fuse to the steel during the firing process. The steel's ability to maintain its shape during the firing process directly affects the temperature for fusing the porcelain onto the substrate. This temperature will affect the composition of the enamel coating. A thick light steel article may distort

or sag at elevated temperatures. Enamel composition must, therefore, allow for a lower maturing temperature so the steel will not distort.

Furnaces for Firing

A wide range of commercial furnaces are used. The type used depends on the size and load of enamelled items. Furnaces can be continuous (on a conveyer), intermittent, or box, and can be heated by propane or natural gas, electricity or oil. All furnaces will have different firing conditions depending on their configuration, firing temperature and process time. Humidity in the furnaces can vary, which can be detrimental when firing enamelled articles. For example, fishscaling may occur if the firing atmosphere has a high moisture content. Furnace design also affects cooling rate, which will affect compression of the fired coating onto the article.

There are three types of gas-fired furnaces: muffle, radiant-tube or luminous wall–direct fired.[14,27] The luminous wall furnace is direct-fired, which allows efficient combustion of the air/gas mixture after it has passed through a porous ceramic brick.[44] Geary[45] gives the advantages of luminous walled furnaces. In radiant tube furnaces, heat is supplied by radiation from the red-hot tubes. Therefore, a lot of heat power is used and wasted.[45] One disadvantage of direct-firing (luminous walled) is the high moisture in the furnace[46] produced when burning fuel (natural gas). This can cause excessive gassing and large bubble structure, producing a grizzled (wrinkled) surface.

1.8 Coating Properties

1.8.1 Viscosity

Viscosity influences the temperature the enamel coating fuses onto the steel. Viscosity decreases with increased temperature[15] and more viscous enamels must be fused at higher temperatures.[7] High viscosities reduce the ability of the enamel to flow over the surface of the substrate. Low viscosities during firing may produce irregular coating thickness because of excessive flow of the melt. Vargin[7] suggests that high viscosity enamels melt slowly, which will decrease gas bubble production. Viscosity also affects separation of opacifiers in the melt. The specific

sized opacifying particles for maximum opacification separate at specific viscosity.[7]

Flow properties of enamel suspensions and their application and levelling properties can be controlled using the relationship between viscosity and the degree of dispersion.[47] Optimum dispersion or full or partial defloculation markedly changes the rheological characteristics. Dispersion reduces the shearing stress of a clay/water suspension, thereby reducing the viscosity. Currie's[20] study showed increasing total electrolytes in a slip (to a maximum) result in small increases in viscosity, but excess electrolytes reduces viscosity. Andrews[15] suggests that fluorides have the greatest effect on lowering viscosity and that titanium oxide decreases the viscosity (up to the point of crystallisation). Mill additions generally increase viscosity.

1.8.2 Thermal Expansion

The enamel coating must closely match the thermal expansion characteristics of the substrate. If the thermal expansion characteristics of a system are not identical, stresses will be generated because of differential contraction during cooling from the coating temperature.[7,12,48] Frit suppliers normally prepare their products so the enamel coating will have a suitable expansion for steel applications.

Porcelain enamels are usually formulated so thermal expansion characteristics place the enamel coating in slight compression under service conditions.[14] Rado[49] showed that coatings are brittle materials that are very strong under compression, but are readily subjected to tensile failures. The tensile stresses causing these failures are produced from differential cooling (contraction) when the coating is fired onto the substrate.

1.8.3 Enamel Microstructure

Bubble Structure

The "bubble structure" is a characteristic feature of one-coat (or ground-coat) enamelling.[21,50] Gas bubbles (or mixtures of holes), are formed when the specimen is fired. The gas originates from carbon and hydrogen in the steel,

combined or absorbed water in the frit, water and organic materials in the clay and the mill additions, and water vapour in the furnace atmosphere.[7,11,50] Water vapour formed from clay decomposition stays in the enamel coat, partly as fine bubbles.[21] Eppler[11] proposes that most of the smaller bubbles have little effect upon the coating quality, but larger bubbles disturb the coating surface (see pinhole defects, section 1.8.4). Smalley[51] suggests that gases formed in the firing process originate from small amounts of free and absorbed organic materials in some of the clays (plastic clays of the ball clay or plastic fire-clay types) and contribute to the bubble structure.

Although bubbles do not contribute to developing adherence of the interface between the glassy enamel and steel during the firing process reaction, they do partially relieve stress on the glass if there is an impact from an external force[52]. Bubbles stop surface cracks going directly to the metal interface by deflecting the cracks. This gives greater glass retention and protection of the metal.[19,52] Bubbles also absorb gases from the steel surface and help minimise the fishscale defect.[16,19,51,52] Bubbles are especially needed in the lower zones near the enamel steel interface to prevent fishscaling.

Smalley[51] considers that the bubble structure also affects corrosion resistance of ground coat enamels. Many bubbles (especially ruptured bubbles) at the surface of the coating increases surface area and therefore the rate the glass solubilises. This reduces the corrosion resistance. Smalley[51] also suggests that the bubble structure affects the subsurface abrasion resistance of an enamel coating. If the size or number of bubbles increases, subsurface abrasion decreases. Sullivan[9] suggests a high alkali content in the glass enamel will cause excessive boiling and large bubbles.

1.8.4 Common Coating Defects

There is a lot of literature on in porcelain enamel coating defects.[7,11,15,16,21,53,54] This section summarises some of the defects relevant for this research.

Carbon Boiling

Carbon oxidation in the steel during enamel firing produces carbon monoxide that causes primary boiling of the enamel.[14,55] Carbon boiling produces black or grey specs on the coating surface; or in severe cases it may appear as blisters (Figure 1.5). General or localised areas of excessive carbon content in steels exacerbate carbon boiling.[53] These defects only occur in the ground coat during the first firing and a cover coat can disguise the defect. The increasing availability of very low carbon steels (<0.005 wt% C), known as decarburised steel - has significantly reduced the gases from carbon boiling during the firing process.

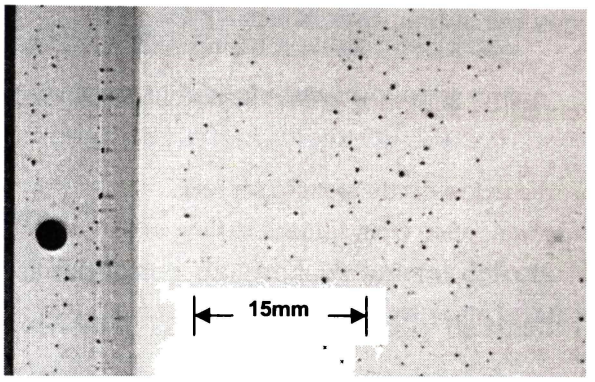

Figure 1.5 Optical micrograph. Example of carbon boiling defect from surface view.

Fishscale

Fishscaling is caused when hydrogen is released from the steel after the enamel coating has hardened.[56] This hydrogen increases the pressure at regions under the enamel coating, creating a stress and consequently a fracture defect.[29,56-58] The enamel then breaks away and produces a fishscale defect (Figure 1.6). The substrate metal reduces water present in the enamel frit during the firing process and the hydrogen is adsorbed by the steel.[21,58,59] Equation 1.5 shows how hydrogen is produced:

$$Fe + H_2O = FeO + H_2 \qquad \textbf{Eq. 1.5}$$

Using a ground coat with a good bubble structure (see section 1.8.3) can often negate the occurrence of fishscale.

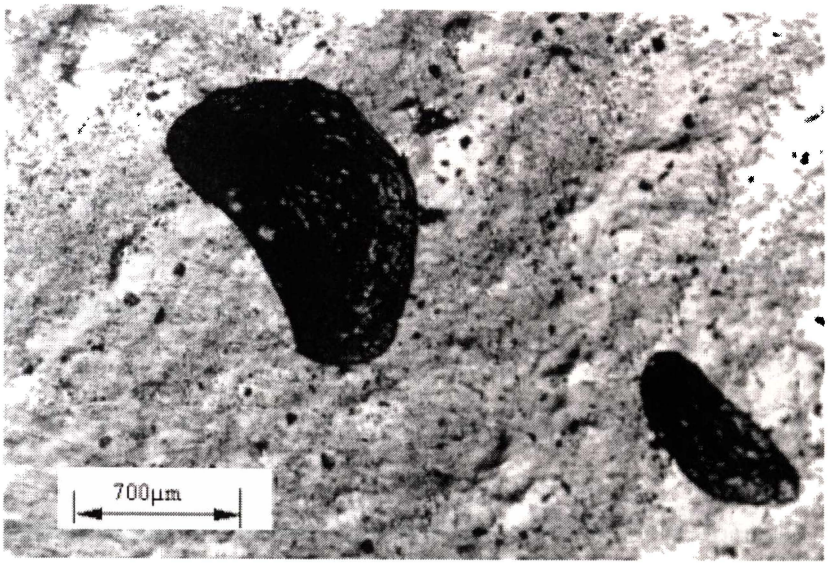

Figure 1.6 Micrograph of fishscale defect on coating surface.

Pinholes and Blisters

The way an article is fabricated can produce several defects. For instance, if the enamel coating is over-fired, bubbles will generally be small; if under-fired, large bubbles may occur. These large bubbles can extend to the surface of the coating, causing dimples, pinholes and blisters.[15] Pinholes are formed where the enamel has not smoothly run back after gas has escaped. Blisters are also caused when gas is evolved during firing.[7,15,53] Taylor and Bull[60] suggest that dimples and pinholes are bubbles that have burst and only partially healed.

Cleland and Morgan[61] investigated leakage of water tanks and found that holes or pore defects in the enamel coatings extended to and exposed the steel substrate to corrosion. They suggested that water had migrated through the pores and caused corrosion of the steel. The enamel coating lifted away from the steel, increasing the steel exposed, resulting in accelerated corrosion.

Orange Peel

This defect arises when the application technique is incorrect.[15,19] For example, the spray gun may have been too close to the substrate or sprayed at too high a pressure. Consequently, the enamel slip is applied with a large force, which causes a shearing effect on the previously applied layer and produces a wavy

surface appearance known as orange peel. Under firing the enamel coating can also cause orange peel.[19,21]

Crazing

Fine cracks or microcracks covering the enamelled item is called crazing.[7] They form when the enamel coating has a thermal expansion much higher than the steel, which creates tension. If the stresses are of high enough magnitude crazing occurs.

Spalling

Spalling occurs when the enamel coating has a much lower thermal expansion than that of the substrate. The coating is in compression during cooling and spalling occurs if the compressive stresses are too high.

Hairlining

Hairlining is a series of nearly parallel lines formed on the surface of the enamelled coating. This happens from cracking during the coat fusion, which has healed over but the steel of the previous coating is still showing.[16] A thick or under fired ground coat can cause hairlining, usually in the region of small or sharp radii of the enamelled part, which causes stresses on the enamel coating.[16,21]

Tearing

If the bisque becomes "too hard" during drying, the resultant shrinkage may develop stresses that concentrate to form cracks.[15,19,31] Andrews[15] suggests that common causes of tearing include applying a slip that is too heavy or too wet, drying the coat too rapidly and allowing the enamel surface to dry before the enamel underneath has dried. These all can cause differential shrinkage.

1.9 Steel for Enamelling

1.9.1 Types of steel

Many types of metal substrates can be used for enamelling, including; cast iron, aluminium and low carbon steel. Sheet steel for enamelling is known as "enamel grade" steel. It must fulfil certain general requirements for enamelling, including

enamelability and formability. Formability is required because many products contain bends (for example, stoves and fireplaces). Many products also require welding and so the steel must have good weldability.

The aim of enamel grade steels is to minimise the volume of austenite, which decreases the probability of forming the martensite phase during cooling.[55] The carbon content of enamel grade steel must be less than 0.05 wt%. Too much carbon causes defects from primary boiling (carbon boiling). Surface impairments can occur when carbon monoxide and carbon dioxide moves through the porcelain enamel coating during firing.[14,55] Carbon monoxide gas evolves when the cementite (Fe_3C) particles at the surface of the steel reacts with oxides in the enamel frit.[55] Removing cementites at the steel surface reduces this problem. However, if large carbide particles in the steel substrate are not concentrated at the surface, the substrate can be enamelled without producing defects from primary boiling.[62] Cold rolling can fracture the carbides and create voids in the steel where hydrogen gas can collect; reducing defects caused by gas diffusing to the interface. Decarburisation can also create voids in the steel because diffusion of carbon in ferrite is faster than self-diffusion of iron.[56] Therefore, carbon diffuses out of the steel and the carbides reduce in size, eventually disappearing and leaving voids that cannot be completely filled by the slower diffusing iron.[56]

Steel suitable for enamelling must also have the correct oxide and precipitate content.

1.9.2 Enamel Grade Steels Available

The types of flat-rolled carbon steels used for enamelling include:[14] low-carbon, decarburised, interstitial-free, titanium-stabilised, common cold-rolled and common hot-rolled steels.

Typical compositions are given in Table 1.7. Cold rolled steels can be cold rolled aluminium-killed steel or cold rolled rimmed steel. Another category is enamelling iron, a premium grade of commercially pure iron.

During the manufacture of sheet steel, oxygen is blown into the molten steel to reduce the carbon content. Before the steel solidifies, carbon oxide escapes while the melt is boiling. This is known as "unkilled" steel casting.[21]

Table 1.7 Typical compositions of steels used for porcelain enamelling.

	Composition % wt									
Steel type	**C**	**Mn**	**P**	**S**	**Al**	**N**	**Si**	**B**	**Ti**	**Nb**
Decarburised[63,64]	0.003-0.005	0.2-0.3	0.01-0.015	0.015-0.028	0.03-0.07				0.-0.019	
Interstitial-free[63]	0.005	0.2	0.01	0.02					0.04	0.09
Hot rolled[65]	0.14-0.17	0.7-1.0	0.2-0.045	0.015-0.02	0.02 min	0.01-0.02				
Cold rolled–aluminium killed[14]	0.02-0.04	0.15-0.3	0.015 max	0.015 max	0.03-0.07		0.015 max	0.006 max		
Cold rolled/rimmed or continuous-cast[14,63]	0.04-0.07	0.25-0.04	0.01	0.02						
Titanium – stabilised[63]	0.05	0.30	0.01	0.02	0.05				0.03	
Enamelling Iron[27]	0.03	0.05	0.025	0.025						

Enamel grade steels available (2000 AD) in New Zealand are given in Table 1.8.

Table 1.8 Enamel grade steel available in New Zealand for 2000.

Enamel grade steel	Manufacturer	New Zealand steel supplier
Decarburised KTSTM steel	Kawasaki Steel Corp., Japan	Fletcher Steel
Enamel grade JISSPP steel	Sunkyong Steel, Korea	Kiwi Steel
Enamel grade cold rolled JISG414	Sumitomo Steel, Japan	Stewart Steel

To process "decarburised steel", the carbon must be removed. This is done by annealing in an atmosphere of nitrogen, hydrogen, and water vapour at approximately 700°C.[26] Other types of decarburised steels available include open-coil decarburised steel and steel that is vacuum decarburised in the smelter.[26]

The process for manufacturing KTSMT (decarburised) steel is in Figure 1.10.[64]

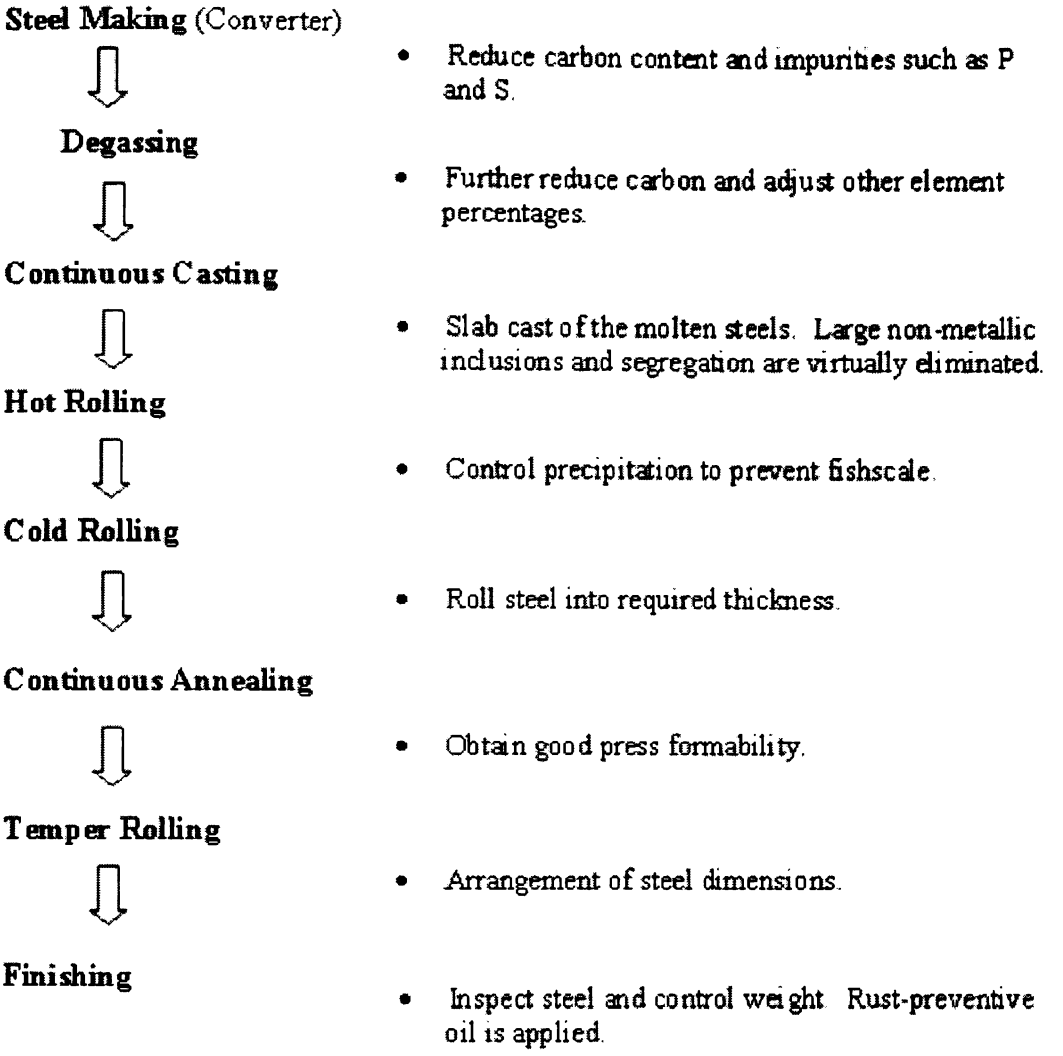

Figure 1.7 Process for manufacturing KTSMT (decarburised steel).[64]

1.9.3 Thermal Deformation (Sagging Distortion)

Steel composition affects the amount of sag during the firing cycle. Carbon and manganese influence the strength of steel at enamel firing temperatures, and consequently the sag characteristics.[66] Blickwede[56] suggests that plastic deformation associated with sagging occurs at enamelling temperatures and is promoted by the ferrite to austenite phase transformation. The carbon content of the steel affects the temperature for the start of this phase transformation and also the degree of transformation at a given temperature. Very low carbon steels have

greater sag resistance.[15,21,56] The temperature at which transformation occurs in enamelling steel (<0.025 wt% C) and the amount of transformation at a given temperature decreases with decreased carbon content.[21,56] If carbon content is above 0.025 wt%, the transformation temperature for thermal deformation is 721°C.[21] One of the aims of enamel grade steels is to prevent distortion at high temperatures. This is achieved by reducing the carbon content, which minimises the austenite formed.

Uniformity stress and temperature during firing minimises sheet steel distortion. Non-uniform steel thickness gives different heating rates, leading to distortion and possible variation in enamel maturity.[14]

1.9.4 Cleaning the Steel

Preparing the Surface for enamelling

The metal surface must be pre-treated (degreased and cleaned) before the enamelling stage to help prevent defects such as blisters, chips, poor adherence and fishscale.[15] The steel being enamelled often has a thin coat of oil to prevent corrosion during storage and transportation. Rust and contamination (such as dust) need to be removed before enamelling. The predominant form of steel surface contamination is surface carbon; the degree of surface cleanliness can be related to the level of carbon on the surface.[67]

Cleaning Methods

There are four general ways to clean the steel surface; detergents, solvents, chemicals or mechanical action.[68] The enamelling industry usually uses pickling (chemical reaction) and the clean-only method (detergents).

Mechanical action by abrasive blasting with sand, steel shot or grit was common, especially for large parts such as water tanks (where only one side is enamelled) and parts without pockets or crevices. The steel sheet must be thick enough to prevent distortion.[14]

- **Clean-Only Method**

The clean-only method, which is often known as the "no-nickel/no-pickle system", is becoming the preferred method for preparing steel for enamelling because it has lower environmental impact. Toton[69] reports that this system is used because of ingredients for the nickel and pickle cleaning system are expensive and there are high costs associated with disposing of hazardous waste. Hyde[70] suggests the preferred metal pre-treatment for pickle-free coating is by cleaning of any oils, drawing compounds and dirt, followed by several rinses. The soils must be completely removed in the alkaline cleaning stage so remaining rinses are not affected.[71]

- **Pickling/ Nickel method**

Cleaning by pickling followed by a nickel dip for adherence is still common for preparing low carbon steel for enamel application.[72,73] Pickling is acid cleaning of the steel surface to remove contaminants such as rust, scale (from grease firing) and etching of the surface. The most commonly used solution is 5-10% wt/wt sulphuric acid (H_2SO_4). Nickel dip (also known as nickel flash) is applied to the surface to help the enamel coating adhere to the steel and to reduce fishscale and copper head defects.[19] Using nickel dip enables direct-on white or light colour enamel to be applied without a ground coat, which contains adherence oxides. A 1-5% wt% of $NiSO_4.7H_2O$ is commonly used as the nickel dip.[26]

1.10 Enamel/Steel interface

Theories of Adherence

There is a lot quantity of literature on the theory of adherence or bonding between the enamel coating and metal substrate. Donald has completed a comprehensive study on the different theories for bonding between glass (enamel) and metal, including: the thermodynamic approach, mechanical bonding, the dendrite theory, the electrolytic theory, mutual solubility and intermediate compound formation and chemical bonding.

Most literature on adherence theories support the concept of an oxide layer at interface between the steel and enamel.[21,40,73,74] An extensive earlier study by

King and co-workers[75] was initially against the oxide layer concept because adherence between the steel and FeO layer at the interface is not particularly good. A major conclusion[75] was that a strong chemical bond could be formed at the glass/metal interface if the glass (enamel) coating became saturated with an oxide of the metal (FeO when using an iron substrate), which when in solution the glass would not be reduced by the metal.

Kyri[21] argues that the steel surface oxidizes during the initial heating of the firing. This thin oxide layer allows the surface to be wetted by the melting vitreous enamel. Fine crystals of metallic cobalt and nickel separate from chemical exchange between iron in the steel and cobalt oxide and nickel oxide in the melted enamel on the steel surface, which promotes iron oxidation. The rough surface allows mechanical fixing of the enamel. Kyri,[21] however, states that this is not sufficient to explain firm adhesion, so other unexplained physical processes must be involved. Other processes do occur when the ground coat is fired. For instance, the iron oxide being formed dissolves in the molten ground coat. Because of a concentration gradient, it diffuses into the enamel layer. The enamel structure changes because the enamel devitrifies (changes from glassy state to minute crystalline state). This enamel has low mechanical strength and is sensitive to hydrogen (which allow hydrogen-associated defects such as fishscale to occur).[21]

Mohyla and co-workers[76] summarised work of Sullivan[9] and Dietzel[77] as follows: Nickel and cobalt promote enamel adherence because they are moderately attracted to the iron-enamel interface by the electrolytic forces of the galvanic micro-cell present on the steel surface.

Lynch[78] suggests three basic requirements for glass-to-metal adherence in porcelain enamelling:

- The enamel must wet the base metal and electrochemical bonding must occur across the interface.
- An oxide of the base metal must saturate the glass-metal interface.
- The oxide must not be reduced by the base metal when in solution.

These conditions are established and maintained if adherence-promoting oxides such as CoO, MnO_2, NiO and CuO are used in ground coats.[78]

Pask[40] proposed a rough interface contributes to adherence and provides a safety factor in terms of the transition zone and greater contact area. However, it is theoretically not needed if a chemical bond (that is, metallic, ionic, and/or covalent) is obtained throughout the interface.

Shieu and co-workers[72] performed adherence tests using various porcelain enamels and low carbon steels. They found that the coating of enamel grade steel treated (dipped) with cobalt adhered better than steel treated with nickel or without transition metal. Good adherence is also associated with high-density anchor points in the enamel/steel interface, with porcelain enamel to steel adherence being controlled by mechanical locking.

Paparazzo and co-workers[79] used X-ray photoelectron microscopy to show that good adherence occurred if the silicate phase reacts fully, giving local chemical continuity between the steel and the enamel. Adherence was associated with a heterogeneous mixture of an iron silicate phase and unreacted FeO.

1.11 Chemical Resistance

1.11.1 Testing Specimens

The porcelain enamels used in this study are commonly coated onto products such as outdoor gas cookers (also known as barbecues) and indoor wood burners. These cookers need to withstand outside environmental exposure, food acids and detergents used for cleaning. The composition of the water in the environment can vary from nearly pure (neutral), to acidic or alkaline.[15] Chemical resistance of the coating, is therefore, an important property. Wood burners are normally used indoors and may be exposed to cleaning detergents, so alkali resistance is an important property. Most porcelain enamels are unaffected by alkalis at room temperature.[80] However, some enamel products (especially outdoor gas cookers) may be exposed to a high temperature, alkaline environment (through cleaning), so the coating must be alkali-resistant.

1.11.2 Weather Resistance / Acid Tests

Weather resistance of porcelain enamels can be indicated using its resistance to boiling citric acid solution (6% wt/wt).[81] The boiling acid test (DIN 51 151) was designed primarily for cookware applications[21] and consists of measuring weight loss after exposure to boiling citric acid (6 % wt/wt) for 2.5 h (for more boiling citric acid test information see section 2.7.1).

Porcelain Enamel Institute (PEI) studies show a relationship between another acid resistance test (DIN 51 150) and corrosion after 15 years of weather exposure.[21,82] The relationship after 30 years was also determined.[83] The DIN 51 150 method is qualitative and involves exposing enamel coating to 10% wt/wt citric acid at room temperature for 15 minutes then grading the corrosion (loss of gloss). This test cannot be used for matte enamels.

The DIN 51 151 (boiling acid test) indicates that blue enamel has a high resistance (2.0 g/m^2 after 2.5 h, Table 1.9), whilst zirconium white enamel is completely removed, indicating that it has very low resistance to acid.

Table 1.9 Acid resistances of different enamels, using the DIN 51 151 test.[21]

Enamel type	Weight loss g/m^2
Blue for household ware interiors	2.0
Transparent enamel, acid resistance, containing boron	3.0
Boron-titanium, acid resistance	5.0
Zinc-titanium	30.0
Boron-titanium enamel soft	50.0
Zirconium white enamel	Completely removed

There is little published data on acid resistance (quantitative-weight loss) of enamelled outdoor gas cookers or wood burners. The specification for maximum weight loss of interior enamel on cooking utensils and for acid resistant bathtubs is 25.0 g/m^2.[21] Outdoor gas cookers are exposed to acids from cooking and acidic water (rain), and require moderate acid resistance. Higher resistance is required

for cooking utensils (which are continuously exposed to cooking acids) and bathtubs (which are exposed to an acid solution). Wood burners are generally not exposed to acids and do not, therefore, need to be acid resistant.

1.11.3 Chemical Corrosion Mechanisms

Corrosion of enamel surfaces by acid, alkali or water may occur in the following ways:[84,85]

- New compounds being formed on the surface from reactions with a corrosive medium.
- Surface leaching (hydrated silica layer) by preferential dissolving of the glass surface.
- Dissolution of the glass surface, which continuously exposes a fresh surface.

In the general corrosion process, there is an initial extraction of alkali ions on the glass surface that leaves an alkali deficit layer.[84] When the enamel surface is exposed to an acid solution, free hydroxyl ions formed by reaction are neutralised,[86] and attack on the silica network is minimised.[84] Maylor[84] proposes that pH of the acid solution and composition of the glass affects the thickness of the hydrated silica layer. Less durable glasses form thicker hydrated layers because the glass has a more open structure; allowing alkali ions to rapidly leach out.

Acid Corrosion

Eppler[87] summarises the principal mechanism for acidic attack as an ion exchange process between a modifier (principally alkali) ion in the glass and a hydrogen ion in the solution (Equation 1.6). The basic glass structure is not disturbed because diffusion occurs through the modifier-depleted surface to the interface, with unreacted glass where the ion exchange occurs.[87]

$$H^+ \text{ (solution)} + Me^+\text{(glass)} \rightarrow H^+\text{(glass)} + Me^+ \text{ (solution)} \quad \textbf{Equ. 1.6}$$

Alkali Corrosion

Surface corrosion in an alkali solution involves ion exchange leaching and dissolution. Glass leaching occurs when hydrogen ions in the solution react with the glass matrix, causing the alkali ions in the glass to be ionised.[30] This reaction is pH-related. Dissolution of the silicate structure generally takes place when the pH is greater than 8, and dissolution increases as pH increases. As the concentration of alkali ions such as Li^+, Na^+ and K^+ in the enamel increases, the number of nonbridging oxygens in the glass also increases, which increases ion exchange leaching and causes a larger hydrated layer to form at the glass surface. Dissolution of the hydrated layer occurs more quickly than dissolution of the rest of the glass.[30]

Enamel coating surfaces contain insoluble salt deposits, which retard alkali corrosion. The temperature during testing affects the degree of corrosion. Testing specimens in hot sodium hydroxide for 48 hours above 80°C impairs reproducibility because of these surface deposits. However, at temperatures below 80°C, reproducibility is impaired because the corrosion is reduced.[88] The alkali corrosion mechanism is further discussed in sections 1.11.5. and 5.1 (Chapter 5).

1.11.4 Microscopy Examination

The effect of acids or alkalis can be examined by microscope. If the enamel is soluble, then the surface will be etched and look like powdered glass. If the outer surface is then mechanically removed, the exposed enamel will have a rough etched surface. If the enamel is resistant to solution, the surface may be crazed, which is a common characteristic of having been heated.[15]

1.11.5 Role of Mill Additions on Chemical Resistance

Changes in enamel composition can effect acid and alkali resistance.[14,16,30] Adding titanium dioxide and increasing the silicon dioxide (with a decrease in boron), can increase acid resistance.[14] The highest degree of acid resistance is achieved by decreasing resistance to other materials, including alkalis.[80] To improve alkali resistance, it is common to maintain a high level of silicon dioxide while adding zirconium oxide or alumina.[14] Any silica added as a mill addition,

might only partially dissolve during firing. Smith[89] reported that less than half of silica mill additions dissolve in the glass when firing some enamel coatings; increasing the firing time made little difference to the amount of silica dissolved. Horton[30] studied the effect of mill additions on alkali resistance in wet enamel systems and found that titanium dioxide forms as titania recrystallises during the cooling stage of the firing cycle. These crystals form insoluble structures and are not attached structurally to the remaining glass. Horton[30] also observed, that some of the boron oxide in the glass coating has a tetrahedral co-ordination while the rest has a triangular co-ordination. He suggested that many glasses do not have sufficient (BO_4)- tetrahedrals to tie up all the alkali ions. Consequently, the alkali ions form nonbridging oxygens on the triangularly co-ordinated boron and make a B-O-R bond. Hydrogen ions can react with this bond and form a hydrated layer. Consequently, the glass has lower alkali resistance.

The alkali resistance durability of glass can be improved by using divalent cations such as Mg^{2+}, Ca^{2+}, Zn^{2+} and Sr^{2+} that prevent alkali exchange with the H^+ ions.[30] The divalent cation occupies two nonbridging oxygens, and hinders ion exchange of alkali ions with the glass structure.[30]

Other components such as clay can also affect alkali resistance of porcelain enamel coatings. Decreasing the clay level in the coating increases weight loss,[90] and decreases the enamel's resistance to alkali attack (Figure 1.8). Reducing the clay level reduced the alumina content in the coating. However, increasing the alumina content in the clays increased alkali resistance (Figure 1.9).[90]

Vargin[7] reports that adding clay reduces acid resistance, especially to strong mineral acids. Enamels applied as powders (without clay) have greater acid resistant than those applied by the wet slip spray method.

Alkaline metal oxides reduce the melting temperature of silica. However, alkaline metals have the detrimental affect of decreasing chemical resistance and increasing thermal expansion.

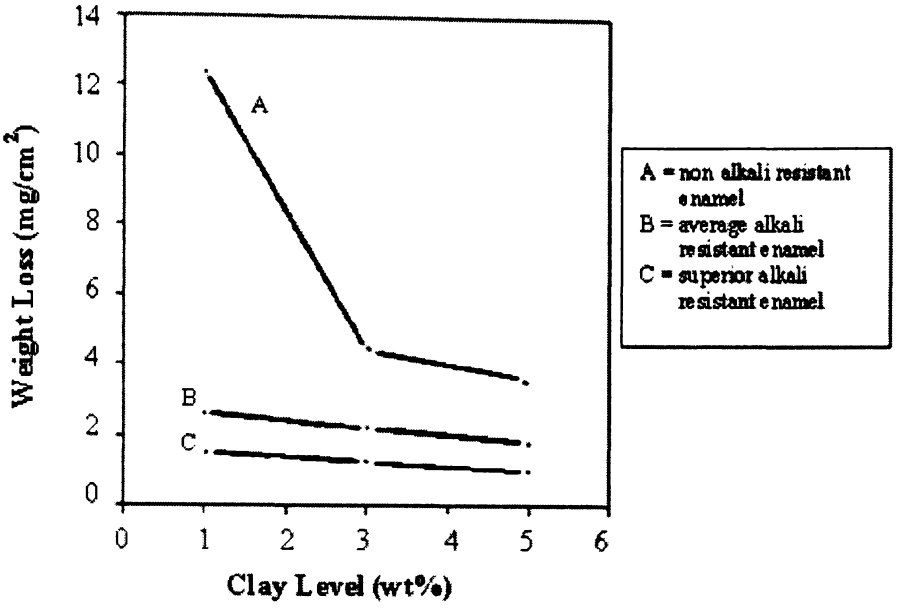

Figure 1.8 Effect of clay content on alkali corrosion weight loss (adapted from Lightner and Nobles[90]).

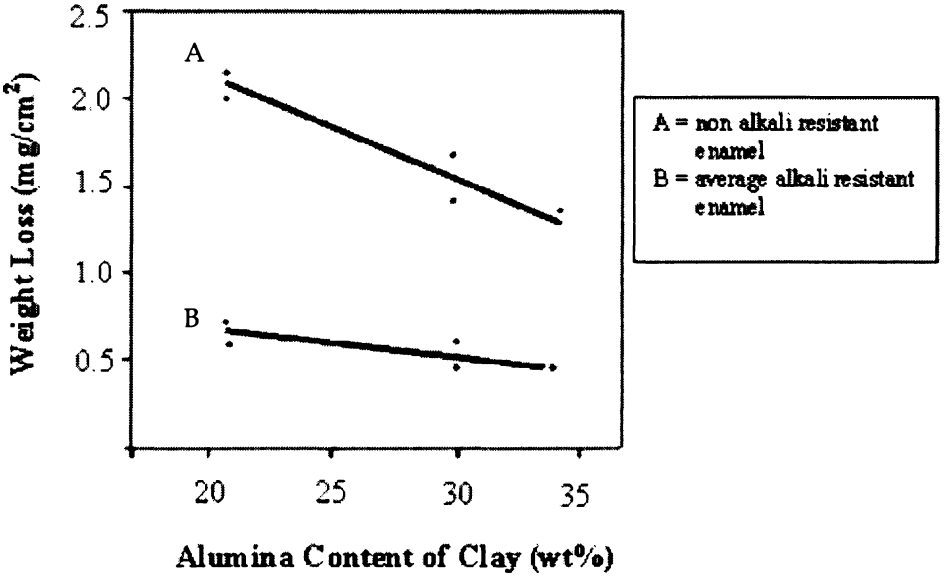

Figure 1.9 Effect of alumina content of clay on weight loss (adapted from Lightner and Nobles[90]).

1.11.6 Effect of bubble structure on chemical resistance

As discussed in section 1.8.3 the bubble structure also effect corrosion resistance of ground coat enamels. After initial dissolution from exposure to acid and alkali

attack, secondary factors such as bubbles or pinholes may play a role in the dissolution process by increasing the surface area to chemical attack and therefore the rate of glass dissolution.

There is literature on bubbles in enamels[50,51,91] and equations that help predict enamel durability as a solid matter without bubbles.[87] However, there were no reports that quantified the effect of bubbles on corrosion of vitreous enamel coatings. The effect of bubble structure on chemical resistance is investigated in Chapter 5.

1.12 Tests for Assessing Porcelain Enamel Coatings

There are many tests for assessing porcelain enamel coatings. The ASTM (American Society for Testing and Materials) is the most extensive and up-to-date compendium of methods, which are summarised in Table 1.10.

1.12.1 Adherence/Bonding Test

The term adherence describes the enamel coating's resistance to mechanical damage and whether the enamel comes cleanly off the metal or leaves variable amounts of broken glass in contact with the metal. Destroying the enamelled sheet steel by mechanical deformation will establish the degree that the enamel coat adheres to the steel. Various electronic instruments can measure the degree the adherence.[21] However, a very common method (because it is easy and inexpensive) is the falling weight (or impact) test. A known weight is dropped from a known height onto the enamel coating (see section 2.7.3) and the visual damage categorised using a standard chart (Table 1.11).

Good quality enamel will have excellent adhesion with little damage. Enamel coatings with 'bad adhesion' category will have a large amount of enamel damage and the steel will appear "clean" in appearance, indicating that the enamel coating has not adhered to the substrate.[92]

Table 1.10 Selected porcelain enamel test methods (ASTM).

Designation	Title
	Adherence
ASTM C 313	Adherence of Porcelain Enamel and Ceramic Coatings to Sheet Metal
PEI T-29*	Adherence of Porcelain Enamel Cover Coats Direct To Steel
	Colour and Gloss
ASTM C 346	45-deg Specular Gloss of Ceramic Coatings
ASTM C 540	Image Gloss of Porcelain Enamel Surfaces
ASTM D 2244	Colour differences of Opaque Materials, Instrumental Evaluation of
	Chemical Resistance and Weather Characteristics
ASTM C 282	Acid Resistance of Porcelain Enamels (Citric Acid Spot Test)
ASTM C 614	Alkali Resistance of Porcelain Enamels
ASTM C 756	Cleanability of Surface Finishes
ASTM C 283	Resistance of Porcelain Enameled Utensils to Boiling Acid
ASTM D 1567	Detergent Cleaners for Evaluation of Corrosive Effects on Certain Porcelain Enamels, Testing
	Chipping Resistance
ASTM C 409	Torsion Resistance of Laboratory Specimens of Porcelain Enameled Iron and Steel
	Abrasion Resistance
ASTM C 448	Abrasion Resistance of Porcelain Enamels
	Thermal Shock
ASTM C 385	Thermal Shock Resistance of Porcelain Enamel Utensils
	Tests Related to Preparation of Coatings and Substrates
ASTM C 285	Sieve Analysis of Wet-Milled and Dry-Milled Porcelain Enamel
ASTM C 715	Compressive Stress of Porcelain Enamels by Loaded-Beam Method
ASTM C 632	Reboiling Tendency of Sheet Steel for Porcelain Enameling
ASTM C 774	Yield Strength of Enameling Steels After Straining and Firing
	Tests Related to Continuity of Coating
ASTM C 743	Continuity of Porcelain Enamel Coatings

*PEI T-29 is a Porcelain Enamel Institute test

The ASTM test for porcelain enamel adherence involves deforming the substrate and measuring the ratio of porcelain enamel in the deformed area to porcelain enamel in the area before deformation (indication of adherence).[80] Shieu and co-workers[72] used conductivity measurement (ASTM C 313 adherence test) and periodic cracking method with a universal tensile testing (Instron) machine to

indicate tensile properties to evaluate adherence of porcelain enamel to low carbon steel. The cracks that developed on loading were examined, the crack spacing measured, and the average shear stress at the enamel/steel interfaces was determined. There was a sigmoidal correlation found between the adherence index (conductivity test) and average shear stress (periodic cracking), with failure occurring at a critical load when the enamel changed from cohesive to adhesive.

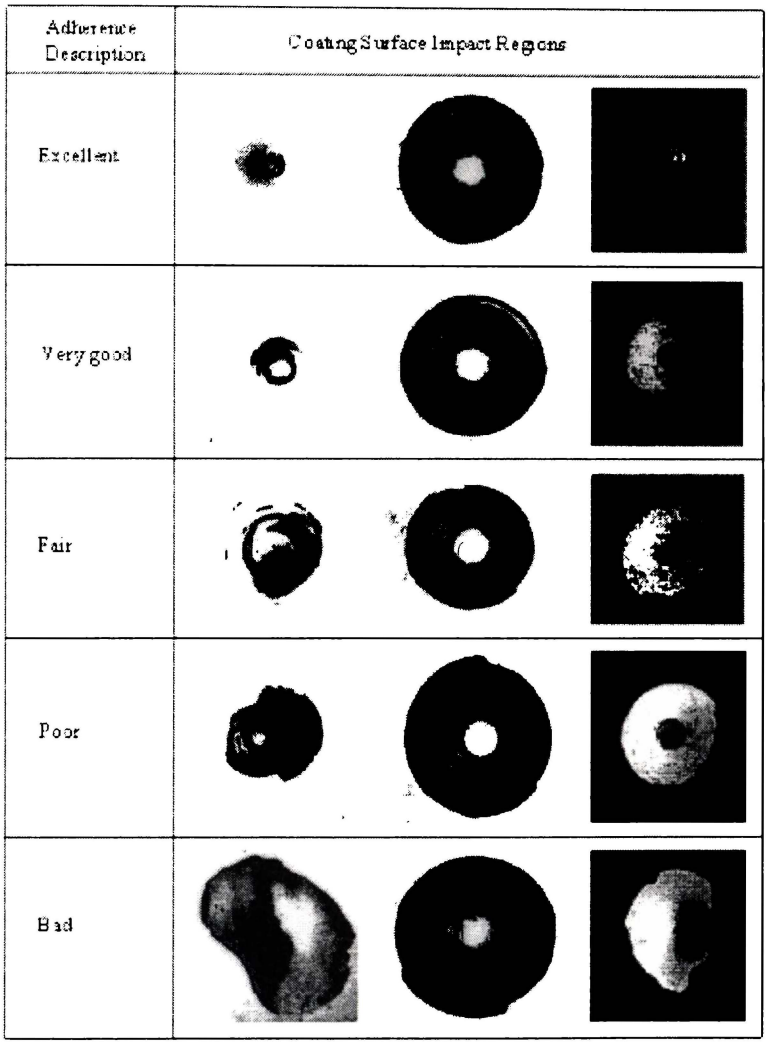

Table 1.11 Impact test categories.[92]

1.13 Spectroscopic Characterisation Review

Raman spectroscopy and infrared spectroscopy have not been widely used in the enamelling research area. However, there is a lot of literature on spectroscopy of

crystalline silica, amorphous silica and many of the mill addition components in the final glassy coating matrix. McMillian[93] completed a review showing a great quantity of literature on Raman spectroscopic studies of alkali and alkaline earth silicate glasses and melts. However, there is much less work done on more complex compositions such as aluminosilicate and borosilicate systems, let alone the very complex alkali-alumino-borosilicate type systems of porcelain enamel coatings.

Both Raman and infrared spectroscopy techniques are used widely for qualitative mineral identification (see Griffith[94]). The published Raman and infrared spectroscopy band positions of many of the solid components used in fabricating porcelain enamel coatings are given in Table 1.12.

The first order spectra of Raman and infrared spectra of amorphous materials are continuous[4] because the structure has no long-range order or periodicity. This irregular arrangement of the structural elements results in a fundamental breakdown of the first order vibrational modes, allowing other modes to exist for a single crystalline structure. The bands are continuous and broad as modes overlap. The main features of a typical spectrum for vitreous silica from Raman and infrared spectroscopy include broad continuous bands at approximately 450 cm^{-1}, 800 cm^{-1} and 1050 cm^{-1} (Figure 1.10). The infrared spectrum has strong broad bands at approximately 450 cm^{-1} and 1100 cm^{-1}, with other bands at 800 cm^{-1} and 1150cm^{-1} (shoulder).

X-ray diffraction of a crystalline solid will show sharp peaks (Figure 1.11a) at certain 2θ angles as X-rays diffract from defined crystal planes. However, the curve of scattered intensity is almost zero in other regions. Amorphous solids and liquids lack periodicity (the tendency to "order"), which results in the X-ray scattering curves typically displaying one or two broad maxima (Figure 1.11b and c).

Table 1.12 Solid components used in the fabrication of porcelain enamel coatings.

Component	Composition	Purpose	Raman (R) and Infrared (IR) band positions (cm^{-1}) (from literature)
Frit	amorphous alkali borosilicate	Frit	R: 450, 800, 1050 (amorphous silica)[4] IR: ca. 450 s,b, 800, 1100s, 1150sh (amorphous silica)[4]
Silica	α-quartz, SiO_2	refractory	R: 128, 207, 265, 356, 394, 401, 450, 464, 509, 697, 795, 807, 1072, 1085, 1162, 1235[96] IR: 257m, 362s, 385sh, 450s, 510sh, 693w, 775m[97]
Colouring Oxide	α-Cr_2O_3	colouring	R: 303, 351, ca. 397, 530, 551, 609[98] IR: 407w, 435w, 555s, 625s[99]
Colouring Oxide	$CuCr_2O_4$, $FeCr_2O_4$, $ZnCr_2O_4$	colouring	R: 171, 373, 495, 615 ($FeCr_2O_4$)[98], 186, 457, 515, 610, 692 ($ZnCr_2O_4$)[100] IR: 450w, 510s, 605s ($CuCr_2O_4$)[101] 176, 370, 510, 625 ($FeCr_2O_4$) 188, 375, 537, 635 ($ZnCr_2O_4$)[99]
HB Clay	SiO_2 (quartz) and kaolinite	refractory	See Silica and Kaolex clay
Kaolex Clay	kaolinite $Al_2O_3.2SiO_2.2H_2O$	refractory	R: 130sh, 143m, 197vw, 245w, 270m, 336m, 418sh, 431m, 463m, 516w, 638m, 710vw, 751w, 790w, 915w[102] IR: 794, 910, 938, 1005, 1030, 1116, 3620, 3651, 3668, 3696 (Keokuk kaolinite)[103]
Bentonite	bentonite $(M^{2+})(M^{3+})_4(Si,Al)_8O_{20}(OH)_4.H_2O$	suspending agent	R: 75, 132, 162, 202, 264, 290, 360, 429br, 608, 708, 800, 916, 1033, 1105, 1162[104] IR: 427, 467, 525, 629,8, 590, 796, 846, 883, 920, 999, 1043, 1116, 1636, 3425, 3630 (Ankeria deposit)[105]
Feldspar	Microcline $KAlSi_3O_8$	refractory	R: 62, 82, 95, 110, 127, 141, 150, 158, 180, 200, 245, 257, 265, 285, 310, 330, 370, 403, 412, 452, 475, 485, 512, 580, 630, 650, 747, 765, 812, 975, 993, 1000, 1035, 1095, 1120, 1123, 1136[106] IR: 97, 115, 141, 147, 165, 185, 200, 220, 280, 330, 370, 420, 460, 530, 585, 605, 650, 720, 740, 765, 790, 1010, 1090, 1140, 2300, 2940($Na_2O.Al_2O_3.6SiO_2$)[107]
Feldspar	Albite $K_{0.06}Na_{0.86}Ca_{0.08}$-$Al_{1.08}$-$Si_{2.92}O_8$	refractory	R: 164, 185, 207, 250, 268, 291, 328, 407, 415, 455, 479, 506, 763, 815, 976[108] IR: 93, 145, 165, 185, 200, 220, 250, 275, 330, 370, 420, 460, 530, 590, 650, 720, 750, 760, 790, 1000, 1040, 1090, 1150, 2300, 2870 ($Na_2O.Al_2O_3.6SiO_2$)[107]
Feldspar	Orthoclase	refractory	R: 1130 and 1005 cm^{-1}[109] IR:?
Antimony Oxide	Sb_2O_3 (senarmonite)	opacifier	R: 87, 121, 144, 193, 218, 256, 298, 359, 376, 434, 452, 717[110] IR: 179, 272, 386, 404, 482, 617, 744, 952, 971[110]
Alumina	Al_2O_3	refractory	R: 378, 418, 432, 451, 578, 645, 751 (a -Al_2O_3) ca.460w[111] IR: 460m, 600s, 660sh, 850s[112]
Boric acid	H_3BO_3	flux	R: 208m, 498m, 880s[113] IR: 1195 s, 1471s, ca 2260m, ca 2360m, ca 2510m, 3223 s,b[114]
Hydrous Borax	borax ($Na_2B_4O_7.10H_2O$)	flux	R: 78w, 90m, 120m, 160w, 361m,390w, 474m, 530wbr, 590vw, 776mbr, 860w, 975m, 1640vw, 3140s, 3357s, 3400s, 3447s, 3495s, 3575s[115] IR: 220s, 235s, 320vvbr, 430w, 465m, 525w, 590w, 660w, 828s, 710w, 785w, 890sh, 947s, 1003vs, 1038sh, 1078m, 1132s, 1140sh, 1175w, 1235m, 1282m, 1350vs, 1385w, 1424s, 1483vs, 1580w, 1656m, 1710sh, 2875w, 2910w, 3060sh, 3357vs, 3503s, 3560s[115]
Magnesium Carbonate	$MgCO_3$	electrolyte-flocculater	R: 212, 332, 735, 1096, 1460[116] IR: 362-459, 747-763, 876-911, 1446-1599[117]
Sodium Nitrite	$NaNO_2$	increases set	R: 119s, 154m, 827m, 1325s[118] IR: 820m, 1270s, 2540w[119]

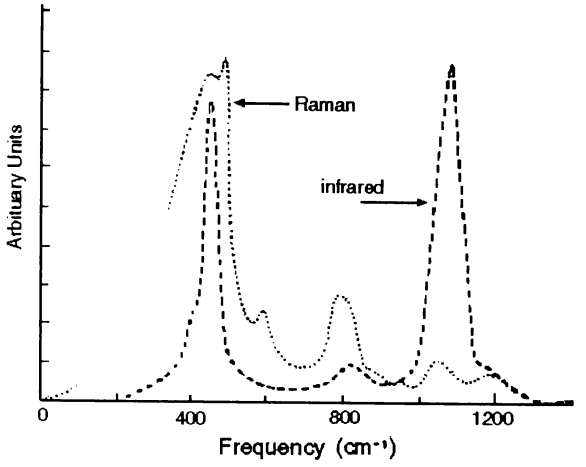

Figure 1.10 Raman and infrared spectra of vitreous silica (adapted from Murray *et al*[4]).

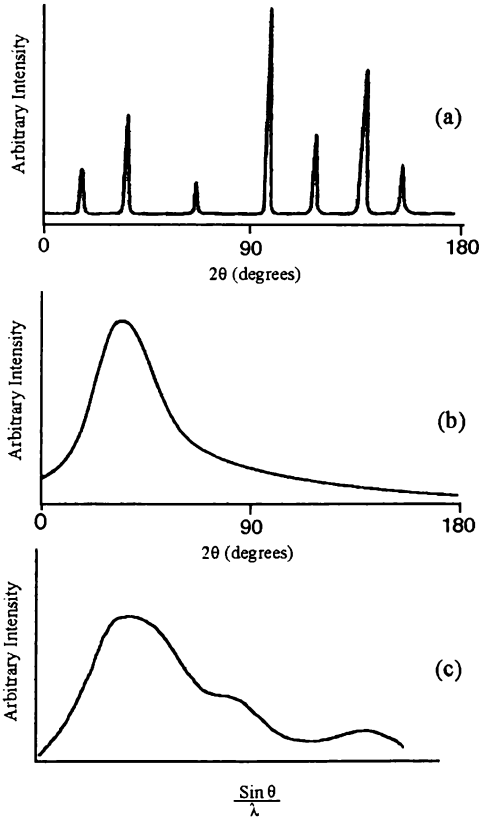

Figure 1.11 Comparative X-ray scattering patterns, (a) crystalline solids, (b) liquid or amorphous solid (a and b adapted from Cullity[95]), and (c) glass example (adapted from Vargin[7]). ($\sin\theta/\lambda$ = °2θ).

Previous Raman Spectroscopy Study

Buerhop and co-workers[1] studied gas and solid inclusions present in glazes on porcelain dishes using Raman microscopy. They showed that the solid inclusions consisted of quartz immersed in a glassy matrix, and cristobalite embedded on the surface of bubbles. Cristobalite is a high temperature phase of SiO_2, and is most stable between 1470° C and 1713°C although it does exist at lower temperatures. Bands were observed at ca. 463 cm^{-1} for α-quartz, and 127, 222, 413, 780 and 1081 cm^{-1} for α-cristobalite. The gas inclusions in glazes on porcelain dishes were air in an incompletely fired sample and CO_2 for an optimum-fired sample.

1.14 Porcelain Enamels – Recent Developments

Porcelain enamelling is an ancient technology but both the coatings and processes have to be improved to remain competitive. This section discusses recent developments in both the enamel product and enamelling processes as well as problems that exist or could occur in the future.

1.14.1 Competitive Organic Coatings

Organic finish technology has been a major competitor over the last 50 years. Although organic coatings are cheaper, and can be used in many more situations, they are not as durable to high temperature, chemicals, microbial degradation and adverse climatic conditions as porcelain enamels.[120] Organic finishes can be scratched, wear more easily and are susceptible to chemical attack.[121] Powder application of organic paints has been an undisputed success in the metal finishing industry and has two basic advantages over vitreous enamel powder.[122] Firstly, the material is inherently highly resistive with a value of $10^{16\text{-}18}$ ohm cm^{-1} compared with 10^6 ohm cm^{-1} of frit. Secondly, organic coatings have a much lower density than frit (1100 compared with 2500-2700 kg m^{-3}).

As organic particles are more resistive than frit particles, they do not lose their charge when attracted by earthed components. Frit particles rapidly lose charge

and drop off. However, encapsulating the frit with an organic silane to simulate properties of organic powders can increase resistivity.[122]

1.14.2 Composition Changes

Enamel formulations are constantly changing to improve particular properties or reduce costs. Adding a second phase or by crystallising the coating after it has been applied have been major developments for controlling the microstructure of enamels.[122] Adding a metallic second phase improves the ability of the final coating to withstand considerable distortion without flaking or chipping,[123] and adding aluminium particles increases toughness of the glass.[124] Introducing a second phase can also increase resistance to high temperatures, which allows enamelled ware to be used at temperatures approaching firing temperatures.[122] Adding crystalline inclusions to conventional base enamel can also improve the resistance for high temperature uses.[125]

There is no comprehensive study on the effect of additives on the properties of enamels or glasses, so this is where the most promising future materials might be found. For example, introducing metal oxides into the surface of vitreous enamel improves properties.[126] Modifying the surface layer by ion–exchange, thermal toughening or crystallisation (normal methods used for modifying normal glass) is also possible.

1.14.3 Light Colours for Direct-On Enamels

To increase adhesion and reduce fishscaling the steel surface must be pickled and nickel dipped (section 1.9.4) before enamelling to produce light-coloured direct-on enamels. Adhesion oxides such as cobalt and nickel allow direct-on enamelling without a nickel dip, but darker colours are produced. Other components have been tried for direct-on white enamels. However, enamels produced from frits with nickel but no cobalt did not adhere sufficiently under service conditions.[127] Adding antimony oxide to the frits during smelting gave varying results, with 3.5% giving the best adhesion.

Developing self-opacifying white enamels, based on zirconia and titanium oxides was a major development.[128] Previously, fluorine or antimony were the only

opaque enamels available and up to 6% tin was required to achieve satisfactory opacity. Two coats were needed for a good enamel finish but newer formulations allow a one-coat application. Titanium opaque enamels have improved impact and acid resistance,[129] and semi-opaque and transparent enamels for a wide range of colours have been developed. The matte enamels developed for both white and colours are also suitable for white and black boards.[129] Enamels with unique appearances such as metallic lustres to simulate copper metal or stainless steel are being developed.

1.14.4 Powder Enamel

Probably the biggest impact on the enamelling industry worldwide has been the development of enamel powders for electrostatic application.[129] Electrostatic spraying is environmentally friendly and more economical than the standard wet spray process. The steel does not need to be degreased, saving in drawing oils, etc. Powder enamel is available as "direct-on" for hot water tanks, heat exchanger panels and pyrolytic ovens and as alkaline resistant coatings for washing machine drums.

1.14.5 Self Clean Enamels

It was originally thought that self-cleaning (or continuous) enamels would be impossible to develop but by the end of the 1960s, new formulations had been developed for internal oven surfaces.[122] The porous components with excess oxygen that catalyse decomposition of organic deposits.[129-132] When organic materials from cooking contact the enamelled surfaces, the organics are oxidised and destroyed.[132] The oxidation temperature is reduced to the 250-300°C of normal domestic oven baking temperatures using the well-known principle that a higher oxygen atmosphere lowers the oxidation temperature. The higher the porosity in the enamel coatings, the more fat residues that can be stored.[131] Volatilisation of the soils also contributes to the cleaning action. Environmentally unfriendly cleaning agents are not needed, only heat as with pyrolytic ovens.[129] Catalytic pyrolytic oven enamels (produced with electrostatic powders) with self-clean properties have therefore become common.[121]

1.14.6 Application Processes

Electrostatic dry powder process

The most commonly used process for producing porcelain enamel is electrostatic dry powder. Dry electrostatic and electrophoresis (EP deposition) processes have many advantages over the older methods of wet suspension spray application and dipping.[122] These processes are environmentally friendly and generate very little waste. The material can be recycled, no drying is needed, and a pickle/nickel treatment is not needed. The only pre-treatment is cleaning, which sometimes can exclude degreasing.

The electrostatic systems first developed were not used by smaller companies because of their high relative cost.[133] However, the development of pre-milled frits (just add water), either as a ground coat or as part of a two-coat/one fire system, has decreased process cost. Enamellers can now blend pre-milled frits to obtain properties required for each application, saving milling cost and eliminating waste. The two-coat/one fire processes for electrostatic spraying also reduce process time. Electrostatic powders and pre-milled powders produce consistent, even coatings and no waste. The enamels produced recently allow greater bond development with thinner applications.[134]

One problem with electrostatic spraying is back ionisation. However, removing free ions between the gun and the item being enamelled significantly reduces back ionisation, thus improving finish quality and uniformity.[134]

Electrophoretic deposition Electrophoresis

The electrophoresis enamelling process was first demonstrated in 1974.[135] This is an anodic process where the metal item is submerged in a bath containing the frits and additions. An electric current causes the particles to deposit onto the metal surface. The item is then fired using conventional methods. This process gives excellent film characteristics including; a uniform thin layer without thickening on corners, dense, low porosity, superior smoothness, but without orange peel defects common in the wet spray process.[135,136] However, this process can have high capital costs.

Electrophoresis can be difficult to control. The metal surface must have consistent electrochemical properties and be active for good deposition. If the surface is passive, deposition is often not good because gaseous oxygen is produced.[137]

High-power diode laser

High-power diode laser (HPDL) treatment can improve wettability characteristics of EN8 mild steel because the metal surface can undergo HPDL-induced melting.[138] This surface treatment reduces surface roughness, increases the polar component of the surface energy, and increases the surface oxygen content. HDPL radiation can be used to change the microstructure of an amalgamated alumina/silica based oxide (AOC).[139] Without laser treatment, the enamel cannot be fired onto the AOC surface but HDPL laser radiation alters the mild steel's wetting characteristics by decreasing the contact angle. After rapid solidification, a range of microstructures is obtained.

1.14.7 New Developments In Testing and Analytical Techniques

Many techniques can be used to test and analyse porcelain enamels. This helps increase information on enamelling, which helps improve quality.

The compositional complexity of vitreous enamels makes quantitative analyses difficult. Conventional methods for characterising elemental compositions include energy dispersive X-ray analysis (EDS), atomic absorption spectrophotometry (AAS) and inductively coupled plasma (ICP). EDS elemental analysis is widely used as a quantitative analysis method, but is not accurate with elements with low atomic mass (often those below Na). Methods such as AAS have simplified some analytical determinations but, because of inter-elemental interferences, accuracy may be questionable unless almost identical enamels are being regularly analysed.[140]

X-ray fluorescence (XRF) can provide accurate and relatively inexpensive analysis of vitreous enamels.[140] However, analysing samples of widely differing

compositions is difficult. A standard must be prepared from the most recent analysis and the comparisons adjusted for any errors detected.

XPS has been used since the early 1908s and can detect all elements. It is surface sensitive and individual phases can be isolated if the peaks are deconvoluted. Therefore, each element's oxidation state can be determined. However, only a 40-50 nm (depending on X-ray source and beam angle) depth, can be analysed. Ion gun sputtering can remove surface artefacts and allow depth profiling but this technique takes a long time and is expensive.[140]

Scanning electron microscopy (SEM) with attached energy dispersive X-ray analysers (EDS) is being used more frequently for semi-quantitative elemental characterisation and specimen image analysis. Fick et al[141] gives an example of in-depth analysis of coating defects using SEM with EDS.

Schreiner et al[142] used SEM-EDS, secondary ion mass spectrometry (SIMS) and atomic force microscopy (AFM) to characterise the surface layers that formed on stained glass under natural environmental conditions and developed new analytical strategies and methods to obtain information on surface processes. SEM-EDS and SIMS were used to analyse corrosion products and the surface layers and tapping mode atomic force microscopy (TM-AFM) was used to study the initial corrosion stages. SIMS has the advantage over EDS for surface analysis in that its high power can detect most elements. Depth profiling with high spatial resolution is also possible. However, the possibility of a strong matrix effect must be considered when interpreting depth profiles quantitatively. High beam energy can disrupt the matrix significantly during sputtering and obscure details on the depth profile. AFM, introduced in the 1980s, allows surface topographies from real space down to the atomic scale on both electrically conductive and non-conductive samples.

1.14.8 New Applications for Porcelain Enamels

Currently, the important enamelling products are household equipment, sanitary ware, hot water tanks, hollowware and architectural panels.[129] The following are some recent porcelain enamel application developments.

Hot Water Cylinders

Because they are very resistant to corrosion and less expensive, vitreous enamel cylinders are effective alternatives to copper for hot-water cylinders. The direct-on enamels and powder enamels now used make the process cost effective. Currently, about 80% of the USA and EU market is enamelled hot-water cylinders.[129]

Solar panels

Solar collectors are essentially high temperature chambers so durability is important.[143,144] Vitreous enamels, in particular special direct-on enamels, have been used to produce solar panels with greater corrosion and UV resistance than other materials. The enamels have emissivities of up to 20% and are often able to absorb more than 90% of the heat energy.[129] These panels have good stability and longevity and are normally in compression during their working life, which helps resist the repeated day/night thermal cycling of temperature encountered on a flat plate collector, especially under no-load conditions. Systems with black enamel coatings and spectral selective tin oxide coatings are effective if atmospheric conditions are poor.

Heat-Reflecting Porcelain Enamel

Heat-reflecting porcelain enamels have been developed to increase energy efficiency and/or decrease cooking times in ovens.[145] These enamels have higher infrared reflectivity so they emit more infrared radiation, which increases the oven air temperature-heating rate.

Architectural Applications

Porcelain enamels have been increasingly used in architectural cladding or panels, especially in tunnels, subway systems and railway stations. The vitreous enamels

have excellent chemical and scratch resistance and important anti-fouling properties, including attack by graffiti vandals. The enamelled steel also has good heat resistance and flame retardant properties.[146]

Other Applications

Enamels have been developed for the electronic market for micro-circuitry and electronic components including baseboards and for printing the actual circuits.[121] Heat exchanger panels of air and gas preheaters in electricity generating plants can also be enamelled.

1.14.9 Developments in Enamelling Substrates

Steel

Decarburised steel with low carbon allows direct-on coats without the need for a cover-coat to cover out-gassing defects. Better quality drawing steel can be made from vacuum decarburised steel.

Aluminium-killed steel was initially not suitable for enamelling because it pickled non-uniformly and fishscale defects occurred when the steel was enamelled. The manufacturing techniques and chemical compositions have been modified to improve enamelling characteristics of aluminium-killed steels. These enamelling iron replacements have better formability than enamelling iron but are less resistant to warping.[147]

Interstitial-free high quality porcelain enamelling steel has been developed using vacuum degassing, continuous casting and conventional batch annealing. This steel replaces the traditional steels produced by ingot casting and open coil annealing. Common enamelling defects such as fishscaling and warping are reduced.[148]

Aluminium

Enamelling aluminium has the advantage that the whole system is very corrosion resistant, even if the aluminium substrate is exposed because the aluminium surface can naturally oxidise and form a passive barrier film. However,

aluminium and aluminium alloys have low softening and melting points (~650°C) compared with standard enamelling steel, so new frits with low maturing temperature properties need to be developed. Electrostatic powder enamels, which are baked on at 200-250°C, are ideal. Frits for wet spraying contained lead to lower the maturing temperature. Components including lithium, barium, antimony, vanadium and bismuth can be used to produce lead-free enamels with low maturing temperatures.[149]

Aluminised Steel

Enamelling on aluminised steel is more environmentally friendly than enamelling on aluminium.[150] Degreasing is the only pre-treatment needed and a ground coat is not needed so direct-on coats can be used. Furthermore, firing temperatures are lower (550-580°C) than for conventional steels (800°C). Aluminised steels tend to warp less and only one side of the aluminium sheet needs to be enamelled as the thin layer of alumina coated onto the steel naturally passivates, which protects against corrosion.

1.14.10 Environmental Aspects

Many countries have introduced more stringent regulations for emissions and disposal of waste. Although pickle/nickel processes are still used in the USA, especially for direct-on coatings,[151] meeting Environmental Protection Agency (EPA) regulations have reduced this sector[152] and two coat/one fire and non-pickle systems are more common. Pickle-free enamels use frits that react chemically and mechanically to form a tight bond directly with the substrate. The clean-only enamelling process has removed many of the problems associated with pre-treatment waste. However, emissions can also originate from pre-treatment, milling operations, spraying and the enamelling furnace. Producing frits uses a lot of energy and chemicals, which can produce potentially environmentally damaging waste. The amount of waste and energy used by new enamelling processes such as two coat/one fire, powder coating and the electropheretic enamelling processes[129,150] produce less waste, use less energy, and produce higher quality products than conventional processes.

Various environmentally "unfriendly" components are still used in enamelling at present. These include fluorine and cadmium pigments. Fluorine is used as a flux and refining agent to give a better surface finish and acid resistance. During the firing process, a lot of the fluorine is volatilised and expensive scrubbing systems are needed. However, the scrubbers still give solid wastes that need to be disposed. Therefore, alternatives without fluorine are needed. Cadmium pigments are used extensively in the enamelling industry for red colouring. No alternatives have been found. Copper compounds, used in the ceramic industry, are not suitable because the copper dissolves in the enamel too slowly for colour to develop in the short firing period[13]. Therefore, a sophisticated effluent treatment programme is needed if they continue to be used.[151] Some companies have installed completely self-contained units for milling, spraying and recovery cadmium-containing finishes. However, products containing toxic cadmium cannot be used for applications in direct contact humans, for example, cooking vessels.

1.15 Scope of Research

Porcelain enamel coatings on steel are competitive with materials such as plastics and organic coatings. To continue to be competitive, the technology must continue to advance. New Zealand industry are researching and developing enamelling technology. This thesis was a joint project with an enamelling company (Ceratec Ltd, New Zealand).

One objective of this thesis was to examine structural and compositional characteristics of porcelain enamel coatings and their many compositional components used in enamel fabrication. Data on enamel characteristics and the effect of compositional changes on these characteristics were obtained from conventional techniques used in the enamel industry such as energy dispersive X-ray analysis (EDS), Inductively coupled plasma spectroscopy (ICP) and X-ray diffraction (XRD) and non-conventional techniques such as Raman and infrared spectroscopy. Past Raman and infrared spectroscopic studies of alkali and alkaline earth silicate glasses have provided useful structural and compositional information. These same techniques can potentially yield a similar type of

information for the more complex porcelain enamel coating systems within the limitations of possible constraints regarding the vibrational interpretations.

The research concentrated on single coat systems rather than the conventional two-coat system (ground coat and cover coat) as single coat technology is now a viable option because decarburised steel, which reduces defects caused by outgasing, is readily available. (The advantages of single coats are discussed in section 1.5.5.).

Another objective of this thesis was to investigate the chemical resistance of some single coat porcelain enamels. The data from this research could help the enamelling industry improve their coating technology. The corrosion of the enamel coatings was examined in terms of being solid matter (destruction of the glass network), but also being heterogeneous in nature, that is containing bubbles, which may affect the corrosion properties.

The methods for fabricating porcelain enamel coated onto steel samples, preparing the samples for testing, and experimental methods used for examining and classifying the samples are given in Chapter 2.

Chapter 3 gives initial characterisation of enamels used in this research, including a discussion on the enamel batch compositions. The chapter also describes the milling and firing procedures performed, and many of the resulting properties including adherence, bubble structure and particle size distribution.

Results from characterising the commercial porcelain enamel ground coatings and their compositional components using energy dispersive X-ray analysis (EDX), X-ray diffraction (XRD), Raman spectroscopy and infrared spectroscopy are presented in Chapter 4.

The resistance to acid and alkali attack of both commercial coatings and trial coatings are detailed in Chapter 5. Different mechanisms for explaining and predicting corrosion performance are discussed. The effect of bubble content on the corrosion of enamels is also investigated. Trial coatings were obtained by

changing the mill additions of one commercial coating formulation regularly used by Ceratec Ltd. The corrosion resistance was determined using AS 2219.1 (boiling citric acid test) and AS 2219.1.4 (hot sodium hydroxide test).

Chapter 6 reports the characterisation of phases present in a single-coat enamel on steel systems and the pinhole defect phenomenon using Raman microscopy, X-ray diffraction (XRD) and scanning electron microscopy coupled with energy dispersive X-ray analysis (EDX).

1.16 References

1. Buerhop, C., Condrate Sr., R.A., Moertel, H. and Hapanowiz, R.P, *Appl. Spectroc.* 1992. **46**: p. 1545.
2. Ritchie, D., Schaffer, H.A. and White, D., *The presence of an iron oxide layer at the enamel/steel interface in one-coat porcelain enamelling.* J. Mat. Sci., 1983. **18**: p. 599-604.
3. Mackeret, J.R., Conner, T.G., Ringle, R.D., Parry, E.E. & Fairhurst, C.W., *X-ray Diffraction Characterization of the Enamel-Steel Interface.* J. Am. Ceram. Soc., 1992. **75**(11): p. 3087-90.
4. Murray, C.A. and Greytak, T.J., *Intrinsic surface phonons in amorphous silica.* Phys. Rev. B, 1979. **20**: p. 3368.
5. Zachariasen, W.H., J. Am. Chem. Soc., 1932. **54**: p. 3841.
6. Duffy, J.A., *Bonding, Energy Levels and Bands in Inorganic Solids*. 1990, Harlow Essex, England: Longman Scientific and Technical. 249.
7. Vargin, V., *Technology of Enamels*. 1968: Maclaren and Sons Ltd.
8. Chiang, Y., Birnie, D. and Kingery, W.D., *Physical Ceramics - Principles for Ceramic Science and Engineering*. 1997: John Wiley and Sons, Inc.
9. Sullivan, J.D., *Glass-Metal Reactions and Physical Properties of Enamels.* Proc. Porc. Enam. Inst., 1980: p. 143-159.
10. Eppler, R.A. and Gill., D., *Glazes & Enamels*, in *Engineered Materials Handbook, Vol 4. Ceramics and Glasses*. 1991, ASM International, The Materials Information Society. USA.
11. Eppler, R.A., *Ceramic Coatings*, in *Engineered Materials Handbook-Ceramics and Glasses*. 1991, ASM International.
12. Donald, I.W., *Preparation, properties and chemistry of glass- and glass-ceramic-to-metal seals and coatings.* Journal of Materials Science, 1993. **28**: p. 2841-2886.
13. Industry, C., *Materials Handbook*, in *Ceramic Industry*. 1992. p. 1-109.
14. ASM Committee on Porcelain Enameling, ed. *Porcelain Enameling*. ASM Handbook (Metals Handbook), Surface Engineering, ed. S.R. Lampman. Vol. 5. 1996, ASM International.
15. Andrews, A.I., *Porcelain Enamels. The Preparation , Application, and Properties of Enamels*. 1961: The Garrard Press, Publishers.
16. Escol, *The Vitreous Enameller's Diary*. 1994: Escol.
17. Bauer, W.C. and Bailey, J.E., *Raw Materials/Batching*, in *Engineered Materials Handbook-Ceramics and Glasses*. 1991, ASM International.

18. Prinzbach, G.R., *The Outlook for Raw Materials Used for Porcelain Enamels.* Ceramic Engineering and Science Proceedings, 1995. **16**(6): p. 90-96.
19. *Enamelling Manual.* , Unknown, Australia.
20. Currie, T.E., *The Effect of Mill Additions on the Rheology of Enamel Slips.* PEI Tech. For. Proc., 1970. **32**: p. 132-139.
21. Kyri, H., *Handbook for bayer enamels.* 1975: Bayer AG.
22. Eppler, R.A., *Ceramic Colorants.* 1986. **A5**.
23. Burgyan, A. and Eppler, R.A., *Classification of Mixed-Metal-Oxide Inorganic Pigments.* American Ceramic Society Bulletin, 1983. **62**(9).
24. Eppler, R.A., *Selecting Ceramic Pigments.* Ceramic Bulletin, 1987. **66**(11): p. 1600-1604.
25. Brosseder, H.W., *Colour in Vitreous Enamel.* The Vitreous Enameller, 1986. **37**(3): p. 49-66.
26. Reporter, E., *Direct -on Enamelling.* Bayer-emails: Bayer, Germany.
27. Boyer, E.H. and Gill, T.L., *Carbon and Alloy Steels*, in *Metals Handbook.* 1985, American Society for Metals: Metals Park, Ohio.
28. Joseph, W.A., *Matte Surfaces-Uses, Problems, Solutions.* PEI Tech. For. Proc., 1983. **45**: p. 176-184.
29. Layne, C.M., *Physical Properties of Grate Enamel Systems.* Ceramic Engineering and Science Proceedings, 1995. **16**(6): p. 103-109.
30. Horton, M., *The Development of Alkali-Resistant Powder Porcelain Enamel Systems.* Ceramic Engineering and Science Proceedings, 1993. **14**(5-6): p. 37-44.
31. Bryant, E.E., *Porcelain Enameling Operations.* 1964, Cleveland, Ohio: Enamelist Publishing Company.
32. Fuller, W.O., *Milling Practices and Parameters.* Ceram. Eng. Sci. Proc., 1991. **12**(5-6): p. 749-754.
33. Phelps, G.W and Silwanowicz A., *The Role of NonClay Particle Size in the Whiteware Slip Casting.* J. Canad. Ceram. Soc, 1970. **39**: p. 17-19.
34. Phelps, G.W., *Particle Size Distribution and Slip Rheology.* PEI Tech. For. Proc., 1976. **38**: p. 1-15.
35. Paulus, H., Muller, S. and Oel, H.J., *Influence of the Grain Size of Glass Frits on the Characteristics of Glass Enamels.* Glastech. Ber., 1991. **64**(2): p. 39-42.
36. Fu, D., *Processing of Porcelain Enamel Glass Powders for Electrostatic Spraying.* Powder Technology, 1995. **85**: p. 65-69.
37. Smart, W.L., *The Fundamentals of Electrostatic Finishing.* PEI Forum, ??
38. Voges, D.L., *Porcelain Enamel: Properties and Applications.* Ceram. Eng. Sci. Proc., 1996. **17**(5): p. 22-25.
39. Report, S., *Porcelain Enameling.. the One-Coat Process.* Metal Progress, 1966. **89**: p. 97-101.
40. Pask, J.A., *Chemical Reactions and Adherence at Glass-Metal Interfaces.* Proceedings of the Porcelain Enamel Inst. Tech Forum, 1971: p. 1-16.
41. Bayer, ed. *1.2 Enamel Types.* Technical Information, Bayer.
42. Von Podesta, W. and Runte., W., *Mitt. Ver Deutsch Email Fach.* 35, 1987: p. 129.
43. Someswar, D., *Acid resistant one coat for power generation plants.* Bull. Mater. Sci., 1998. **21**(5): p. 421-425.
44. Mayer, M.M., *Experiences with Luminous-Wall Furnaces.* PEI Tech. For. Proc., 1982. **44**: p. 434-438.
45. Geary, J., *Luminous Wall Furnaces in Australia.* PEI Tech. Form. Proc., 1979. **41**: p. 132-134.
46. Wright, J.F. and Layne, C.H., *Reaction of Various Enamel Sytems to Direct Firing.* Porc. Enam. Ins. Tech. For. Proc., 1982. **44**: p. 447-458.
47. Murray, H.H., *Rheology.* PEI Tech. For. Proc., 1973. **35**: p. 97-102.
48. Clark, K., *Practice pottery and ceramics.* 1968: Studio Vista Ltd, London.

49. Rado, P., *An Introduction to the Technology of Pottery*. 2nd ed. 1988, Oxford: Pergamon Press.
50. Nakazato, Y., Kuguminato, H., Soeda, N., and Takahashi, I., *A study of Bubble Structure in Porcelain Enamel.* Transactions ISIJ, 1980. **20**: p. 1-8.
51. Smalley, H.F., *The Effect of Bubble Structure on Chemical and Physical Properties of Ground Coat Porcelain Enamels.* PEI Tech. For. Proc., 1964. **26**: p. 172-176.
52. Biller, L.N., *Investigation of Fired Bubble Structure-Wet and Dry.* Ceramic Engineering and Science Proceedings, 1990. **11**(5-6): p. 396-405.
53. Collins, M.A., *Atlas of Enamel Defects*. 1995: The Institute of Vitreous Enamellers.
54. Dowdell, G., *Vitreous Enamel Defects - Causes and Remedies.* Enamelling Seminar - New Zealand, 1988.
55. Samuels, L.E., *Optical Microscopy of Carbon Steels*. 198?: American Society for Metals (ASM).
56. Blickwede, D.J., *Enameling and the Microconstituents in Steel.* Proc. Porcelain Enamel Inst. Tech. Forum, 1972. **34**: p. 5-29.
57. Rarey, C.R.R., *Enameling Steels-Focus on Hydrogen.* Ceram. Eng. Sci. Proc., 1993. **14**(5-6): p. 98-106.
58. Maskall, K.A., Richens., M.J. and White, D., *The Importance of Hydrogen in the Application of Vitreous Enamel to Ferrous Metals.* Hydrogen in Steel, 1982: p. 113-117.
59. Moore, D.G., Mason, M.A. and Harrison, W.N.,, *J. Am. Ceram. Soc.* 1952. **35**(33).
60. Taylor, J.R.and Bull, A.C., *Ceramics Glaze Technology*. 1986, Oxford: Pergamon Press.
61. Cleland, J.H.and Morgan, P.G., *Failure of Vitreous Enamelled Coatings.* Engineering Failure Analysis, 1996. **3**(3): p. 149-155.
62. Martinek, C.A., *Porcelain Enamel Properties and Tests.* PEI Tech. For. Proc., 1964. **26**: p. 189-195.
63. Wright, J.F., Bereron, C.G. and Oliver, J.C., ed. *Porcelain Enamel.* Engineered Materials Handbook, Vol 4. *Ceramics and Glasses*. 1991, ASM International, The Materials Information Society. USA.
64. Kawasaki, *Kawasaki KTSMT, Steel Sheet for Porcelain Enamelling.* 1987: Kawasaki Steel Corporation.
65. Sollac, *Hot Rolled Steel - specifications.* .
66. Toland, D.A. and Ludwigson, D.C., *Characterization of the Properties of Enameling Steels to Enamel Firing Temperatures.* PEI Tech. Forum., 1977. **39**.
67. Coduti, P.L. and Earl, D.G., *Cleanliness Measurement Techniques on Sheet Steel Surfaces.* PEI Tech. Forum Proc., 1979. **41**: p. 167-172.
68. Scott, T.M., *Metal Preparation for Porcelain Enameling Appliance Components: Clean-Only Systems.* Ceram. Eng. Sci. Proc., 1998. **19**(5).
69. Toton, L.G., *Production Experiences with N0-Nickel/No-Pickel System.* Ceram. Eng. Sci. Proc., 1990. **11**(5-6): p. 390-392.
70. Hyde, R.L., *Effect of Neutralizers on Clean-Only Systems.* Ceram. Eng. Sci. Proc., 1992. **13**(5-6).
71. Bernett, T.W.and Krebs, H.W., *Theories of Alkaline Cleaners.* Ceram. Eng. Sci. Proc., 1990. **11**(5-6).
72. Shieu, F.S., Lin, K.C. and Wong, J.C., *Microstructure and adherence of porcelain enamel to low carbon steel.* Ceramics International, 1999. **25**: p. 27-34.
73. Pask, K.A. and Fulrath, R.M., *Fundamenatals of Glass-to-Metal Bonding: Nature of Wetting and Adherence.* J. Am. Ceram. Soc., 1962. **45**(12).
74. Ritchie, D. and White, D., *The mechanism of Direct-on Enamelling of Steel.* The Vitreous Enameller, 1972. **23**: p. 1-12.

75. King, B.W., Tripp, H.P. and Duckworth, W.H., *Nature of Adherence of Porcelain Enamels to Metals.* J. Am. Ceram. Soc., 1959. **42**(11): p. 504-525.
76. Mohyla, M., Podjuklova, J. and Bastl, Z., *A Contribution to the Study of the Phase Boundry Between Metal and Vitreous Enamel.* Ceramics-Silikaty, 1990. **c. 4**: p. 299-306.
77. Dietzel, A.H., *Emaillierung.* 1981: p. 119-121.
78. Lynch, A.M., *Role of Cobalt Oxide in Porcelain Enamel.* Ceram. Eng. Sci. Proc., 1993. **14**(5-6): p. 52-57.
79. Paparazzo, E., Fierro, G., Ingo, G.M. and Sturlese, S., *Microchemistry and Mechanisms of Adherence in Steel/Enamel Interfaces.* J. Am. Ceram. Soc., 1988. **71**(12): p. C-494-C-497.
80. Davis, J.R., ed. *Corrosion, Porcelain Enamels.* ASM Handbook (Metals Handbook), ed. J.R. Davis. Vol. 13. 1996, ASM, International, The Materials Information Society.
81. Sweo, B.J., *Correlation of Weather Resistance of Porcelain Enamels With Chemical-Test Data.* J. Am. Ceram. Soc., 1949. **32**(11): p. 356-59.
82. Baker, A.K., *Weather Resistance of Porcelain Enamels-15-Year Inspection of the 1956 Exposure Test.* NBS Building Science Series 50, 1974. **50**: p. 1-12.
83. Baker, M.A., *1939 Exposure Test of Porcelain Enamels on Steel. 30-Year Inspection.* Building Science Series 38, 1971. **38**: p. 1-9.
84. Marlor, A.J., Bergeron, C.G. and Gardner, J., *Mechanism of Corrosion of Vitreous Coatings.* PEI Tech. For. Proc., 1973. **34**: p. 139-143.
85. Holland, L., *Surface Chemistry and Corrosion of Glasses.* The Properties of Glass Surfaces, 1966: p. 122-192.
86. Douglas, R.W. and El-Shamy, T.M.M., *Reactions of Glasses with Aqueous Solutions.* J. Am. Ceram. Soc., 1967. **50**(1): p. 1-8.
87. Eppler, R.A., *Resistance of Porcelain Enamels to Attack by Aqueous Media: II, Equations To Predict Enamel Durability.* Ceramic Bulletin, 1977. **56**(12): p. 1068-1070.
88. Australia, S.A., *AS 2219.1.1, Determination of Resistance of Vitreous Enamel Coatings to Hot Sodium Hydroxide.* Methods of Test for Vitreous Enamel Coatings. 1978.
89. Smith, H., J., *The Effect of Refractory Mill Additions on the Corrosion and Abrasion Resistance of Porcelain Enamels.* PEI Tech. For. Proc., 1963. **25**: p. 37-48.
90. Lightner, L.F. and Nobles, E., *Processing and Testing Variables Affecting Alkali Resistance Determinations.* PEI Tech. Forum Proc., 1964. **26**: p. 202-207.
91. Joseph, W.A., *Structure of Enamel Coatings.* The Vitreous Enameller, 1988. **39**(1).
92. Instit. Vit.Enamellers, ed. *Visual Classification of Adhesion of Vitreous Enamel to Steel.* , Institute of Vitreous Enamellers.
93. McMillan, P., *Structural Studies of Silicate Glasses and Melts - Applications and Limitations of Raman Spectroscopy.* American Minreralogist, 1984. **69**: p. 622-644.
94. Griffith, W.P., *Advances in the Raman and Infrared Spectroscopy of Minerals,.* 1987, John Wiley and Sons Ltd.
95. Cullity, B.D., *Elements of X-ray Diffraction.* 1978: Addison-Wesley Publishing Company, Inc.
96. Scott, J.F. and Porto, S.P.S., Phys. Rev., 1967. **161**: p. 903.
97. McDevitt, Spectrochim. Acta, 1964. **20**: p. 799-808.
98. Beattie, I.R. and Gilson, T.R., J. Chem. Soc. (A), 1970: p. 980.
99. Preudhomme, J. and Tarte, P., Spectrochim. Acta, 1971. **27A**: p. 1817-35.
100. Lutz, H.D., Muller, B. and Steiner, H.J., J. Solid State Chem., 1991. **90**: p. 54-60.
101. Basak, D. and Ghose, J., Spectrochim. Acta, 1994. **50A**: p. 713-18.

102. Frost, R.L., Fredeicks, P.M. and Shurvell, H.F., Can. J. Appl. Spectrosc., 1996. **41**: p. 10.
103. Johnston, C.T., Agnew, S.F. and Bish, B.L., Clays and Clay Minerals, 1990. **38**: p. 575-583.
104. Frost, R.L. and Rintoul, L., Appl. Clay Sci., 1996. **11**: p. 171.
105. Chgristidis, G.E., Scott, P.W. and Marcopoulos, T., Clays and Clay Minerals, 1995. **43**: p. 63-77.
106. Vodop'yanov, V.P., Migorodskii, A.P. and Lazarev, A.N., Inorg. Mater., 1984. **19**: p. 1667.
107. Nyquist, R.A., Infrared of Organic Compounds, 1997. **4**.
108. Frogner, P., Broman, C. and Lindblom, S., Chemical Geology, 1988. **151**: p. 161-168.
109. Velde, B. and Boyer, H., J. Geophys. Res., 1985. **90**: p. 3675.
110. Sourisseau, C. and Mercier, R., Spectrochim. Acta, 1978. **34A**: p. 173-8.
111. Porto, S.P.S and Krishnan., R.S., J. Chem. Phys., 1967. **47**: p. 1009-1012.
112. Nyquist, R.A. and Kagel, R.O., *Infrared Spectra of Inorganic Compounds 3800-45 cm^{-1}*. 1971: Academic Press, New York.
113. Erdemir, A., Halter, M. and Fenske, G.R, Wear, 1997. **205**: p. 236-9.
114. Kim, Y.Y., Lim, J.T. and Park, S.H., Phys. Chem. Solids, 1999. **60**: p. 969-73.
115. Devi, S.A., Philip, D. and Aruldhas, G., J. Solid State Chem., 1994. **113**: p. 157.
116. Krishnamuti, D., Proc. Indian Acad. Sci., 1956. **43A**: p. 210.
117. Pilati, T., Demartin, F. and Gramaccioli, C.M., Acta Cryst., 1998. **54B**: p. 515-523.
118. Degan, I.A.and Newman, G.A., Spectro. Acta, 1993. **49A**(5/6): p. 863.
119. Craver, C.D., ed. *Desk Book of Infrared Spectra.* . 1986, The Coblentz Society. 484.
120. Basso, S., Hoens, M., and Vuyk, J., *Considerations on Modern Pretreatment Techniques and Coating Procedures for Steel.* The Vitreous Enameller, 1977. **28**(4): p. 64-75.
121. Phipps, K.J., *The Changing Face of Vitreous Enamel.* The Vitreous Enameller, 1985. **36**(1).
122. Maskall, K.A.and White, D., *Vitreous Enamelling - A Guide to Modern Enamelling Practice.* 1986.
123. Wratil, J., *High Temperature Enamels With Outstanding Qualities.* The Vitreous Enameller, 1981. **32**(2): p. 42-48.
124. Krstic, V.V., Nicholson, P.S. and Hoagland, R.G., *Toughening of glass by metallic particles.* J. Am. Ceram. Soc., 1981. **64**(9): p. 499-504.
125. Hennicke, H.W., and Padel, A., *Enamelling with Crystalline Inclusions for High Temperature Applications.* The Vitreous Enameller, 1991. **42**(2): p. 27-39.
126. Stevenson, R., *British Patent 53567/72*, in *British Gas Corporation*. 1974.
127. Feltser, K., and Valo, M., *Experiments with Bright Coloured Direct-On Enamels.* The Vitreous Enameller, 1976. **27**(2).
128. Clarke, J.A., *Enamel and its Development.* The Vitreous Enameller, 1969. **20**(2): p. 65-68.
129. Verboom, D.W.A., *Trends and Developments in the Enamelling Industry.* The Vitreous Enameller, 1995. **46**(2): p. 33-49.
130. Viquesnel, A., *The Influence of Porosity on the Efficiency of Self-Cleaning Systems.* The Vitreous Enameller, 1975. **26**(4): p. 70-75.
131. Denny, P., and Robertson, R., *Devlopments in Self-Clean Enamels.* The Vitreous Enameller, 1973. **24**(1): p. 59-65.
132. Piva, R., *Self-Cleaning Enamels.* The Vitreous Enameller, 1973. **24**(4): p. 110-112.
133. Faust, W.D., *Current Status of Enamelling in the USA.* The Vitreous Enameller, 1993. **44**(2): p. 16-25.

134. Guskov, S., *Electrostatic Charging and Powder Coating With Porcelain Enamels.* PEI Tech. Form. Proc., 1997. **59**: p. 1-15.
135. Hoffmann, H. and Zybell, P, *The Effect of New Base Materials, Technologies and systems on Enamelling.* The Vitreous Enameller, 1977. **28**(2): p. 76-89.
136. Hoffmann, H., *The EP Process-Electro-Dip Enamelling.* The Vitreous Enameller, 1979. **30**(4): p. 79-91.
137. Hughes, E.W., *A Report on the Status of Electrodeposition for Porcelain Enamels.* The Vitreous Enameller, 1969. **20**(2).
138. Lawrence, J. and Li. L., *A Laser-Based Technique for the Coating of Mild Steel with a Vitreous Enamel.* Surface and Coatings Technology, 2001. **140**: p. 238-243.
139. Lawrence, J. and Li., L., *Effect of Laser Indused Rapid Solidification Structures on Adhesion and Bonding Characteristics of alumina/silica based oxide to vitreous enamel.* Materials Science and Technology, 2000. **16**: p. 220-226.
140. Bennett, H., *Chemical Analysis of Vitreous Enamels by Modern Methods.* The Vitreous Enameller, 1980. **31**(2): p. 37-41.
141. Fick, D.K., Holger, F.E., and Layne, C.H., *Scanning Electron Microscopy as a Tool in Porcelain Enamel Defect Analysis.* PEI Tech. For. Proc., 1999. **61.** p 155-166.
142. Schreiner, M., Woisetschlager, G., Schmitz, I. and Wadsak, M., *Characterisation of Surface Layers Formed Under Natural Environmental Conditions on Medieval Stained Glass and Ancient Copper Alloys Using SEM, SIMS and Atomic Force Microscopy.* J. Anal. At. Spectrom., 1998. **14**: p. 395-403.
143. de Jong, J., *Vitreous Enamelling and Glass Research.* The Vitreous Enameller, 1972. **23**(2): p. 20-28.
144. Hoens, M., and Van der Vliet, W., *New Application for Porcelain Enamel Substrates.* The Vitreous Enameller, 1986. **37**(2): p. 34-38.
145. Baldwin, C., *Heat-Reflecting Porcelain Enamel.* PEI Tech. For. Proc., 2000. **62**.
146. Hoffmann, H., *The Future Outlook for Enamel.* The Vitreous Enameller, 1990. **42**(4): p. 82-86.
147. Hingsbergen, J.P. and Hall, B.J., *Evaluation of Steels for Replacement of Enamelling Iron.* The Vitreous Enameller, 1991. **42**(3).
148. Thorpe, M.D., *Development of Interstitial-Free Porcelain Enamelling Steel.* The Vitreous Enameller, 1993. **44**(3): p. 12-37.
149. Viquesnel, A., and Krist, O., *New Application of Aluminium Enamels.* The Vitreous Enameller, 1986. **37**(2): p. 17-26.
150. Cholet, V., Gousselot, P., and Spehner, D., *Development of Aluminized Sheet for Enamelling.* The Vitreous Enameller, 1998. **49**(2): p. 47-61.
151. Whitelock, K.E., *Towards a 'Green' Enamel Insustry.* The Vitreous Enameller 44, 1993. **1**(11-16).
152. Sheppard, L.M., *The Porcelain Enamel Industry: New Developments and Challenges.* Ceramic Industry, 2000: p. 30-35.

Chapter Two
Experimental Methodology

Chapter Two
Materials and Methodology

2.1 Introduction

The methods for fabricating porcelain enamel coated onto steel substrate samples, preparing the samples for testing, and experimental methods used for examining and classifying the samples are given in this chapter.

2.2 Materials Used in Sample Fabrication

2.2.1 Steel

The steel used for the substrate is KTSMT enamel-grade steel with carbon content not greater than 0.005 wt% manufactured by Kawasaki Steel Ltd, Japan. The typical chemical composition is given in Table 2.1 and the Fe-C phase diagram of KTSMT is shown in Figure 2.1.

Table 2.1 Typical Chemical Composition of KTSMT (wt%).[1]

C	Mn	P	S	Al	O	N	Ti	Special elements
0.003	0.260	0.010	0.028	0.040	0.0035	0.0083	0.108	0.007

2.2.2 Enamels

The enamels frits and mill additions were imported from Bayer Ltd (Belgium); Ferro Corp. (Australia) and Escol Ltd (England).

Because of commercial confidentiality, formulations of the five commercial ground-coat enamels (often used as a single functional coat) obtained from the manufacturers were coded gloss brown A (GBA), gloss green A (GGA), matte

black A (MBA), gloss brown B (GGB) and gloss brown C (GBC). The composition information for the commercial enamels is given in section 3.2.1 and for the trial coatings in section 3.3.1.

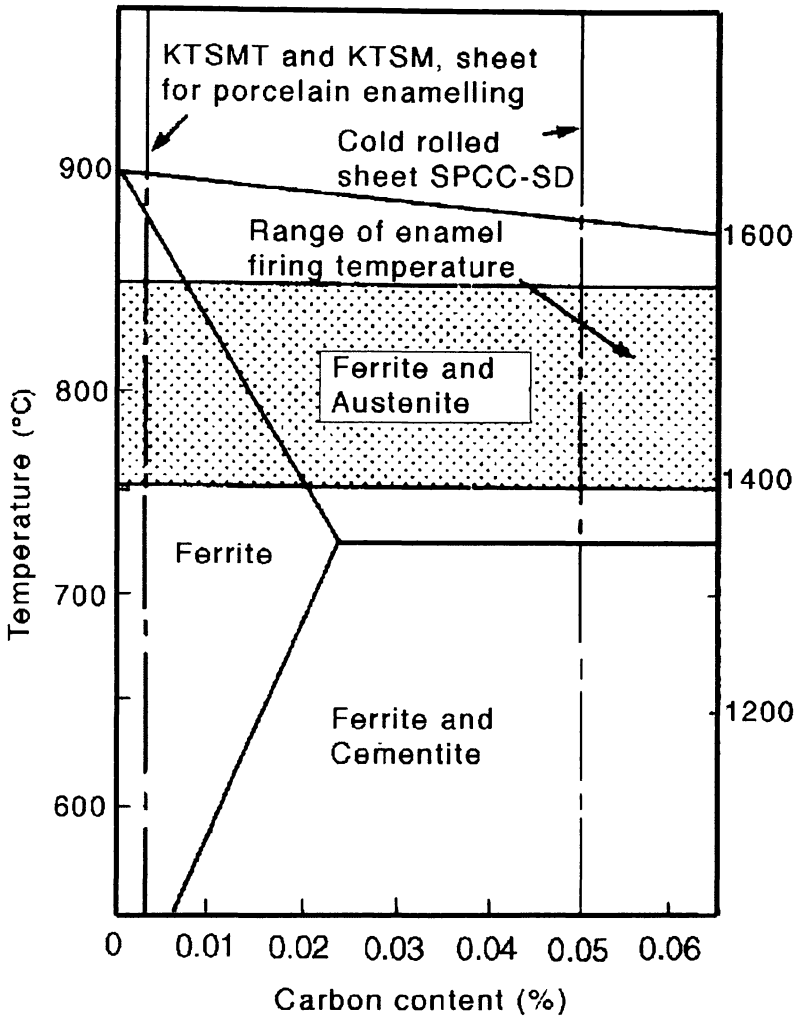

Figure 2.1 Fe-C phase diagram for KTSMT steel (from KTSMT specs[1]).

2.3 Preparing the Enamel Slip

2.3.1 Milling

All of the enamel batches were milled at Ceratec Ltd - Auckland, New Zealand. Wet milling of frits, mill additions and water was performed in ball mills. The commercial ball mill (external view - Figure 2.2; internal view - Figure 2.3) had a 1.05-m long, 1.04-m diameter drum lined with silex (natural silica) blocks. The

commercial enamel milled normally consists of a 200 kg charge of enamel frits and mill additions. Approximately 114 litres of water is added to this before milling. A 60:40 (by volume) mix of 51-mm and 38-mm ceramic balls (made of porcelain) normally occupies 55% of the milling drum. Grinding is performed at a mill speed of approximately 40 r.p.m. for approximately 90 minutes. However, the time can be varied to get the milling fineness specified by the enamel manufacturer (section 2.3.3). The commercial ball mill was used to mill the enamel batch for the GGA enamel coating examined in Chapter 6.

One-litre test batches of slip were milled in a 10-litre porcelain ball mill (Figure 2.4), 0.26 m long and 0.25 m in diameter. Grinding was performed at a mill speed of approximately 80 r.p.m. for approximately 70 minutes (depending on the milling fineness required). The 10-litre porcelain ball mill was used for all the commercial coatings and trial formulation coatings examined in Chapters 3, 4 and 5. The milling parameters for the commercial and trial enamels are given in sections 3.2.2 and 3.3.2 respectively.

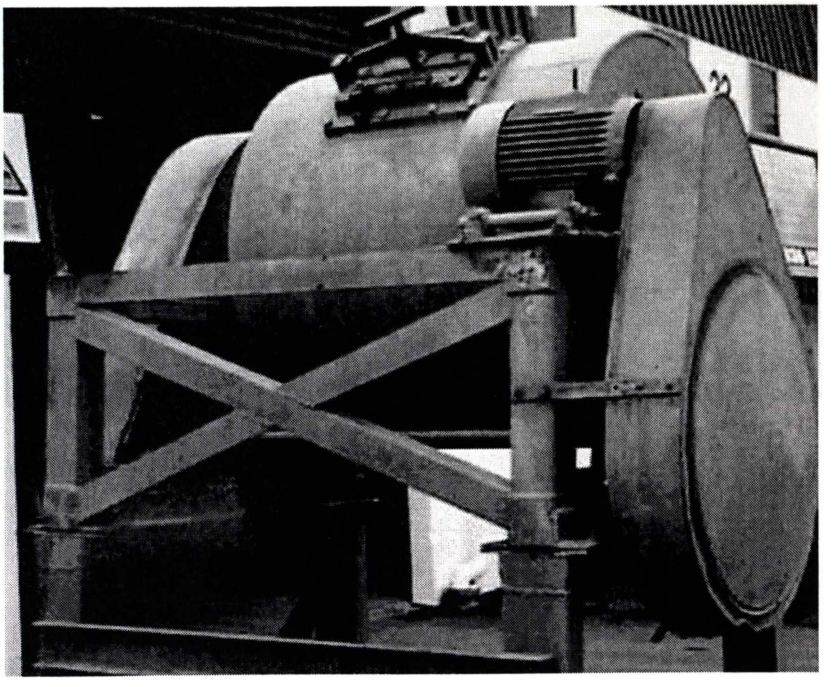

Figure 2.2 External view of commercial mill.

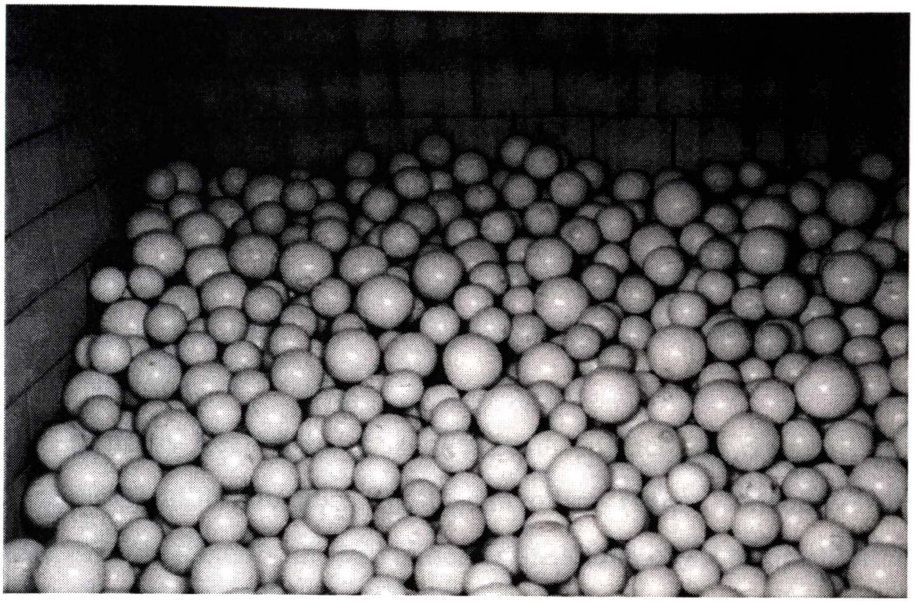

Figure 2.3 Internal view of commercial mill.

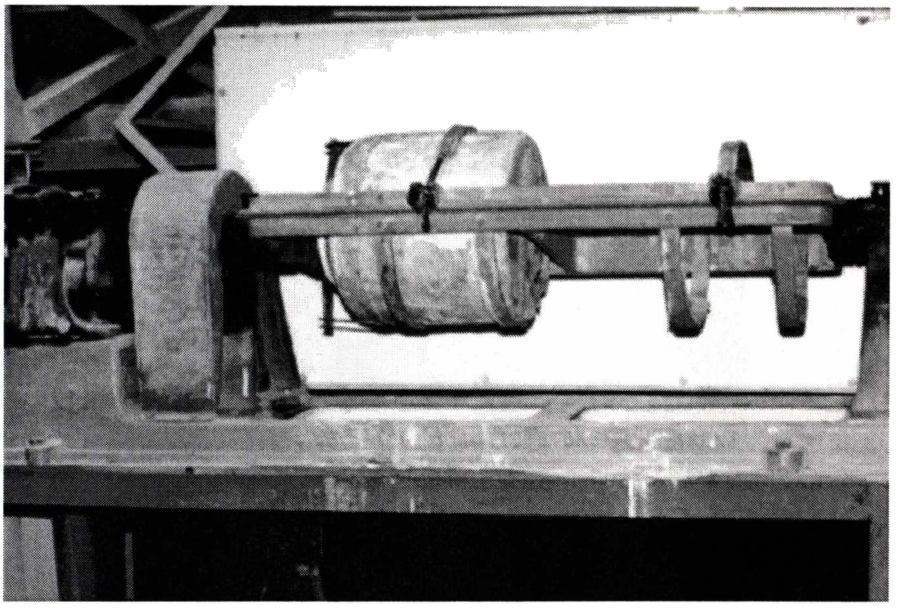

Figure 2.4 External view of trial mill.

2.3.2 Specific Gravity

Specific gravity, as the weight per unit volume of enamel slip, was determined by weighing a 50-ml sample of enamel slip that had passed through a 60-mesh (250 μm) sieve.

2.3.3 Milling Fineness

Milling fineness is the residue from a 50-ml slurry sample retained on a 75-μm (#200 mesh sieve) sieve. Milling fineness can be expressed as grams/50-ml/75-μm sieve, but it is commonly expressed in grams.

2.3.4 Slump Test

A 100-ml stainless steel cylinder is filled with enamel slip (Figure 2.5). The cylinder is raised uniformly, allowing the slip to flow (slump) smoothly over a flat steel plate. The diameter of the slip indicates the slump of the sample.

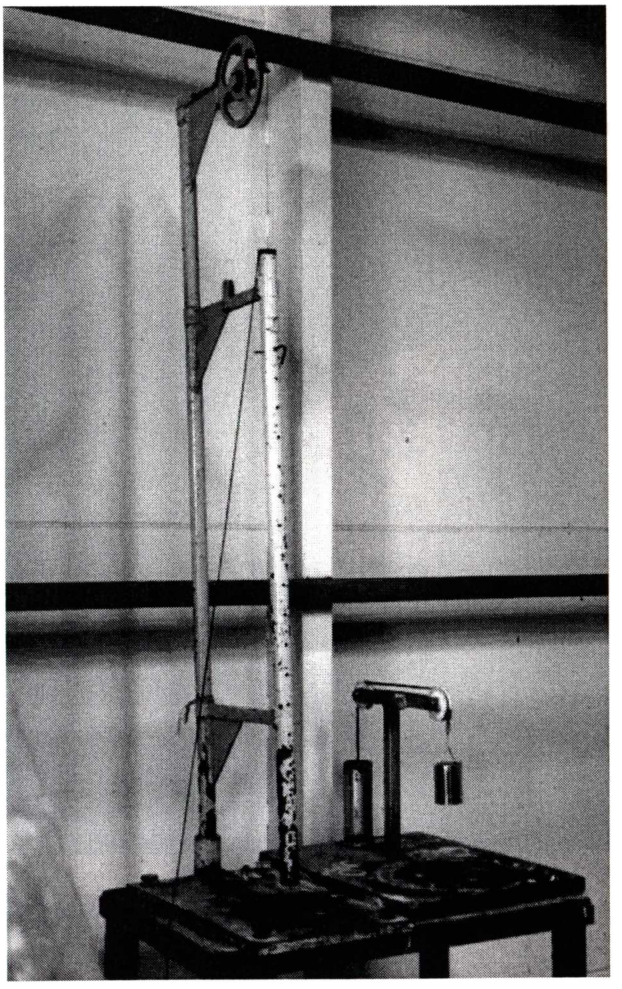

Figure 2.5 Slump tester (right) and impact tester.

2.4 Substrate Preparation (Pre-treatment)

2.4.1 Washing system

The steel was pre-treated before enamelling by the "clean only" or non-pickle process. Samples are conveyed through the washing plant (Figure 2.6) manufactured by Industrial Ovens and Fabrications Ltd, Onehunga, New Zealand. The pre-treatment unit consists of a stainless steel tunnel with a series of tanks containing the cleaning solutions. The unit also has a pump, piping and nozzles for spraying the various solutions onto the steel components as they pass (conveyered) through the system. There are six stages (spray-zones) in the operating cycle (Table 2.2).

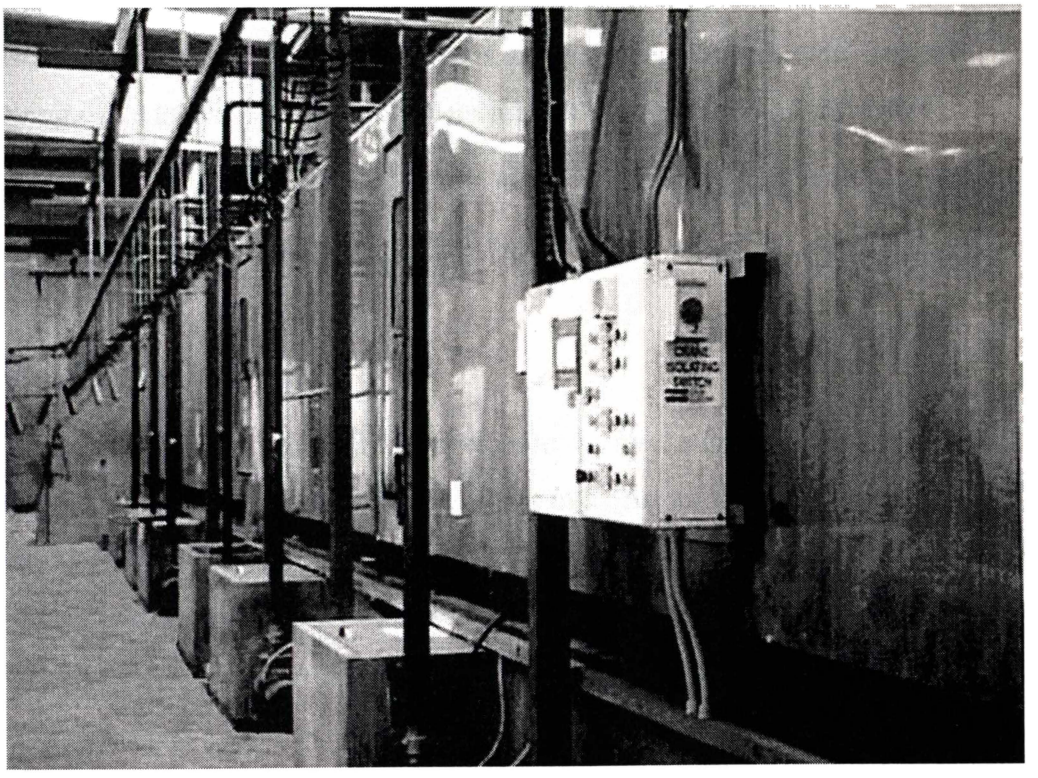

Figure 2.6 Washing plant.

Table 2.2 Washing system, operation cycle.

Stage	Solution	Pressure (kPa)	Cycle time (Sec)	Temp (°C)
1	Alkaline cleaner (caustic soda)	140-120	120	55-60
2	Water rinse	80-120	60	55-60
3	Alkaline cleaner (caustic soda)	140-160	120	55-60
4	Water rinse	80-120	60	55-60
5	Water rinse	80-120	60	Ambient
6	Deionized water rinse	80-120	60	Ambient

2.4.2 Drying

After being cleaned, the steel continued on the conveyer through a drying tunnel, also manufactured by Industrial Ovens and Fabrications Ltd, New Zealand. The drying cycle takes approximately 7 minutes at a temperature of 160-180°C.

2.5 Enamelling Process

2.5.1 Manual spraying

The enamel slip was manually sprayed onto the steel substrate using an AGN-502 Automatic gun (DeVilbiss, an ITW company). An air pressure system feeds the coating material supply. Remotely positioned valves control the air for atomisation and diaphragm operation. The commercial and test-pot spray guns used for enamelling are shown in Figure 2.7.

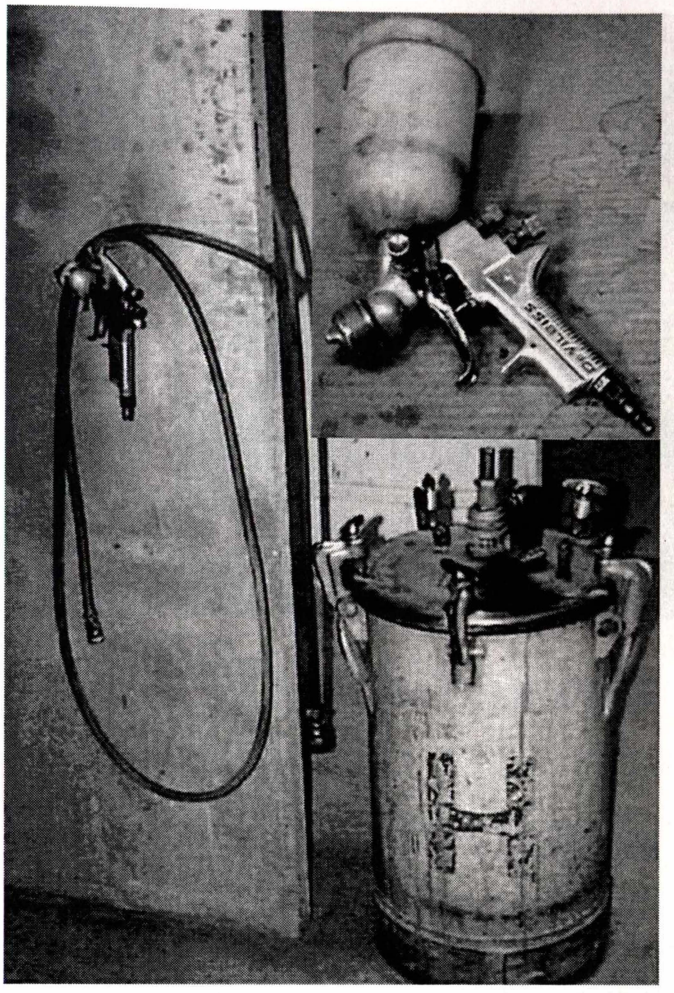

Figure 2.7 Commercial enamel pot and gun and test pot and gun (insert).

2.5.2 Bisqueing

After applying the enamel coating, but before firing, the enamel coating was dried onto the steel substrate by being conveyed through a medium-wave radiant heat drier (Figure 2.8) manufactured by Phoenix Electrical, New Zealand. The heated radiating tubes are powered by electricity. Drying times for the test panels were approximately 5 minutes at approximately 150°C.

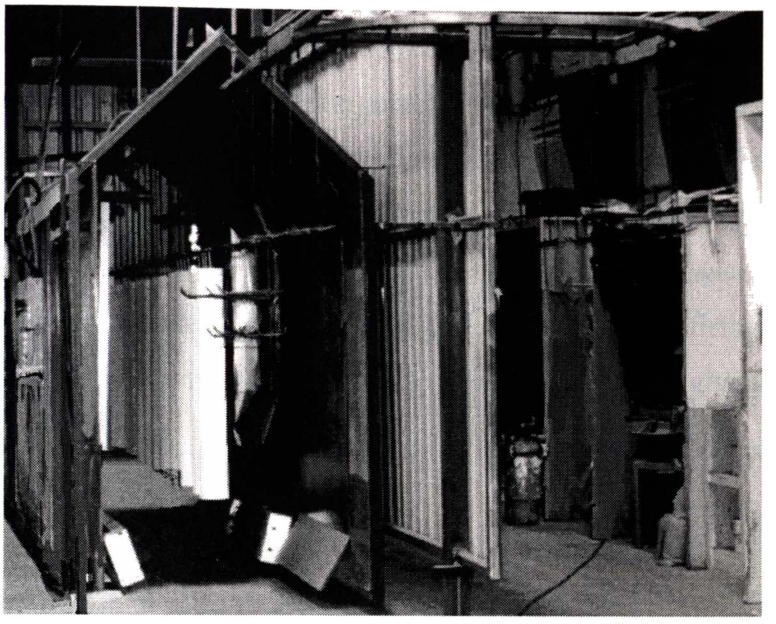

Figure 2.8 Enamel slip drier.

2.5.3 Coating thickness

Coating thickness is measured after bisqueing and firing. Samples were only fired if the bisque thickness was between 100 μm to 180 μm thick (See Coating Thickness, section 1.7.3). Coating thickness was measured using an elcometer (Figure 2.9).

Figure 2.9 Elcometer for the measuring of enamel coating thickness.

2.5.4 Sample Firing

All samples were conveyed at the designated chain speed through a direct radiant heated, luminous walled furnace (specifications are given in Table 2.3). The enamel manufacturers specify an approximate firing time and temperature for commercial coatings. A typical temperature cycle for the furnace used in the trials is given in Figure 2.10. A detailed description of firing times and temperatures for the commercial and trial enamel coatings is given in sections 3.2.2 and 3.3.2.

Table 2.3 Furnace specifications.

Manufacturer	Tempo Holden Furnaces Pty Ltd (Australia)
Type	Direct radiant heated luminous wall
Purpose	Firing porcelain enamel onto enamel grade steel
Heat source	Gas
Maximum temperature	880°C
Process area (m)	L*W*H = 15.4*1.6*1.8

Table 2.4 Effect of dial reading on time in furnace.

Reading on dial	40	50	60	70
Conveyor speed (m/s)	0.028	0.032	0.036	0.038
(seconds/m)	36.0	31.5	28.0	26.5
Time in Firing Zones (min/sec)	2:37	2:17	2:02	1:55
Total time in furnace (min/sec)	9:14	8:05	7:11	6:48

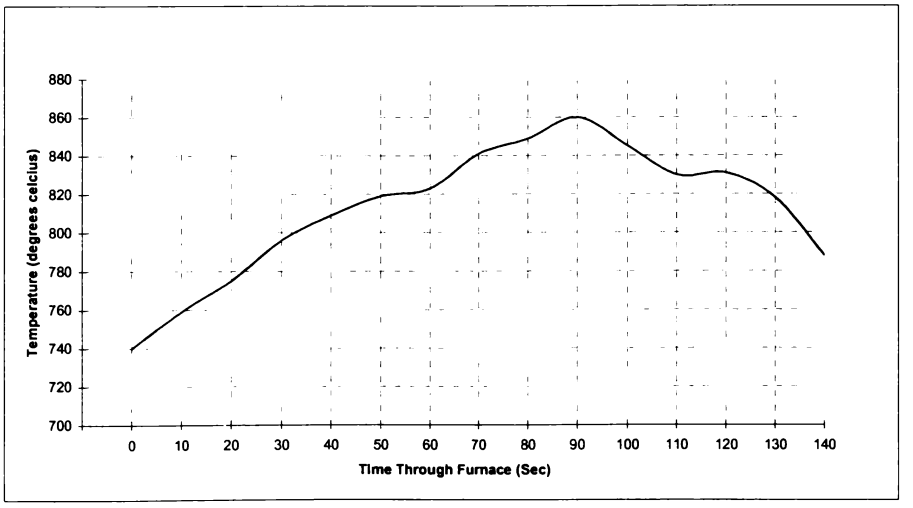

Figure 2.10 Typical temperature cycle for furnace operation.

2.6 Characterisation Techniques

2.6.1 Sample Preparation

Surface and cross-sections of the enamelled samples were cut from the test panels using a guillotine or diamond cutter. Care was taken to protect the area to be examined by cutting the sample at least 5 mm from the region to be examined. The sample was then mounted in cold epoxy resin, followed by grinding to the region to be examined, and polishing to a 1 μm grit size. To prevent iron contamination, the enamelled sample was placed in an ultra-sonic bath before each abrasive disk was used.

2.6.2 Microscopy

Surface and cross-sectional samples were examined with optical light, stereo and scanning electron (SEM) microscopes.

Optical Light Microscopy

The samples were examined using two optical microscopes. The first is an Olympus microscope (BH, B071), and camera (C-35DA-2). The second is an Olympus BX60 optical microscope used in conjunction with a Polaroid digital microscope camera (DMC 1) coupled with the Polaroid DMC Direct software program, used for image capture.

Stereo Microscopy

A Wild M3B optical microscope (Wild Co, Switzerland) with an intralux 5000 light source was used for some analyses. The microscope was used in conjunction with a Polaroid digital microscope camera (DMC) coupled with the Polaroid DMC Direct software program, used for image capture.

Scanning Electron Microscopy (SEM)

A Hitachi S4000 scanning electron microscope was used for surface and cross-sectional microanalysis. Samples that exhibited charging were vacuum sputter coated with metal (gold – palladium).

2.6.3 Energy Dispersive X-ray Analysis (EDS)

A Kevex micro-analyser was attached to the SEM system to perform qualitative analysis of samples and also to determine approximate elemental concentrations within the samples (semi-quantitative analysis). Elemental distribution maps were used to identify the dispersive nature of identified elements within the samples. The sampling depths for all characterisation techniques are reviewed in Chapter 4.

2.6.4 Raman Spectroscopy

A Jobin Yvon U 1000 double beam spectrometer, with a microscope stage that uses 180° incident geometry to analyse small samples, was used for Raman spectroscopy on enamel surfaces, polished cross-sections and compositional components. An uncoated x50 objective lens was utilised with the microscope stage. A Spectra Physics argon-ion laser was employed to excite laser Raman spectra using a 514.5 nm laser line at an incident power of ca. 10-20 mW for the compositional components and 100 mW for surface specimens. A water-cooled Hammamatsu R943-02 photomultiplier tube was used for signal detection. Spectra were obtained using 400 μm or 500 μm slit width and the scanning rate used to collect the spectra was kept at 0.5 $cm^{-1}s^{-1}$ for the compositional components and 0.2 $cm^{-1}4s^{-1}$ for the surface spectra. The spectrometer was calibrated using the 1086 cm^{-1} calcite band. Surface and cross-sectional spectra were obtained in the range 25-1000 cm^{-1} at 0.5 $cm^{-1}s^{-1}$ rate. A comparison spectrum of air was obtained using the macro sample chamber and ca. 300 mW laser power, with the same spectrometer settings. Spectral characterisation and manipulations such as smoothing were achieved using GRAMS/32® software (Galactic Industries Ltd).

2.6.5 X-ray Diffraction (XRD)

A Philips X'pert system with a 40 mA, 45kV CuK_{α} radiation source and a scanning rate of $0.02°s^{-1}$ averaging for 5 seconds per increment, was used to study the crystal structure of the porcelain enamel samples. Frits and mill additions were ground into powder and pressed into aluminium holders, with sample space

dimensions of ca. 2x15x10 mm for analysis. The coating surfaces were analysed in original form, flush to the plane of the sample holder. Phases from the XRD patterns were identified using the best fitting ICDD (International Centre for Diffraction Data) reference cards.

2.6.6 Mid-Infrared Spectroscopy

Mid-infrared spectroscopy was performed on frit and mill additions using a Digilab FTS-40 Fourier transform-infrared spectrometer, employing a dry nitrogen purged bench. The spectra were recorded in the range 400-4000 cm^{-1} with a resolution of 8 cm^{-1} and averaging over 64 scans. The powdered samples of frits and oxides were diluted with dry KBr powder and pressed into pellets for scanning.

Attenuated Reflectance Spectroscopy (ATR) of enamel coating surfaces was performed using a specular reflectance cell and the spectra were transformed using a Kebulka Munk transform calculation. A range of 400-4000 cm^{-1} at a resolution of 8 cm^{-1} was used. Spectral analysis and manipulations was carried out using a WinIR® (Galactic Industries) software.

2.6.7 Far-Infrared Spectroscopy

A Digilab FTS-40 Fourier transform-infrared spectrometer with a 6.25-μm beamsplitter, on an evacuated bench, was used to obtain far-infrared spectra in the range 50-450 cm^{-1} with a resolution of 8 cm^{-1} and averaging over 256 scans.

The powdered samples of frits and oxide mill additions were examined as Vaseline mulls on a polyethylene plate. Spectral analysis and manipulations was carried out using a WinIR® (Galactic Industries) software. Spectra were subtracted from a control spectrum of Vaseline on polyethylene to remove any background spectral profile.

2.6.8 Bubble Size/Distribution

An indication of the bubble structure (size and size distribution) and iron oxide diffusion layer for each enamel coating was executed by examining micrographs of 490 μm length of cross-section (at 90° to the surface) for each enamel coating. The bubble size and size distributions were analysed using scion-image (Scion Corporation) software. Six cross-sections were analysed for each enamel coating type.

2.6.9 Particle Size/Distribution

Samples of porcelain enamel slips were analysed with a Malvern Mastersizer E laser diffraction system. This system was used primarily to determine particle size and particle size distribution of the milled enamel slips.

2.7 Chemical Resistance Testing

2.7.1 Boiling Citric Acid

The Australian Standards method for testing Vitreous Enamel Coatings, AS 2219.1.4[2] (ISO 2742), was used to determine acid resistance. The full test procedure is given in Appendix 1. Test equipment (Figure 2.12) is constructed in accordance to Appendix A of AS 2219.1.2.[3] It consists of a cylinder sealed top and bottom with two samples of pre-weighed test panel. The cylinder is connected to a 500-W heater and a reflux condenser. The bottom test panel is exposed to a boiling solution (64 g/L) of AR citric acid ($C_6H_8O_7.H_20$) in distilled water and the top panel is exposed to acid vapour. The test panels are exposed for 2.5 hours, then cleaned with distilled water. The samples are then dried at 110°C for 2 hours and then stored in a dessicator for 2 hours to constant mass before re-weighing. The corrosion after 2.5 hours testing is expressed as the loss in mass per square metre (g/m^2). The test was replicated six times for each enamel sample.

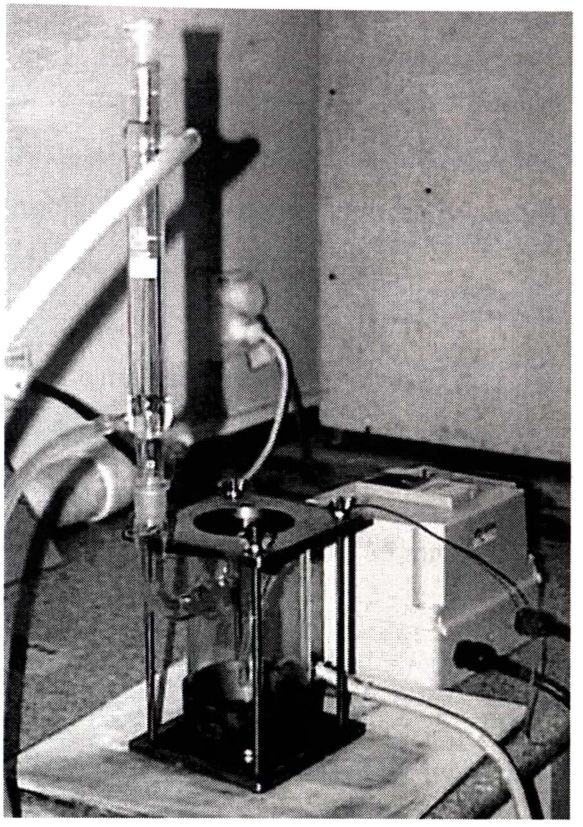

Figure 2.11 Boiling acid test apparatus.

2.7.2 Hot Sodium Hydroxide Test

The AS 2219.1.1[4] (ISO 2745) test method was used to determine the resistance of the coatings to hot sodium hydroxide. The method is described in full in Appendix 1. The test apparatus to hold the test panels is constructed in accordance to AS 2219.1.1. and is placed in a thermostatically controlled water bath. Two pre-weighed panels are tested simultaneously by exposing them to NaOH (40 g/L distilled water) at 80°C ± 0.1°C for 48 hours. Six test panels were tested for each enamel type. After testing, the samples are cleaned with acetic acid, followed by distilled water. The panels are then dried at 110°C for 2 hours. The dried samples are stored in a dessicator for 2 hours to constant mass and then re-weighed. The rate of corrosion is expressed as loss of mass per square metre per day ($g/m^2/d$).

2.7.3 Impact Resistance

The *"Visual Classification of Adhesion of Vitreous Enamel to Steel"* was used to assess impact resistance.[5] In this test, the results of a specified impact using an impact tester (Figure 2.5) on the enamel is visually assessed and classified. The following test conditions were used:

- Weight of hardened steel ball 450 g
- Height of fall 1,000 mm
- Diameter of anvil hole 25 mm
- Diameter of ball 25 mm

Three impact tests, over as widely distributed an area as possible, were performed for each coating type. After the weight had been dropped onto the surface of the sample, the damage area was visually classified by comparing it with the impact test categories displayed in Table 1.11.

2.8 References

1. Kawasaki, *Kawasaki KTSMT, Steel Sheet for Porcelain Enamelling.* 1987: Kawasaki Steel Corporation.
2. Standards Association of Australia, *AS 2219.1.4, Determination of Resistance of Vitreous Enamel Coatings to Boiling Citric Acid.* Methods of Test for Vitreous Enamel Coatings. 1978.
3. Standards Association of Australia, *AS 2219.1.2, Determination of Resistance of Vitreous Enamel Coatings to Boiling Water and Water Vapour.* Methods of Test for Vitreous Enamel Coatings. 1978.
4. Standards Association of Australia, *AS 2219.1.1, Determination of Resistance of Vitreous Enamel Coatings to Hot Sodium Hydroxide.* Methods of Test for Vitreous Enamel Coatings. 1978.
5. Institute of Vitreous Enamellers, ed. *Visual Classification of Adhesion of Vitreous Enamel to Steel.* Institute of Vitreous Enamellers.

Chapter Three
Preliminary Characterisation and Coating Properties

Chapter Three
Preliminary Characterisation and Coating Properties

3.1 Introduction

This chapter describes the porcelain enamels used in this research, including the enamel slip compositions (enamel batches). The compositions of the frits, colouring pigments and fired porcelain enamel coatings are discussed. The chapter also describes particle size distribution of the enamel slips, the milling and firing procedures used and coating adherence and bubble structure and size distribution in the fired porcelain enamels.

3.2 Commercial Enamel Ground Coats

Enamel Batch (Slip) Compositions

For commercial confidentiality, coatings used are coded gloss brown A (GBA), gloss green A (GGA), matte black A (MBA), gloss brown B (GBB) and gloss brown C (GBC).

Frits are the main components in the commercial enamels (Table 3.1). Ground coats for the 'A' enamels consisted of three frit types whilst GBB had two frit types. It is useful to blend multiple frit types (hard and soft) to get a good firing range, bond and appearance.

Table 3.1 Enamel (slip) batch formulations for commercial ground-coat enamels (1 kg batch*).

GBA	(g)	GGA	(g)	MBA	(g)	GBB	(g)	(g)	GBC	(g)
Frit A1	500	Frit A1	500	Frit A3	300	Frit B1	400	500	Frit C1	750
Frit A2	300	Frit A2	300	Frit A4	500	Frit B2	600	500	Frit C2	250
Frit A3	200	Frit A3	200	Frit A5	200					
Sub total	1000	Sub total	1000	Sub total	1000	Sub total	1000	1000	Sub total	1000
Colouring pigment GBA1	40	Colouring pigment GGA1	50	Colouring pigment MBA1	60	Colouring pigment GBB1	7	40	White clay	60
Silica	40	Silica	40	Silica	50	Colouring pigment GBB2	18	50	Quartz	50
HB clay	40	HB clay	40	HB clay	20	Silica	70	2	Soda nitrite	1.5
Kaolex clay	30	Kaolex clay	30	Kaolex clay	30	Blue clay	35	3	Bentonite	2.5
Bentonite	2	Bentonite	2	Benonite	2	Mill addition	10	2	Compound	1.5
Borax	5	Borax	5	Borax	2	Boric acid	2		Oxide GBC1	20
Magnesium carbonate	1	Magnesium carbonate	1	Feldspar	5	Magnesium carbonate	2			
Sodium nitrite	1	Sodium nitrite	1	Sodium nitrite	2	Sodium nitrite	2			
				Calcined alumina	80					
				Antimony	5					
Batch total	1158	Batch total	1168	Batch total	1206	Batch total	1146	1097	Batch total	1135.5
Water	570	Water	570	Water	600	Water	500	520	Water	400

* The normal convention for showing enamel batch formulations is for the frits to add up to 100 wt% then the mill additions are added to the formulation.

The EDX spectra (Figures 1-7, Appendix 3) and ICP data (Table 3.2) indicate that each frit had many elements, with silica being the main constituent. This is expected, as the enamels are alkali borosilicate glasses. Many of the frits had high calcium contents. This calcium may come from the $CaCO_3$, added for fluxing, but can also be a common impurity of the many frit components.

Mill additions and colouring pigment oxides used to obtain different enamel slips are given in Table 3.1. Although the GBC composition is given in Table 3.1, individual enamel batch components could not be analysed because the manufacturer supplied this commercial enamel in a dry milled condition.

Clays are used to suspend the frit particles and to promote bubble structure. The high calcined alumina content of the MBA coating decreases the gloss and promotes a matte finish. However, using alumina as a mill addition can also reduce the coating's acid resistance.[1]

Colouring pigment oxides are also in the batch composition (Table 3.1). The EDX spectra for each pigment indicate that GBA (with pigment GBA1) contain the elements Si, Al, Cr, Fe and Zn (Figure 3.1a). Data from literature[2-4] (Table 1.3) indicate that $(Zn,Fe)(Fe,Cr)_2O_4$ (zinc-iron-chromite brown spinel) is the closest matching colouring pigment. The colouring oxides were not expected to contain silica (indicated by the intense band in the spectrum). This element is typically used as a refractory and to give a white colour. Silica may have been included to change the colour or as an extender (to increase melting temperature).

Colouring pigment GGA1 (Figure 3.1b) used in the GGA coating contains the elements Cr (intense peak), Fe and a small amount of Si. The elemental composition (with the exception of the Si) closely matches that of $(Cr,Fe)_2O_3$.

The MBA enamel uses pigment MBA1, which has an intense Cr peak and a smaller Cu peak (Figure 3.1c). This colouring oxide is presumed to be $CuCr_2O_4$ (Copper-chromite black spinel).

GBB enamel uses two mill addition pigments for colouring - GBB1 and GBB2. Elemental analyses indicate that these contained many constituents. The most intense peak for colouring pigment GBB1 is Cr, with intense peaks for Fe and Si. The other peaks include Zn and a small peak representing Al. The elemental composition most closely matches $(Zn,Fe)(Fe,Cr)_2O_4$ (zinc-iron-chromite brown spinel). Pigment GBB2 used in GBB enamel is similar to pigment GGB1, except it contains Ti, often added as titania, to give the porcelain enamel opacity. The pigment could be a mix of zinc-iron-chromite brown spinel and iron-titanium brown spinel, Fe_2TiO_4, although elemental Si and Al were also detected.

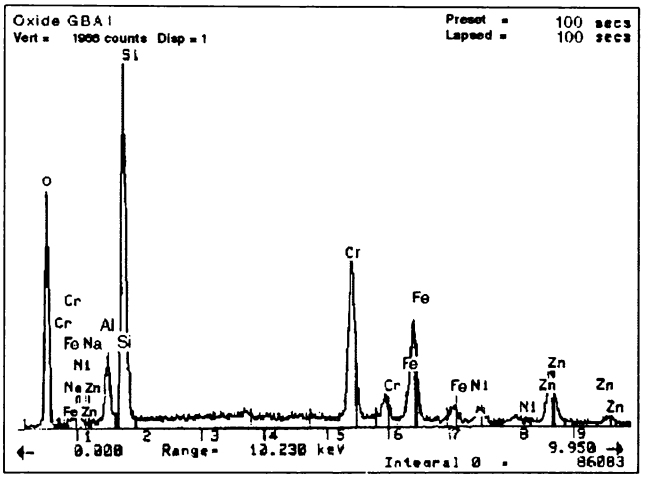

Figure 3.1(a) EDX spectrum of colouring pigment for GBA.

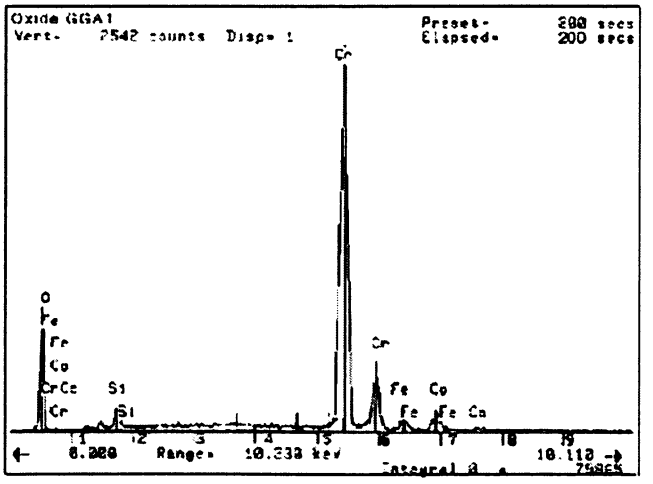

Figure 3.1(b) EDX spectrum of colouring pigment for GGA.

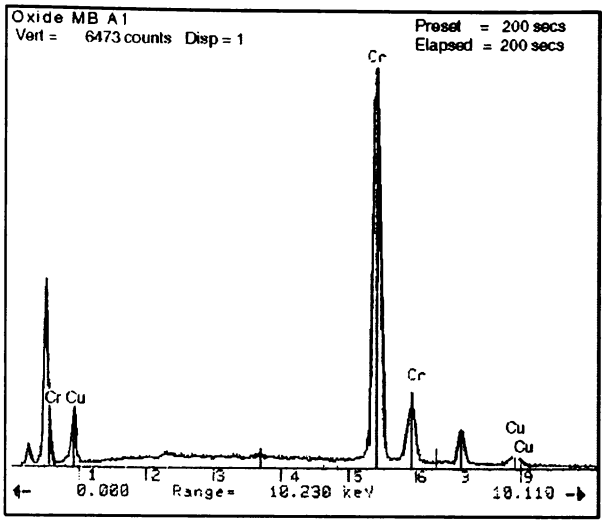

Figure 3.1(c) EDX spectrum of colouring pigment for MBA.

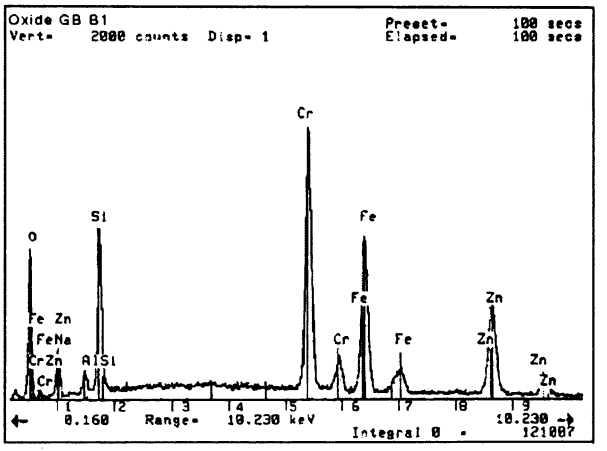

Figure 3.1(d) EDX spectrum of colouring pigment 1 (GBB1) for GBB.

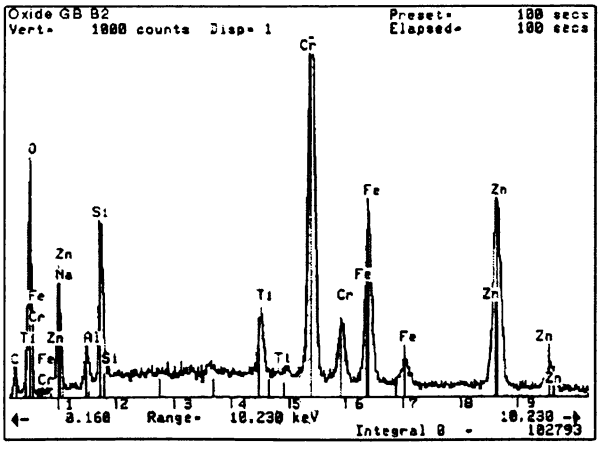

Figure 3.1(e) EDX spectrum of colouring pigment 2 (GBB2) for GBB.

Porcelain enamels are complex because they have many constituents (up to 15). This can be shown by quantitative ICP analysis (Table 3.2). As expected, silica is the most dominant component, ranging from 49 wt% for frit A2 to 71 wt% for frit A5. Frits with the highest silica content tend to have the lowest boron oxide content and vice versa.

GGA and GBA contain the same frits - A1, A2 and A3 (Table 3.1). Frits A1 and A3 have slightly more silica (52.3 and 52.9 wt% respectively) than frit A2 (49.1 wt%) (Table 3.2). The A5 frit used in the MBA enamel has the most silica (70.84 wt%), and can be termed a "hard" frit. The frits all have similar alumina content. The principle source of this alumina is likely to be feldspar.[5]

Table 3.2 Composition (weight percent) of ground-coat enamel frit (ICP).*

	Composition (Wt %)						
Constituent	**Frit A1**	**Frit A2**	**Frit A3**	**Frit A4**	**Frit A5**	**Frit B1**	**Frit B2**
SiO_2	52.26	49.13	52.90	51.53	70.84	68.93	61.25
Na_2O	14.39	13.25	8.24	19.68	9.17	11.69	10.47
Al_2O_3	3.03	6.34	3.53	3.46	6.06	0.55	1.60
CaO	7.45	11.89	3.67	7.19	1.24	5.86	5.03
K_2O	0.21	0.35	0.48	0.71	3.72	0.23	0.21
MnO_2	0.82	1.15	0.08	0.02	0.06	0.10	0.06
NiO	1.64	0.63	3.17	1.71	1.12	3.13	2.10
CoO	0.36	0.40	0.65	0.42	0.87	1.35	0.41
BaO	2.89	00	8.77	0	0.06	00?	1.86
FeO	1.29	0.44	2.19	0.28	0.32	0.10	1.09
Cr_2O_3	0.10	0.11	0.09	0	0	0.09	0.10
TiO_2	0.14	0.14	0.10	0.09	0.09	1.26	4.51
CuO	0.36	0.05	1.41	0.08	0	0.05	0.48
B_2O_3	13.15	14.05	14.10	12.58	5.85	6.65	10.65
MgO	1.87	2.10	0.56	2.02	0.59	1.13	0.09

*Constituents expressed as metal oxides. See Appendix 2 for method.

3.2.2 Milling and Firing Commercial Ground Coat Enamels

Milling time, specific gravity and milling fines for each commercial ground-coat enamel are in Table 3.3. Milling fineness is the residue in grams retained on a 75 μm sieve from a 50 ml sample of slurry (expressed as grams / 50 ml / 75 μm sieve (#200 mesh sieve), but for the following results only the number of grams will be

shown). To obtain good adherence between the steel substrate and the enamel, and good aesthetic qualities for the fired enamel, an attempt was made to match specific gravity and milling fineness specs of the frits. The manufacturers/suppliers had tested these frit characteristics.

Table 3.3 Milling parameters for commercial ground-coat enamels.

Enamel	GBA	GGA	MBA	GBB1	GBB2	GBC
Mill time (mins)	70	70	72	86+15	97	Supplied premilled
Specific gravity (g/cm^3)	1.74	1.74	1.78	1.72, 1.72	1.70	-
Milling fineness	6	6.1	4.5	4.1, 1.5	0.8	-

The GBA and GGA samples were milled for 70 minutes to obtain a specific gravity of 1.74 g/cm^3 and milling fineness of 6 (GBA) and 6.1 (GGA). These values are within the manufacturer's milling specifications of 1.72 to 1.74 g/cm^3 for specific gravity and 5.5 to 6.5 for milling fineness. The MBA specifications of 4 to 4.5 milling fineness and 1.78 g/cm^3 specific gravity was achieved by milling the sample for 72 minutes.

The specifications for GBB are 0.5 milling fineness and 1.72 g/cm^3 specific gravity. After 86 minutes milling, the milling fineness value was 4.5 and the specific gravity was 1.72 g/cm^3 (Table 3.3). As the manufacturer's fineness specifications had not been obtained, the batch was milled for 15 minutes more to achieve the milling fineness of 1.5. A second batch, which had been milled for 97 minutes, had a fineness of 0.8 and a specific gravity of 1.70 g/cm^3.

Firing times for each enamel slip were varied to get the best bond and surface appearance (Table 3.4). Enamel slips higher in refractory silica (GBB and GBC), required longer firing times to get better coat fusion.

Table. 3.4 Firing time and speed for commercial ground coat enamels.

Enamel	GGA	GBA	MBA	GBB	GBC
Time in furnace (min:sec)	7:11	7:11	7:11	8:05	8:05
Total time in firing zones (min:sec)	2:00	2:00	2:00	2:15	2:15
Zone 1 temperature (°C)	820	820	820	820	820
Zone 2 temperature (°C)	850	850	850	850	850

3.2.3 Impact Test and Adherence for Commercial Coatings

Descriptions of visual adherence and photographs of impact regions of the commercial enamels used in this investigation are summarised in Table 3.5.

Table: 3.5 Drop weight impact data and description of adherence for commercial ground-coat enamels (3 tests per sample, 2 samples tested for each enamel type).

Enamel	Adherence Description	Photograph of Impact Region of Coating Surface (Scale 1:1)
GBA	Fair-very good	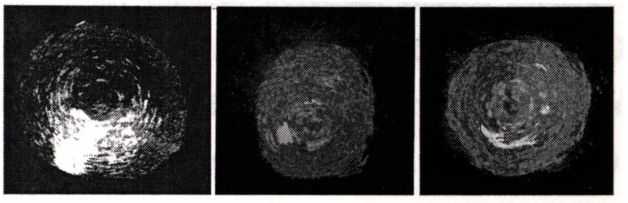
GGA	Fair-very good	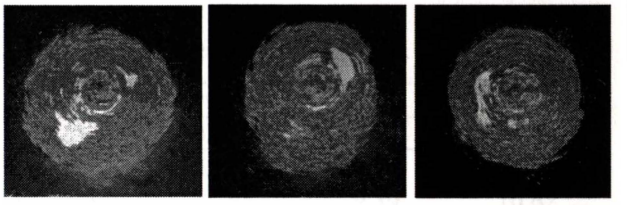
MBA	Fair-very good	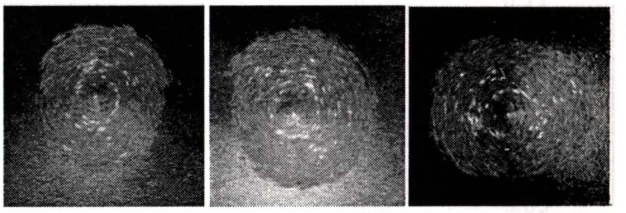
GBB	Excellent	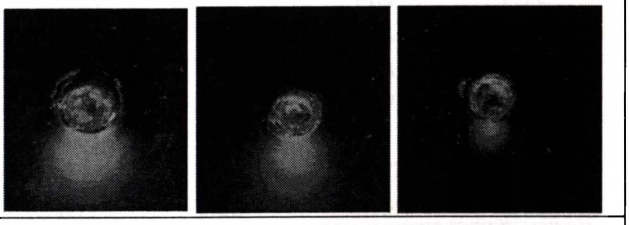
GBC	Fair-very good	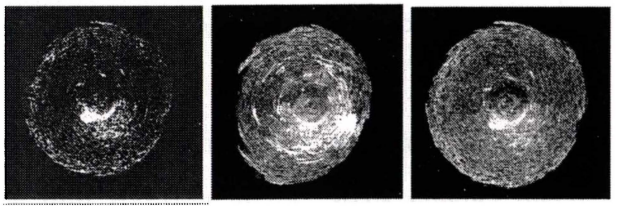

The GBA and GGA enamels have similar compositions (Table 3.1). The adherence classification (Table 1.11) indicates that both coatings had a fair to very good adherence. The MBA enamel, which was made from the same frits as GBA

and GGA) also has a fair to very good adherence as only a small amount of enamel coating was removed from the steel. The GBB coating has excellent adherence and very little enamel was removed from the steel base in the impact test. Impact damage to the GBC coating was similar to that of commercial "A" coatings, with fair to very good adherence.

3.2.4 Melted Coating Compositions

The ICP data for compositions of the finished porcelain enamel coatings are shown in Table 3.6. The high silica content (from the glass former) in the GBB and GBC frits (Table 3.2) contribute to the high silica content of the finished coating (62.16 wt% and 54.76 wt% for GBB and GBC respectively, Table 3.6).

Table 3.6 Melted ground-coat enamel compositions (ICP).*

	Composition (wt %)				
Constituent	**GBA**	**GGA**	**MBA**	**GBB**	**GBC**
SiO_2	48.73	51.72	43.75	62.16	54.76
Na_2O	10.13	12.55	7.20	9.39	10.62
K_2O	0.25	0.22	0.24	0.17	0.11
CaO	6.68	6.70	4.37	4.44	3.93
ZnO	0.27	0.04	0.12	0.28	0.41
Al_2O_3	5.03	4.60	12.02	1.96	2.08
TiO_2	0.18	0.19	0.46	2.80	3.67
CuO	0.34	0.39	1.08	0.23	0.44
MnO	0.75	0.69	0.10	0.06	0.65
NiO	1.16	1.40	1.21	2.09	1.23
CoO	0.33	0.40	0.33	0.63	0.40
BaO	2.64	3.22	7.44	0.93	0
FeO	10.56	5.41	11.40	2.87	11.55
Cr_2O_3	0.43	0.65	0.46	0.21	0.53
B_2O_3	11.58	10.66	9.76	11.67	9.78
MgO	0.96	1.17	0.06	0.13	0.11

*Constituents expressed as metal oxides. See Appendix 2 for method

The content of boron oxide, another glass former, was similar in all enamel coatings. The calcined alumina mill addition in the MBA enamel batch, presumably used to reduce surface gloss, produced a high Al_2O_3 content in the coating. The CoO and NiO present in all samples and are used to promote adherence to the substrate, but also impart darker shades. The FeO content of the fired enamels (up to 11.55 %) is much higher than in the

contributing frits. This higher content is caused by iron oxide diffusion from the substrate into the coatings during firing.

3.3 Variations in Ground-Coat Enamel Composition

3.3.1 Enamel Batch (Slip) Composition of Trial Coat Enamels

To investigate the effect of composition on chemical resistance, samples of the commercial enamel coating, GBA, were obtained by adding different amounts of mill additions silica and/or HB clay (Table 3.7).

Table 3.7 Enamel batch composition for ground-coat enamel trial formulations (1kg batch). (Changes from the GBA composition are bolded.)

Batch Component	GBA	GBI	GBII	GBIII	GBIV
Frit A1	500	500	500	500	500
Frit A2	300	300	300	300	300
Frit A3	200	200	200	200	200
Frit Total	1000	1000	1000	1000	1000
Colouring pigment GBA1	40	40	40	40	40
Silica	40	**140**	40	**70**	**90**
HB clay	40	40	**140**	**70**	40
Kaolex clay	30	30	30	30	30
Bentonite	2	2	2	2	2
Borax	5	5	5	5	5
Magnesium carbonate	1	1	1	1	1
Sodium nitrite	1	1	1	1	1
Total	1158	1258	1258	1218	1208
Water	570	570	570	570	570

Adding 100g of silica (GBI) was done to give a pronounced effect on the acid resistance properties of the enamel coating. Increasing the HB clay by 100 g (GBII), was done to obtain a pronounced effect on the alkali properties of the resultant enamel coating. The main elements in the HB clay are Si, Al, and O, with traces of Ti (Figure 15-Appendix 3). GBIII had an increase in both silica and HB clay by 30 g for each addition. GBIV had an increase in silica by 50 g to investigate the chemical resistance while maintaining similar adherence and appearance to GBA.

3.3.2 Milling and Firing Trial Coat Enamels

The specific gravity and milling fineness of the slips for the trial enamels are given in Table 3.8. After around 70 minutes milling, all slips had the similar specific gravities. However, GBI and GBII samples had a milling fineness 4.0 - 4.4 whereas the GBIII and GBIV had a milling fineness of 6.1.

Table 3.8 Milling parameters for trial ground coat enamels.

Enamel	GBI	GBII	GBIII	GBIV
Mill time (mins)	73	71	69	69
Specific gravity (g/cm^3)	1.70	1.70	1.69	1.70
Milling fineness	4.4	4.0	6.7	6.1

The same firing times and temperatures were used for each trial enamel coating (Table 3.9) because previous research[10] showed that mill additions such as silica only partially dissolve during firing and this was not affected by firing time. In other words, increasing the firing time to get better fusion for trial coatings high silica contents would not increase the amount of silica dissolved.

Table 3.9 Firing time and temperature for trial ground-coat enamels.

Enamel	GBI	GBII	GBIII	GBIV
Total Time in Furnace (min:sec)	7:11	7:11	7:11	7:11
Time in Firing Zones (min:sec)	2:00	2:00	2:00	2:00
Firing Temp (°C) Zone 1	820	820	820	820
Firing Temp (°C) Zone 2	850	850	850	850

3.3.3 Impact Test and Adherence of Trial Coatings

The GBA (4 wt% silica) had fair to very good adherence but the GBI enamel (9 wt % silica increase) had the lowest adherence of the four trial coatings tested (Table 3.10). Large amounts of enamel coating flaked off after the impact test, giving it a rating of poor to fair. Occasionally the bond was acceptable (middle photograph for GBI, Table 3.10). The data indicate that increasing silica content to 13 wt% adversely affected adherence. This may be because the coating is too refractory (hard), which weakens the bond. A second reason is that increasing the silica content effectively decreases the content of the adherence oxides Co and Ni.

Table 3.10 Drop weight impact test results and adherence description for trial coat enamels (3 tests per sample, 2 samples were tested for each enamel type).

Enamel	Adherence Description	Photograph of Impact Region of Coating Surface (Scale 1:1)
GBI	Poor – fair	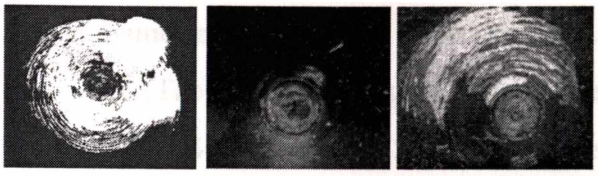
GBII	Fair-very good	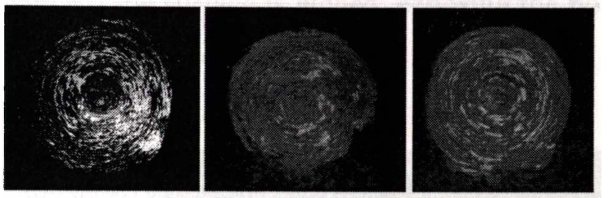
GBIII	Fair-very good	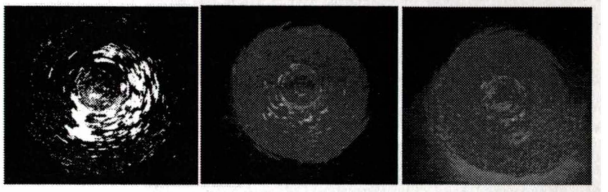
GBIV	Fair-poor	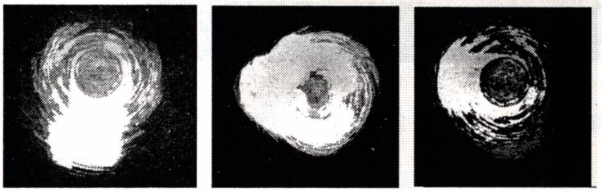

The adherence of GBII (9 wt% more HB clay) was fair to very good, which was between that of GBI and GBA. This adherence would be acceptable for commercial use but the coating differs from that GBA coating by having a non-aesthetically acceptable speckled appearance.

The adherence of GBIII (3 wt % increase of HB clay and silica) and GBII was similar (fair to very good), and acceptable for commercial use. However, the adherence of GBIV (4 wt% extra silica) is not acceptable for commercial use.

3.4 Cross Section

Bubble structure and the iron oxide diffusion layer of each porcelain enamel coating cross-section (90° to the surface) are shown in Figures 3.2 to 3.9 and bubble size and size distributions are in Table 3.11 and Figures 3.10 to 3.12.

The lighter coloured iron oxide diffusion layer in the commercial coat enamel, GBA, seen in the dark field illumination (Figure 3.2b) extends from the enamel/steel interface, 30 μm into the enamel coating. The evenly dispersed bubbles vary from 1 μm to 32 μm in diameter (Figure 3.2a). This enamel has the highest number of bubbles per unit area (Table 3.11 and Figure 3.10) and a high percentage bubble area (approximately 23 ± 4% - Figure 3.12). Both factors may adversely affect chemical resistance if the surface is etched, exposing the pores to chemicals.

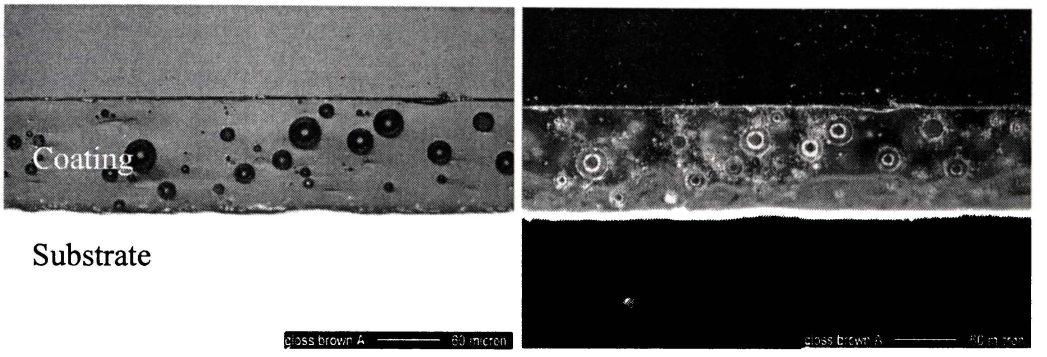

Figure 3.2 Optical micrograph of GBA coating on steel substrate using bright field (a) and dark field illumination (b).

The GGA enamel has a similar composition to GBA, and is discussed in detail in Chapter 6. MBA has the second highest number of bubbles per unit area (Table 3.11, Figure 3.11), with many being near the surface of the coating (Figure 3.3). This could decrease chemical resistance because more surface area is exposed to a chemical if the enamel surface is etched.

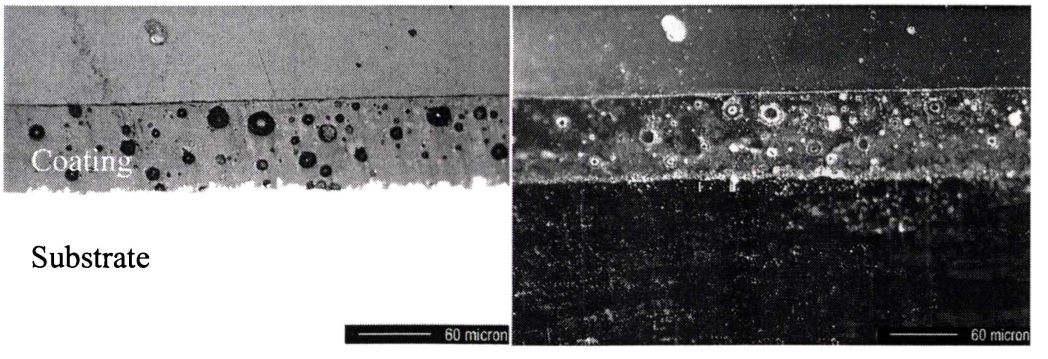

Figure 3.3 Optical micrograph of MBA coating on steel substrate using bright field (a) and dark field illumination (b).

Bubbles in GBB are well dispersed in the lower zone near the steel surface (Figure 3.4). This could help absorb gases from the steel substrate and help prevent defects such as fishscale.[11-15] Literature indicates that the bubble zone required to absorb the gases should be approximately 25 μm thick from the steel-coating interface.[11,16] The zone near the surface does not have many bubbles, and no large bubbles (>40 μm) that can cause defects such as pinholes/blisters. The bubble structure in this zone is mainly small bubbles, less than 10 μm diameter, with no bubbles greater than 30 μm in diameter. The percentage bubble area (Figure 3.12) for GBB is much lower than the other coatings, which could help increase its chemical resistance (by having a decreased surface area). The impact adherence for GBB was excellent (Table 3.10). The bubble structure in GBB (small bubbles, and low bubble density) may increase the mechanical strength of this enamel. This is supported by Smalley,[13] who also reported that some ground coats with little bubble structure, along with an increased iron oxide layer, had good mechanical strength. This is opposite to the assumption that a good bubble structure (many well-dispersed bubbles that help relieve stress from external impact) is needed for good mechanical strength.[12] Dark field illumination shows that the iron oxide diffusion layer extends about 30 μm from the enamel/steel interface (Figure 3.4b).

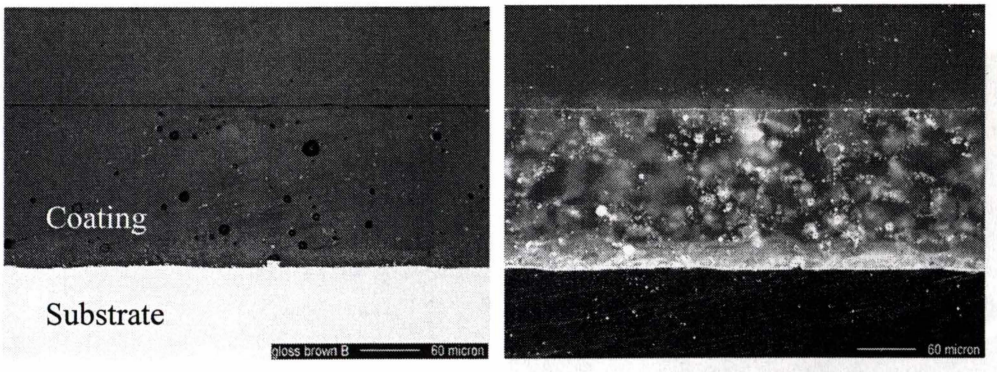

Figure 3.4 Optical micrograph of GBB coating on steel substrate using bright field (a) and dark field illumination (b).

Although the GBC coating cross-section has few bubbles (Figure 3.5), most are very large (diameters of 40-50 μm and >50 μm) (Table 3.11; Figure 3.11). The average cross-section contains 700 ± 220 bubbles per mm^2 (Table 3.11, Figure

3.10), indicating that the GBC coating has the highest percentage bubble area (see Figure 3.12). This high percentage bubble area could adversely affect chemical resistance. However, most bubbles are not near the surface (Figure 3.5), so increased area for chemical attack is be minimised.

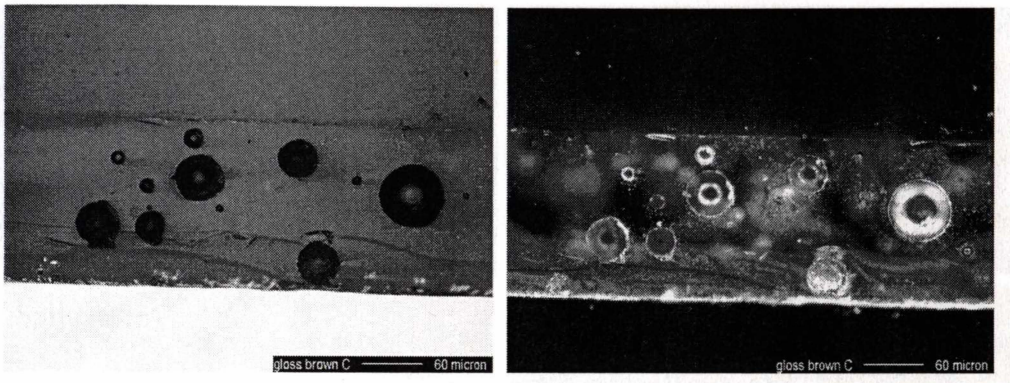

Figure 3.5 Optical micrograph of GBC coating on steel substrate using bright field (a) and dark field illumination (b).

The bubbles in GBI tend to be small (diameter <20 μm; Figure 3.10; Figure 3.11). and in the upper and lower sections (Figure 3.6). Bubbles near the surface could increase the surface area exposed to chemicals, thus increasing the corrosion rate. However, percentage bubble area is small (approximately 12%, Figure 3.12), which would increase chemical resistance.

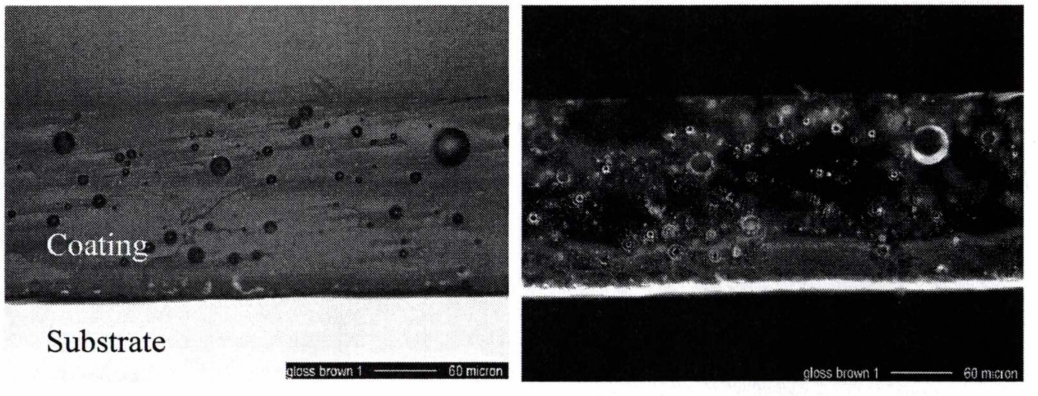

Figure 3.6 Optical micrograph of GBI coating on steel substrate using bright field (a) and dark field illumination (b).

Bubbles in the GBII coating are near the steel substrate (Figure 3.7) so gases produced can be adsorbed easily. The percentage bubble area (Figure 3.12) is 22

± 14 %. The high standard deviation indicates the wide range in bubble numbers; size and distribution in the six cross-sections examined. Variability in bubble structure may contribute to the variable adherence data (fair to good range; Table 3.10).

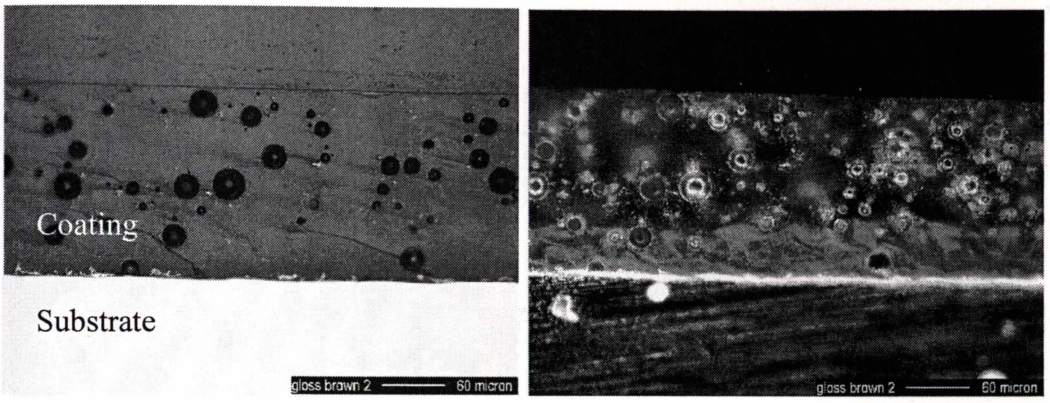

Figure 3.7 Optical micrograph of GBII coating on steel substrate using bright field (a) and dark field illumination (b).

The GBIII coating has a different bubble structure from GBA, I and II (Figure 3.8). It has mainly large-diameter (30-40 and 40-50 μm) bubbles (Table 3.10, Figure 3.11), similar to the GBC enamel (Figure 3.11). Very few bubbles are near the steel interface (Figure 3.8), which would not aid in the prevention of fishscale defects. Decreasing the firing time may produce more, smaller-diameter bubbles. The large iron oxide diffusion zone (Figure 3.8b) extends 69 μm upwards from the enamel/steel interface.

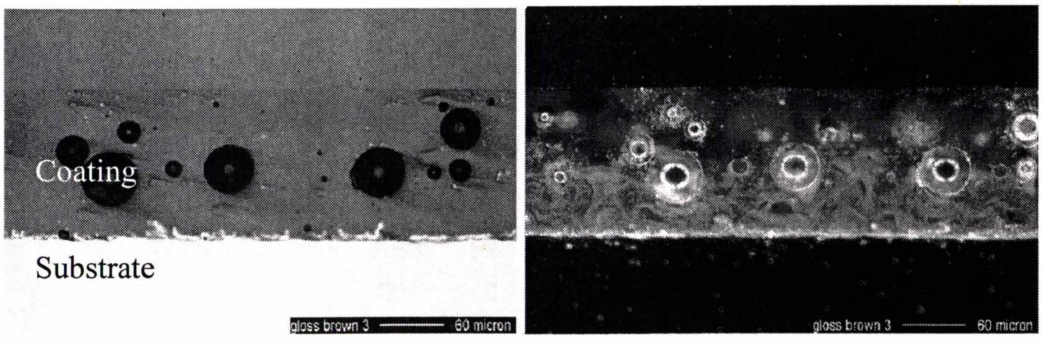

Figure 3.8 Optical micrograph of GBIII coating on steel substrate using bright field (a) and dark field illumination (b).

The GBIV coating has a wide range of bubble sizes (Figure 3.9a, Figure 3.11, Table 3.11). Although there are more bubbles than for GBIII, the percentage bubble area is similar (Figure 3.12). The diffusion zone (Figure 3.9b) extends 40 μm upwards from the enamel/steel interface.

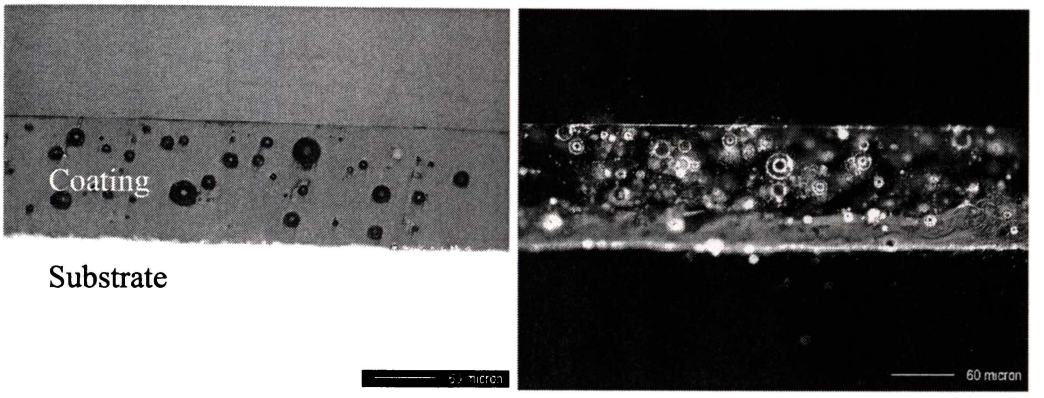

Figure 3.9 Optical micrograph of GBIV coating on steel substrate using bright field (a) and dark field illumination (b).

Table 3.11 Distribution of mean bubble sizes (μm diameter) and number of bubbles per unit area (mm^2) for each coating.

	Porcelain Enamel Coating Types							
Diameter Range (μm)	Gloss brown A	Gloss brown B	Gloss brown C	Gloss brown I	Gloss brown II	Gloss brown III	Gloss brown IV	Matte black A
<10	1813 ± 297	1173 ± 273	400 ± 42	997 ± 163	634 ± 287	330 ± 45	630 ± 290	1722 ± 450
10-20	702 ± 149	154 ± 82	106 ± 44	386 ± 82	381 ± 144	156 ± 89	367 ± 81	389 ± 119
20-30	91 ± 110	7 ± 10	58 ± 39	5 ± 61	134 ± 100	63 ± 17	120 ± 77	49 ± 27
30-40	15 ± 17	0	46 ± 19	8 ± 9	24 ± 31	59 ± 23	40.0 ± 33	0
40-50	5 ± 12	0	49 ± 27	3 ± 7	9 ± 10	30 ± 18	10 ± 15	0
>50	0	0	42 ± 27	0	0	7 ± 12	3 ± 8	0
Total Bubble Number	2626 ± 388	1333 ± 273	700 ± 220	1444 ± 213	1182 ± 230	644 ± 116	1170 ± 305	2160 ± 546

± = Standard deviation

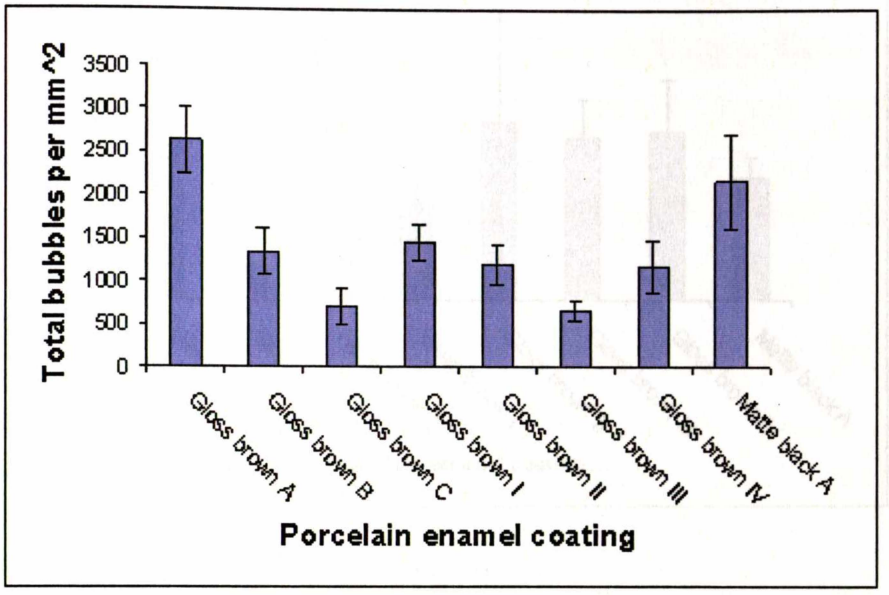

Figure 3.10 Bubbles per unit area (mm^2).

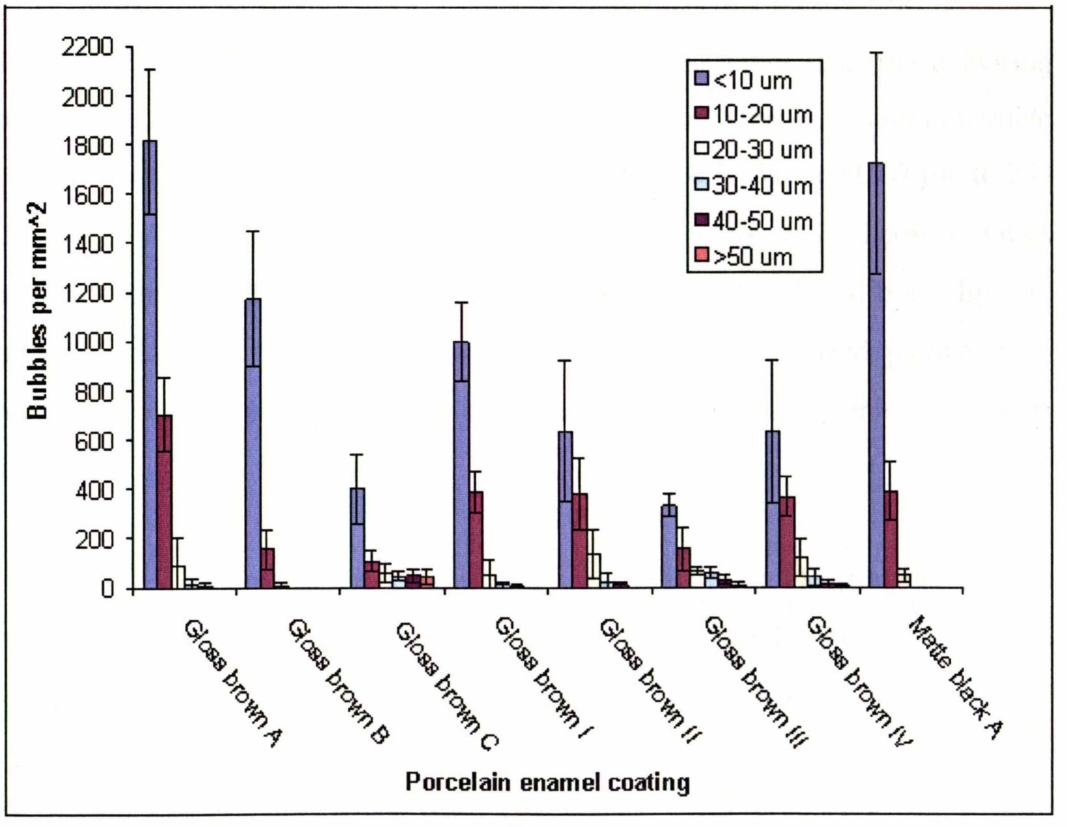

Figure 3.11 Size distribution of bubbles per unit area (mm^2).

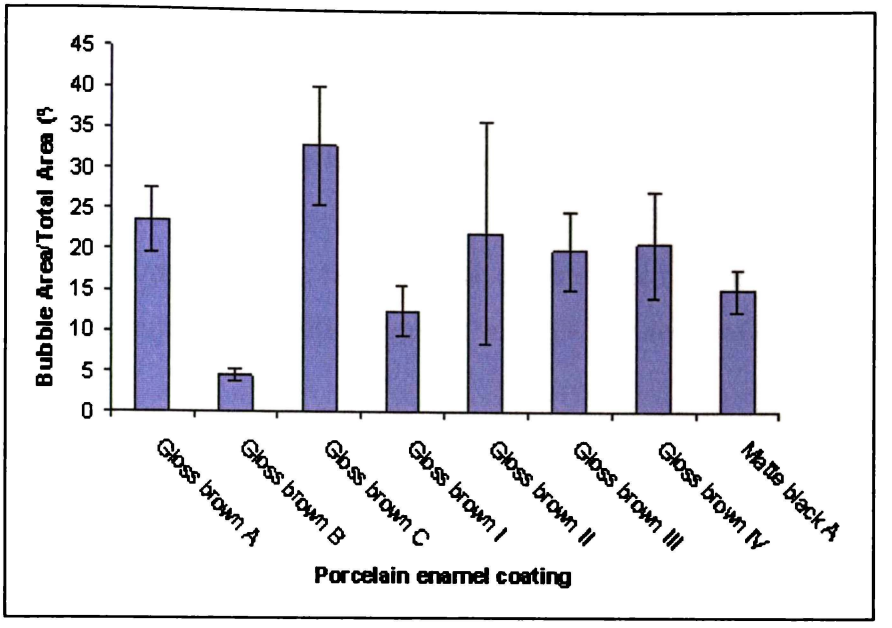

Figure 3.12 Percentage bubble area in coatings.

3.5 Enamel Slip (Before Firing) Particle Size Analysis

The GGA and GBA slips have similar compositions other than the colouring oxides. Laser diffraction data indicate that these enamel slips have similar particle size distribution - 0.08 μm to 222 μm for GBA (Figure 3.13a) and 0.07 μm to 259 μm for GGA (Figure 3.13b). The mean particle diameters are 35.1 μm for GGA and 39.9 μm for GBA. Approximately 11.5 % of the particles in both slips are less than 2 μm in diameter. Currie[17] proposes that this sized particle may represent colloidal material such as secondary glass particles, organic compounds and clays.

Particles in GBB enamel slip (Figure 3.13c) are 0.1 μm to 115 μm with a mean particle size diameter of 28.67 μm. This smaller mean particle size is possibly due to a long milling time to achieve the specified milling fineness.

Particles in GBC enamel slip (Figure 3.13d) are 0.1 μm to 105 μm with a mean particle diameter of ca. 26 μm. This enamel slip was made from pre-milled enamel batch supplied by the manufacturer, so the milling time is not known.

A particle size analysis showed that the GBI, GBIII and GBIV enamel slips had similar sized particles - between ca. 0.1 μm and 112 μm. (Figures 3.13e-g). The GBI, with more silica (to 13 wt%) has the lowest mean particle diameter (36.13 μm compared with 39.22 μm and 37.99 μm for GBIII and GBIV slips respectively). A longer milling time may have contributed to the smaller particle size for GBI. (73 minutes for GBI compared with 69 minutes for GBIII and IV).

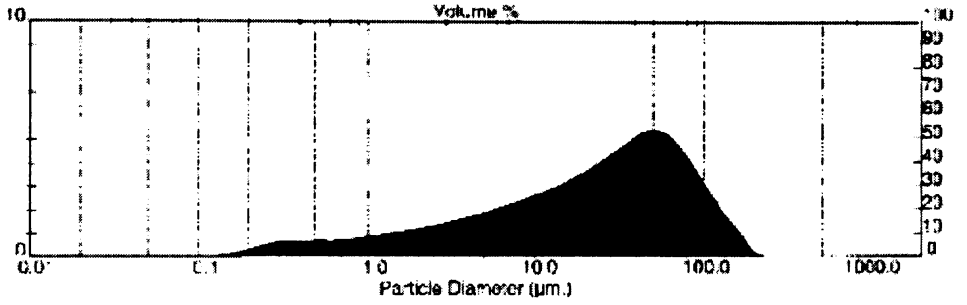

Figure 3.13(a) Particle size distribution of GBA enamel slip after milling.

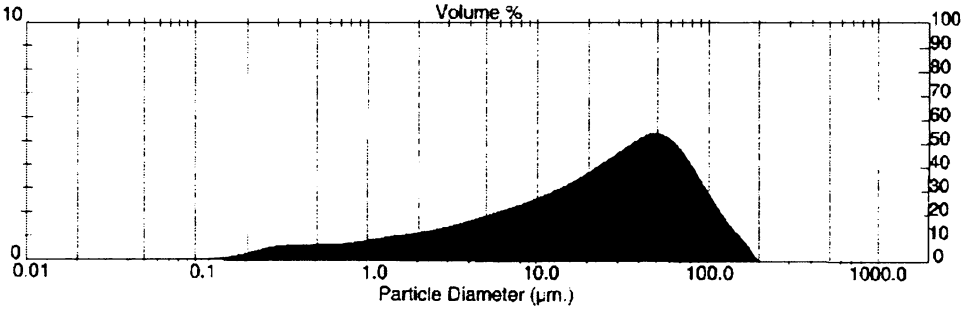

Figure 3.13(b) Particle size distribution of GGA enamel slip after milling.

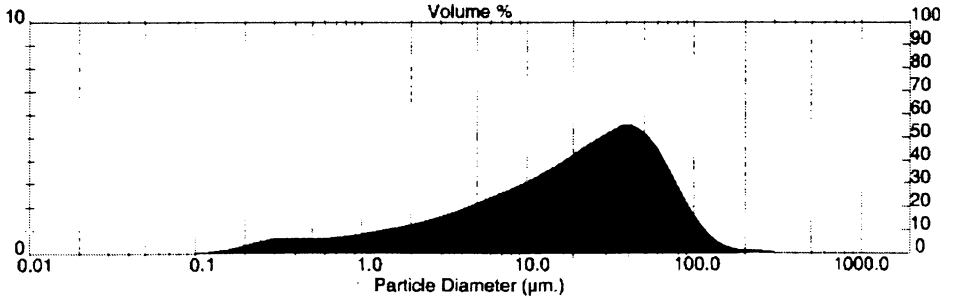

Figure 3.13(c) Particle size distribution of GBB enamel slip after milling.

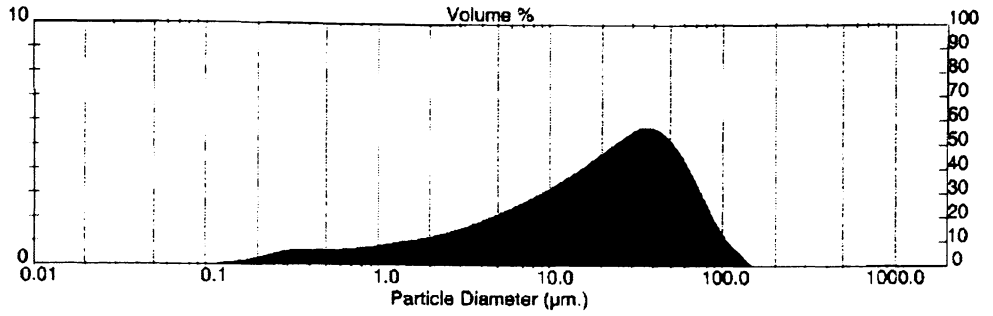

Figure 3.13(d) Particle size distribution of GBC enamel slip after milling.

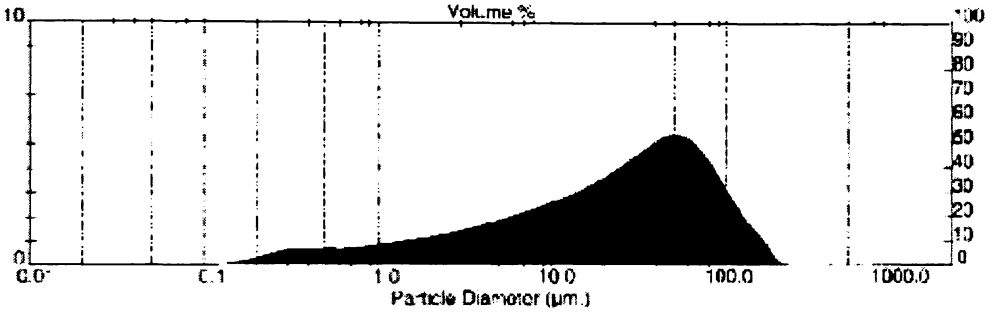

Figure 3.13(e) Particle size distribution of GBI enamel slip after milling.

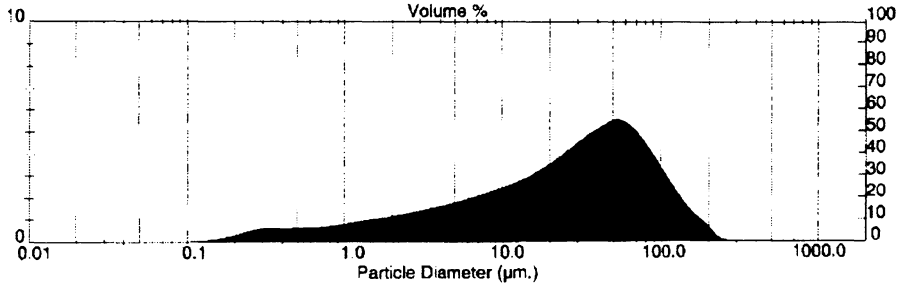

Figure 3.13(f) Particle size distribution of GBIII enamel slip after milling.

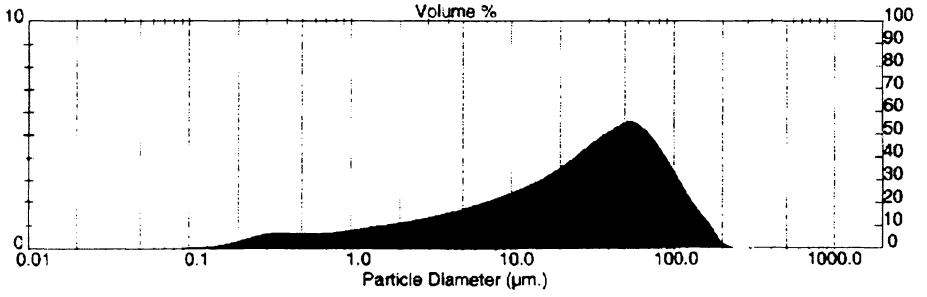

Figure 3.13(g) Particle size distribution of GBIV enamel slip after milling.

3.6 Summary

The preliminary characteristics of the porcelain enamel coatings used in this research were presented. This information assists the research undertaken in the following chapters.

Quantitative analysis of the frits and the fired enamel coating by ICP showed that SiO_2 was the major component in the frits and enamel coatings, followed by Na_2O and B_2O_3. The coatings had more FeO than the frits because FeO diffuses from the steel substrate during firing. The iron oxide diffusion layer in cross-sections of coating could be identified using dark field optical microscopy.

The GBB commercial enamel had excellence adherence, while other commercial coatings were rated fair to very good. Adherence ratings of trial enamels made by varying the composition of the commercial enamels ranged from poor to very good. GBII and GBIII, with increased HB clay and HB clay/silica contents respectively had the best ratings for the trial enamels. By only increasing the silica content of the trial formulations reduced adherence ratings.

The commercial and trial enamels had a range of bubble structures. GBA and MBA had the highest number of bubbles per unit area. Chemical resistance may depend on the surface area exposed to chemicals.

3.7 References

1. Layne, C.M., *Physical Properties of Grate Enamel Systems.* Ceramic Engineering and Science Proceedings, 1995. **16**(6).
2. Eppler, R.A., *Ceramic Colorants.* 1986. **A5**.
3. Burgyan, A. and Eppler, R.A., *Classification of Mixed-Metal-Oxide Inorganic Pigments.* American Ceramic Society Bulletin, 1983. **62**(9).
4. Eppler, R.A. and Gill, D., *Glazes & Enamels*, in *Engineered Materials Handbook, Vol 4. Ceramics and Glasses.* 1991, ASM International, The Materials Information Society. USA.
5. Ceramic Industry, *Materials Handbook*, in *Ceramic Industry.* 1992.
6. Vargin, V., *Technology of Enamels.* 1968: Maclaren and Sons Ltd.
7. Andrews, A.I., *Porcelain Enamels. The Preparation , Application, and Properties of Enamels.* 1961: The Garrard Press, Publishers.

8. ASM Committee on Porcelain Enameling, *Porcelain Enameling*. ASM Handbook (Metals Handbook), Surface Engineering, ed. S.R. Lampman. Vol. 5. 1996, ASM International.
9. Wright, J.F., Bereron, C.G. and Oliver, J.C., ed. *Porcelain Enamel*. Engineered Materials Handbook, Vol 4. *Ceramics and Glasses*. 1991, ASM International, The Materials Information Society. USA.
10. Smith, H., J., *The Effect of Refractory Mill Additions on the Corrosion and Abrasion Resistance of Porcelain Enamels*. Proc. Porc. Enam. Inst. Tech. Forum, 1963. **25**.
11. Nakazato, Y., Kuguminato, H., Soeda, N., and Takahashi, I., *A study of Bubble Structure in Porcelain Enamel*. Transactions ISIJ, 1980. **20**.
12. Biller, L.N., *Investigation of Fired Bubble Structure-Wet and Dry*. Ceramic Engineering and Science Proceedings, 1990. **11**(5-6).
13. Smalley, H.F., *The Effect of Bubble Structure on Chemical and Physical Properties of Ground Coat Porcelain Enamels*. Proc. Porc. Enam. Inst. Tech. Forum., 1964. **26**.
14. *Enamelling Manual.*, Unknown, Australia.
15. Escol, *The Vitreous Enameller's Diary*. 1994: Escol.
16. Bergeron, C.G., J. Amer. Ceram. Soc., 1953. **36**.
17. Currie, T.E., *The Effect of Mill Additions on the Rheology of Enamel Slips*. Proc. Porc. Enam. Inst. Tech. Forum, 1970. **32**.

Chapter Four
Phase Characterisation

Chapter Four
Phase Characterisation

4.1 Introduction

This chapter presents structural and compositonal information on commercial "end use" porcelain enamel ground coatings characterised using conventional techniques such as Energy Dispersive X-ray analysis (EDS) and X-ray diffraction (XRD) and less commonly used techniques such as Raman and Fourier transform infrared spectroscopy (Mid-IR and Far-IR). XRD and Raman spectroscopy were used to obtain data on frits, mill additions and enamel coatings, transmission infrared spectra were obtained for frit and mill additions and attenuated total reflectance (ATR) infrared was used to obtain spectra of the enamel coatings.

4.1.1 Sampling Depth

Penetration depths and effective sampling volumes must be considered when comparing characterisation data of frits, mill additions and coating surfaces. All techniques, except ATR, are bulk specific for effective volume analysed. ATR was only used to obtain spectra of the coating surface and subsurface. A summary of the spectroscopic techniques used in this study and their respective sampling depths are presented in Table 4.1.

The penetration depth of the X-ray for energy dispersive X-ray spectrometry (EDS) is a function of the electron beam energy (accelerating voltage) and whether the material contains elements with high atomic numbers. Typical penetration depths are micrometers[1] so this technique can be considered a sub-surface to bulk analysis. EDS is used to obtain bulk information from cross-sectional area analysis or powdered samples.

In vibrational spectroscopy, penetration depth is dependent on both wavelength and refractive index of the sample.[2] Raman spectroscopy is based on the

comparably weak interaction of photons with matter. Even under strong absorbing conditions, penetration depth of photons is more than fifty atomic layers[4] and so the Raman signal is bulk specific.

Table 4.1 Effective sample volumes for different spectroscopic techniques.

Technique	Sample Type	Penetration depth/Effective Volume
Raman	Powdered samples Glass enamel surface	bulk bulk
Mid IR	Powdered samples	Bulk
Far IR	Powdered samples	Bulk
ATR	Glass enamel surface	0.2 – 4 μm/sub-surface
EDS	Powdered samples Glass enamel surface	bulk 1-3 μm/sub- surface to bulk
XRD	Powdered samples Glass enamel surface	bulk 4-10 μm/bulk

Penetration depth for ATR is wavelength dependent. This method is useful for measuring surface films and coatings as the effect depends on the composition of the outer layer, to a maximum of 25 μm.[3] Typical depths are up to 4 μm.[2]

XRD is considered a bulk technique as the penetration depth of the X-rays range from 4-10 μm. Penetration depth is dependent on the wavelength of radiation used and on the type of material under study.[5]

4.2 Results and Discussion

4.2.1 Frit Characterisation

Many phase changes occur when raw materials and additives are smelted into a uniform glassy sheet to produce frits.[6] A homogeneous chemical composition is only obtained if the melt has been stirred efficiently; this gives rise to other structural groups.

Data from XRD (Figures 4.1 to 4.3) and vibrational spectroscopy (Table 4.6a) indicate that all frits (A1-A5, B1, and B2) have broad spectral features

characteristic of amorphous phases and no crystalline phases were detected. When the melt is cooled rapidly (quenched), crystallisation cannot occur and hence, an amorphous melt phase (solid solution) of the siliceous compound is formed.[7] Data (Tables 4.2 and 4.3) indicate that the predominant phase is amorphous silica (vitreous silica), which is very unstable at the enamel melt temperature and therefore highly soluble.[8] This silica can react with other constituents to form other phases. For example, borosilicate is formed when it reacts with B_2O_3.

The generally accepted structural model for bulk amorphous silica is a continuous random network of interconnected SiO_4 tetrahedral units through bridging oxygen atoms.[9,10] Slight twisting in the bonding produces structural pattern irregularity.[11] Any B_2O_3 and Al_2O_3 in the bulk composition will affect the structure. When alkali oxides are added, Al_2O_3 will exist as AlO_4 in the structural network and B_2O_3 will exist as BO_3 or BO_4 units, depending on the availability of alkali oxides. Interpretation of Raman, IR and XRD spectra must therefore account for these phases.

Qualitative EDS analyses of the frits indicate high silica concentrations (Figures 1 to 7 - Appendix 3) and ICP analyses show silica concentrations of 49 to 71 wt% (Table 3.2). Boron oxide was not detected by EDS but was observed using ICP at concentrations of 5.85 to 14.10 wt%.

The XRD patterns for all frits (Figures 4.1-4.3) have a broad peak at approximately 30 degrees (2θ) similar to the typical X-ray pattern for glass (Figure 1.11). The broad peaks indicate lack of periodicity with overlapping modes. The XRD pattern did not show any crystalline phases even though the bulk composition was analysed. As with EDS, boron oxide was not detected.

Raman spectra of the frits (Table 4.6a) indicate a weak broad band between 490-560 cm^{-1}. Virgo et al[12] attributed a band between 500–700 cm^{-1} (in alkali silicate glass system) to bonding vibrations of Si and non-bonding oxygen (NBO) atoms so the 490-560 cm^{-1} band is tentatively assigned to Si-NBO vibrations.

All frits had another weak broad band between 950-1091 cm^{-1} (Table 4.6a). Raman bands between 550–1200 cm^{-1} (silicate glasses) are generally attributed to Si-O vibrations in SiO_4 tetrahedra as well as Si-O-Si bonds linking the tetrahedra.[13] More precisely, the bands at the higher frequency range, 800 – 1200 cm^{-1}, are attributed to symmetric stretching vibrations of SiO_4 tetrahedra with different numbers of non-bridging oxygen atoms.[12-14] The bands observed between 950-1091 cm^{-1} are most likely due to these SiO_4 vibrations.

IR spectra for all the frits have broad bands at approximately 500(m), 1000(s) and 1400(m) cm^{-1} (Table 4.6a, Figures 3 to 9 - Appendix 4). Bands at 500 and 1000 cm^{-1} are probably associated with amorphous silica[9]. The 1000 cm^{-1} band is tentatively assigned to Si-O-Si and B-O bond vibrations because Stoch et al[15] assigned a band at 1040 cm^{-1} to this effect. The shift to lower frequency is probably because the Si-O-Si and B-O moieties give stronger bonding interactions. The band at 1400 cm^{-1} may be B-O bonds.[15]

The IR spectra of all the frits also have a feature between 700 and 740 cm^{-1} (Table 4.6a), which ranged in intensity from medium in frit A5 to weak in frit A3. This feature is probably due to an amorphous phase in the glassy matrix and is attributed to variation in the bonds of the SiO_4 tetrahedra and/or Si-O-Si bonds.

4.2.2 Characterisation of Mill Additions

Colouring Oxides

Colouring pigments are added when the frits were being milled. During firing, colouring oxides develop as small homogeneous crystals on the phase boundaries. These crystals include opacifiers (for example, antimony oxide and titanium oxide) and various compounds including metal-alumina-silicates.[16] The colouring pigments used in this study are coded as gloss brown A1 (GBA1), gloss green A1 (GGA1), matte black A1 (MBA1), gloss brown B1 (GBB1) and gloss brown B2 (GBB2).

Raman spectra of the colouring pigments yielded little useful information due to poor signal-to-noise ratio, caused mainly by the laser light being absorbed by the

dark pigmentation. The GBA1 spectra had weak and broad bands at 575 and 1093 cm^{-1}, which are attributed to an amorphous phase (Table 4.6b, Figure 11 - Appendix 4). The band at 1093 cm^{-1} was assigned to amorphous silica.[9]

The EDS spectra indicated that all pigments except MBA1 had Si in the bulk phase (Figures 21-25 – Appendix 3). The XRD data (Figures 4.1-4.3) and IR analysis (Table 4.6b) indicated crystalline silica was present and IR spectroscopy detected amorphous silica in the matrix (between 1084 and 1107 cm^{-1}).

The EDS spectra show that all pigments contained Cr, which IR and XRD data indicated was present in different crystalline phases (Tables 4.2 and 4.3; Figures 4.1-4.3). The IR spectra for the pigments showed bands between 369-373 and 501-511 cm^{-1} (Table 4.6b), which are assigned to $FeCr_2O_4$.[17] Bands between 609-620 cm^{-1} could be attributed to $FeCr_2O_4$, Cr_2O_3[18] or $CuCr_2O_4$.[19] However, EDS data showed that none of the pigments except MBA1 contained copper (Figure 23 - Appendix 3). Hence, this band in GBA1, GBB1 and GBB2 can be assigned to $FeCr_2O_4$ or Cr_2O_3 type compounds. The $FeCr_2O_4$ is similar to $(Cr,Fe)_2O_3$ (chromium green hematite) commonly used for colouring porcelain enamels.[20,21]

The XRD and IR data confirmed the presence of elements such as Cr, Si and Fe detected by EDS. For example, the EDS spectrum of GGA1 detected Cr, Si, and Fe (Table 4.2, Figure 22 – Appendix 3) and the XRD pattern indicated that these elements were in the phases $FeCr_2O_4$, SiO_2 and Cr_2O_3 (Figure 4.1). IR spectra also indicated $FeCr_2O_4$ and SiO_2 (Table 4.6b). Some pigments contained trace elements that were only detected by EDS. For example small concentrations of Zn, Na, Al and Ni were found in GBA1 (Figure 22 – Appendix 3).

The XRD and IR spectra of MBA1 (Figure 4.2 and Table 4.6b) indicate the presence of $CuCr_2O_4$ and the IR spectra indicated that $FeCr_2O_4$ and/or Cr_2O_3 were in the matrix. However, Fe was not detected by EDS (Figure 23 – Appendix 3), therefore $CuCr_2O_4$ or Cr_2O_3 is the likely phase.

The XRD and IR spectra of GBB1 and GBB2 indicated that $FeCr_2O_4$ and SiO_2 (Table 4.3) were present. XRD data also indicated that GBB1 contained

$ZnFeCrO_4$ (zinc chromite) and that GBB2 contained $NiFe_2O_4$ (trevorite), $ZnCr_2O_4$ (zincochromite) and Zn_2SiO_4 (willemite) (Figure 4.3). These phases were not detected by IR spectroscopy. The EDS data for GBB1 and GBB2 (Figures 24 and 25 – Appendix 3), indicate elements Zn, Cr, Fe and Si, which are present in the XRD phases.

Other Mill Additions

The EDS analysis indicated that feldspar contained Si, Al, K, Na and O (Table 4.2, Figure 14 - Appendix 3) and XRD data revealed three closely matching phases - microcline ($KAlSi_3O_8$), orthoclase ($KAlSi_3O_8$) (microcline and orthoclase are polymorphs), and albite ($NaAlSi_3O_8$) (Figure 4.2). The vibrational spectroscopy band positions matched the microcline and albite phases (Table 4.6c). Andrews[8] reports that orthoclase and albite are typical commercial feldspars.

Silica is a mill addition in all the enamel batches. Raman and IR spectra indicated the presence of α-quartz (Table 4.6d). The XRD pattern also indicated that silica was present as crystalline quartz (Figure 4.1).

The three clays (HB clay, Kaolex and GBB) for suspending and adjusting the slip were added to their respective enamel slip batches before milling. Vibrational spectra (Table 4.6d) of all clays were similar, indicting that similar phases were present. IR spectra of the clays were more defined than the Raman spectra with IR bands at 800 to 3700 cm^{-1} closely matching the $Al_2Si_2O_5(OH)_4$ (kaolinite) reported by Johnson et al.[22] Features attributed to microcline and albite phases were also observed. These are dominant phases detected in the feldspar mill addition (Table 4.6c). The XRD pattern indicated SiO_2 and $Al_2Si_2O_5(OH)_4$ (kaolinite) were the dominant phases for the three clays (Figures 4.1-4.3).

The chief constituent of the clay-like mill addition bentonite is the clay mineral montmorillonite ($Al_2O_3.5SiO_2.7H_2O$).[23] The XRD pattern shows that montmorillonite ($Na_{0.3}(Al,Mg)_2Si_4O_{10}(OH)_2.8H_20$) and SiO_2 are present (Figures 4.1 and 4.2), but Raman spectral bands were not observed because of the poor

signal-to-noise ratio. However, the IR spectrum bands could be attributed to bentonite[24] (Table 4.6e, Figure 19 - Appendix 4).

Boric acid is a mill addition that introduces boric oxide into the melt. The XRD pattern indicated that H_3BO_3 (hydrogen borate) was present (Figure 4.3), and vibrational spectra indicated that boric acid was present[25,26] (Table 4.6f, Figure 26 - Appendix 4). The EDS analysis indicated that borax (fluxing agent) contains B, Na and O (Table 4.2, Figure 11 - Appendix 3). The B peak is very weak because the detector is insensitive to low atomic number elements. However, sodium borate hydroxide hydrate ($Na_2B_4O_5(OH)_4.8H_2O$) was identified by XRD (Figures 4.1 and 4.2). Raman and IR spectra of the borax (Table 4.6g) closely matched those reported in the literature.[27]

The mill addition magnesium carbonate is added to enamel batches (except MBA) for flocculation (electrolyte) and to control particle suspension. Its elemental composition is predominantly Mg, O, and Al, with lower concentrations of Ca (Table 4.2, Figure 17 - Appendix 3). Two principal phases, $Mg_5(CO_3)_4(OH)_2.4H_2O$ (hydromagnesite) and $MgCO_3.5H_2O$ (lansfordite), were determined from XRD patterns (Figure 4.1). Raman and IR spectra (Table 4.6h, Figure 21 - Appendix 4) support the presence of these phases, indicating the presence of magnesium carbonate ($MgCO_3$). The Al and Ca identified by EDS are probably impurities in the mill addition.

The MBA batch contains calcined alumina to decrease coating gloss and produce a matte finish. EDS analysis indicated the presence of Al and O (Table 4.2, Figure 8 - Appendix 3) whilst XRD analysis indicated Al_2O_3 was present (Table 4.2, Figure 4.2). Raman and IR spectral bands matched the reported bands[28,29] for α-Al_2O_3 (Table 4.6i), so α-Al_2O_3 is considered to be the phase in the mill addition.

The MBA batch also contains antimony oxide. The EDS spectrum indicates that Sb, Ti and possibly Ca were present (Table 4.2, Figure 9 - Appendix 3). The XRD pattern indicated the possible presence of calcium antimony oxide ($Ca_2Sb_2O_7$) and antimony oxide (Sb_6O_{13}) phases, suggesting that Ca is a component of the mill

addition (Figure 4.2). The band positions produced from both vibrational techniques most closely matched those reported for Sb_2O_3[30] (Table 4.6j).

4.2.3 Characterisation of Enamel Coatings

Raman and IR spectra and XRD patterns were obtained for the enamel coatings. These techniques indicated many amorphous phases were present, which is consistent with the bulk of the enamel being made of the amorphous silica-based frit. However, the frits were totally amorphous whereas crystalline phases were observed in the amorphous material of the porcelain enamel coatings. These crystalline phases are introduced though mill additions and fusing of the enamel slip onto the base metal. Most of these crystalline phases are attributed to colouring oxides.

Amorphous Phases

The XRD patterns of all the coatings (Figures 4.1, 4.2 and 4.3) have a broad peak at approximately 30 degrees (2θ) indicating a mainly amorphous silica phase, similar to that for the frits.

Raman spectra of all coatings (Figure 4.5) have a band at approximately 840 cm^{-1}, which is attributed to a silicate phase reported by McMillian.[13] The intensity of this band is weak in all samples except MBA, which ICP analysis (Table 3.6) indicated had the most Al_2O_3. Higher concentration of Al_2O_3 and/or alkali oxides can influence band intensity. Fukumi et al[31] reported that alkali oxide concentration could also affect Raman scattering intensities of silicate bands.

Raman spectra showed that all frits had a weak broad band between 480 and 550 cm^{-1} (Figure 4.5, Table 4.6k). This most closely reported band at 475 cm^{-1} is attributed to the bending or rocking of the B-O-Si or Si-O-Si bridging[14] or SiO_4 and Si-O-Si bonds.[13] The weak bands at about 1296 cm^{-1} (Figure 4.5, Table 4.6k) for most coatings are attributed to the B-O stretching modes of SiO_2-B_2O_3 glass.[14]

ATR-IR spectra of the coatings (Figure 4.6, Table 4.6k) are more surface specific than Raman and FT-IR spectra. Two dominant bands were observed – at 1200-

1250 cm^{-1} and at 1408-1480 cm^{-1} (medium and broad bands). Both bands are attributed to B-O stretch modes [15,32] indicating that boron is distributed near the sample surface.

Crystalline phases

The XRD and vibrational spectroscopic analyses of the coatings indicate that oxides are present as crystalline phases in the amorphous material of the glassy matrix. Many of the crystalline phases are similar to those for powdered samples of the colouring pigments.

The XRD pattern for the GGA coating (Table 4.4, Figure 4.1) indicated the crystalline phases Cr_2O_3 and SiO_2. These phases were also in the colouring pigment GGA1 (Table 4.2, Figure 4.1). The quartz phase matches the quartz phase in HB clay and Kaolex clay. The $FeCr_2O_4$ in the colouring pigment GGA1 was not detected in the coating by XRD or vibrational spectroscopy. However, the EDS spectrum indicated a small Fe peak in the GGA1 colouring pigment (Figure 22 - Appendix 3) and coating (Figure 27 - Appendix 3). Consequently, the $FeCr_2O_4$ phase is postulated to be only a very small component in the overall structure.

Raman analysis of the GGA coating detected crystalline phases attributed to Cr_2O_3, and SiO_2 (Table 4.6k, Figure 4.5) supporting the XRD data (Figure 4.1). The well-defined shoulder at 549 cm^{-1} observed on the band at 475 cm^{-1} (Figure 4.5) has been assigned to Cr_2O_3.[33] This band was not in the spectra of other coatings and notably was not present in the spectrum of GBA, in which the only difference in composition is from the colouring pigments. The more sub-surface specific technique, ATR-IR spectroscopy, indicated the presence of Cr_2O_3, SiO_2 and Al_2O_3 (Figure 4.6, Table 4.6k), which was not detected in the bulk of the coating by Raman spectroscopy.

The XRD pattern for the GBA coating indicated the crystalline phases SiO_2 and $FeCr_2O_4$. The SiO_2 phase peaks for the coating (Figure 4.1) match those for the colouring pigment (GBA1), the mill addition silica, and the silica phase in HB

clay. The $FeCr_2O_4$ phase matches the phase present in the colouring pigment GBA1 pattern (Figure 4.1). The $FeCr_2O_4$ is detected in GBA coating possibly because the colouring pigment has a high Fe content (Figure 21 - Appendix 3). Raman spectroscopy of the GBA coating indicated Cr_2O_3 and possibly a microcline or albite phase (Tables 4.6k; Figure 4.5). Cr_2O_3 is also present in the colouring pigment spectrum. The bands detected by ATR-IR spectroscopy of the coating can be attributed to Cr_2O_3 and Al_2O_3 (Table 4.6k).

The EDS spectrum indicates that the MBA coating has many elements (Figure 28 - Appendix 3). The highest peaks correspond to Si, Al and O. The XRD pattern revealed the presence of two crystalline phases (Table 4.4, Figure 4.1). The major phase, $CuCr_2O_4$, matches that of the mill addition MBA1 (Figure 4.1) and the phase orthoclase $(K,Ba,Na)(Si,Al)_4O_8$ is also present. The ATR-IR spectrum (Table 4.6k; Figure 4.6) shows bands that match $CuCr_2O_4$ and SiO_2.

The EDS analysis of the GBB coating (Figure 29 - Appendix 3) indicated Si as the dominant element and the XRD pattern (Figure 4.3) indicates a major peak for crystalline SiO_2. This SiO_2 is consistent with peaks in the silica mill addition spectra. The XRD pattern also indicates that the coating contains $FeCr_2O_4$ and Raman spectra (Table 4.6k, Figure 4.5) indicate that α-quartz (SiO_2) and amorphous silica are present. ATR-IR spectroscopy detected crystalline SiO_2 at 775 cm^{-1} (Table 4.6k, Figure 4.6). The band at 586 cm^{-1} (Table 4.6k) could be attributed to Al_2O_3 (600 cm^{-1}).[29]

4.3 Summary

Spectroscopic investigations of porcelain enamels demonstrate that these systems are very complex with many different amorphous and crystalline phases.

The XRD and vibrational spectra of frit samples showed that amorphous phases are dominant. The main composition of the frits was determined as silicates and borates. Si-O and Si-O-Si (950-1091 cm^{-1}) vibrations (broad bands) characteristic of SiO_4 tetrahedra, were found in both the Raman and IR data. However, only the IR technique was capable of identifying the presence of B-O bonds associated

with B_2O_3 (as BO_3 or BO_4 units). The XRD data was in agreement with the vibrational analysis. In all cases, a broad peak at approximately 30° (2θ) typically associated with glass dominated the spectra.

By contrast, the colouring pigments appeared to be crystalline. All the pigments contained Cr as shown by EDS. The IR and XRD spectra indicated that Cr was present in many crystalline phases including $FeCr_2O_4$, Cr_2O_3 and $CuCr_2O_4$. The EDS, IR and XRD results also showed that all the pigments except MBA1 contained Si in the form of crystalline SiO_2.

Vibrational spectroscopy and XRD data indicated that amorphous phases were present in the fired glass enamel coatings. However, crystalline compounds could be detected in the amorphous material of the glassy matrix. The dominant components in the amorphous phase are borates and silicates. These compounds were identified through the presence of B-O-Si, Si-O-Si and B-O stretching modes in the Raman spectra. The presence of amorphous silica was confirmed by XRD analysis. The ATR-IR spectra of the coatings, which are surface specific, are dominated by B-O stretching modes at 1200-1250 and 1408-1480 cm^{-1}. This suggests that borates were found at the coating surface. Many of the crystalline phases in the fired enamel coating detected by XRD and vibrational spectroscopic analysis including $FeCr_2O_4$, Cr_2O_3 and SiO_2 matched those in the colouring pigments.

The results in this chapter showed that Raman and IR spectroscopy provides useful structural and compositional information on oxide materials. Vibrational spectroscopy, XRD and EDS data allowed finger printing (phase characterisation) of the batch components and the resultant porcelain enamel coatings. This information can be used to develop new formulations, which will improve the performance of porcelain enamel coatings and their finish quality.

Table 4.2 Characterisation summary of components used in fabrication of GBA, GGA and MBA porcelain enamel coatings.

Component	EDS*	XRD Formula/name/matched ICDD reference cards	Raman	Infrared
Frit A1	**Ca**, Na, Al, **Si**, K, Ba, Mn, Fe, Ni, Mg, O	amorphous	amorphous silica, Si-O, B-O-Si, Si-O-Si, SiO_4,	amorphous silica
Frit A2	**Na**, Al, **Si**, K, **Ca**, O	amorphous	amorphous silica, Si-O, B-O-Si, Si-O-Si, SiO_4,	amorphous silica, Si-O-Si, BO_4, B-O
Frit A3	Na, Al, **Si**, K, Ca, Ba, Fe, Co, Ni, Cu	amorphous	amorphous silica, B_2O_3, Si-O, B-O-Si, Si-O-Si, SiO_4	amorphous silica, Si-O-Si, BO_4, B-O
Frit A4	**Si**, Na, Al, K, Ca, Ba, O	amorphous	amorphous silica, Si-O, B-O-Si, Si-O-Si, SiO_4,	amorphous silica, Si-O-Si, BO_4, B-O
Frit A5	**Si**, **Al**, Na, K, Ca, Co, O	amorphous	amorphous silica, Si-O, B-O-Si, Si-O-Si, SiO_4,	amorphous silica, Si-O-Si, BO_4, B-O
Colouring GBA1	**O**, Zn, Na, Al, **Si**, **Cr**, **Fe**, Ni	$FeCr_2O_4$, #34-0140, Chromite, syn; SiO_2, #46-1045, Quartz	Cr_2O_3	$FeCr_2O_4$, Cr_2O_3, quartz and amorphous silica
Colouring GGA1	**Cr**, Si, Fe, O	Cr_2O_3, Chromium oxide (Eskolaite), #38-1479; $FeCr_2O_4$, Chromite, #34-0140; SiO_2, Silica, #46-1045		$FeCr_2O_4$ quartz and amorphous silica
Colouring MBA1	**Cr**, Cu, C, O	$CuCr_2O_4$, Copper Chromite, #34-0424		$CuCr_2O_4$, Cr_2O_3 and $FeCr_2O_4$
Silica	**Si**, O	SiO_2, Quartz, #46-1045	α-quartz	α-quartz
HB Clay	**Si**, **Al**, Ti, **O**	SiO_2, Quartz, #46-1045: $Al_2Si_2O_5(OH)_4$, Kaolinite, #29-1488	kaolinite	kaolinite, α-quartz, microcline, albite
Kaolex Clay	**Al**, **Si**, K, Ti, Fe, **O**	$Al_2Si_2O_5(OH)_4$, Kaolinite, #29-1488; SiO_2, Quartz, #46-1045	kaolinite	kaolinite, α-quartz, microcline, albite
Feldspar	**Si**, **Al**, **K**, Na, **O**	$KAlSi_3O_8$, Microcline, #19-0926; $KAlSi_3O_8$, Orthoclase, #22-0687; $NaAlSi_3O_8$, Albite, #19-2284	microcline and albite	microcline and albite
Bentonite	**Al**, **Si**, Ca, Fe, Na, **O**, C	SiO_2, Quartz, #46-1045; $Na_{0.3}(Al,Mg)_2Si_4O_{10}(OH)_2 \cdot 8H_20$, Montmorillonite, #29-1499	-	bentonite
Borax	**B**, **Na**, **O**	$Na_2B_4O_5(OH)_4.8H_2O$, Sodium borate hydroxide hydrate, #33-1215	borax	borax
Magnesium Carbonate	**Mg**, C, **O**, **Al**, Ca	$Mg_5(CO_3)_4(OH)_2.4H_2O$, Hydromagnesite, #25-0513; $MgCO_3.5H_2O$, Lansfordite, #21-0959	magnesium carbonate	magnesium carbonate
Calcined Alumina	**Al**, O	Al_2O_3, Corundum, #43-1484; Al_2O_3, Aluminium oxide, #29-0063	α-Al_2O_3	α-Al_2O_3
Antimony Oxide	**Sb**, Ti, Ca	amorphous phase, $Ca_2Sb_2O_7$, Calcium antimony oxide, #02-1348; Sb_6O_{13}, Antimony oxide, #33-0111	Sb_2O_3	Sb_2O_3

*Elements with high intensity peaks from EDS spectra are shown in bold.

Table 4.3 Characterisation summary of components used in the fabrication of GBB porcelain enamel coating.

Component	EDS*	XRD Formula/name/matched ICDD reference cards	Raman	Infrared
Frit B2	O, **Na**, Al, **Si**, K, Ti, Ni	Amorphous phases	Amorphous Si-O, B-O-Si, Si-O-Si, SiO_4,	Amorphous silica, BO_4, Si-O-Si, B-O
Frit B1	O, Na, **Si**, P, K, Ca, Ti, Co, Ni	Amorphous phases	Amorphous Si-O, B-B_2O_3O-Si, Si-O-Si, SiO_4, B_2O_3	Amorphous silica BO_4, Si-O-Si, B-O
Colouring pigment 1 GBB1	**O**, Na, **Si**, Al, **Cr**, **Fe**, **Zn**	$FeCr_2O_4$, Chromite, #34-0140 SiO_2, Quartz, #46-1045 $ZnFeCrO_4$, Zinc chromite, #43-0554		Amorphous silica $FeCr_2O_4$, quartz
Colouring pigment 1 GBB2	C, **O**, **Zn**, Na, Al, **Si**, Ti, **Cr**, **Fe**	$ZnCr_2O_4$, Zincochromite, #22-1107 $NiFe_2O_4$, Trevorite, #10-0325 SiO_2, Quartz, #46-1045 Zn_2SiO_4 willemite #01-1076		$FeCr_2O_4$, Quartz, Amorphous silica
Silica	O, Si	SiO_2,Quartz, #46-1045	α-quartz	α-quartz
Clay GBB	O, **Al**, **Si**, K, Ti, Fe	$Al_2Si_2O_5(OH)_4$, Kaolinite, #29-1488 SiO_2, Quartz, #46-1045	Kaolinite	kaolinite, α-quartz, microcline, albite
Suspension agent	C, O, **Si**, Al	amorphous phase	Amorphous silica	Amorphous silica
Boric Acid	**O**, B	H_3BO_3, Hydrogen borate, #30-0620	Boric acid	Boric acid
Magnesium Carbonate	C, **O**, **Mg**, Al, **Ca**	$Mg_5(CO_3)_4(OH)_2.4H_2O$, Hydromagnesite, #25-0513 $MgCO_3.5H_2O$, Lansfordite, #21-0959	$MgCO_3$	$MgCO_3$

*Elements with high intensity peaks from EDS spectra are shown in bold.

Table 4.4 Characterisation summary results of porcelain enamel coatings.

Enamel Coating	EDS*	XRD Formula/name/matched ICDD reference cards	Raman	Infrared
GBA	**Si**, Al, Ca, Na, K, Fe, Ni, Cu, Cr, O, Co	Amorphous phase $FeCr_2O_4$, Chromite, #34-0140 SiO_2, Quartz, #46-1045	Amorphous silica, Cr_2O_3	Cr_2O_3, B-O
GGA	**Si**, Al, Ca, Na, K, Fe, Ni, Cr, **O**, Co	Amorphous phase Cr_2O_3, Chromium oxide, #38-1479 SiO_2, Quartz, #46-1045	Amorphous silica, Cr_2O_3	Cr_2O_3, B-O
MBA	**Si**, **Al**, Ca, K, Na, Ba, Cr, Ni, Cu, Co, **O**	Amorphous phase, $CuCr_2O_4$, Copper chromite, #26-0509 $(K,Ba,Na)(Si,Al)_4O_8$, Orthoclase, #19-0002	Amorphous silica, B_2O_3	$CuCr_2O_4$, α-quartz, B-O
GBB	Ni, Al, **Si**, K, Ca, Ti, Mn, Co, Cr, Zn	SiO_2, Quartz, #46-1045 $FeCr_2O_4$, Chromite, #34-0140	Amorphous silica, α-quartz	α-quartz, B-O
GBC	Ba, Ni, Al, **Si**, Cu, Cr, Zn, Co	$ZnFeCrO_4$, Zinc chromite, #43-0554 $FeCr_2O_4$, Chromite, #34-0140 SiO_2, Quartz, #46-1045	Amorphous silica, B_2O_3	Cr_2O_3, B-O

*Elements with high intensity peaks from EDS spectra are shown in bold.

Table 4.5 Symbols representing compounds in XRD patterns (Figures 4.1 - 4.4).

Symbol	Compound Formula	Name
ø	SiO_2	Quartz
Ù	$Ca_2Sb_2O_7$	Calcium antimony oxide
+	Sb_6O_{13}	Antimony oxide
†	Al_2O_3	Aluminium oxide
Y	H_3BO_3	Hydrogen borate
∞	$MgCO_35H_20$	Lansfordite
þ	$Mg_5(CO_3)_4(OH)_24H_2O$	Hydromagnesite
Σ	$Na_2B_4O_5(OH)_4.8H_2O$	Sodium borate hydroxide hydrate
λ	Cr_2O_3	Chromium oxide
#	$CuCr_2O_4$	Copper chromite
Φ	$FeCr_2O_4$	Chromite
α	$ZnFeCrO_4$	Zinc Chromite
X	$ZnCr_2O_4$	Zincochromite
β	$NiFe_2O_4$	Trevorite
Ψ	Zn_2SiO_4	Willemite
θ	TiO_2	Rutile
¶	$Al_2Si_2.O_5(OH)_4$	Kaolinite
Π	$KAlSi_3O_8$	Orthoclase
Λ	$NaAlSi_3O_8$	Albite
Ω	$Na_{0.3}(Al,Mg)_2Si_4O_{10}(OH)_2.H_2O$	Montmorillonite
Δ	$Mg_5(CO_3)_4(OH)_2.4H_2O$	Hydromagnesite
O	$MgCO_3.5H_20$	Lansfordite

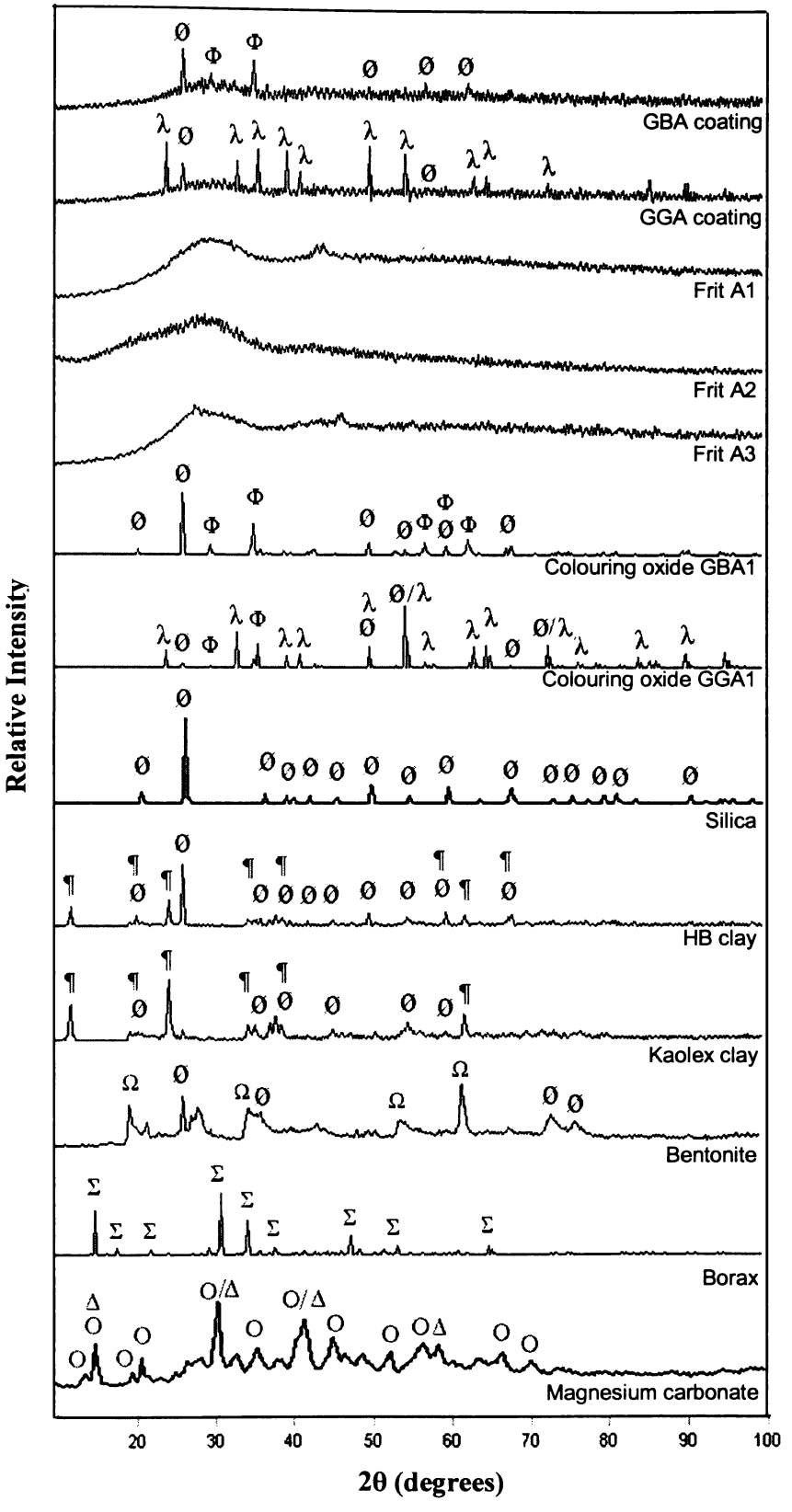

Figure 4.1 XRD patterns of GBA and GGA coating surfaces and their compositional components used in fabrication of the coatings. (Compound formula for each symbol is given in Table 4.5.)

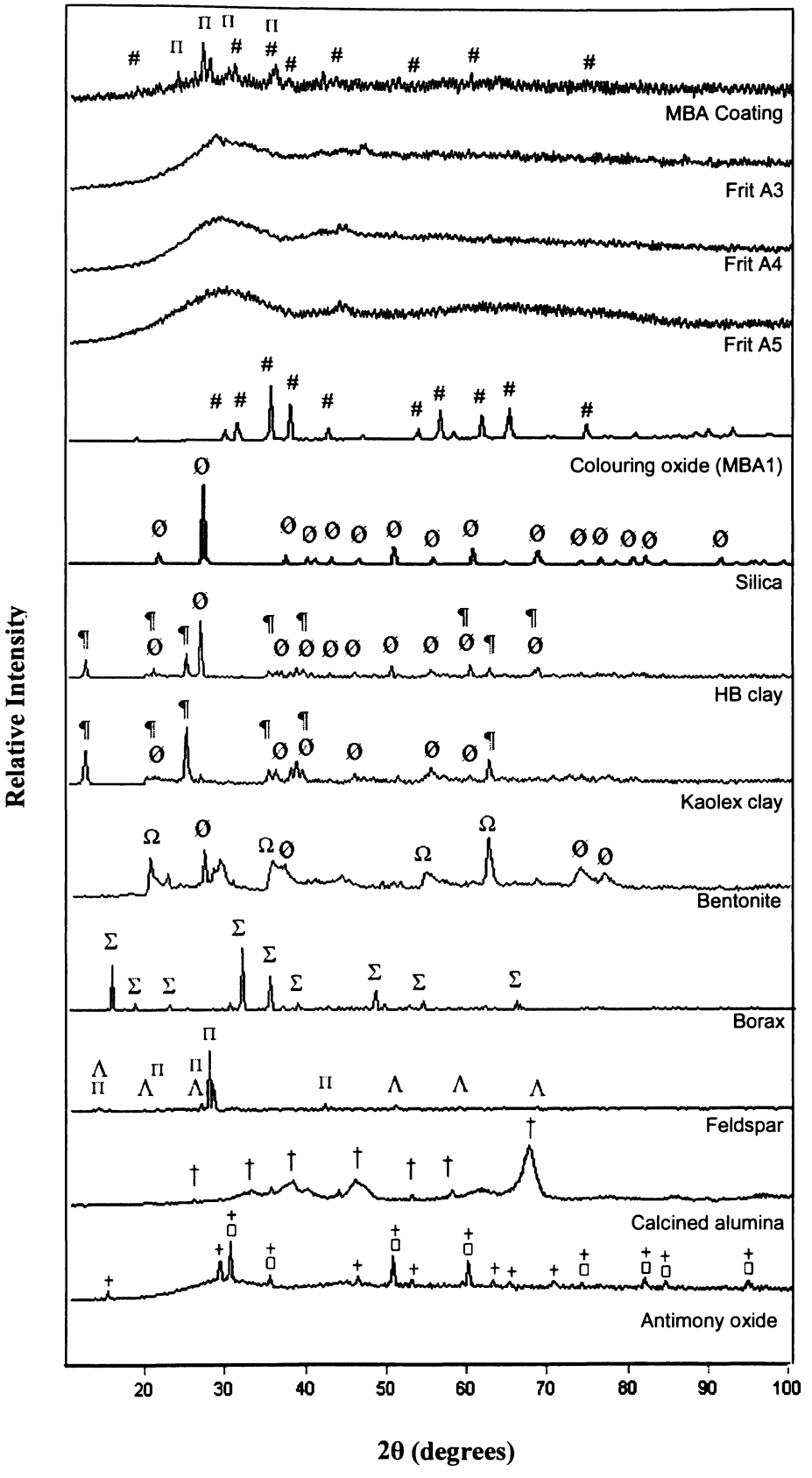

Figure 4.2 XRD patterns of MBA coating surface and compositional components used in fabrication of the coating. (Compound formula for each symbol is given in Table 4.5.)

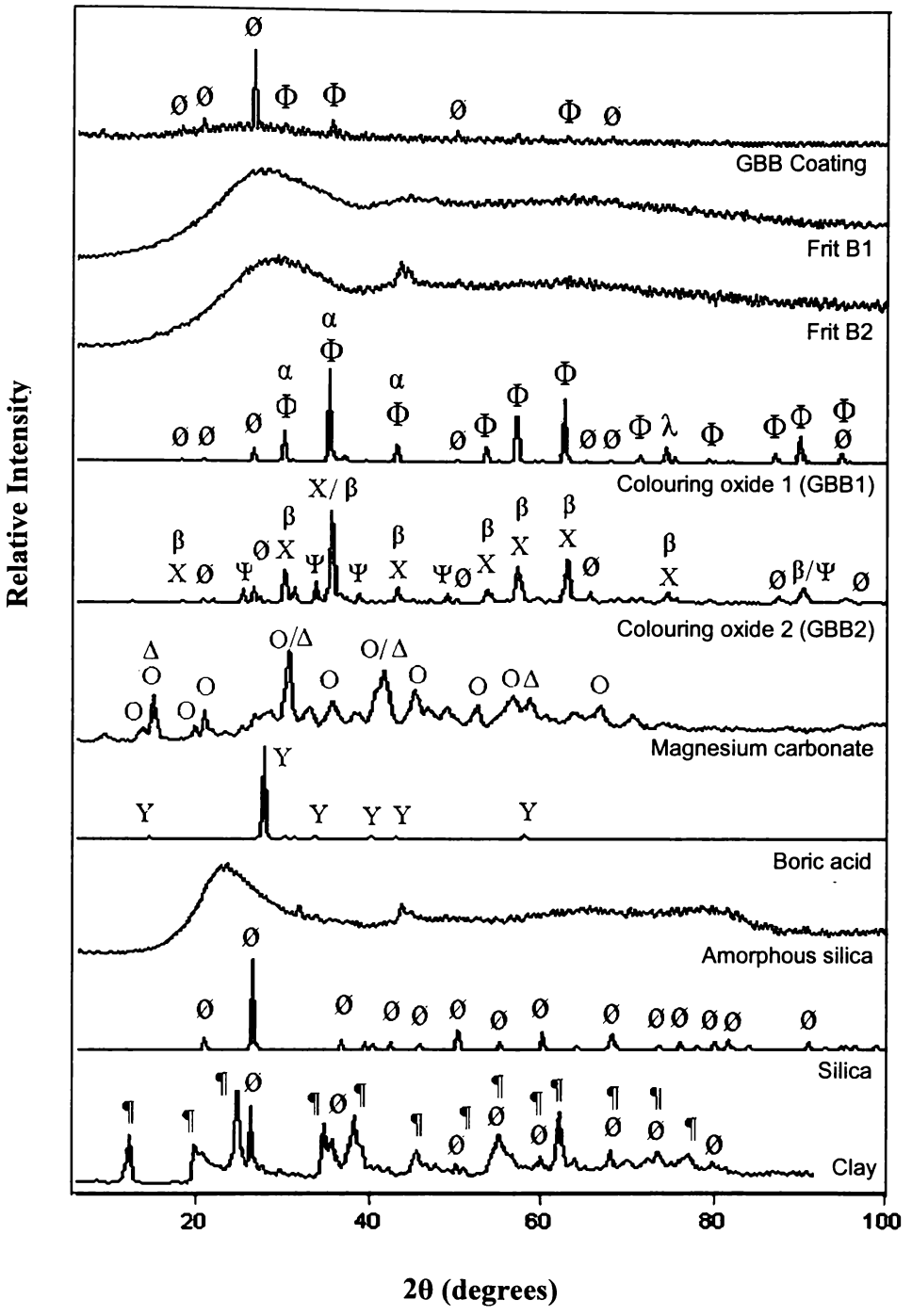

Figure 4.3 XRD patterns of GBB coating surface and compositional components used in fabrication of the coating. (Compound formula for each symbol is given in Table 4.5.)

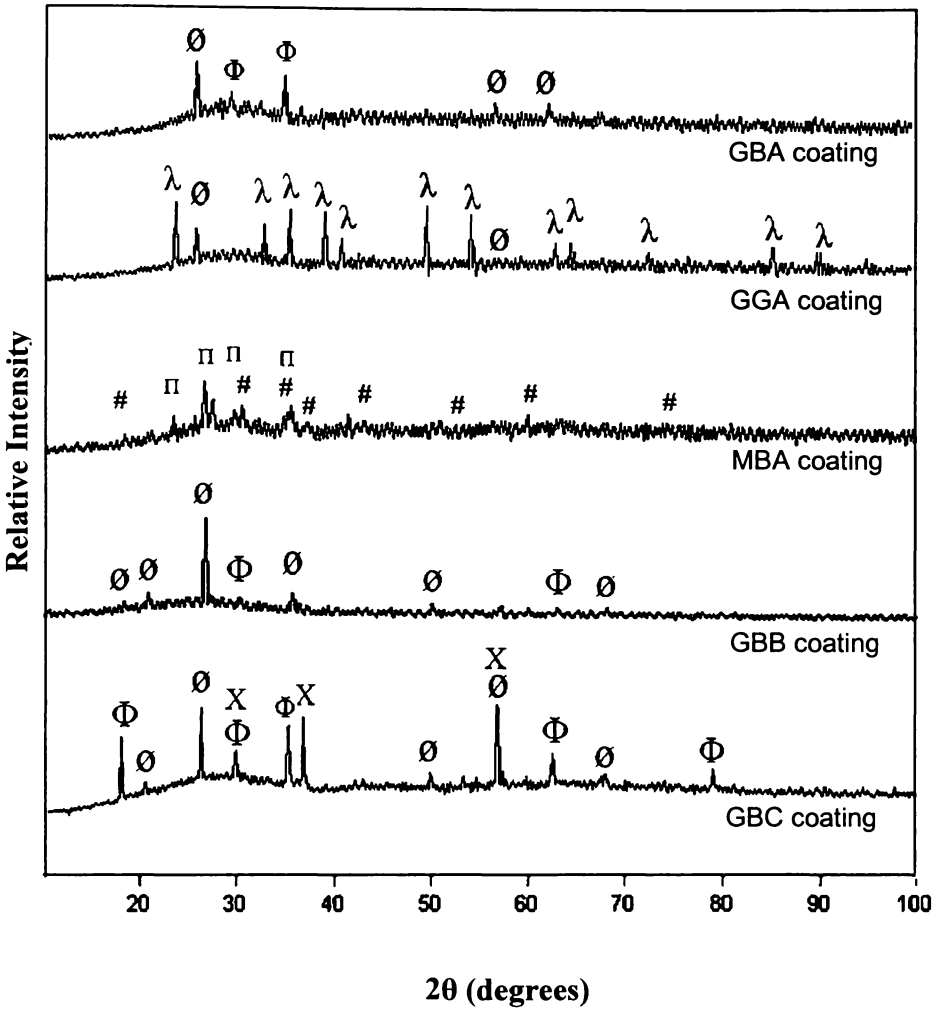

Figure 4.4 XRD patterns of porcelain enamel coating surfaces. (Compound formula for each symbol is given in Table 4.5.)

Table 4.6(a) Raman (R) and Infrared (IR) band assignments* of commercial enamel coatings and compositional components used in fabrication of coatings.

Frit A1		Frit A2		Frit A3		Frit A4		Frit A5		Frit B1		Frit B2		Assignment	Assignment
IR	R	IR	R	IR	R	IR	R	IR	R	IR	R	IR	R	IR	R
	313 w								319w						
480 s,b		487 s,b		485 s,b		444 s,b		450s,b		455 m,b				450 amorphous silica[9]	
	500 w,b		559w, b		534 w,b		500 w,b		491 w,b		538 w				475 B-O-Si, Si-O-Si;[14] 500-700 Si-NBO;[12] 550-1200 SiO_4, Si-O-Si[13]
740 sh		718 w,b		742w		714w		703m, b		711 sh		741 w,b			SiO_4, Si-O-Si (this study)
					813w, b					787 sh	846 w		844 b		800 amorphous SiO_2;[9] 862 B_2O_3[15]; 800-1200 SiO_4[12]; 550-1200 SiO_4, Si-O-Si[13]
1018 s,b		1014 s,b		1020 vs,b		985vs, b		995s,b		1022 s,b		1006 s,b		1000 amorphous silica;[9] 1040 Si-O-Si and B-O[15]	
	1000 w,b		1086 w,b		1091 w,b		1050 w,b		1053 w,b		1058 w,b		950 w,b		1100 amorphous SiO_2;[9] 1050-1100 SiO_4;[13] 800-1200 SiO_4, Si-O;[12]; 1000-1200 Si-O stretching[14]
1430 m		1432 m,b		1410s		1402 s		1414 m,b		1425 m,b		1494 m,b		1400 B-O[15]	

*Relative intensity: vw = very weak, w = weak, m = medium, s = strong, br = broad, sh = shoulder

Table 4.6(b)

Colouring Pigment GBA1		Colouring Pigment GGA1		Colouring Pigment MBA1		Colouring Pigment GBB1		Colouring Pigment GBB2		Assignment	Assignment
IR	R	IR	R	IR	R	IR	R	IR	R	IR	R
				119s							
131w				131s							
262w										257 α-quartz[34]	
370s		373w		369s						370 $FeCr_2O_4$[17]	
395s		400s				401s		402w			
424sh		441w						430w		450 α-quartz[34]; 450w $CuCr_2O_4$[19]	
462s		467m				457m					
510s		508w		524s		501s		511s		510 $FeCr_2O_4$[17]; 510sh quartz[34]	
	575w,b			559s						555s Cr_2O_3[18]	
614s				612vs		609s		620s		625 $FeCr_2O_4$[17]; 625s Cr_2O_3[18]; 605s $CuCr_2O_4$[19]	
		652s									
779m		778w				785w		779w		775 α-quartz[34]	
798m		796w						794w		800 amorphous silica[9]	
1084s,b	1093w,b	1087w,b				1107w,b		1088w,b		1100 amorphous silica[9]	1100 amorphous silica[9]
1168m,b		1148w								1150 amorphous silica[9]	

Table 4.6(c)

Feldspar			
Infrared	Assignment - Microcline[37]/albite[37]	Raman	Assignment - microcline[35]/albite[36]
52w		68w	62
96s	97/93	86w	82
112s	115	113w	110
136m	141,147/-	141w	141
185w	185/185	151w	150
277w	280/275	161w	158/164
327s	330/330	170sh	
374s	370/370	185m	180/185
418s	420/420	209w	200/207
		252w	245/250
		269w	265/268
420s	420/420	291s	285/291
462sh	460/460	329w	330/328
535m	530/530	404w,b	403/407
			412/415
580m	585/590	456w	452/455
605m	605/-	479m	475/479
646m	650/650	507s	512/506
742m	740/750	580vw	580,
769m	765/760	763w	765/763
1008vs	1010/1000	815w	812/815
1046sh	1040	843vw	
1091s	1090/1090	976w	975/976
1139s	1140/1150	1032vw	1035
	-/2300	1099w	1095
	-/2870		1120
			1123
			1136

Table 4.6(d)

Silica		HB clay		Kaloex clay		Clay GBB		Assignment	
IR	R	IR	R	IR	R	IR	R	IR	R
		54w		55s					
	128m				107w				128 α-quartz[38]
			146s		148m				143m kaolinite[39]
		193m		193m		194w			
	206m,b								207 α-quartz[38]
262w	264w							257 α-quartz[34]	265 α-quartz[38]
		277s		277s		277w		280 microcline[37]; 275 albite[37]	
					279vw				270 kaolinite[39]
		347s		345s		347w			
	356w								356 α-quartz[38]
374w		371s		365w	381w	371w		362 α-quartz[34]; 370 microcline[37]; 370 albite[37]	
398w	395w	397w							394 α-quartz[38]
		432s		430s		430m		427 bentonite[24]	
442s							438w	450s α-quartz[34]	
461w	464s							467 bentonite[24]	464 α-quartz[38]
		471vs		471vs		471s			
517m								510sh α-quartz[34]	
		540vs		539vs		538s		530 microcline[37]; 530 albite[37]	
				598sh				590 bentonite[24]	
		647w		648sh				650 microcline[37]; 650 albite[37]	
693m		693m		693m		696m		693w α-quartz[34]	
		756w		751w		754w		740 microcline[37]; 750 albite[37]	
779m		780w						775m α-quartz[34]	
797m		797m		792w				794 kaolinite[22]; 796 bentonite[24]	
								846 bentonite[24]	
						878sh		883 bentonite[24]	
1006s		915s		914m		914m		910 kaolinite[22]; 920 bentonite[24]	
		939w		938sh		937sh	972w	938 kaolinite[22]	
1084s		1006s		1005m		1008s		1005 kaolinite[22]	
	1022w	1033vs		1032m		1032s		1030 kaolinite[22]	
		1097m		1102w		1107m		1116 kaolinite[22]	
1172sh	1154w								1162 α-quartz[38]
		3621s		3618m		3622w		3620 kaolinite[22]	
		3652m		3651w		3654w		3651 kaolinite[22]	
		3666w		3665sh		3672w		3668 kaolinite[22]	
		3694s		3694s		3698m		3696 kaolinite[22]	

Table 4.6(e)

Silica		Mill addition GBB		Bentonite		Assignment	
IR	R	IR	R	IR	R	IR	R
	128m						128 α-quartz[38]
	206m,b						207 α-quartz[38]
262w	264w					257 α-quartz[18]	265 α-quartz[38]
	356w			339w,b			356 α-quartz[38]
374w						362 α-quartz[18]	
398w	395w	388w					394 α-quartz[38]
442s		475s,b		466s		450s α-quartz[18]; 467 bentonite[24]	
461w	464s		468b				464 α-quartz[38]
517m				523s		510sh α-quartz[18]; 525 bentonite[24]	
		594w		590sh		590 bentonite[24]	
				626w		629 bentonite[24]	
693m						693w α-quartz[18]	
779m			779b	795w		775m α-quartz[18]	α-quartz[38]
797m		802w				796 bentonite[24]	
				845w		846 bentonite[24]	
				886w		883 bentonite[24]	
			981b	914w		920 bentonite[24]	
	1022w		1050 b	1016sh		999 bentonite[24]	1072 α-quartz[38]
1084s, b				1048s,b		1043 bentonite[24]	
		1108s		1117sh		1116 bentonite[24]	
	1154w						1162 α-quartz[38]
1172sh		1200sh					
				1637w		1636 bentonite[24]	

Table 4.6(f)

Boric acid			
Infrared	Assignment - H_3BO_3[26]	Raman	Assignment - H_3BO_3[25]
547m		35w	
607sh		104w	
647m		119w	
674w		210m	208m
741sh		500m	498m
793m,b		881s	880s
884m		1169w	
1165sh			
1194s	1195 s		
1227sh			
1420sh			
1468s,b	1471 s,b		
2263w			
2345sh			
2263w	ca 2260		
2345sh			
2363w	ca 2360		
2514w,b	ca 2510		
3223s,b	3223 s,b		
3745w			

Table 4.6(g)

Borax			
Infrared	Assignment - borax[27]	Raman	Assignment - borax[27]
85w		73w	78w, 90m
113m		107w	120m
139w		161w	
162sh		191w	160w
176m		319w	
213m	220s	346m	361m
234w	235s	384m	390w
282sh		407w	
306w	320vb	461m	474m
372w			530wbr
406w		576vs	590vw
445w	430w		
448m	465m	766m	776mbr
525s	525w		
618s	590w	842w	860w
665sh	660w	945m	
773w	710w, 785w	996w	975m
816s			1640vw
833s	828s, 890sh		3140s
948s	947s	3359s,b	3357s
997s	1003vs	3428s,b	3400s, 3447s
1039sh	1038sh	3491s,b	3495s
1072s	1078m	3568m,b	3575s
1128s	1132s		
1151s	1140sh, 1175w, 1235m, 1282m		
1356s	1350vs		
1386s	1385w		
1429vs	1424s, 1483vs		
1650s	1580w, 1656m		
1684s	1710sh		
2151w			
2336w			
3206sh	2875w, 2910w, 3060sh		
3369s	3357vs		
3447s			
3505s	3503s		
3583m	3560		

Table 4.6(h)

Magnesium carbonate			
Infrared	Assignment - $MgCO_3$[41]	Raman	Assignment - $MgCO_3$[40]
431m	362-459		212
485w			332
594m			735
667w		1119w	1096
743w	747-763		
802m			
877sh	876-911		
885m	876-911		
1422s	1446-1599		
1483s	1446-1599		

Table 4.6(i)

Calcined alumina			
Infrared	Assignment - Al_2O_3[29]	Raman	Assignment - Al_2O_3[28]
319s		460w	ca. 450 (514.5 nm)
365s			
406sh			
449w	460m		
493m			
478s,b	600s, 660sh		
771sh	850s		
1379sh			
1505sh			
1650wb			

Table 4.6(j)

Antimony oxide			
Infrared	Assignment - Sb_2O_3[30]	Raman	Assignment - Sb_2O_3[30]
	179	84w	87
	272	120w	121
334b	386		144
	404	191m	193
	482		218
	617	255s	256,
741s	744		298
959w	952, 971		359
		374w	376
			434
		451w	452
			717

Table 4.6(k)

GGA coating		GBA coating		GBB coating		GBC coating		MBA coating		Assignment	
IR	R	IR	R	IR	R	IR	R	IR	R	IR	R
	305										303 Cr_2O_3[33]
			321(w)						320		330 microcline[35]; 328 albite[36]
425 w										435w Cr_2O_3[18]	
	520										510 $CuCr_2O_4$[19]
		538w						540m		555s Cr_2O_3[18]	
	549s		554w,b		560m,b		567m,b		480 w,b		450 amorphous silica[9]; 551 Cr_2O_3[33]; 475 B-O-Si, Si-O-Si[14]; 550-1200 SiO_4, Si-O-Si[13]
593m	611w	591m		586w				597m		600s Al_2O_3[29]; 605 $CuCr_2O_4$[19]	609 Cr_2O_3[33]
	637w			642w	649sh	622w				635 Cr_2O_3[18]	
663m								660m		660s Al_2O_3[29]; 665 Borax[27]	
	687w,b		679w,b		702w,b		689w,b		683w,b		697 α-quartz[38]
740m		745m				748w				750 albite[37]; 720 B-O-B[32]	
				775w				775m		775 α-quartz[34]	
	841w		838m		847w		840w		839m		850 SiO_2[9]
							860w		862w		862 B_2O_3[15]
	883w		895w				893w		890w		893, 894 silicates[42]; 900 SiO_4[13]
	917w		915w		915w		907w		914w		915 kaolinite[39]
1204vs		1207vs		1250vs		1231vs		1198vs		1265 B-O[32]	
	1292w		1296w						1296w		1250-1500 B-O[14],800-1200[12]
1480s		1408s		1467m, b		1467m, b		1451s		1400 B-O[15]; 1350 BO_4[32]	

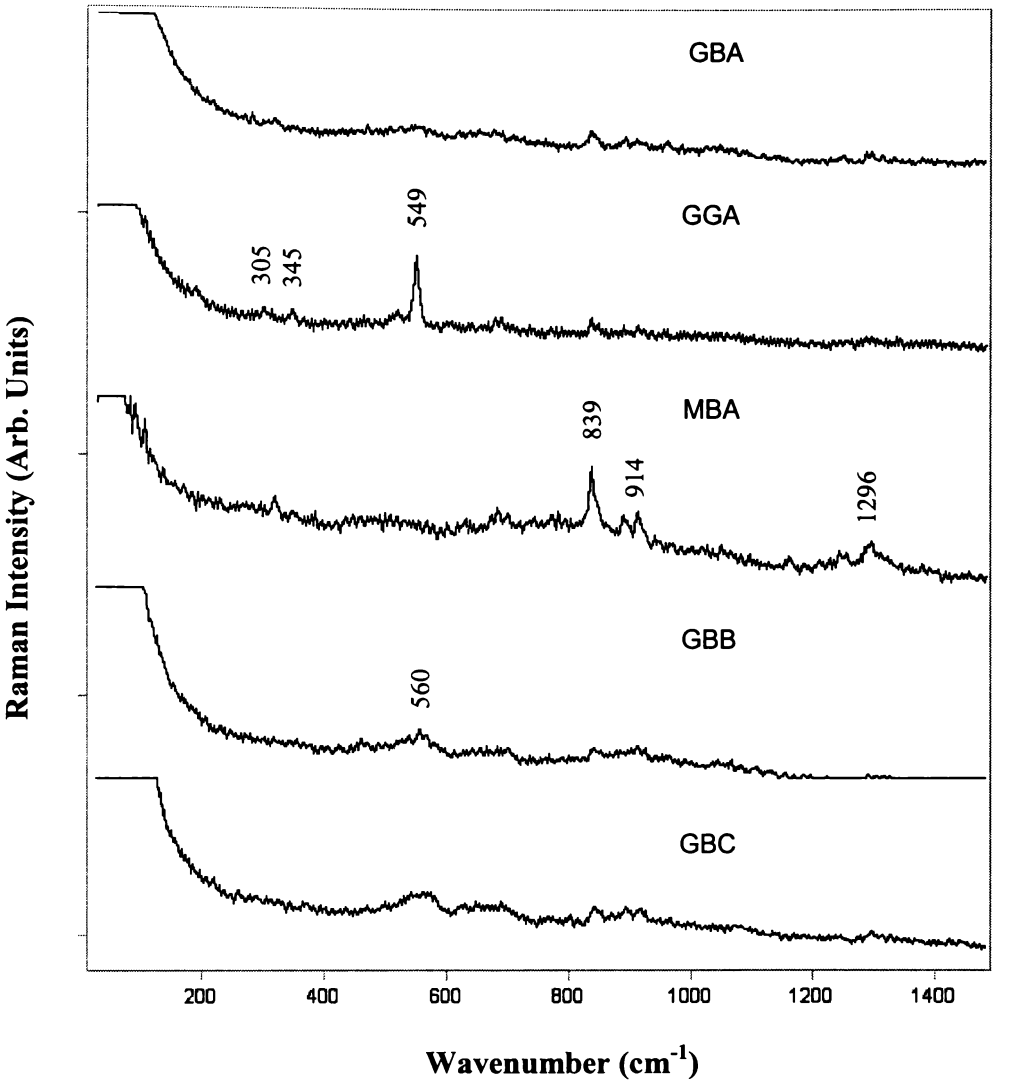

Figure 4.5 Raman spectra of porcelain enamel coating surfaces.

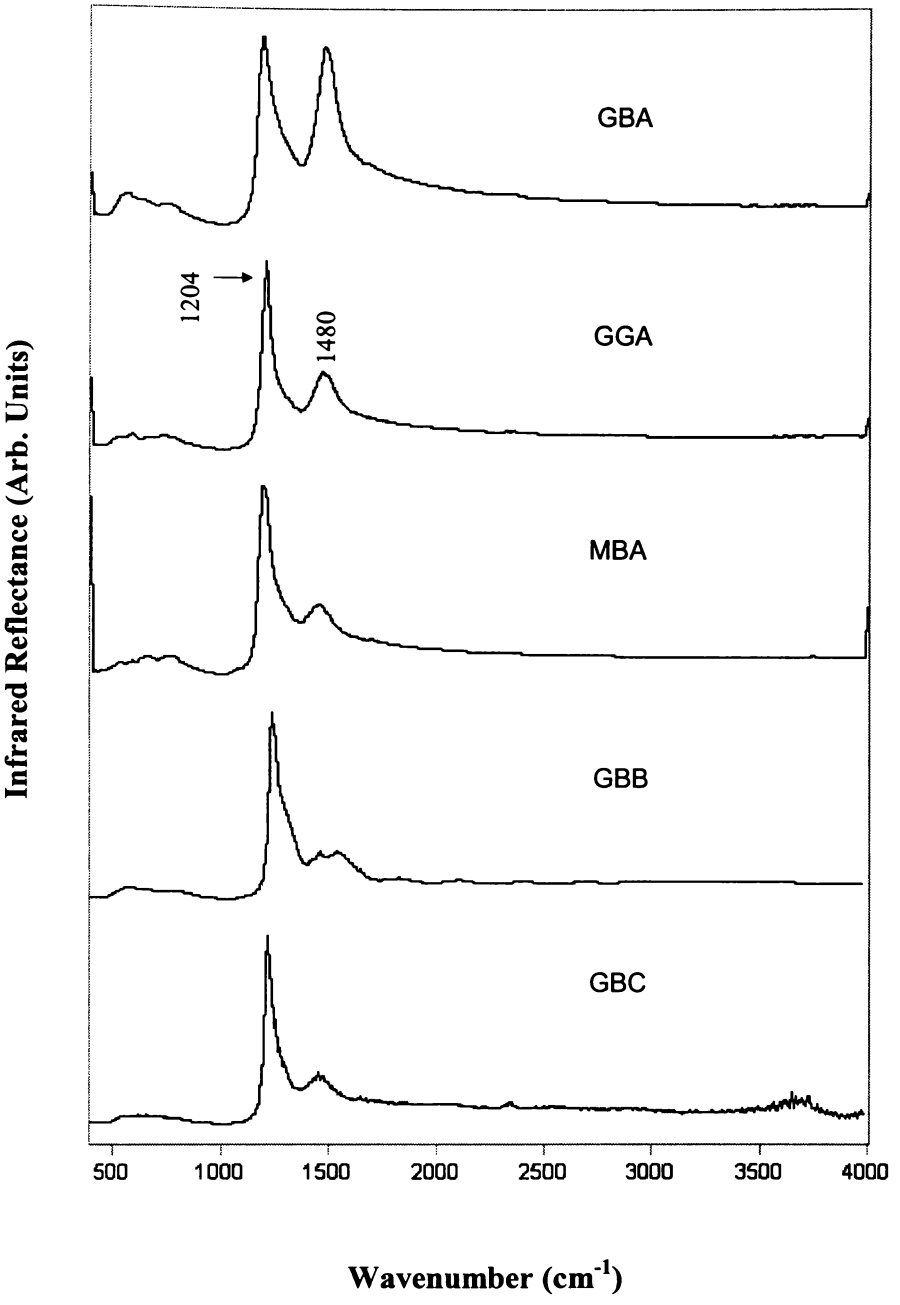

Figure 4.6 Infrared reflectance (ATR) spectra of porcelain enamel coating surfaces.

4.4 References

1. Wells, O.C., *Scanning Electron Microscopy*. 1974: McGraw-Hill.
2. Coleman, P.B., *Practical Sampling Techniques for Infrared Analysis*. 1993: CRC Press.
3. Browning, D.R., *Spectroscopy*. 1969: McGraw-Hill London.
4. Esser, N., Hinrichs, K., and Richter, W, *Raman Scattering from Surface Phonons on Semiconductors*. http://www.pcross.org/icorsxm/paper/richter.pdf., .
5. IBM-Microelectronics, *X-Ray Diffraction (Polycrystalline)*. www-3.ibm.com/chips/services/asg/capabilities/asweb43.html., .
6. Bryant, E.E., *Porcelain Enameling Operations*. 1964, Cleveland, Ohio: Enamelist Publishing Company.
7. Vargin, V., *Technology of Enamels*. 1968: Maclaren and Sons Ltd.
8. Andrews, A.I., *Porcelain Enamels. The Preparation , Application, and Properties of Enamels*. 1961: The Garrard Press, Publishers.
9. Murray, C.A.and .Greytak., T.J., *Intrinsic surface phonons in amorphous silica.* Phys. Rev. B, 1979. **20**: p. 3368.
10. Zachariasen, W.H., J. Am. Chem. Soc., 1932. **54**: p. 3841.
11. Duffy, J.A., *Bonding, Energy Levels and Bands in Inorganic Solids*. 1990, Harlow Essex, England: Longman Scientific and Technical. 249.
12. Virgo, D., Mysen, B.O., and Kushiro, I., *Anionic constitution of 1-atmosphere silicate melts: implications for the structure of igneous melts.* Science, 1980. **208**: p. 1371.
13. McMillan, P., *Structural Studies of Silicate Glasses and Melts - Applications and Limitations of Raman Spectroscopy.* American Minreralogist, 1984. **69**: p. 622-644.
14. Furukawa, T., and White, W.B., *Raman Spectroscopy of Heat-Treated B_2O_3-SiO_2 Glasses.* J. Amer. Ceram. Soc., 1981. **64**(8): p. 443-447.
15. Stoch, A., Stoch, J. and Paluszkiewicz, C., *Spectroscopic Investigations of Metal-Ceramic Enamel Interface.* : p. 45-52.
16. Maskall, K.A. and White, D., *Vitreous Enamelling - A Guide to Modern Enamelling Practice*. 1986.
17. Allen, G.C.and Paul, M., Appl. Spectrosc., 1995. **49**: p. 451-8.
18. Preudhomme, J. and Tarte, P., Spectrochim. Acta, 1971. **27A**: p. 1817-35.
19. Basak, D. and Ghose, J., Spectrochim. Acta, 1994. **50A**: p. 713-18.
20. Eppler, R.A., *Ceramic Coatings*, in *Engineered Materials Handbook-Ceramics and Glasses*. 1991, ASM International.
21. Burgyan, A. and Eppler, R.A., *Classification of Mixed-Metal-Oxide Inorganic Pigments.* American Ceramic Society Bulletin, 1983. **62**(9).
22. Johnston, C.T., Agnew, S.F. and Bish, B.L., Clays and Clay Minerals, 1990. **38**: p. 575-583.
23. Industry, C., *Materials Handbook*, in *Ceramic Industry*. 1992. p. 1-109.
24. Chgristidis, G.E., Scott, P.W. and Marcopoulos, T., Clays and Clay Minerals, 1995. **43**: p. 63-77.
25. Erdemir, A., Halter, M. and Fenske, G.R, Wear, 1997. **205**: p. 236-9.
26. Kim, Y.Y., Lim, J.T. and Park, S.H., Phys. Chem. Solids, 1999. **60**: p. 969-73.
27. Devi, S.A., Philip, D. and Aruldhas, G., J. Solid State Chem., 1994. **113**: p. 157.
28. Porto, S.P.S. and Khrishnan, R.S., J. Chem. Phys., 1967. **47**: p. 1009-1012.
29. Nyquist, R.A. and Kagel, R.O., *Infrared Spectra of Inorganic Compounds 3800-45 cm^{-1}*. 1971: Academic Press, New York.
30. Sourisseau, C. and Mercier, R., Spectrochim. Acta, 1978. **34A**: p. 173-8.

31. Fukumi, K., Hayakawa, J. and Komiyama, T., *Intensity of Raman Band in Silicate Glasses.* Journal of Non-Crystalline Solids, 1990. **119**: p. 297-302.
32. Tang, Y., Jiang, Z. and Song, X., *NMR, IR and Raman Spectra Study of the Structure of Borate and Borosilicate Glasses.* Journal of Non-Crystalline Solids, 1989. **112**: p. 131-135.
33. Beattie, I.R. and Gilson, T.R., J. Chem. Soc. (A), 1970: p. 980.
34. McDevitt, Spectrochim. Acta, 1964. **20**: p. 799-808.
35. Vodop'yanov, V.P., Migorodskii, A.P. and Lazarev, A.N., Inorg. Mater., 1984. **19**: p. 1667.
36. Frogner, P., Broman, C. and Lindblom, S., Chemical Geology, 1988. **151**: p. 161-168.
37. Nyquist, R.A., Infrared of Organic Compounds, 1997. **4**.
38. Scott, J.F. and Porto, S.P.S., Phys. Rev., 1967. **161**: p. 903.
39. Frost, R.L., Fredeicks, P.M. and Shurvell, H.F., Can. J. Appl. Spectrosc., 1996. **41**: p. 10.
40. Krishnamuti, D., Proc. Indian Acad. Sci., 1956. **43A**: p. 210.
41. Pilati, T., Demartin, F. and Gramaccioli, C.M., Acta Cryst., 1998. **54B**: p. 515-523.
42. Nakamoto, K., *Infrared and Raman Spectra of Inorganic and Coordination Compounds*. 4th ed. 1986: John Wiley and Sons.

Chapter Five
Chemical Resistance

Chapter Five
Chemical Resistance

5.1 Introduction

In this chapter acid and alkali corrosion resistance of ground coat porcelain enamels, often used as a single functional coat are investigated. Five commercial coatings were fabricated and tested and the effects of mill additions, clay and silica content on the chemical resistance of one of these were determined.

When discussing corrosion of enamelled specimens, corrosion of the enamelled coating and the metal substrate need to be differentiated. Using a passive barrier (glass coating), usually prevents corrosion of low carbon steel, but this barrier can undergo acid and alkaline corrosion and the glass can be selectively leached in corrosive environments.

This chapter mainly discusses the corrosion when the enamel layer is exposed to acid and alkali, which destroys the finish. Any exposed underlying metal corrodes by a different corrosion mechanism but it mainly is an electrochemical process. The most common corrosion is uniform attack over the entire exposed surface, which often leaves a scale or deposit of corrosion products.

Many factors affect the corrosion rate of vitreous enamel coatings and these can be classified into primary and secondary factors.

Primary Factors - corrosion of the enamel as a solid matter (glass-network decomposition related).

Secondary Factors - the enamel coating is not homogeneous or solid but contains bubbles (pores) that may affect corrosion resistance.

Corrosion resistance is normally discussed in terms of the solid matter, that is, glass structure. However, once the glass is attacked, bubbles in the coating may also affect the dissolution process. The affect of bubbles on corrosion potential is presented after examining the corrosion potential due to primary factors. Opacifiers/colouring pigments are used in enamel coatings and therefore their affect on corrosion potential also needs to be determined.

5.1.1 Solid Glass Composition

Composition of the commercial coatings was identified using ICP (Table 3.6). The basic glass matrices used in this investigation are made up of the following types of oxides:

1. Glass formers, which are SiO_2 and B_2O_3. These form the main structural network.
2. Modifying oxides, which are Na_2O, K_2O, CaO and MgO. Modifiers change the glass lattice, distorting the basic structure of the glass formers, thus weakening the bonds and promoting easier melting. This improves fluidity and workability of the glass-enamel.
3. Intermediate oxides, Al_2O_3. This oxide plays an important part in the glass matrix by acting as a glass former or modifier depending on the availability of modifying ions.
4. Adherence oxides, NiO and CoO.
5. Colouring pigments and opacifiers, which include TiO_2 and Cr_2O_3.

The glass structure or network principally determines chemical resistance (ignoring the affect of any secondary factors on corrosion). Porcelain enamels are complex alkali metal borosilicates. The glass structure is based on a network of mainly SiO_4 tetrahedra and some BO_3 triangular units (arrangements). The B_2O_3 is introduced to reduce the melting point but breaks the Si-O bonds, thus creating an irregular network. The lattice interstices contain alkali metals such as sodium and alkaline earth metals such as calcium. Introducing alkali and alkaline metals into the lattice further disrupts the network, so more Si-O bonds are broken. The alkali metal oxides (also called modifiers) do not participate in the network but

provide extra oxygen ions to the lattice, thereby increasing the O/Si ratio. However, Al^{3+} can be incorporated into the composition by substituting for Si^{4+} when using an oxygen ion from an adjacent alkali compound (Equation. 5.1).

$$Al_2^{3+}O_3^{2-} + Na_2^{+}O^{2-} \Rightarrow 2[Al^{3+} (O^{2-}/2)_4 Na^{+}] \quad \textbf{Eq. 5.1}$$

5.1.2 Chemical Attack Mechanisms

Acid Attack

Eppler[1] summarises the principal mechanism for acidic attack as an ion exchange process between a modifier (principally alkali) ion in the glass and a hydrogen ion in the solution (Equation 5.2). This does not disturb the basic glass structure because hydrogen ions diffuse through the modifier-depleted surface to the interface of the unreacted glass, where ion exchange occurs.

$$H+ \text{ (solution)} + Me+\text{(glass)} \Rightarrow H+\text{(glass)} + Me+ \text{ (solution)} \quad \textbf{Eq. 5.2}$$

Alkali Attack

Surface corrosion in an alkali solution involves ion exchange leaching and dissolution. The hydroxyl (OH) group from the alkaline solution also takes part in the reaction by penetrating into the network, causing destruction.[2] Glass leaching occurs when hydrogen ions in the solution react with the glass matrix, causing alkali ions in the glass to be ionised.[3] As the concentration of alkali ions such as Li^{+}, Na^{+} and K^{+} in the enamel increases, the number of non-bridging oxygens (NBOs) in the glass also increases. This increases ion exchange leaching, causing a larger hydrated layer to form at the glass surface. Dissolution of the hydrated layer occurs more quickly than dissolution of the bulk of the glass.[3]

Eppler[1] describes the principle mechanism of alkali corrosion of a glass structure as:

$$Si\text{-}O\text{-}Si + NaOH \Rightarrow Si\text{-}O\text{-}Na + Si\text{-}OH \quad \textbf{Eq. 5.3}$$

The predominantly silica glass network then dissolves from sequential attack by alkali hydroxides on the fundamental Si-O-Si bonds of the glass structure.[1,4]

5.2 Chemical Resistance Testing

5.2.1 Acid Test Weight Loss Results

Of the five commercial enamel formulations investigated, matte black A (MBA) enamel coating had the lowest resistance to boiling citric acid solution and vapour (Figure 5.1; Table 1 - Appendix 6). Because the average weight loss after 2.5 h exposure (366 ± 113 g/m^2) was extremely high, samples were not tested at longer exposure times. The variation in the large areas of coating removed from the MBA sample resulted in the high standard deviation.

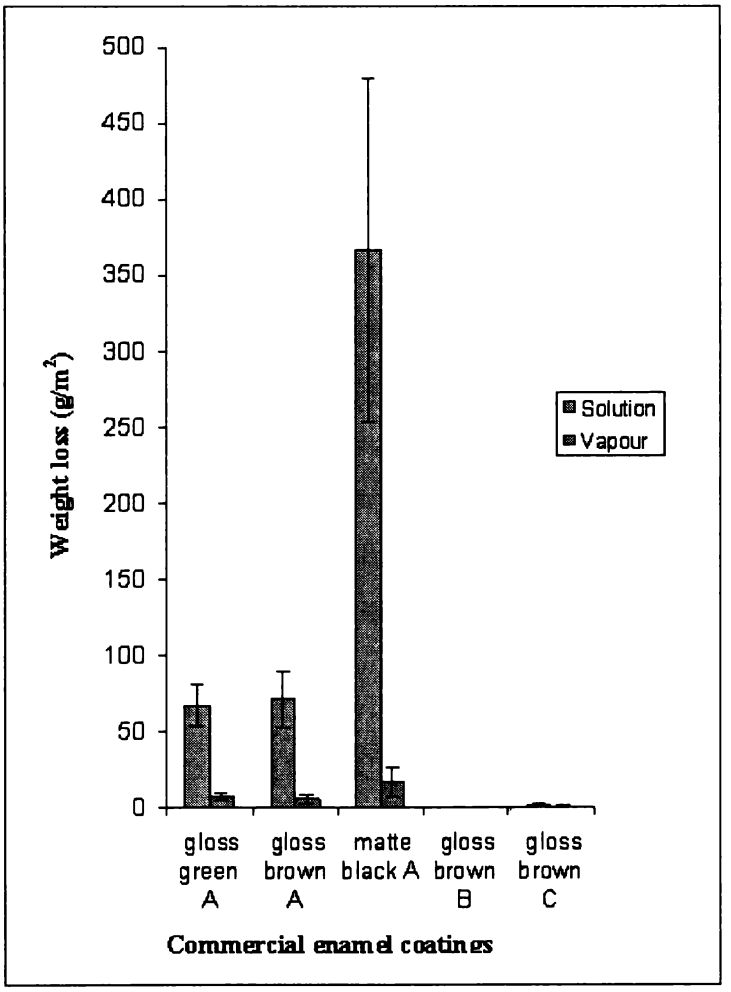

Figure 5.1 Average weight losses of commercial enamel coatings after 2.5 hours of surface exposure to boiling citric acid solution and vapour. (n=6)

Gloss green A (GGA) and gloss brown A (GBA) samples also had large weight losses (67 and 71 g/m^2) after 2.5 h exposure to boiling citric acid solution (Figure 5.1), therefore were not tested for longer periods. GGA and GBA enamels had similar weight losses (and standard deviations) because they have similar compositions (Table 3.1), differing only by the colouring oxides added. The weight loss of 67–71 g/m^2 is much higher than the 25 g/m^2 specified[5] for cooking utensils and bathtubs. However, the service conditions of the enamel coatings on outdoor gas cookers and wood burners will be less demanding than for cooking utensils, so this weight loss (indicating acid resistance) may be acceptable. Gloss brown B (GBB) and gloss brown C (GBC) coatings had negligible weight loss after 2.5 h exposure to both acid solution and vapour, so the test period was extended. After 24 h exposure to boiling solution, GBB samples had lost 3.6 ± 0.5 g/m^2 and GBC samples had lost 9.9 ± 4.3 g/m^2 (Table 1 - Appendix 6).

Enamels with less than 5 g/m^2 weight loss after 2.5 h are classified as acid resistant (Table 1.9). Thus, GBB could be classified as acid resistant. The data obtained that appliances coated with matte black enamel have lower chemical resistance than gloss enamel coatings.

5.2.2 Alkali Test Weight Loss Results

Of the samples tested, MBA coating had the least resistance to hot sodium hydroxide after 48 h (Figure 5.2 and Table 2-Appendix 6). If only comparing the gloss coatings then GBB and GBC are the least resistant to alkali corrosion (10.4 ± 0.6 and 13.2 ± 0.9 g/m^2 respectively after 48 h). This result is the opposite of the acid resistance test, where GBB and GBC had the best resistance.

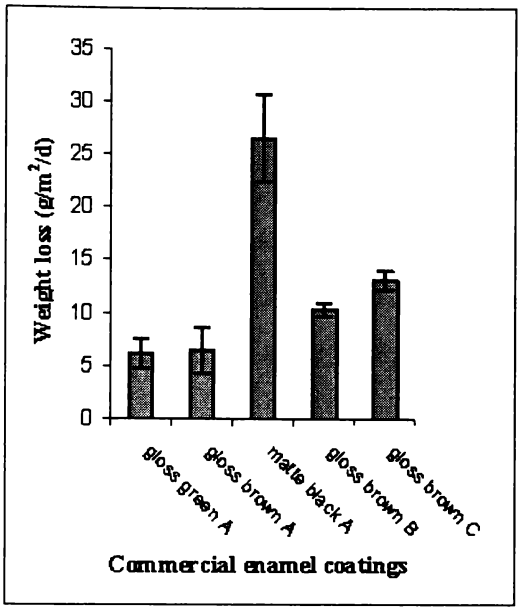

Figure 5.2. Average weight loss of commercial enamels after surface exposure to hot sodium hydroxide for 48 hours. (n=6)

5.2.3 Explanation of Results

Triangular Composition Diagrams

To help explain corrosion and predict chemical resistance of vitreous enamels, triangular composition diagrams were developed from the ICP data. This type of diagram has been used for vitreous enamels with various oxide formulations, to examine differences in colour and opacification of various enamels[6,7] and for chemical properties and chemical resistance of vitreous enamels[8] (Figure 5.3). Behrenbeck et al[8] proposed that higher SiO_2 + B_2O_3 contents increases acid resistance whilst a higher ZrO_2 (RO_2) content increases alkali resistance. The composition diagrams used by these authors do not include Al_2O_3 and its relationship with modifiers.

Kingery et al[9] and Chiang et al[10] report that up to 30 mole% alkali oxide is needed to convert BO_3 triangular units to BO_4 tetrahedra. However, above this concentration the alkali may behave as a modifier, increasing the NBO content between tetrahedra. Horton[3] reports that the ratio of tetrahedral to triangular boron has not been determined for complex glasses such as porcelain enamels.

This is because porcelain enamel systems contain SiO_2, B_2O_3, Al_2O_3, R_2O and RO, which directly affect the arrangement of the network.

The composition diagram (Figure 5.3) in the literature[6,7,8] are insufficient to explain the corrosion properties of the enamel coatings used in this study because they contain Al_2O_3 (Table 3.6) and the Al_2O_3/modifier oxide equivalence is not constant for enamels tested. This variation will have a large effect on chemical resistance.

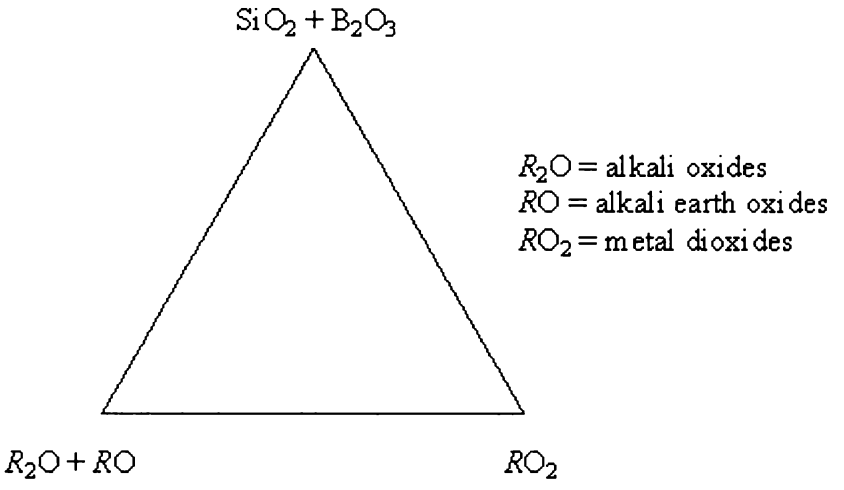

Figure 5.3 Composition diagram for porcelain enamels.[7,8]

Doweidar[11] assumed that Al_2O_3 associates with an equal quantity of modifiers to form AlO_4 tetrahedra. When $(Al_2O_3/R_2O) \leq 1$, the conversion occurs at two AlO_4 tetrahedra per Al_2O_3 molecule. The remaining R_2O (alkali oxide) will form silicate units containing NBO ions. For this investigation, the number of NBO per unit depends on a ratio that must also involve B_2O_3 and SiO_2.

To help explain the corrosion data obtained, and to predict chemical resistance of enamels, two composition diagrams for phases in the glass matrix were developed. Each diagram is based on different sets of oxide formulations that impart different specific properties and therefore chemical resistance to porcelain enamels.

There are three regions in each composition diagram. Composition diagram 1 (Figure 5.4) has the glass forming oxide SiO_2, the alkali oxides R_2O, and R_2O_3 whereas composition diagram 2 (Figure 5.5) includes the RO modifiers with R_2O.

SiO_2 provides chemical resistance to the system, so enamels with high SiO_2 contents (i.e. towards the apex of the diagram) should have greater chemical resistance. High alkali and alkaline earth oxides are loosely attached to the network and easily removed, which reduces chemical resistance. Varying R_2O and Al_2O_3 contents gives different structural properties and therefore different corrosion potentials. In both composition diagrams, B_2O_3 and Al_2O_3 are combined because amorphous B_2O_3 (like Al^{3+}) can increase connectivity from triangular BO_3 units to tetrahedral BO_4 units with local charge compensation from alkali additions. RO introduces divalent cations to the network, which occupy two rather than one NBO, thus improving glass durability. Composition diagrams were developed with and without RO to see if RO content affected corrosion potential.

Discussion of Composition Diagrams

The commercial enamel coatings GBB and GBC have the highest mol% of SiO_2 and are near the centre where $R_2O/R_2O_3 = 1$ (Figure 5.4). They also had the highest acid resistance of the enamels tested (Figure 5.1) because compact tetrahedra are formed, with most of the alkali additions increasing connectivity thereby reducing NBOs. The modifiers assist charge neutrality, with Al^{3+}, forming AlO_4 tetrahedral units and increasing connectivity from triangular BO_3 units to tetrahedral BO_4 units. When compact tetrahedra are formed, density increases and fewer NBOs are available to attract hydrogen ions from the chemical reagent. MBA enamel is at the furthest bottom-right of the composition diagram, indicating excess R_2O_3 and the lowest SiO_2 content. Its lower chemical resistance is because it has a less dense structure and excess Al_2O_3, acting as modifier ions, which are easily leached during chemical attack. However, Diagram 1 (Figure 5.4) does not indicate that GBB and GBC compositions have lower resistance to alkali attack than GBA and GGA.

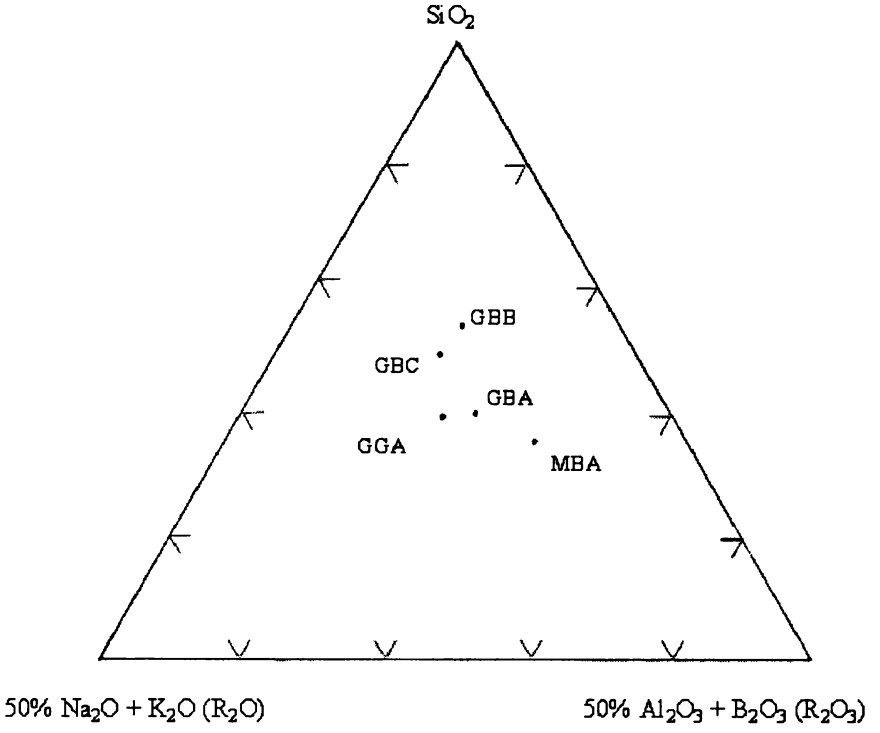

Figure 5.4 Composition diagram 1 for SiO_2-R_2O_3-R_2O system (mol%).

When RO is included in the compositional presentation (Figure 5.5) the relative positions of each enamel changes slightly. The increase in modifiers content shifts all enamels towards the bottom left corner [R_2O + RO]. There is a larger shift for GGA, GBA and MBA towards the [R_2O + RO] region because they have more RO than GBB and GBC enamels. When RO is included in the composition matrix, all enamels other than MBA have [$(R_2O+RO)/Al_2O_3$] >1. This implies an excess of modifier ions, which form NBOs that are readily attacked by hydrogen ions.

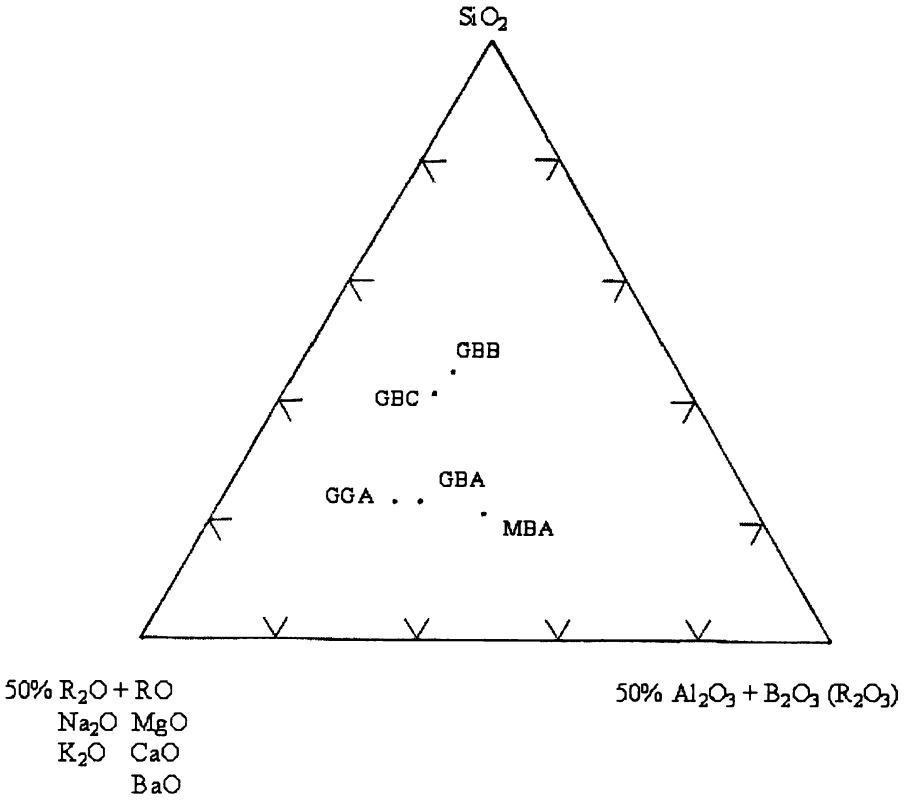

Figure 5.5 Composition diagram 2 showing SiO_2-R_2O_3-R_2O-RO system (mol%).

When explaining chemical resistance properties, composition diagram 2 does not allow for valency differences between R_2O and RO. Modifier oxides such as CaO introduce divalent cations into the network. These occupy two NBOs instead of one, thus improving resistance to alkali attack. GBA and GGA enamels, which were more resistant to alkali attack, have higher RO concentrations than GBB and GBC. The latter two also have lower alumina concentrations (Table 3.6), so there is insufficient AlO_4 tetrahedrals to tie up all the alkali ions. Excess alkali ions would be more readily leached by hydrogen ions, giving higher weight loss for GBB and GBC samples during alkali attack. However, as for composition diagram 1, the enamel composition with the highest acid resistance (GBB) occurs when $(R_2O+RO)/R_2O_3$ is close to 1 and SiO_2 content was greatest.

Composition diagrams are useful in explaining and predicting chemical resistance (and in particularly acid resistance in this study) for porcelain enamels. They allow for different phases in the glass matrix, which impart different properties

and influence resistance to corrosion. The components used in these diagrams do not account for all the phases in the enamels that may affect the chemical resistance. For example, TiO_2 is used for opacification but also increases acid resistance.[12] GBB and GBC enamels have more TiO_2 than other commercial enamels, (Table 3.6), which further increases their acid resistance.

5.3 Chemical Resistance Testing of Trial Formulations

Gloss brown I to IV (GBI to GBIV) were produced by adding various mill additions to the original commercial GBA (Table 5.1).

Table 5.1 Mill addition increases for trial formulations (see Table 3.7 for full enamel batch formulations).

Coating specimen	Mill addition increase (wt%)	
	Silica	HB clay
GBA	0	0
GBI	9	0
GBII	0	9
GBIII	3	3
GBIV	4	0

Acid Resistance

Increasing silica content by 9 wt% (from 3 wt% for GBA to 12 wt%) increased acid resistance (2.5 h exposure to boiling citric acid) from 70.8 ± 17.9 (GBA) to 40.4 ± 4.3 g/m^2 (GBI) (Figure 5.6 and Table 3 – Appendix 6). Adding 9 wt% content of refractory material silica has made a more insoluble coating structure, with improved acid resistance. GBI also had a lower bubble area than GBA (Figure 3.12), which would decrease the surface area exposed to the acid. However, adding only 4 wt% silica (GBIV) did not improve acid resistance. The GBIV coating was more soluble and had a higher bubble area than GBI (Figure 3.12), which would increase the surface area exposed to the acid.

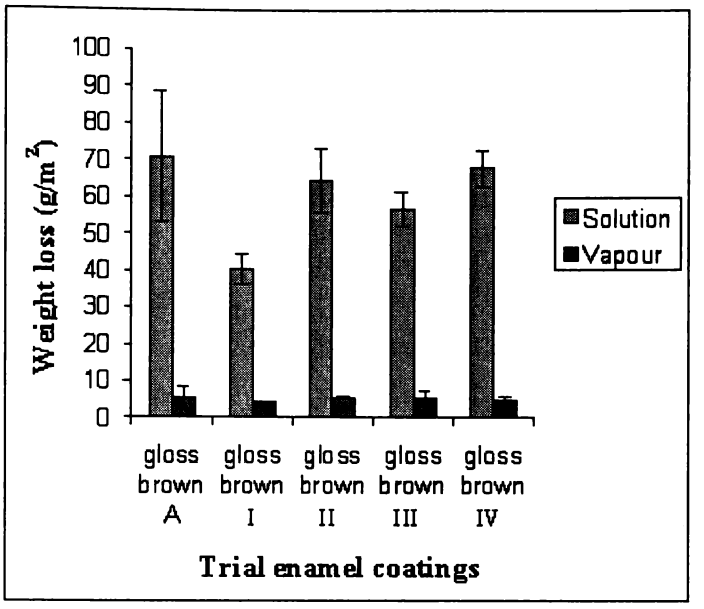

Figure 5.6 Effect of different mill additions on average weight loss of enamel coating surfaces exposed to boiling citric acid solution and vapour for 2.5 h (n = 6).

Increasing silica by 3 wt% and HB clay by 3 wt% (GBIII) increased acid resistance (weight loss of 56.7 ± 4.7 g/m^2), suggesting a synergistic affect from the two mill additions. However, increasing the HB clay (+9 wt %) did not improve acid resistance (weight loss of 64.5 ± 8.7 g/m^2). The large standard deviation for the base formulation (GBA) meant that some of the changes observed were not statistically significant (Figure 5.6).

Weight loss after 2.5 h exposure to citric acid vapour is similar for all samples (Figure 5.6). GBI (+9 silica wt%) had the lowest weight loss (best resistance). Although samples with higher silica contents had the best acid resistance, other properties were affected. For example, GBI had the lowest adherence rating (Table 3.10). Adherence for GBII was greater than for GBI (Table 3.10). Another disadvantage of adding extra HB clay was that the surface changed from that of GBA (Figure 1a - Appendix 5) and became speckled with darker regions (Figure 16a - Appendix 5). GBIII and GBA had similar appearance (Figures 17a and 1a - Appendix 5) and the same adherence (Tables 3.5 and 3.10). GBIV, which did not have a significant increase in acid resistance, also has a lower adherence rating than to GBA (Tables 3.5 and 3.10).

Alkali Resistance

GBI (+9 wt% silica), GBIV (+4 wt% silica) and the commercial enamel, GBA, had similar weight losses (5.9 ± 0.2, 5.8 ± 0.5 and 6.4 ± 1.1 g/m^2/d respectively), indicating that adding silica did not affect alkali resistance (Figure 5.7).

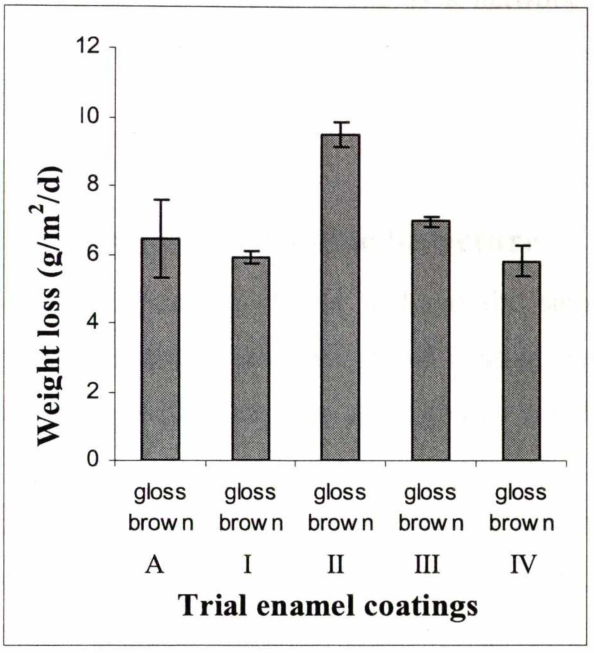

Figure 5.7 Effect of adding different mill additions to the average weight loss of enamel coating surfaces exposed to hot sodium hydroxide for 48 hours (n = 6).

Increasing HB clay content decreased alkali resistance. GBII (+9 wt% HB clay) lost 9.5 ± 0.4 g/m^2/d compared with 6.4 ± 1.1 g/m^2/d for GBA. Slightly increasing HB clay (3 wt%) and silica (3 wt %) did not significantly change alkali resistance (GBII - 7.0 ± 0.2 g/m^2/d weight loss). HB clay, which contains mainly Si, Al and a small amount of Ti (Figure 15-Appendix 3), is known as high bubble clay[13] and is used in ground coatings to achieve the desired set and bubble structure. Increasing Si and Ti increases acid resistance, while increasing Al increases alkali resistance. However, too high an alumina content has a deleterious affect on acid resistance.[3,14] The alkali test results showed increasing HB clay content (GBII and GBIII) made the enamels more susceptible to alkali attack than the original gloss brown coating (GBA). Adding zirconium oxide or

aluminium oxide (usually as zirconia or alumina) to the frit while maintaining a high silicon dioxide content can increase alkali resistance of enamels.[12] Lightner and Nobles[15] found that increasing clay from 1 wt% to 5 wt% increased alkali resistance, probably due to the alumina in the clay. Although HB clay contains Si and Al, increasing HB clay to 7% (GBIII) or 13 wt % (GBII) in the present study did not increase alkali resistance of the enamels. The alumina content may have been too high, resulting in the alumina acting as a network modifier and thus decreasing alkali resistance.

5.4 Secondary Processes

5.4.1 Chemical Resistance and Bubble Structure

Coatings of the same composition should undergo the same corrosion when exposed to a chemical reagent. However, if the coating contains bubbles, or voids, a greater surface area will be exposed and a greater weight loss will occur.

A coating's susceptibly to corrosion and the corrosive environment will affect the initial dissolution rate. Corrosion penetrability on initial exposure to acid or alkali is important before secondary factors such as bubbles or pinholes play a role in the dissolution process. The corrosion rate can vary for different compositions. If alkalis are easily leached out of the solution during the reaction process, this would in turn raise the pH, causing accelerated corrosion.

The relationship of bubbles on corrosion behaviour of enamel coatings needs to be considered. It was postulated that the greater the bubble to total area, the more susceptible the enamel coating will be to chemical attack.[16]

As previously discussed in Chapter 1, there is literature on bubbles in enamel coatings[16-18] and equations help predict enamel durability[1] as a solid matter (without bubbles). However, there were no reports that quantified the affect of bubbles on corrosion of vitreous enamel coatings. This investigation explores the correlation between bubbles and corrosion behaviour by plotting bubble area/total area of coating with weight loss of commercial and trial enamel coatings after exposure to acid and alkali solutions.

5.4.2 Bubble (Entire Coating Depth) and Corrosion Performance

Initially, the bubble area across the entire depth of the coating was examined to correlate weight loss after exposure to acid and alkali solutions. However, no correlations or trends were observed (Figures 5.8). Examining cross-sections after the corrosion tests revealed that corrosion in all enamel samples other MBA penetrated only to a certain depth and not to the substrate. The corrosion for MBA penetrated 80 microns from the surface into the coating.

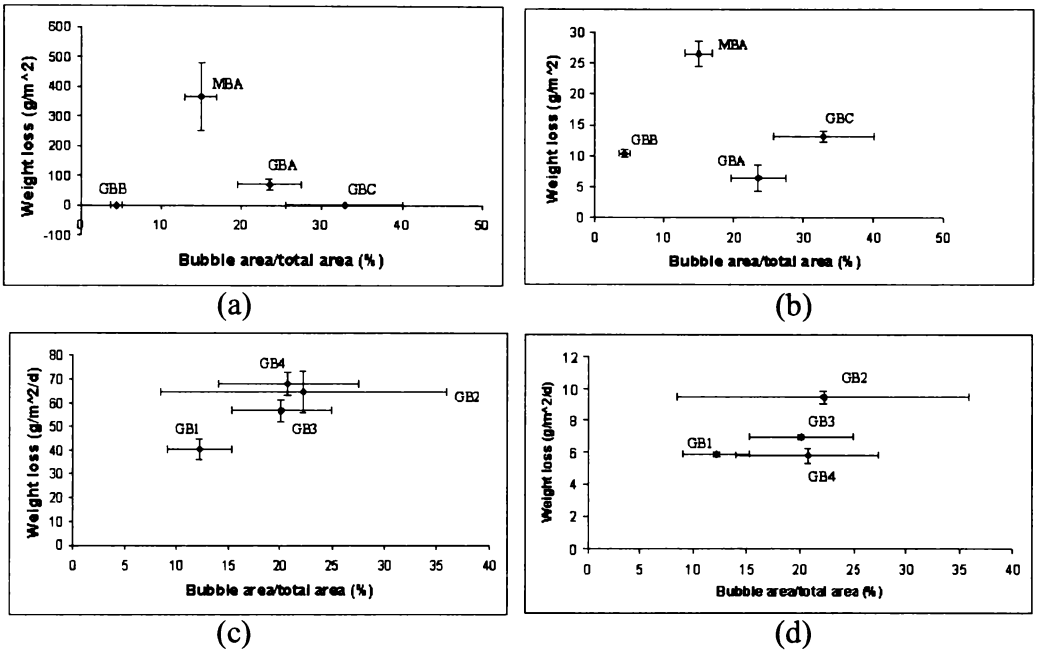

Figure 5.8 Average weight loss versus bubble area/total area for (a) commercial coatings after acid attack, (b) commercial coatings after alkali attack, (c) trial coatings after acid attack, and (d) trial coatings after alkali attack.

One reason acid corrosion did not progress further into the coating is because alkali ions are leached under acid conditions and a silicic skin may have formed on the coating surface. The barrier layer (hydrated) that forms on the surface stops further diffusion of ions into and out of the surface, thus slowing corrosion. The barrier layer doesn't form under alkali attack but the rate of glass removal by alkaline solutions also may slow with time.[19] The rate of attack slows when large amounts of glass go into solution.[19]

If the coating only dissolves close to the surface, then bubbles in the lower region will not be involved in the corrosion process, and only bubbles in the upper region will have a significant affect. This process is shown in Figure 5.9. Bubbles in the lower region (Figure 5.9a) do not affect the surface area and therefore, corrosion resistance. However, bubbles closer to the enamel surface (Figure 5.9b) are directly involved in the corrosion mechanism and provide a larger surface area for corrosion to occur.

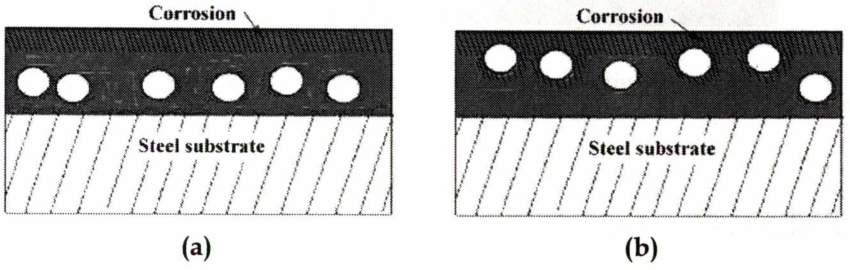

Figure 5.9 Schematic-showing: (a) bubbles positioned far from surface, not affecting corrosion, and (b), bubbles positioned closer to surface, affecting corrosion.

The region near the surface of the coating, therefore, can significantly affect the corrosion mechanism because it determines the surface area exposed to a corrosive environment and consequently the rate the glass will dissolve. Thus, there is an initial depth into the coating where bubbles and total bubble area is more significant. It is suggested that the bubble area in an arbitrary upper zone depth should be correlated with chemical resistance.

Cross-sections of enamel coatings after exposure to corrosive media (Figure 5.10) shows the typical corrosion depth into the coating. The average corrosion depth was found to be approximately 20 μm so it was proposed that this should be the depth of the upper zone for investigating if bubble area correlated with corrosion.

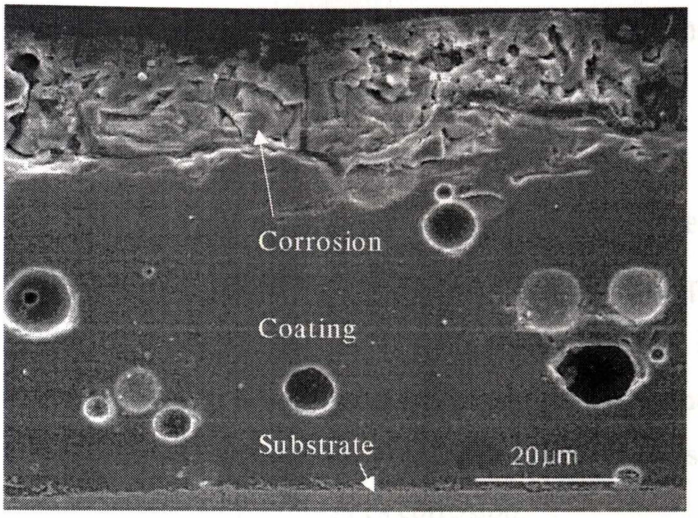

Figure 5.10 SEM micrograph of GBA coating cross-section after surface exposure to boiling citric acid (2.5 h).

Bubble area, expressed as a percentage of the area in the top 20 μm, for each enamel coating was measured and compared with percentage bubble area for the entire thickness (Figure 5.11).

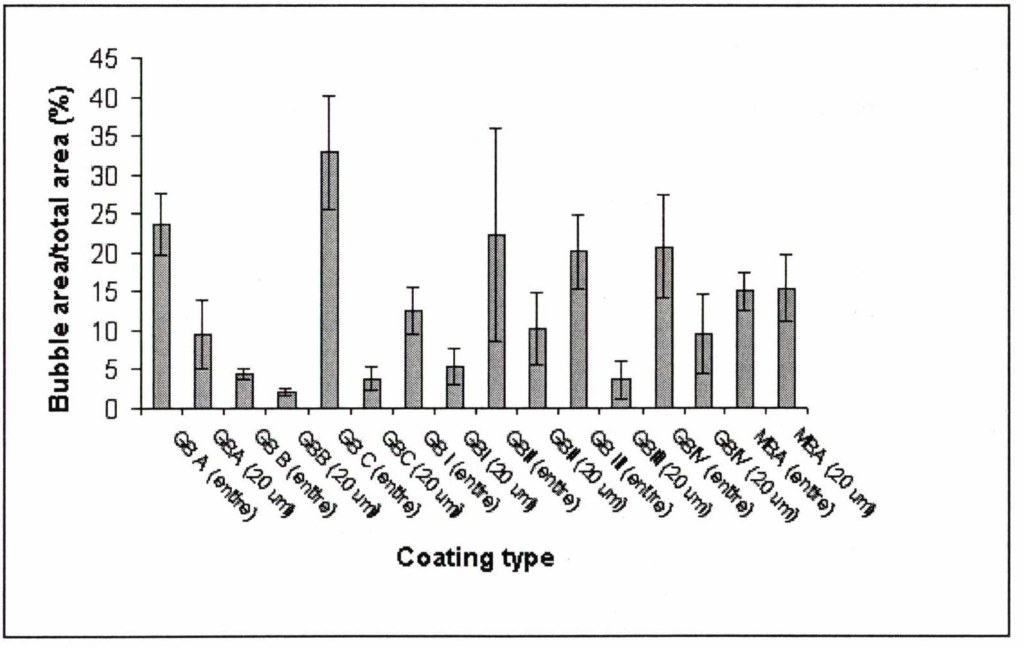

Figure 5.11 Percentage bubble area of entire thickness and top 20 μm for each coating.

In most coatings other than MBA, the proportion of bubbles in the top 20 μm is less than that over the entire coating thickness. In MBA, bubbles were uniform across the entire region. The lower proportion of bubble area

in the top 20 μm for most coatings implies that bubbles will have less influence on corrosion rate than if measured across the whole layer.

5.4.3 Bubbles (Top 20 μm) and Corrosion Performance

There is a general trend for weight loss to be correlated with proportion bubble area in the top 20 μm of coating (Figures 5.12). For example, MBA has the largest bubble area and highest weight loss (Figure 5.12a and b). The same trend can be seen for the other commercial enamels (Figure 5.12a and b), supporting the hypothesis that upper bubble area influences corrosion.

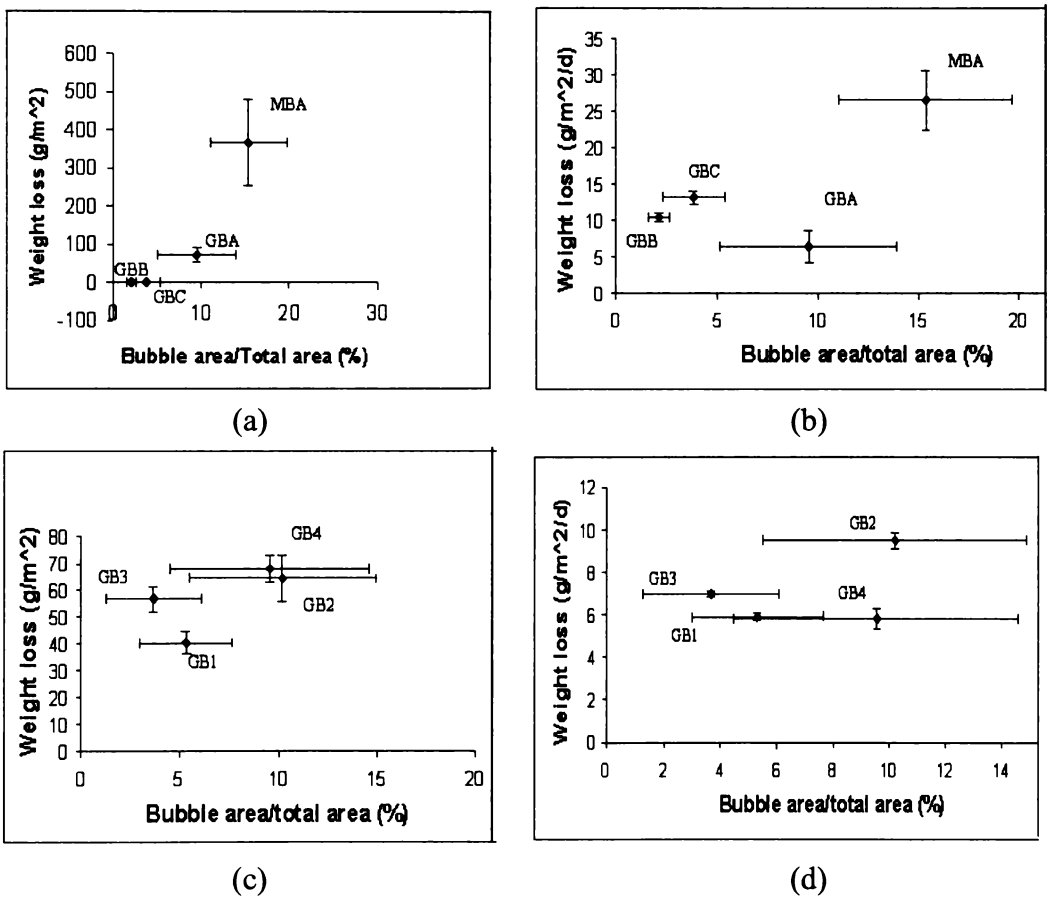

Figure 5.12 Average weight loss versus top 20 μm bubble area/total area for (a) commercial coatings after acid attack, (b) commercial coatings after alkali attack, (c) trial coatings after acid attack, and (d) trial coatings after alkali attack.

Although corrosion and upper bubble proportion in trial formulations appear to be directly correlated (Figures 5.12c and d), the effect was not significant because of the large experimental variation.

Glass formulation should have the most significant affect on the corrosion ability of glass. When examining the affect of bubble structure as a secondary factor on corrosion, some of the discrepancies could be due to the differing compositions. It is recommended that future studies on corrosion resistance of coatings should use a single composition and examine the affect of firing different bubble structures on chemical resistance properties. Bubble structure in the upper zone is critical and this information could be used with the primary factors to help predict corrosion rates.

5.5 Summary

Enamel corrosion was examined in terms of primary factors such as solid matter (glass network decomposition related) and secondary factors such as non-homogeneity of the coating caused by bubbles. Composition diagrams were developed that could account for the phases in the glass matrix that give different properties and therefore influence the rate of corrosion. These composition diagrams helped explain corrosion data and predict chemical resistance. The enamels in the region of higher SiO_2 content with similar modifier to R_2O_3 ratios were more acid resistant because more compact tetrahedra formed, reducing the number of NBOs, thus decreasing ion exchange between hydrogen ions from the solution and modifier ions from the coating. Enamels placed further to the bottom right of the composition diagrams indicate excess of R_2O_3 and less SiO_2. This is correlated with lower chemical resistance because the structure is less dense and excess Al^{3+} act as modifier ions, which are leached during acid attack.

Increasing mill addition silica from 3 to 12 wt% increased the coating's acid resistance but did not change the alkali resistance. Increasing HB clay from 3 to 12 wt% decreased the alkali resistance. This is also postulated to be due to excess of Al^{3+}, which act as modifier ions.

There was no correlation between bubble area over the entire depth of the coatings and weight loss after acid or alkali exposure. This was explained as corrosion generally being less than total coating depth because a barrier builds up on the coating surface over time, which inhibits further ion diffusion and prevents further corrosion. Therefore only bubbles in the top region the coating influence corrosion.

There was a general trend for increased corrosion to be correlated with increased bubble area in the top 20 μm of coating, suggesting that upper bubble area is an important factor in chemical corrosion.

5.6 References

1. Eppler, R.A., *Resistance of Porcelain Enamels to Attack by Aqueous Media: II, Equations To Predict Enamel Durability.* Ceramic Bulletin, 1977. **56**(12): p. 1068-1070.
2. de Jong, J., *Vitreous Enamelling and Glass Research.* The Vitreous Enameller, 1972. **23**(2): p. 20-28.
3. Horton, M., *The Development of Alkali-Resistant Powder Porcelain Enamel Systems.* Ceramic Engineering and Science Proceedings, 1993. **14**(5-6): p. 37-44.
4. Schumacher, L., and Schweite, H-E., *Attack of Fire-Polished Glass Surfaces by Caustic Soda Solution.* Glasstech. Ber., 1960. **33**(1): p. 1-7.
5. Kyri, H., *Handbook for bayer enamels.* 1975: Bayer AG.
6. Zubekhin, A.P., Manysheva, E.A, and Ochkurova, L.D., *Technological Specifics of Devitrified Composite Heat-Resistant Coatings for Nichrome Alloys.* Glass and Ceramics, 2000. **57**(1): p. 30-33.
7. Davis, J.R., ed. *Corrosion, Porcelain Enamels.* ASM Handbook (Metals Handbook), ed. J.R. Davis. Vol. 13. 1996, ASM, International, The Materials Information Society.
8. Behrenbeck, H.and Patzke, K., *Glassy and Crystalline Vitreous Enamel for the Chemical Industry - As Material Against Corrosion and Abrasion.* The Vitreous Enameller, 1985. **36**(2).
9. Kingery, W.D., Bowen, H.K. and Uhlmaunn, D.R., *Introduction to Ceramics.* 1976: John Wiley and Sons N.Y.
10. Chiang, Y., Birnie, D. and Kingery, W.D., *Physical Ceramics - Principles for Ceramic Science and Engineering.* 1997: John Wiley and Sons, Inc.
11. Doweidar, H., *Modelling of Density Structure Relations in Silicate Glasses Containing Al_2O_3.* Phys. Chem. Glasses, 2001. **42**(1).
12. ASM Committee on Porcelain Enameling., ed. *Porcelain Enameling.* ASM Handbook (Metals Handbook), Surface Engineering, ed. S.R. Lampman. Vol. 5. 1996, ASM International.
13. *Enamelling Manual.* , Unknown, Australia.
14. Layne, C.M., *Physical Properties of Grate Enamel Systems.* Ceramic Engineering and Science Proceedings, 1995. **16**(6): p. 103-109.

15. Lightner, L.F. and Nobles, E., *Processing and Testing Variables Affecting Alkali Resistance Determinations.* PEI Tech. Forum Proc., 1964. **26**: p. 202-207.
16. Smalley, H.F., *The Effect of Bubble Structure on Chemical and Physical Properties of Ground Coat Porcelain Enamels.* PEI Tech. For. Proc., 1964. **26**: p. 172-176.
17. Nakazato, Y., Kuguminato, H., Soeda, N., and Takahashi, I., *A study of Bubble Structure in Porcelain Enamel.* Transactions ISIJ, 1980. **20**: p. 1-8.
18. Joseph, W.A., *Structure of Enamel Coatings.* The Vitreous Enameller, 1988. **39**(1).
19. Weyl, W.A. and Marboe, E.C., The Constitution of Glasses – A Dynamic Interpretation. Vol 2, Part 2. Constitution and Properties of Some Representative Glasses. Interscience Publishers

Chapter Six
Study of Porcelain Enamel Coating and Pinhole Defect

Chapter Six
Study of Porcelain Enamel Coating and Pinhole Defect

6.1 Introduction

In this chapter, the phases present in a commercially used single-coat enamel (GGA) on steel substrate system are characterised using Raman microscopy, X-ray diffraction (XRD), scanning electron microscopy (SEM), and energy dispersive X-ray analysis (EDS). The change in distribution and types of phases due to the pinhole defect phenomena is also investigated.

6.2 Characterisation of a One-Coat Porcelain Enamel*

6.2.1 Optical Microscopy

An optical micrograph of a polished GGA coating cross section (90° to the surface) is presented in Figure 6.1 (200x magnification, dark field illumination). The microstructure consists of several visible phases and contains spherical solid and gas "bubble" inclusions. The enamel coating is approximately 145 μm thick. The enamel coating has a light coloured phase, approximately 65 μm thick, adjacent to the steel. This phase is due to iron oxide diffusion into the enamel coating during the enamel/steel firing process. Other researchers have also observed iron oxide diffusion into enamel coatings.[1-3]

*Part of this research was published "Raman Spectroscopy and Scanning Electron Microscopy Study of a One-Coat Porcelain Enamel" *The Ceramic Engineering and Science Proceedings* 20(3), 39-51, 1999.

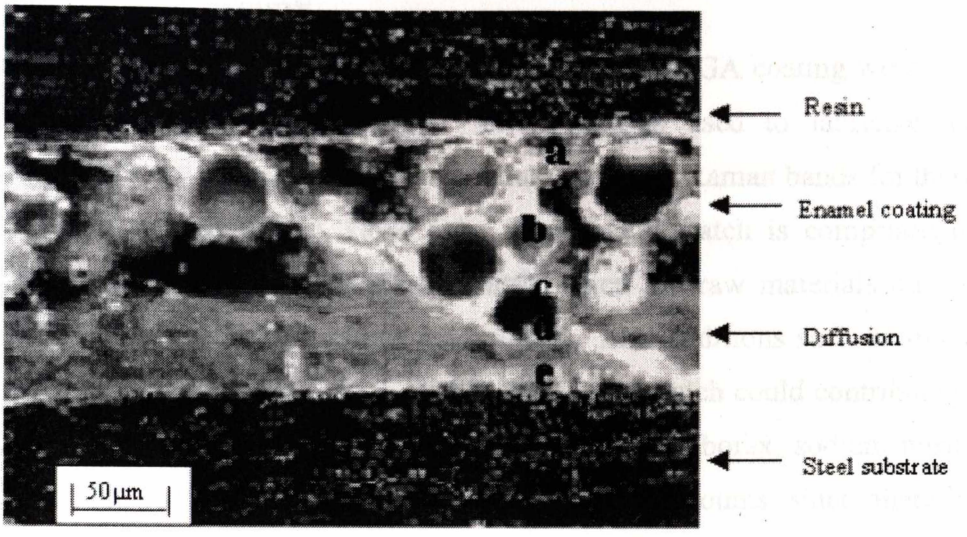

Figure 6.1 Optical micrograph of enamel coating cross-section using dark field illumination. A to E indicate the positions at which Raman spectra were obtained.

6.2.2 X-ray Diffraction

The phases of the GBA surface were initially characterised using XRD (Figure 6.2). Two crystalline phases, α-Cr_2O_3 (λ) and SiO_2 ($\varnothing$), were determined using the standard ICDD cards #38-1479 and #46-1045 respectively. The XRD pattern also has a broad background profile at ca. 30 degrees (2θ) due to the amorphous silica matrix present in the porcelain material.

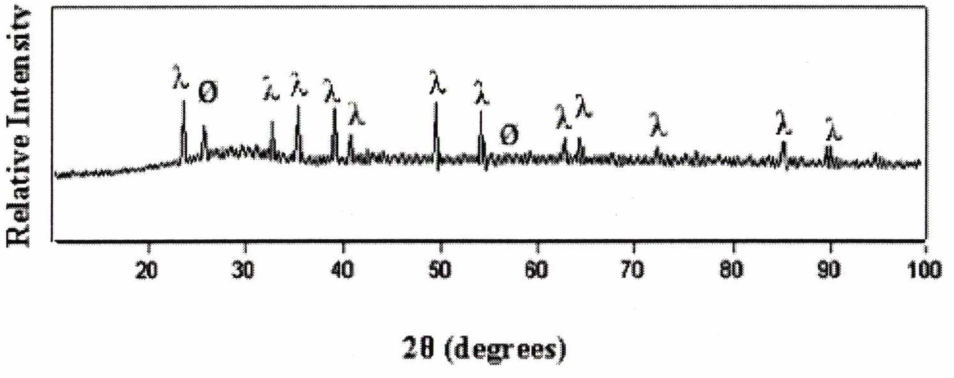

Figure 6.2 X-ray pattern of gloss green A enamel coating surface (λ = Cr_2O_3 and $\varnothing$ = SiO_2).

6.2.3 Raman Microscopy

The phases present in the porcelain enamel matrix of the GGA coating were also determined using Raman microscopy. The materials used to fabricate the porcelain enamel coating and the literature values of major Raman bands for these compounds are summarised in Table 6.1. The enamel batch is comprised of mainly frits, which form an amorphous matrix when the raw materials quartz, feldspar, borax and other components are smelted. Mill additions such as silica, clay, opacifiers and colouring oxides used in the enamel batch could contribute to significant phases in the enamel coating. The compounds borax, sodium nitrite and magnesium carbonate are present only in trace amounts since there is significant decomposition from firing. These are unlikely to contribute to any major phases in the fired enamel coating.

The Raman microprobe technique gives information about the surface and near-surface band vibrations since the focal cylinder of the incident light, formed by the optical microscope objective has a typical diameter and length of approximately 1 μm to 2.5 μm respectively.[4] A surface area as small as 1 μm can be resolved to collect Raman spectra. Hence, individual components in a heterogeneous sample can be selectively investigated.

Raman spectra, using the 514 nm laser line, were obtained at various points across the polished cross-section of the enamel coating (**a** to **e** as indicated in Figure 6.1). The Raman spectra are shown in Figure 6.3 and the corresponding band positions are listed in Table 6.2. At different depths through the coating cross-section, the Raman spectra show differing profiles. The predominant band observed at 549 cm^{-1} is assigned to α-Cr_2O_3 with reference to the literature.[5] Several weak bands at ca. 305, 345, 525 and 611 cm^{-1} are also assigned to α-Cr_2O_3. A weak band observed at ca. 456 cm^{-1} for cross-section positions b and d, was assigned to α-quartz.[6] At position e (the enamel-steel interface), only weak bands were observed, assigned to α-Cr_2O_3. The presence of a band at approximately 845 cm^{-1} in the spectra of all the coatings is attributed to SiO_2[7].

Table 6.1 Solid components used to fabricate GGA enamel coating (enamel batch composition).

Component	Composition	Purpose	Raman band positions (cm^{-1}) from literature*
Frit	Amorphous borosilicate	frit	450br, 800, 1050 (amorphous silica)[8]
Silica	Quartz, SiO_2	refractory	207, 356, 464, 1085, 128, 265, 394, 401, 450, 509, 697, 795, 807, 1072, 1162, 1235[6]
Oxide	Cr_2O_3, $FeCr_2O_4$	colouring	303, 351, ca. 397, 530, 551, 609[5]
HB Clay	SiO_2 (quartz) and kaolinite	refractory	See Silica and Kaolex clay
Kaolex Clay	Kaolinite $Al_2O_3.2SiO_2.2H_2O$	refractory	130sh, 143m, 197vw, 245w, 270m, 336m, 418sh, 431m, 463m, 516w, 638m, 710vw, 751w, 790w, 915w[9]
Bentonite	Bentonite $(M^{2+})(M^{3+})_4(Si,Al)_8O_{20}(OH)_4.H_2O$	suspending agent	75, 132, 162, 202, 264, 290, 360, 429br, 608, 708, 800, 916, 1033, 1105, 1162[10]
Hydrous Borax	Borax ($Na_2B_4O_7.10H_2O$)	flux	78w, 90m, 120m, 160w, 361m,390w, 474m, 530wbr, 590vw, 776mbr, 860w, 975m, 1640vw, 3140s, 3357s, 3400s, 3447s, 3495s, 3575s[11]
Magnesium Carbonate	$MgCO_3$	electrolyte-flocculater	212, 332, 735, 1096, 1460[12]
Sodium Nitrite	$NaNO_2$	increases set	119s, 154m, 827m, 1325s[13]

*Relative intensity: vw = very weak, w = weak, m = medium, s = strong, br = broad, sh = shoulder

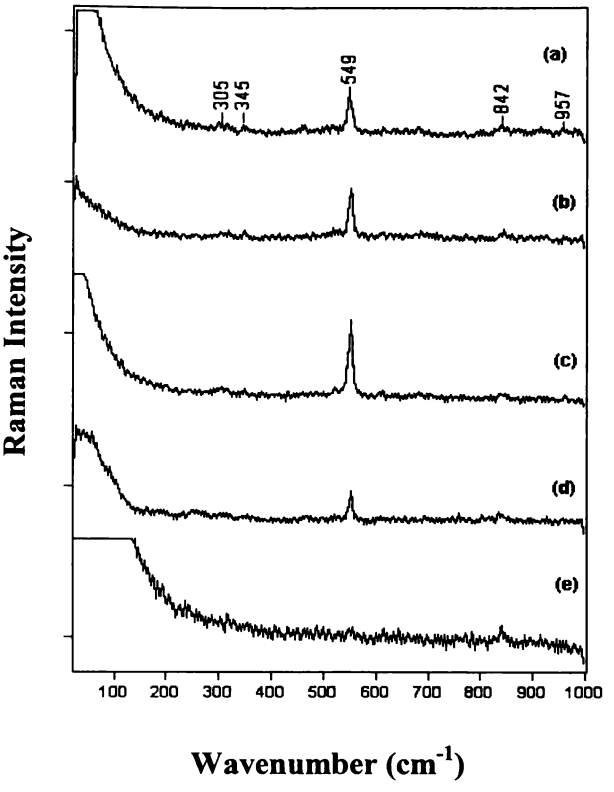

Figure 6.3 Comparison of Raman spectra of the enamel-coating cross-section obtained at positions **a** to **e** from Figure 6.1.

Table 6.2 Raman band and assignments (cm^{-1}) observed for the GGA cross-section.

Position					
(a)	**(b)**	**(c)**	**(d)**	**(e)**	**Assignment**
305w	302w	315w	302w	318w	α- Cr_2O_3[5]
345w	350w	350w	352w		α- Cr_2O_3[5]
	456w		467w		α- quartz[6]
	525w	527w			α- Cr_2O_3 [5]
549s	554s	552s	554s	555w	α- Cr_2O_3 [5]
	614w	611w	611w		α- Cr_2O_3[5]
	687w,br	686w	699w		
842w	844w	843w	839w	841m	SiO_2[7]

Relative intensity: w = weak, m = medium, s = strong, b = broad

6.2.4 SEM and EDS Analyses

The study region for the porcelain enamel coating and steel substrate is shown in Figure 6.4. The qualitative EDS Spectrum used to represent the background of the coating cross-section (Figure 6.5a) was collected from a 140-μm square region. Typical penetration depths are in the order of micrometers (1-3 μm), therefore this technique can be considered a sub-surface to bulk analysis. Intense peaks, corresponding to Si and Fe, were observed. As porcelain enamel coatings are complex alkali borosilicate, the intense Si peak was expected. Boron is present in the coating as shown by ICP analysis (Table 3.6), but cannot be detected by EDS due to the element's low atomic number. The high Fe peak is postulated to be caused by iron oxide diffusing into the enamel coating during the firing process. The spectrum also contains a relatively intense Ca peak (Figure 6.5a). Ca may originate from calcium carbonate often added to the mill of a ground coat charge as a fluxing agent and/or to alter the bubble structure[14].

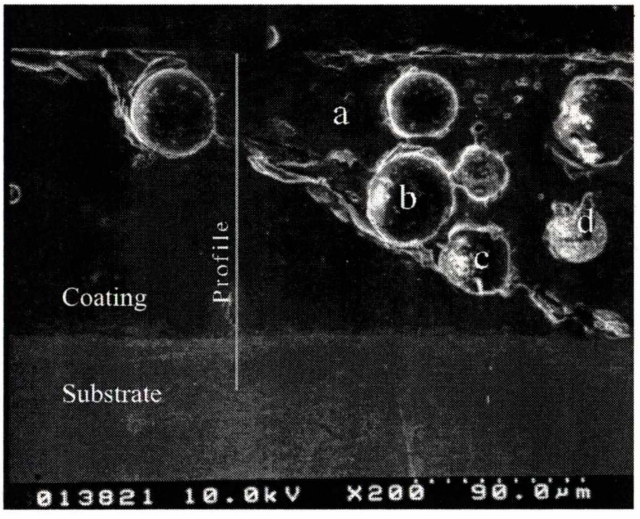

Figure 6.4 SEM micrograph displaying a cross-section of enamel coating and steel substrate. Qualitative spectra were taken at points **a** to **d** (see Figure 6.5) and semi-quantitative at profile (see Figure 6.6).

The EDS spectrum taken from the "bubble structure" (point b, Figure 6.4) has a very low count rate of 233 counts after 100 seconds compared with 2090 counts after 100 seconds for the background (Figure 6.5a and b). This low count rate for the spectrum is due to the pore (or bubble) where the sample was taken. There was an intense Fe peak and less intense Si, Ca, Cr and Ni peaks in the spectrum. The count rate at point (c) is also much lower than the background count rate,

which suggests it may be a pore. The dominant peak in spectrum Figure 6.5c corresponds to Cr. This corresponds well with the Raman spectroscopic data, where the predominant band at phase was assigned to α-Cr_2O_3.

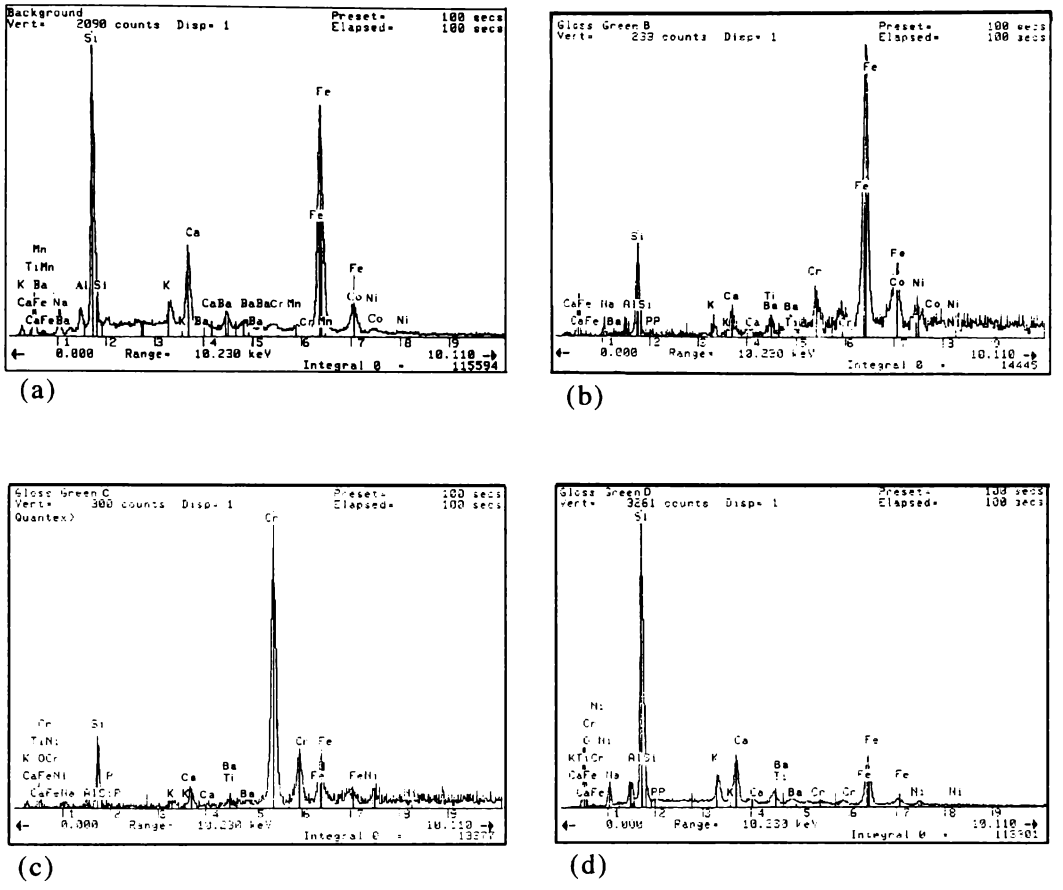

Figure 6.5 Comparison of EDS spectra of GGA coating cross-section obtained at positions **a-d** from Figure 6.4.

The EDS spectrum (Figure. 6.5d) of the inclusion at point d (Figure 6.4), has a high-count rate, indicating that the inclusion is solid. The predominant peak is Si, which is part of the amorphous silica phase or a crystalline quartz phase.

6.2.5 Elemental Profile

A semi-quantitative EDS analysis profile (Figure 6.6) of the cross-section shown in Figure 6.4 indicates that the enamel coating has a high Fe content. This corresponds to the light coloured phase in Figure 6.1 (approximately 0 - 65 μm from the steel-enamel interface). Low levels of Fe (approximately 5 wt%) are present above this phase to the surface of the enamel coating. As expected, the

steel substrate has a high Fe content and low levels of other elements such as Ca, Si, Mn, Co.

The elemental profile (Figure 6.6) shows that the enamel has a high Si content. Si, as silica, is one of the major constituents of the enamel coating. However, the Si concentration gradually decreases from 15 μm to the interface (0 μm), which matches an incremental increase in Fe concentration towards the interface.

6.2.6 EDS Elemental Mapping

Areas of highest brightness in the EDS spectrum (Figure 6.7) correspond to higher concentrations of the specified element. For example, the map for Fe (Figure 6.7, top middle) shows high Fe concentrations in the steel substrate with Fe dispersion from the substrate to approximately 70 μm into the coating. The Fe map matches the elemental profile (Figure 6.6), which shows high Fe concentrations in the substrate and decreasing amounts through to the coating surface.

There are high concentrations of the element Co (used for adherence and colouring) in the substrate and small concentrations in the coating (Figure 6.7, centre). The Fe $K\beta$ peak overlaps and exaggerates the Co $K\alpha$ peak, in the EDS spectra, so the intense Co distribution seen in the substrate is possibly an artefact of the system. Ni like Co is used for adherence. The Ni map (Figure 6.7, bottom centre) displays a mostly even dispersion throughout the cross-section. The Ni concentrated at the interface between the coating and substrate is postulated to be from substitution with the iron oxide at the interface when the enamel is fired onto the steel.

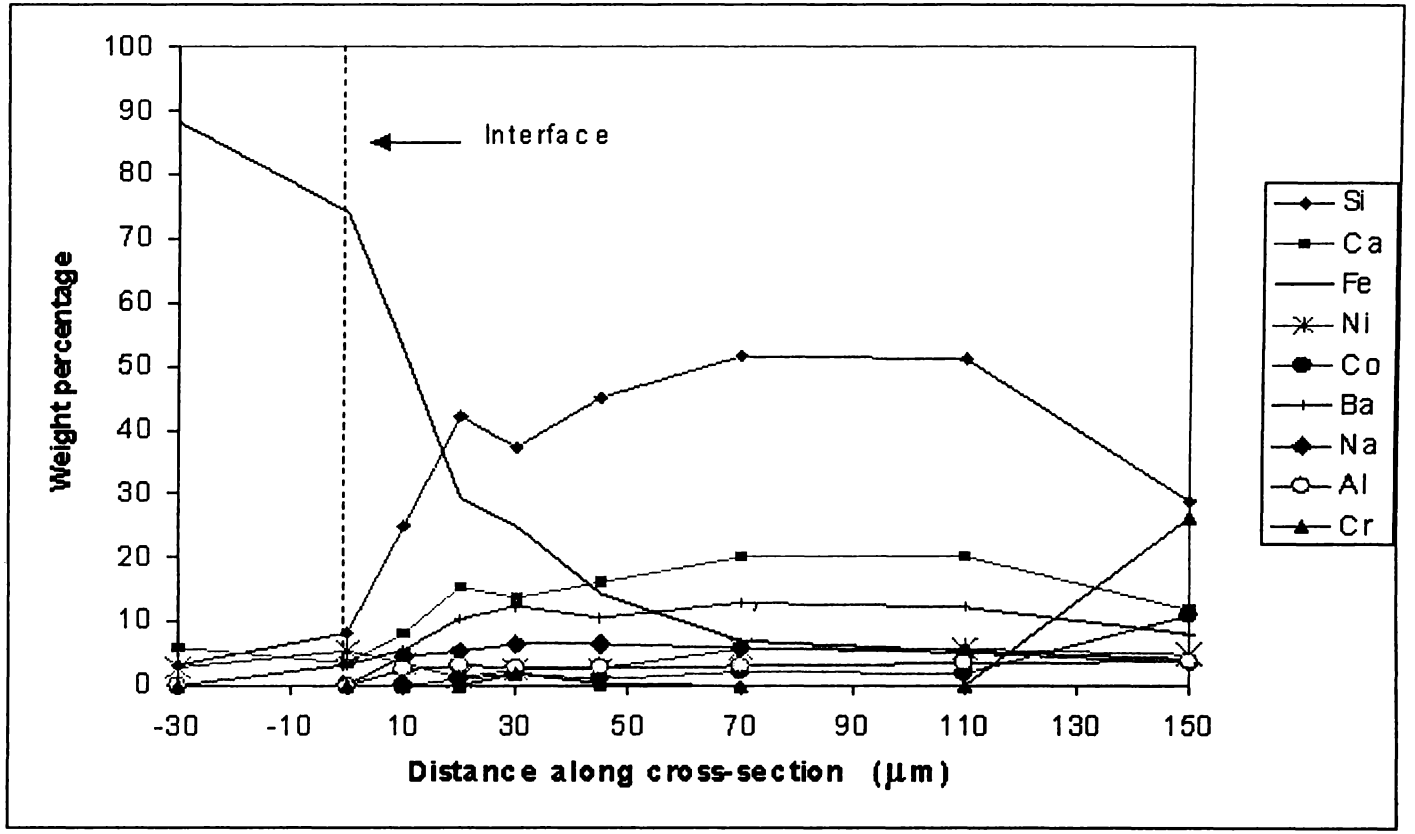

Figure 6.6 Elemental profile of enamel coating on steel cross-section.

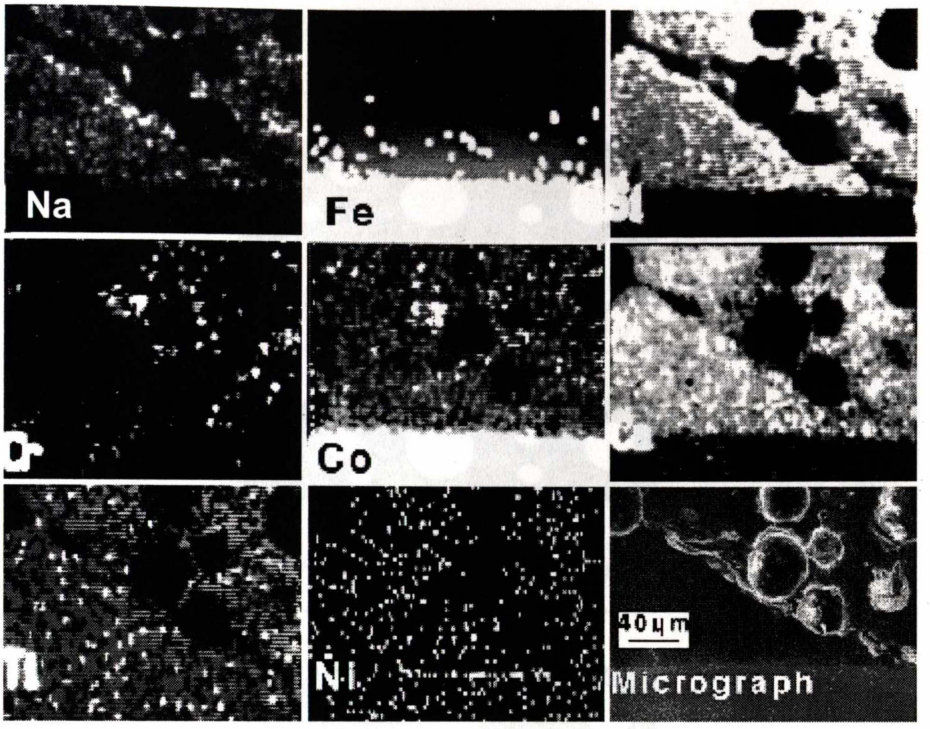

Figure 6.7 EDS elemental concentration mapping of cross-section.

Si (top right of Figure 6.7) is dispersed throughout most areas of the coating, constituting a high percentage of the porcelain matrix. Cr (left centre) is dispersed in small discrete regions in the coating cross-section. There appears to be higher concentrations of Cr around the pores within the coating. This corresponds to the EDS spectrum given in Figure 6.5(c).

6.3 Study of Pinhole Defect

6.3.1 Description

The pinhole defects investigated in this study originate mainly from large bubbles in the ground coat (single coat), and can also result from under-firing the coating. If the large bubble extends to the surface, a pinhole or blister is formed. Figure 6.8 schematically illustrates the formation process of a pinhole defect. Initially there is a large bubble in the central region of the coating (Figure 6.8a). When the bubble moves closer to the surface (Figure 6.8b), a depression or dimple forms in the surface of the coating above the bubble because gases in the bubble contract during the cooling stage of the firing process. The enamel at the surface may then fail, with the pinhole extending to the bottom of the bubble (Figure 6.8c).

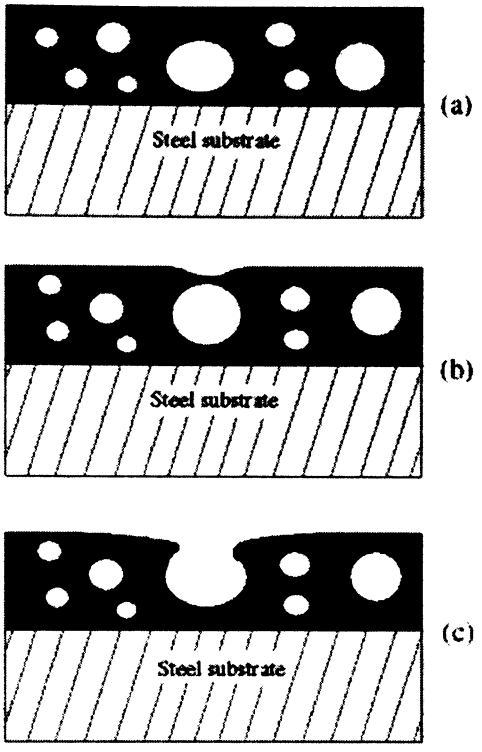

Figure 6.8 Schematic of pinhole defect

The pinhole defect is detrimental for several reasons. Firstly, this defect can be seen by the naked eye, and hence it spoils the appearance of the enamel coating. Secondly, the pinhole can be the origin of corrosion if the steel substrate is exposed at that point.

6.3.2 Microscopy

The appearance of a pinhole defect similar to what is observed using the naked eye is shown from stereo microscopy in Figure 6.9. The pinhole from the surface perspective, using optical microscopy (Figure 6.10), is approximately 30 μm in diameter and has a concave ring (depression from the coating surface to the hole).

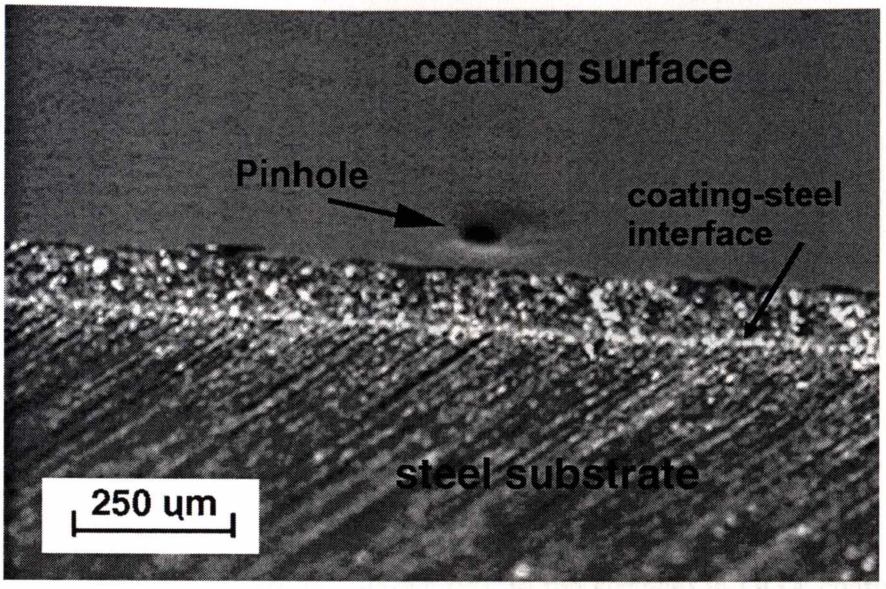

Figure 6.9 Stereo micrograph of enamel coating surface showing a pinhole.

Another example of a pinhole defect from the surface perspective at a higher magnification, observed using SEM, is shown in Figure 6.11a. This defect appears as a depression (or dimple), probably created when the bubble contracted during the cooling stage of the firing process. The small perforation at the top left of the depression (Figure 6.11b) could have occurred when gas was released during or after the firing process, causing the enamel coat to burst outwards.

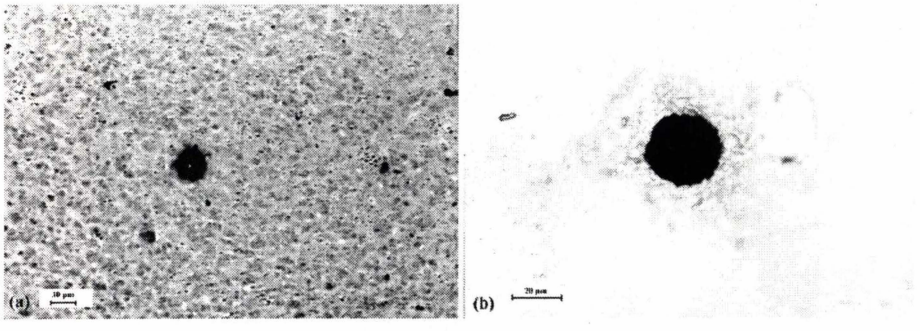

Figure 6.10 Surface perspective of pinhole using an optical microscope (bright field illumination.

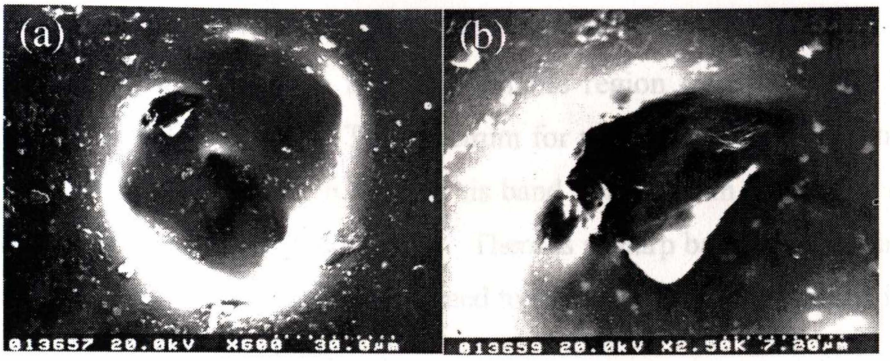

Figure 6.11 Surface perspective of a pinhole using SEM; (a) whole defect region and (b) perforation region.

A cross-section through a pinhole defect (90° to the surface) in GGA coating was prepared for SEM by polishing through to the defect. Figure 6.12 shows that at the top of the defect the coating surface is slightly concave, so a depression (or dimple) would be observed from the surface (as seen in Figure 6.9). Beneath the surface (Figure 6.12) is the void or pore of the so-called pinhole defect.

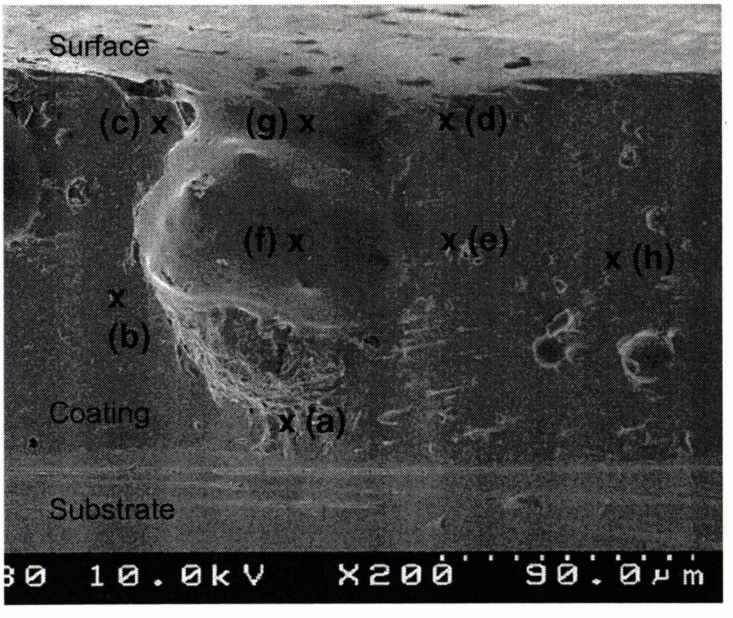

Figure 6.12 SEM micrograph of pinhole in cross section of sample (**a** to **h** indicate positions at which Raman spectra were obtained).

6.3.3 Raman Microscopy of Pinhole Region

The Raman spectra of samples from the pinhole region (positions **a-h**, Figure 6.12) are shown in Figure 6.13. The spectrum for position (a) has only one very weak band at 845 cm^{-1} (Figure 6.13a). This band is present in all spectra (Table 6.3) and is most likely attributed to SiO_2[7]. There is a sharp band at approximately 550 cm^{-1} in profiles b to g, which is assigned to α-Cr_2O_3.[5] This compound is used for colouring in enamel coatings.

The spectrum for point b (Figure 6.13b) taken at the side of the defect also has a band at 461 cm^{-1} indicating the presence of the silica phase, α-quartz. The spectrum at position (h) was obtained from another region, away from the defect as a reference of the coating glassy matrix. Only a band for α-Cr_2O_3 can be identified in the spectrum.

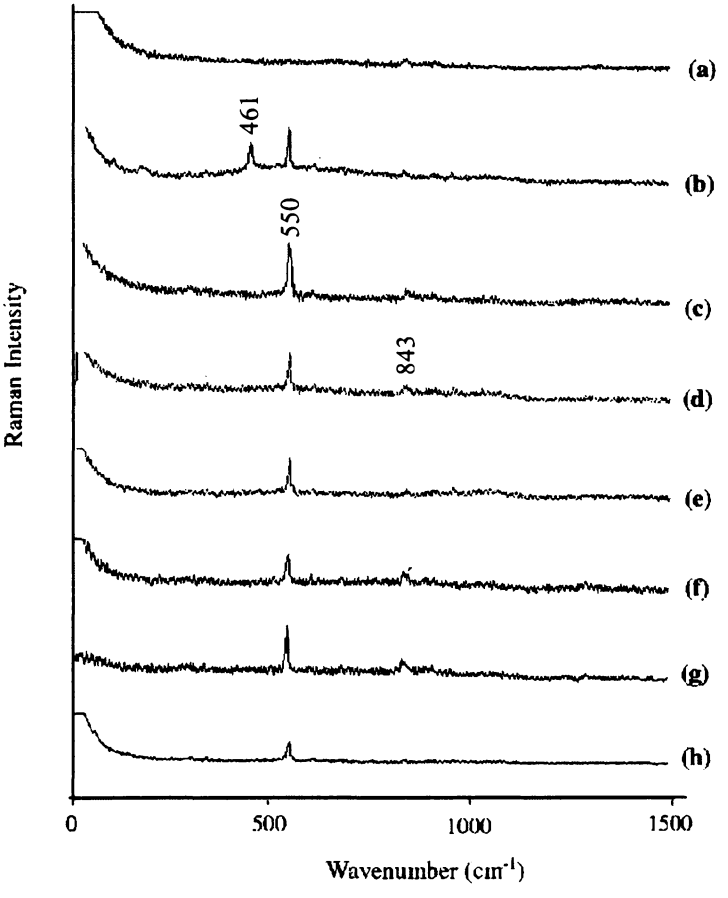

Figure 6.13 Raman spectra from pinhole region of sample cross-section (Figure 6.12).

Table 6.3 Raman band and assignments (cm^{-1}) from spectra of pinhole region (Figure 6.13).

Position								
(a)	(b)	(c)	(d)	(e)	(f)	(g)	(h)	Assignment
	123vw							α- quartz[6]
	191w							α- quartz[6]
	300vw	304vw		309vw	311vw		306vw	α- Cr_2O_3[5]
	350vw	349vw	352vw	346vw			350vw	α- Cr_2O_3[5]
						357vw		α- quartz[6]
	461m							α- quartz[6]
	527vw		526vw					α- Cr_2O_3[5]
	555s	551s	553s	555s	554s	553s	550s	α- Cr_2O_3[5]
	615vw	611vw	615vw	611vw			611vw	α- Cr_2O_3[5]
842vw	839vw	845w	843w	843w	843w	843m	841w	SiO_2[7]

Relative intensity: vw = very weak, w = weak, m = medium, s = strong, b = broad

Raman spectra of the defect region were also taken from the surface of the porcelain enamel coating sample (see Figure 6.14). One spectrum was taken along side the pinhole defect and compared with a profile within the defect region. The band positions and assigned phases are listed in Table 6.4. The major compound in the Raman spectra is α-Cr_2O_3. The main difference in the spectrum of the surface and from within the defect region is the presence of bands assigned to α-quartz.[6] This observation corresponds with the results from the following EDS elemental mapping.

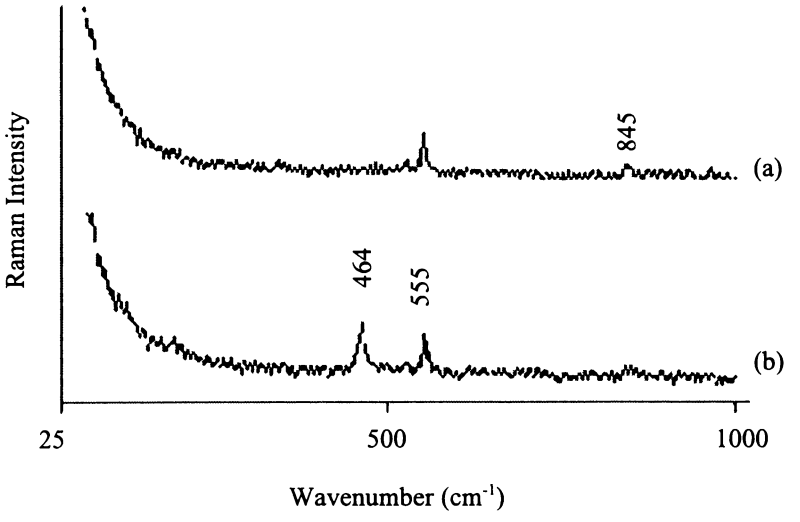

Figure 6.14 Raman spectra of GGA surface and defect region, (a) spectrum of coating alongside defect, (b) spectrum from within defect region.

Table 6.4 Raman band and assignments (cm^{-1}) for GGA surface, (a) and dimple (b and c).

Position		
(a)	(b)	Assignment
	116vw	α- quartz[6]
160w		
	198vw	α- quartz[6]
	464s	α- quartz[6]
530vw		α- Cr_2O_3[5]
554s	555s	α- Cr_2O_3[5]
		α- Cr_2O_3[5]
845m	843vw	SiO_2[7]

Relative intensity: vw = very weak, w = weak, m = medium, s = strong, b = broad

6.3.4 EDS Elemental Mapping

Cross-section

The dispersion of the elements Si, Al, Fe, Na and Cr within the defect cross-section was investigated using EDS elemental mapping (Figure 6.15). The areas of highest brightness correspond to higher concentrations of that particular element.

The EDS map for Fe (top left, Figure 6.15) shows high Fe concentrations in the steel substrate. Fe is also present in the coating due to Fe oxide diffusion from the interface into the coating. This corresponds to the profile in Figure 6.6 and the elemental mapping shown in Figure 6.7. There appears to be high Fe concentrations below the pinhole. This may have formed during the firing process when a gas bubble opens at the surface and exposes the base metal to ambient oxygen. Fe oxidises extremely rapidly and hence would give rise to the very high iron oxide levels in the zone beneath the pinhole. Conversely, it is possible that the outward diffusion of Fe was stopped by the pinhole resulting in accumulation of Fe at the edge of the pinhole.

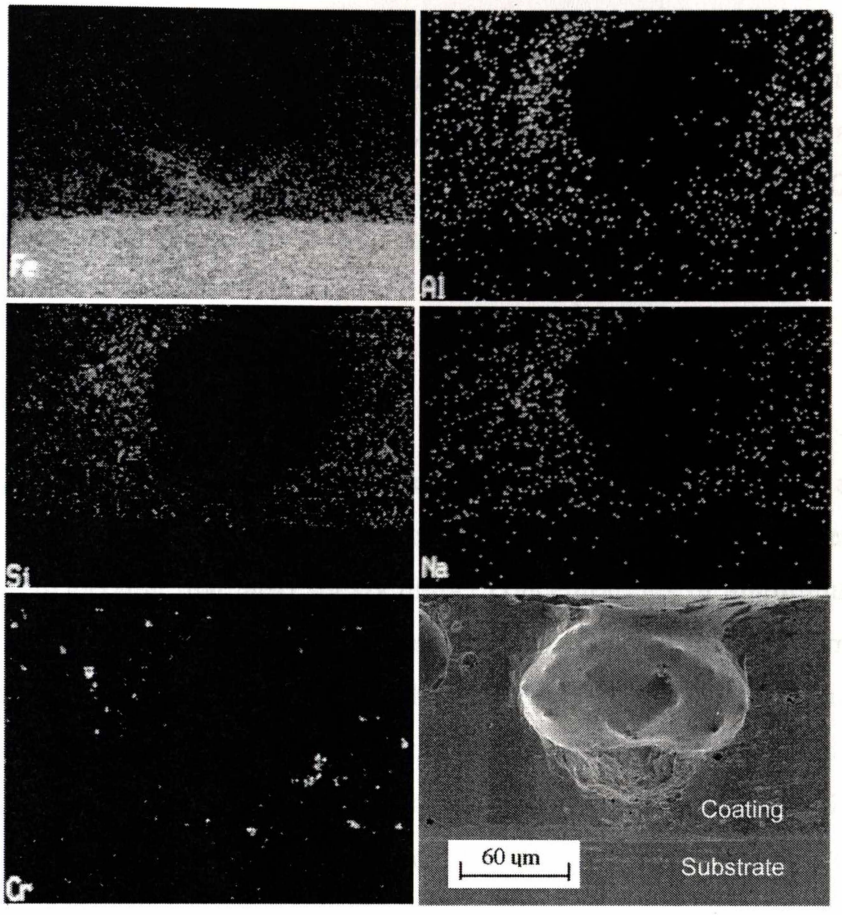

Figure 6.15 EDS elemental mapping of sample cross-section of the pinhole region.

A defect, known as copper head because of its reddish colour can result when iron oxidation contaminates the enamel coating.[1,16,17] It is typically associated with a pinhole in the enamel layer when a large bubble opens up during firing, exposing the steel to oxygen. The iron oxidises and mixes with the glass enamel, producing the red colour.

The elements Si, Al and Na (from their respective maps, Figure 6.15) tend to be evenly dispersed in the coating around the defect region. However, there are higher concentrations of Si, Al and possibly Na in the upper left side of the pinhole, indicating that these elements are part of a sodium-alumina-silicate phase. The Raman spectrum taken at a similar area at the side of the defect (point b,

Figure 6.13b) indicated the presence of a crystalline silica phase (α-quartz) as well as chromium oxide (α-Cr_2O_3).

The chromium map (Figure 6.15, bottom left) indicates that Cr clusters in small discrete areas around the pinhole. This is similar to the elemental mapping of the GGA coating cross-section (Figure 6.7), which showed higher concentrations of Cr at the boundaries of the bubble inclusion within the enamel coating. Cr is part of the compound, chromium oxide (α-Cr_2O_3) identified by Raman analysis (Figure 6.13).

Surface

Elemental mapping a pinhole from the surface shows that there is a higher concentration of Na on the left surface of the defect (Figure 6.16, top left). The aluminium dispersion map also shows higher concentrations of aluminium in the same region (Figure 6.16, towards bottom left). Si (Figure 6.16, bottom left) is found in all areas of the coating around the defect. The Cr (Figure 6.16, top right) dispersion map corresponds well with the mapping of the cross-section. Cr is present in small discrete areas with higher densities around the edge of the defect (similar to Figures 6.7 and 6.15). Ni and Co are sparsely scattered around the pinhole.

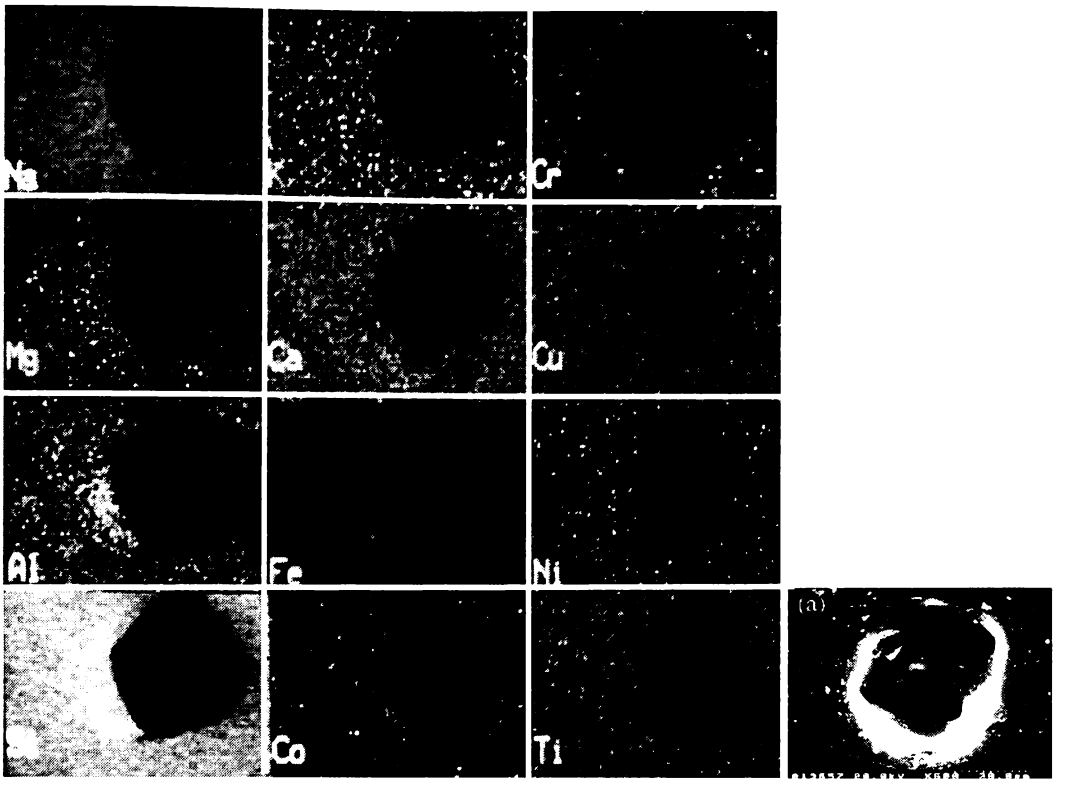

Figure 6.16 Elemental mapping of pinhole region from coating surface.

6.4 Summary

The phases present in a single-coat enamel on steel substrate system were characterised using Raman microscopy, and EDS in conjunction with SEM. Raman microscopy gave information on the crystalline phases present in the enamel coating and pinhole defect region and expands the information collected from EDS.

The Raman spectra of a cross-section of coating indicates a predominant band at 549 cm^{-1}, corresponding to α-Cr_2O_3, and a weak band at ca. 456 cm^{-1}, which was assigned to α-quartz.

The EDS elemental profile and mapping indicated that the porcelain enamel has a high Fe content on the metal surface to 65 μm into the coating. This is postulated to be due to iron oxide diffusing from the substrate into the enamel coating during the firing process, and is part of the adhesion mechanism. The major compositional constituent, Si (as silica), was well dispersed throughout the coating, while other elements such as Ca, Mn, Ni and Co were present at lower

percentages. EDS elemental mapping also indicated high Fe concentrations below the pinhole defect. One reason that caused this effect was the original bubble opening at the coating surface and exposing the base metal to oxygen, thereby increasing iron oxidation and diffusion below the defect region. Conversely, it is possible that the outward diffusion of Fe was stopped by the pinhole resulting in accumulation of Fe at the edge of the pinhole.

The Raman spectra of a cross-section of the pinhole defect had a sharp band at ca.550 cm^{-1}, indicating α-Cr_2O_3. Spectra of the coating away from the defect region as well as the coating surface in the defect region showed the presence of α-Cr_2O_3 and α-quartz. EDS elemental mapping of the cross-section and the surface of the coating showed Cr clusters in small discrete areas with greater concentrations around the boundary of the pinhole defect.

6.5 References

1. Kyri, H., *Handbook for bayer enamels*. 1975: Bayer AG.
2. Pask, J.A., *Chemical Reactions and Adherence at Glass-Metal Interfaces.* Proceedings of the Porcelain Enamel Inst. Tech Forum, 1971: p. 1-16.
3. Ritchie, D., Schaffer, H.A. and White, D., *The presence of an iron oxide layer at the enamel/steel interface in one-coat porcelain enamelling.* J. Mat. Sci., 1983. **18**: p. 599-604.
4. Schrader, ed. *Infrared and Raman Spectroscopy - Methods and Applications.*. 1995, VHC.
5. Beattie, I.R. and Gilson, T.R., J. Chem. Soc. (A), 1970: p. 980.
6. Scott, J.F. and Porto, S.P.S., Phys. Rev., 1967. **161**: p. 903.
7. McMillan, P., *Structural Studies of Silicate Glasses and Melts - Applications and Limitations of Raman Spectroscopy.* American Minreralogist, 1984. **69**: p. 622-644.
8. Murray, C.A.and Greytak, T.J., *Intrinsic surface phonons in amorphous silica.* Phys. Rev. B, 1979. **20**: p. 3368.
9. Frost, R.L., Fredeicks, P.M. and Shurvell, H.F., Can. J. Appl. Spectrosc., 1996. **41**: p. 10.
10. Frost, R.L. and Rintoul, L., Appl. Clay Sci., 1996. **11**: p. 171.
11. Devi, S.A., Philip, D. and Aruldhas, G., J. Solid State Chem., 1994. **113**: p. 157.
12. Krishnamuti, D., Proc. Indian Acad. Sci., 1956. **43A**: p. 210.
13. Degan, I.A. and Newman, G.A., Spectro. Acta, 1993. **49A**(5/6): p. 863.
14. Escol, *The Vitreous Enameller's Diary.* 1994: Escol.
15. Buerhop, C., Condrate Sr., R.A., Moertel, H. and Hapanowiz, R.P, *Appl. Spectroc.* 1992. **46**: p. 1545.
16. Vargin, V., *Technology of Enamels.* 1968: Maclaren and Sons Ltd.
17. Andrews, A.I., *Porcelain Enamels. The Preparation , Application, and Properties of Enamels.* 1961: The Garrard Press, Publishers.

Chapter Seven
Conclusions and Recommendations

Chapter Seven
Conclusions and Recommendations

7.1 Conclusions

7.1.1 Phase Characterisation

The structural and compositional characteristics of five different commercial porcelain enamel coatings and their component raw materials were examined using Raman and infrared (IR) spectroscopy. These techniques extend data from the more conventional analytical methods for characterising porcelain enamels - energy dispersive X-ray analysis (EDS), inductively coupled plasma spectrometry (ICP) and X-ray diffraction. Data showed that the enamels and the individual components investigated were very complex with various amorphous and crystalline phases.

The XRD and vibrational spectra of frit samples showed that amorphous phases were dominant. The main compounds of the frits were determined as silicates and borates. Vibrations (medium broad bands) characteristic of SiO_4 tetrahedra (Si-O and Si-O-Si at 950-1091 cm^{-1}), were found in both the Raman and IR spectra. However, only the IR technique was capable of identifying the presence of B-O bonds associated with B_2O_3 (as BO_3 or BO_4 units). The XRD data was in agreement with the vibrational analysis. In all cases, a broad peak at approximately 30° (2θ), typically associated with glass dominated the spectra.

By contrast, the colouring pigments appeared to be mainly crystalline. EDS analysis showed that all the pigments contained Cr. From the IR and XRD spectra, Cr was detected in many crystalline phases including $FeCr_2O_4$, Cr_2O_3 and

$CuCr_2O_4$. The EDS, IR and XRD results also showed that all the pigments except MBA1 contained Si in the form of crystalline SiO_2.

Vibrational spectroscopy and XRD data indicated that amorphous phases were present in the fired glass enamel coatings. However, crystalline compounds could be detected in the amorphous material of the glassy matrix. The dominant components in the amorphous phase are borates and silicates. These compounds were identified through the presence of their B-O-Si, Si-O-Si and B-O stretching modes in the Raman spectra. The presence of amorphous silica was confirmed by XRD analysis. The surface sensitive ATR-IR spectra of the coatings are dominated by B-O stretching modes at 1200-1250 and 1408-1480 cm^{-1}, suggesting that borates are present at the coating surface. Many of the crystalline phases in the fired enamel coating detected by XRD and vibrational spectroscopic analysis including $FeCr_2O_4$, Cr_2O_3 and SiO_2 matched those in the colouring pigments.

Raman and IR spectroscopy provide complementary information on phase compositions and should be used together. For example, Raman data of the colouring pigment gloss green A did not reveal any distinct bands, mainly because the laser light was absorbed by the dark pigmentation. However, bands in the IR (absorbance) spectrum indicated chromite, quartz and amorphous silica, which could be matched with the chromite and quartz phases detected using XRD.

Raman and IR spectroscopy data, supplemented with more conventional analytical techniques for porcelain enamels, provide useful structural and compositional information about porcelain enamels. This can be used to develop new formulations that will improve porcelain enamel coating performance and finish quality.

7.1.2 Chemical Resistance

Enamel corrosion can be examined in terms of primary factors such as solid matter (related to decomposition of the glass network) and secondary factors such as non-homogeneity of the coating caused by bubbles in the material.

Composition triangular diagrams were developed by grouping different oxides together. These diagrams can be used to predict how compositional changes affect the chemical resistance of the glass matrix. Enamels with higher SiO_2 content but similar modifier to R_2O_3 ratios on the SiO_2-R_2O_3-R_2O composition diagram, (for example GBB), have greater chemical resistance because more compact tetrahedra are formed. These are associated with less modifier ions being available for ion exchange by hydrogen ions from the acid solution.

Of the enamels tested, the MBA enamel had the least resistance to acid and alkali attack. The SiO_2-R_2O_3-R_2O composition diagram indicated this enamel had excess R_2O_3 and the lowest SiO_2 content. Its lower chemical resistance is due to a less dense structure; the excess Al_2O_3 acts as modifier ions and are easily leached during acidic attack.

There was no correlation between bubble area over the entire depth of the coatings and weight loss after acid or alkali exposure. However, there was a general trend for increased corrosion to be correlated with increased bubble area in the top 20 μm of coating. This indicates that that the upper bubble area rather than the bubble area through the coating depth is an important factor in chemical resistance. The barrier that builds on the coating surface with time during acid attack inhibits further ion diffusion and prevents further corrosion. Therefore, only bubbles in the top region of the coating influence corrosion.

Increasing the silica content of GBA commercial coating from 3 to 12 wt% increased its acid resistance but not its alkali resistance. However, other properties such as adherence were adversely affected. Increasing silica from 3 to 7 wt% also reduced adherence rating. The extra silica may have made the coating too refractory (hard) and weakened the enamel-steel bond.

Increasing HB clay in the coating from 3 to 12 wt% decreased alkali resistance. This is probably because the alumina content was increased sufficiently changing its function of network former to network modifier. Adding HB clay also gave greater adherence than the addition of extra silica. However, the surface appearance changed and became speckled with darker regions. Increasing both

silica and HB clay by 3 wt% improved the acid and alkali resistance of the GBA enamel without adversely affecting adherence or appearance.

7.1.3 Coating and Pinhole Study

Raman microscopy analyses of the crystalline phases present in the GGA coating and near pinhole defects were used to extend EDS spectral and elemental mapping information. The Raman spectra of a coating cross-section revealed bands indicating α-Cr_2O_3 and α-quartz. The EDS elemental profile and mapping indicated high Fe content on the metal surface to 65 μm into the coating. This is caused by iron oxide diffusing from the substrate into the enamel coating during the firing process, and is part of the adherence mechanism.

Raman microscopy cross-sectional studies of a pinhole defect also indicated the presence of α-Cr_2O_3. By contrast, α-Cr_2O_3 and α-quartz were detected away from the defect region. The high Fe concentrations detected by EDS below the pinhole defect were caused by the original bubble opening at the coating surface and exposing the base metal to oxygen. This increases iron oxidation and diffusion below the defect region.

Elemental mapping showed similar dispersions of Si and Al throughout the enamel cross-section. However, Si and Al concentrations increased at the upper edge of the pinhole defect, indicating that these elements are part of an alumina-silicate phase. Elemental mapping also revealed the presence of elemental Cr clusters in small discrete areas of the coating. Greater concentrations of Cr were found around the margin of the pinhole defect.

7.2 Recommendations for Future Work

Increased knowledge on the structural and compositional characteristics of complex porcelain enamel glasses will help identify factors that affect corrosion and wear, which can be used to develop new formulations and/or processes to replace the current finish technology. Glass formulation has a significant affect on the corrosion resistance of glass. Further development of composition

diagrams are recommended to sufficiently explain and predict corrosion from alkali attack by allowing for the differences between R_2O and RO modifiers and their affect on corrosion.

This research showed that bubble area also affects the corrosion of porcelain enamels. Bubble structure in the upper zone seems to be the most important. Further corrosion studies are recommended using only one base composition, and a standard process but changing the type and number of bubbles in the coating, and especially in the upper zone. This information would extend the current work on the affect of composition on the corrosion resistance of enamel coatings.

Further studies are needed to elucidate the corrosion mechanism of enamel coatings. This will help develop formulations with improved corrosion resistance. Common methods for quantitatively measuring corrosion are time consuming and use expensive equipment. It is recommended that inexpensive and easily performed analytical methods be developed so industry can quantify and/or predict acid and alkali resistance. The qualitative tests used by most companies may incur subjective errors and cannot be used for inter-company comparisons.

During firing, iron oxide diffuses from the base metal into the enamel coating and could affect the mechanical and chemical properties of the porcelain enamel. Future work could be carried out to quantify the diffusion of iron from the substrate into the enamel as a function of time and temperature, and determine how this affects enamel characteristics.

Other studies that could be undertaken to further characterise porcelain enamel coatings include:

- Identifying the Raman and IR spectral bands associated to the enamel coatings in this study that could not be easily matched with current literature.
- Characterising cover coatings and their enamel batch components using Raman spectroscopy, IR spectroscopy, XRD, EDS and ICP.

- Use of other techniques such as X-ray fluorescence (XRF) and nuclear magnetic resonance (NMR) to help understand structural and compositional characteristics of porcelain enamel coatings and their enamel batch components.

Boiling Citric Acid Test

The following methodology is taken from the Australian Standard AS 2219.1.4 – Determination of Resistance of Vitreous Enamel Coatings to Boiling Citric Acid.

(a) Position one panel on the bottom of the test apparatus with the test surface exposed to the test solution. The top of the cylinder is formed by another test panel with the same enamel or by a stainless steel panel. Screw down the three wing nuts to make the apparatus airtight.

(b) Pour 350 mL of the citric acid solution into the socket for the return flow cooler, replace the latter and switch on the heater. As soon as the citric acid begins to boil (2 to 4 bubbles per second) adjust the heater control so that the citric acid solution gently boils during the remainder of the test.

(c) The test period shall be 2.5, 6 or 24 hours, as specified in the relevant product specimen.

(d) At the conclusion of the test period, empty the test apparatus and after cooling rinse with distilled water. Remove each test panel from the apparatus and wipe it three times with a sponge moistened with distilled water.

(e) Carefully remove any packing residues from the edges of test panels and dry the test panels for 2 hours at 110 ± 5 °C.

(f) Cool in a desiccator for 2 hours. Reweigh to the nearest 0.2 mg to obtain the final mass.

The extent of corrosion is calculated in grams per square metre (g/m^2)

Hot Sodium Hydroxide Test

The following methodology is taken from the Australian Standard AS 2219.1.1 – Determination of Resistance of Vitreous Enamel Coatings to Hot Sodium Hydroxide.

(a) Locate the test panels in the protective envelope and position in the test apparatus with the test surface exposed to the test solution. Screw down the fixing screws to make the apparatus water tight.

(b) Place the sealed test apparatus in the hot water bath at 80 ± 0.1°C in such a way that the frame plates are just submerged. Allow panels to remain for 10 min before filling the apparatus with approximately 320 mL of hot test solution (80 ± 1°C). Allow any air bubbles to escape and seal with the stopper. Cover the bath to prevent loss by evaporation. The thermostatically controlled bath should regain the test temperature within 20 minutes.

(c) After 48 hours remove the test apparatus from the bath and pour off the test solution. Rinse the test apparatus with distilled water.

(d) Remove the test panels from the apparatus and the protective envelope. Wipe them three times with the sponge moistened with acetic acid and finally rinse in distilled water.

(e) Carefully remove reside of the protective envelope from the test panels and dry the test panels for 2 hours at 110 ± 5°C.

(f) Cool in a desiccator for 2 hours. Reweigh to the nearest 0.2 mg to obtain the final mass.

The extent of corrosion is calculated in grams per square metre per day ($g/m^2/d$)

Inductively Coupled Plasma Spectroscopy (ICP)

A GBC Integra XL Inductively Coupled Plasma Atomic Emission Spectrometer (ICP-AES) was used for quantitative analysis of the powdered frits and enamel coatings. The University of Waikato Chemistry Department performed this analysis.

The digestions were carried out in 100mL polypropylene beakers, which were soaked overnight in 2 M HNO_3, then rinsed with distilled water and dried.

HF was used for digestion of the glass powders samples for analysis. To each sample, 14 mL of HF and 6 mL of AR grade HNO_3 were added. The solutions were evaporated overnight leaving a residue. 40 mL of 4 M AR grade HNO_3 was added and warmed to dissolve the residue and create the digest solutions.

For validation and quality control, method blanks were prepared by carrying them through the digestion procedure along with the samples.

Samples were analysed in a single batch manually. Between samples the sample probe was washed with distilled water.

Multi-element standard solutions were used to calibrate each run, and were prepared in the same final acid matrix as the samples.

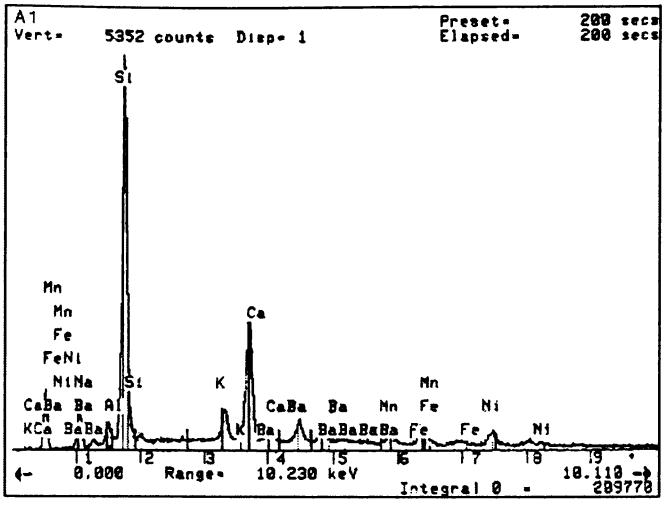

Figure 1 EDS spectrum of frit A1.

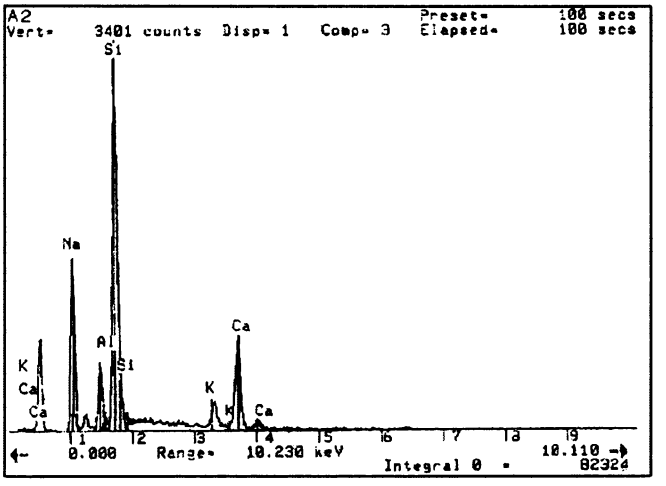

Figure 2 EDS spectrum of frit A2.

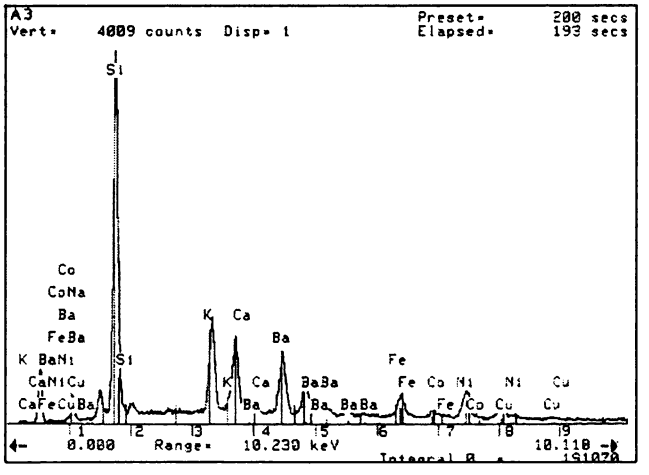

Figure 3 EDS spectrum of frit A3.

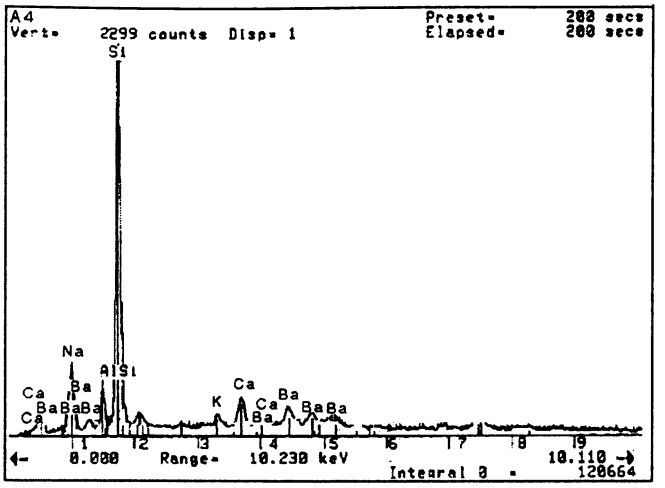

Figure 4 EDS spectrum of frit A4.

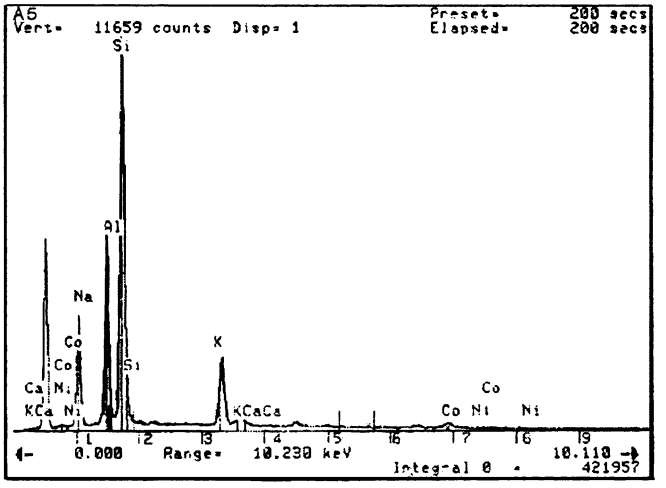

Figure 5 EDS spectrum of frit A5.

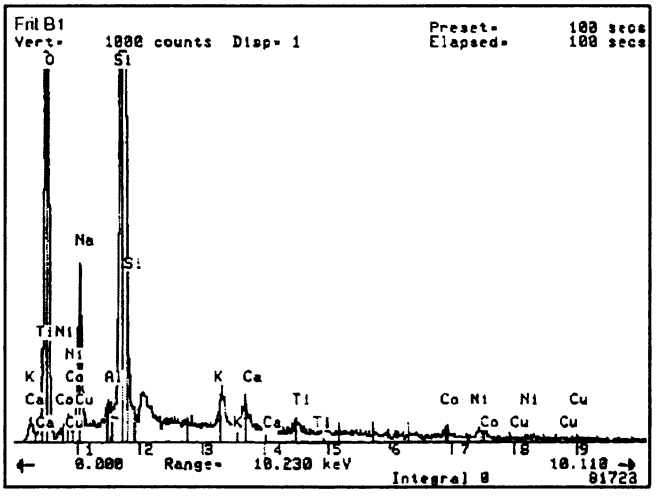

Figure 6 EDS spectrum of frit B1.

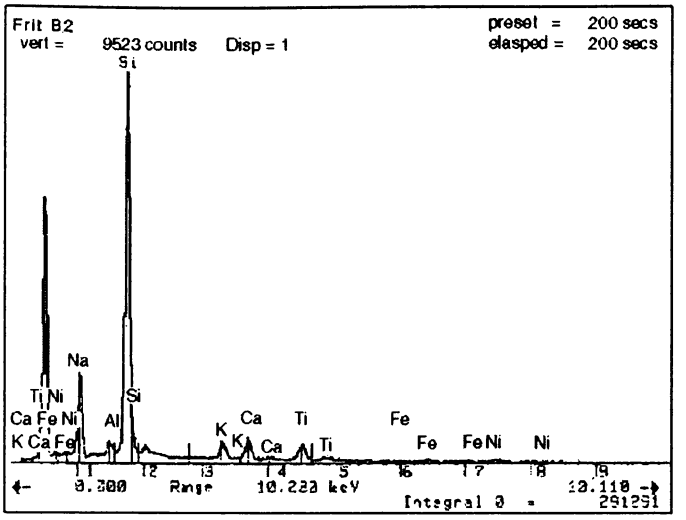

Figure 7 EDS spectrum of frit B2.

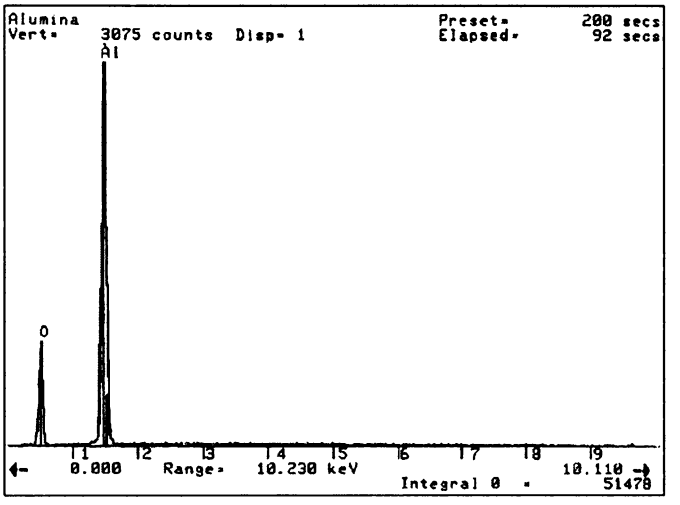

Figure 8 EDS spectrum of alumina.

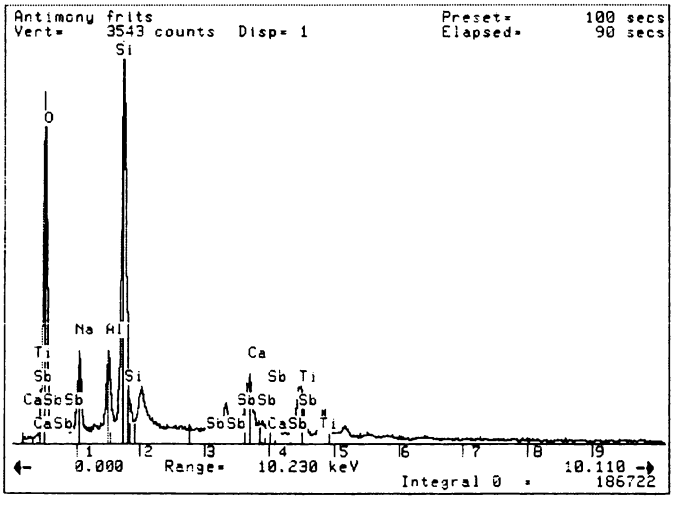

Figure 9 EDS spectrum of antimony frits.

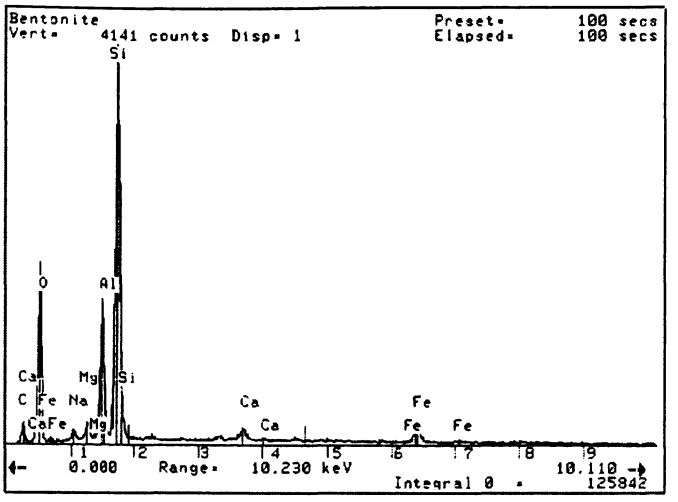

Figure 10 EDS spectrum of bentonite.

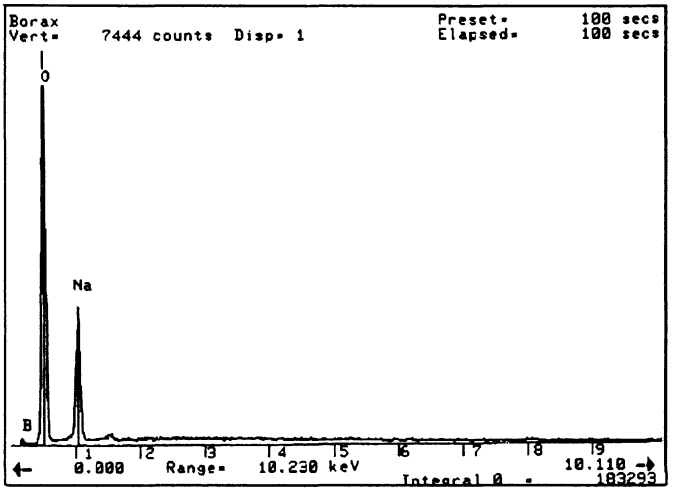

Figure 11 EDS spectrum of borax.

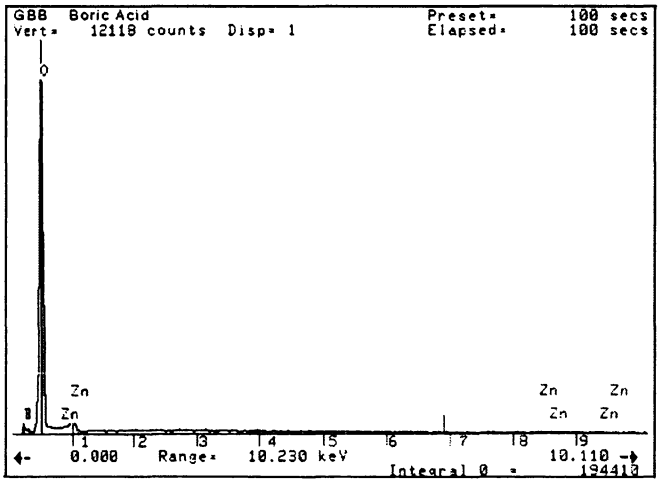

Figure 12 EDS spectrum of boric acid.

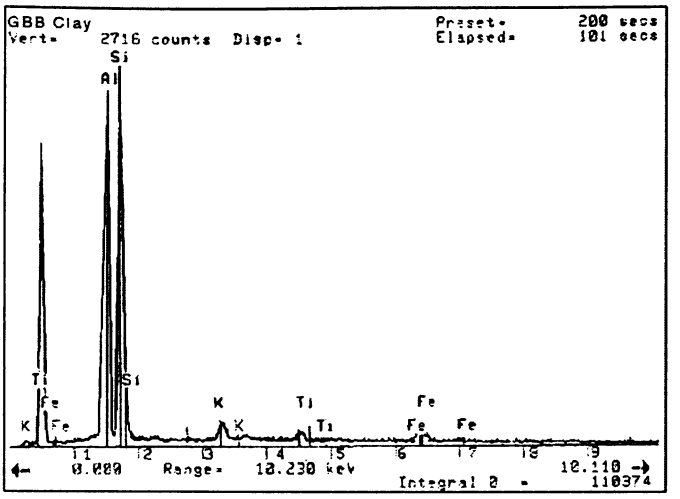

Figure 13 EDS spectrum of clay.

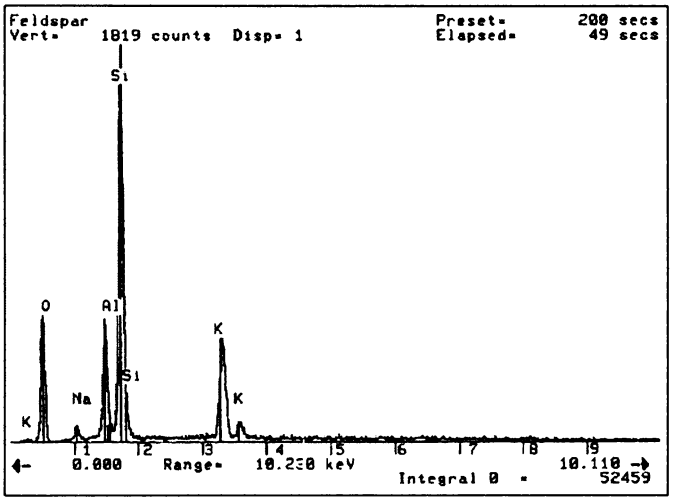

Figure 14 EDS spectrum of feldspar.

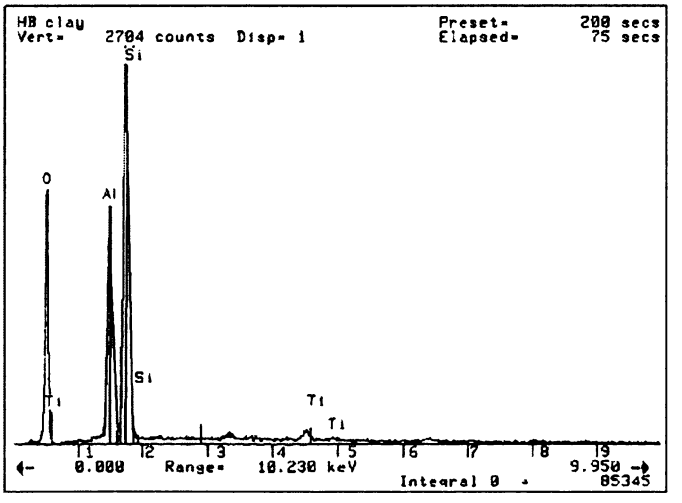

Figure 15 EDS spectrum of HB clay.

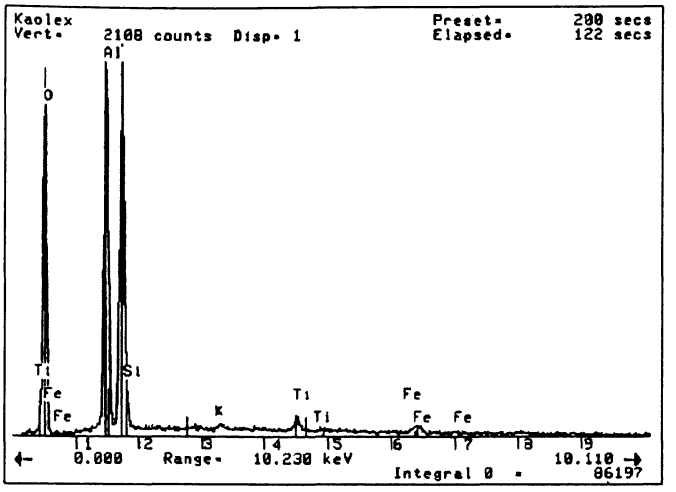

Figure 16 EDS spectrum of kaolex clay.

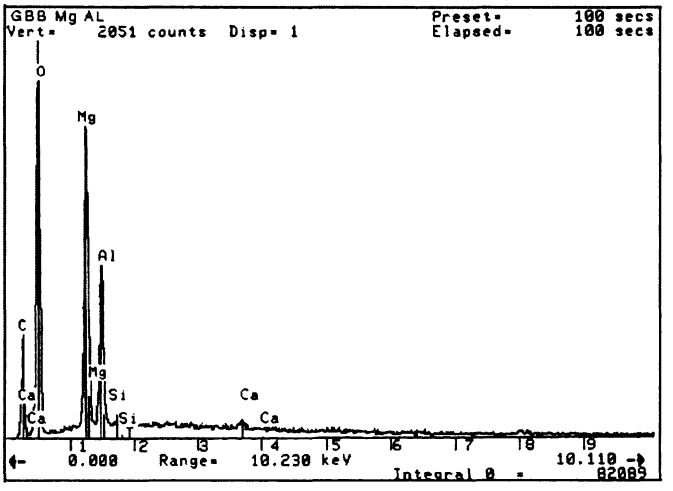

Figure 17 EDS spectrum of magnesium carbonate.

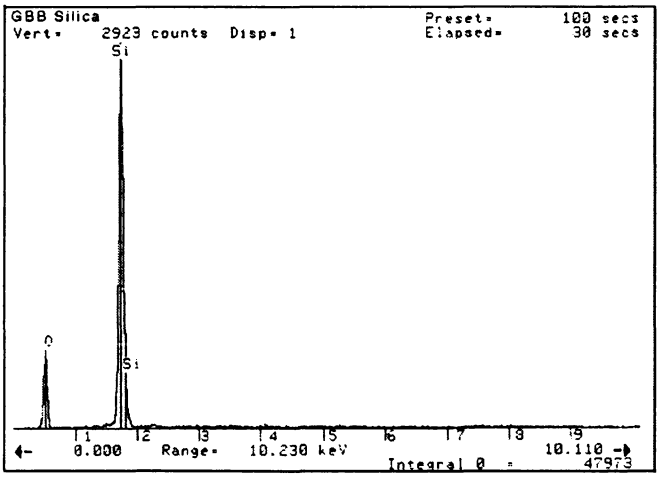

Figure 18 EDS spectrum of silica.

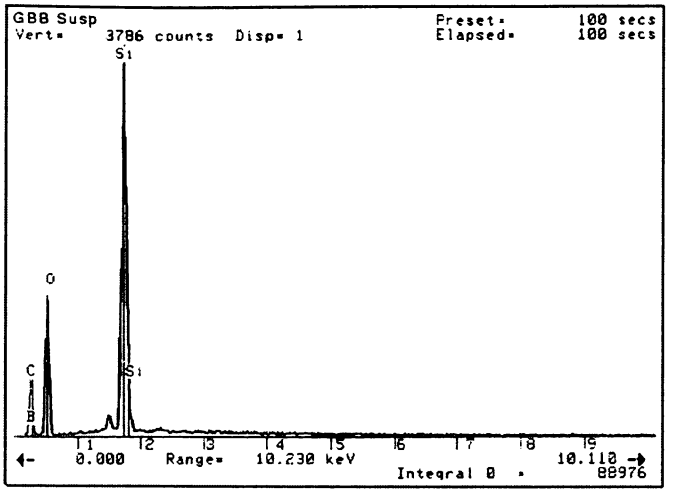

Figure 19 EDS spectrum of mill addition for GBB.

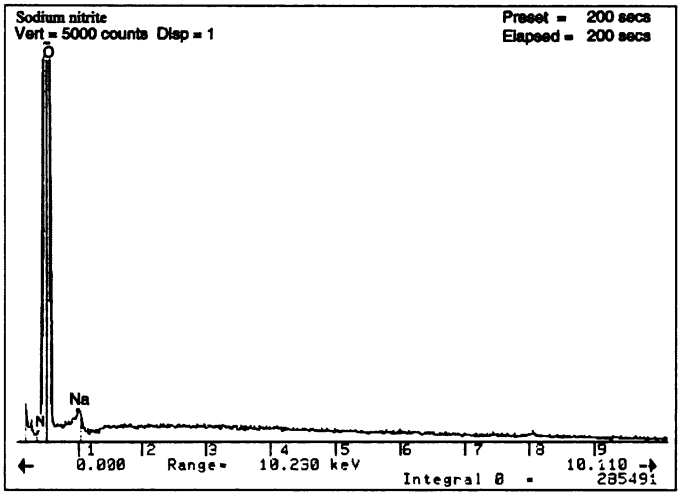

Figure 20 EDS spectrum of sodium nitrite.

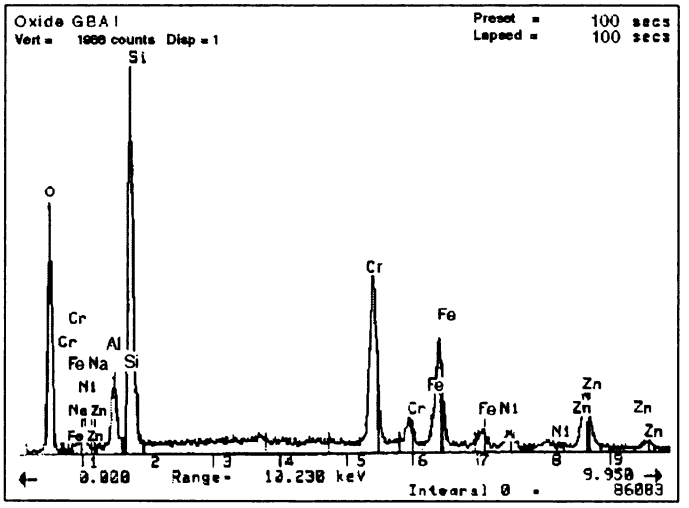

Figure 21 EDS spectrum of colouring oxide GBA1.

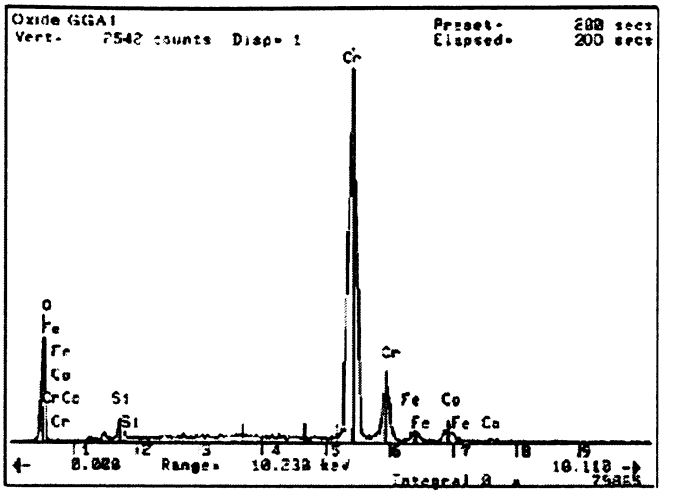

Figure 22 EDS spectrum of colouring oxide GGA1.

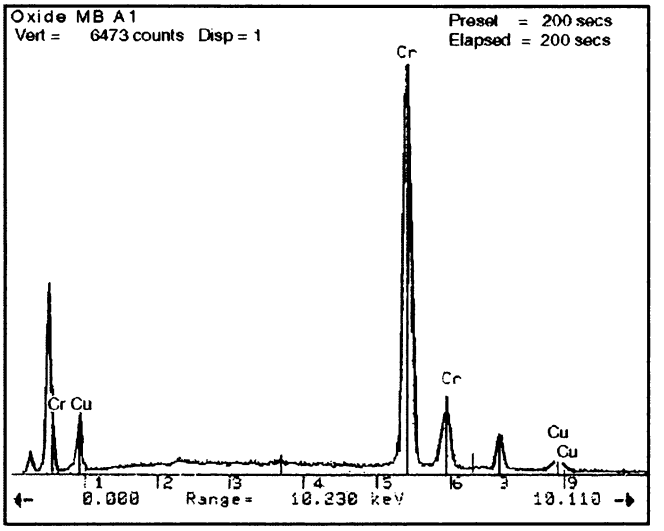

Figure 23 EDS spectrum of colouring oxide MBA1.

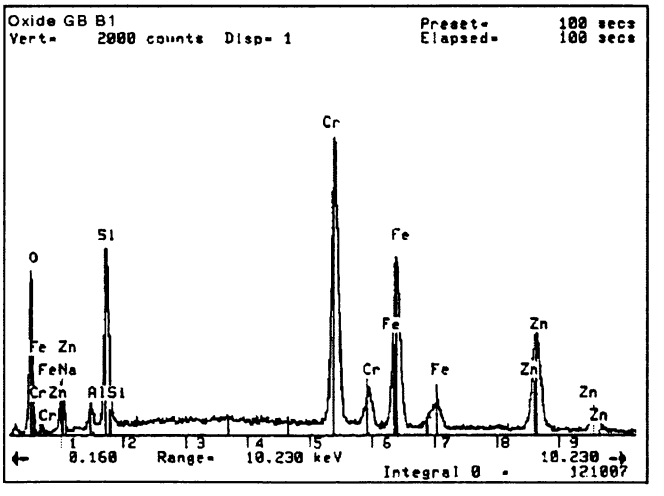

Figure 24 EDS spectrum of colouring oxide GBB1.

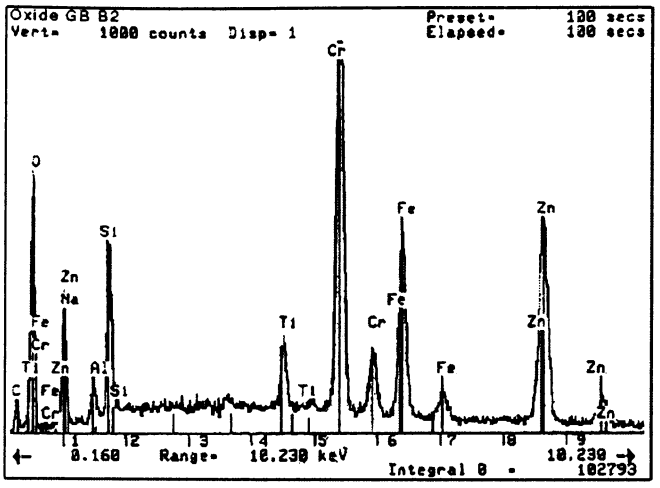

Figure 25 EDS spectrum of colouring oxide 2 GBB2.

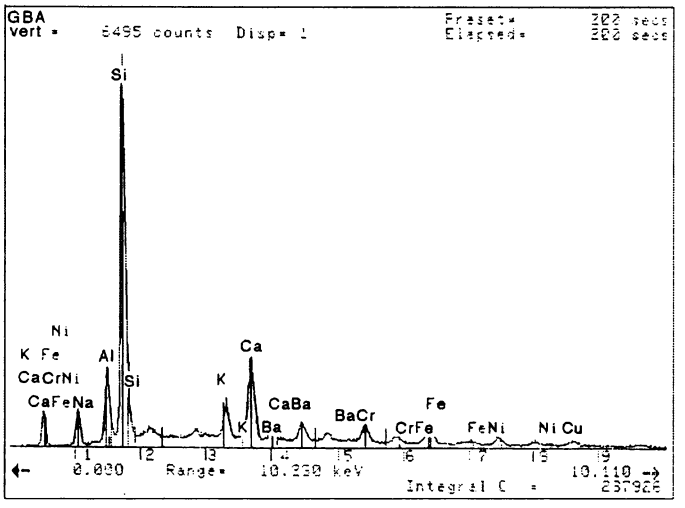

Figure 26 EDS spectrum of GBA coating surface.

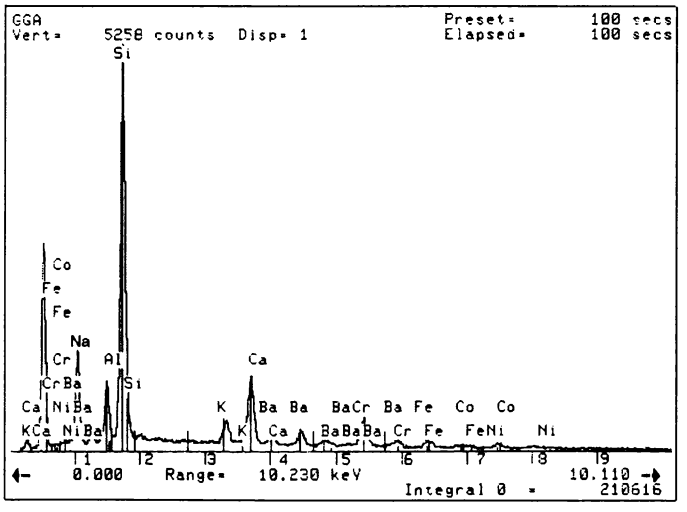

Figure 27 EDS spectrum of GGA coating surface.

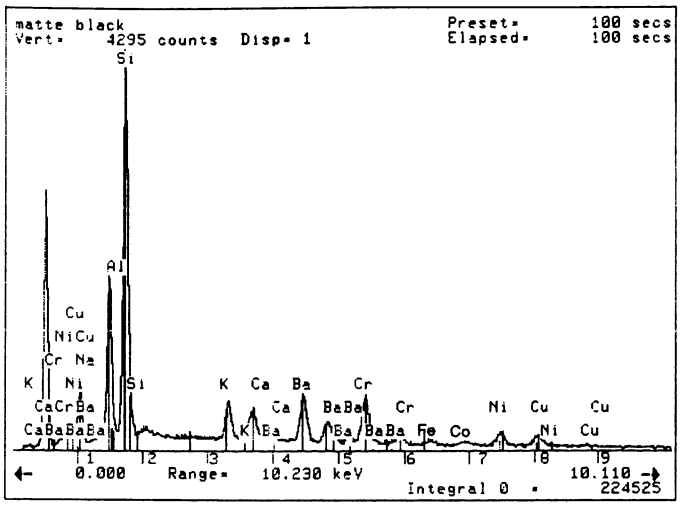

Figure 28 EDS spectrum of MBA coating surface.

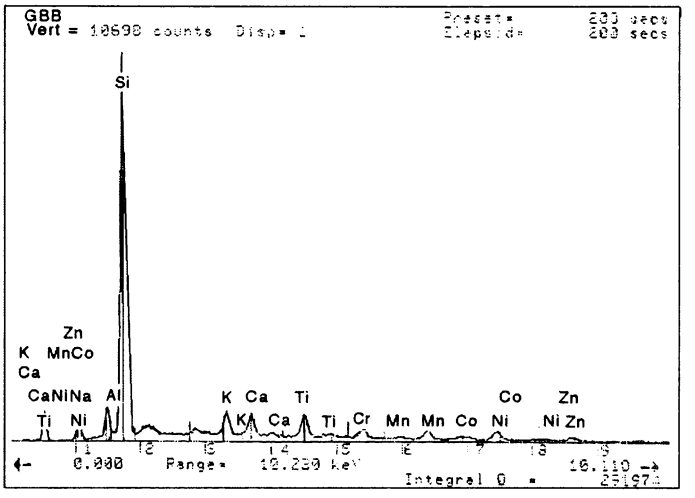

Figure 29 EDS spectrum of GBB coating surface.

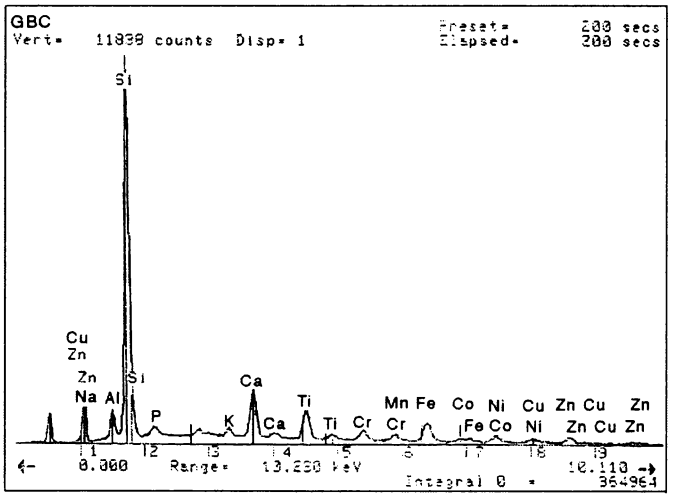

Figure 30 EDS spectrum of GBC coating surface.

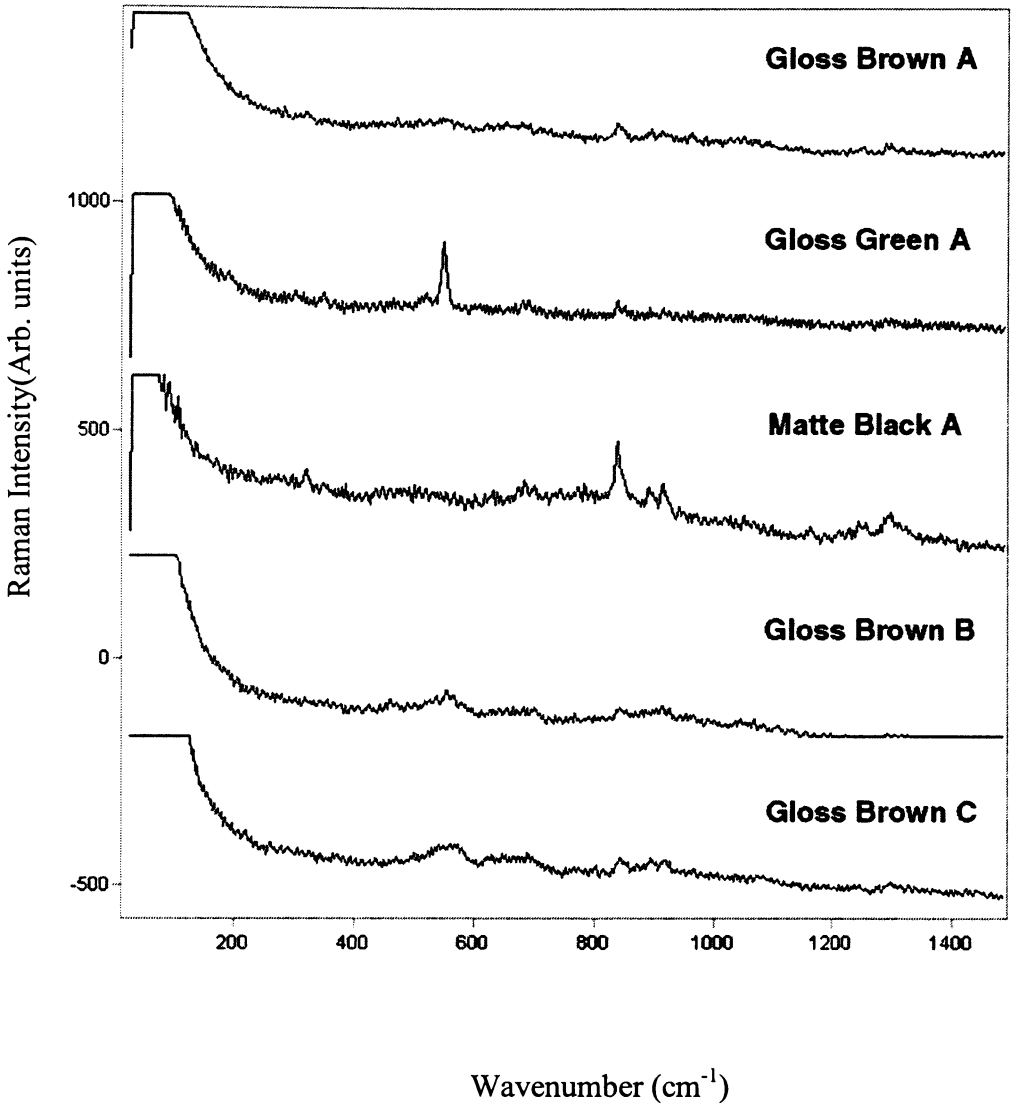

Figure 1 Raman spectra of porcelain enamel coating surfaces.

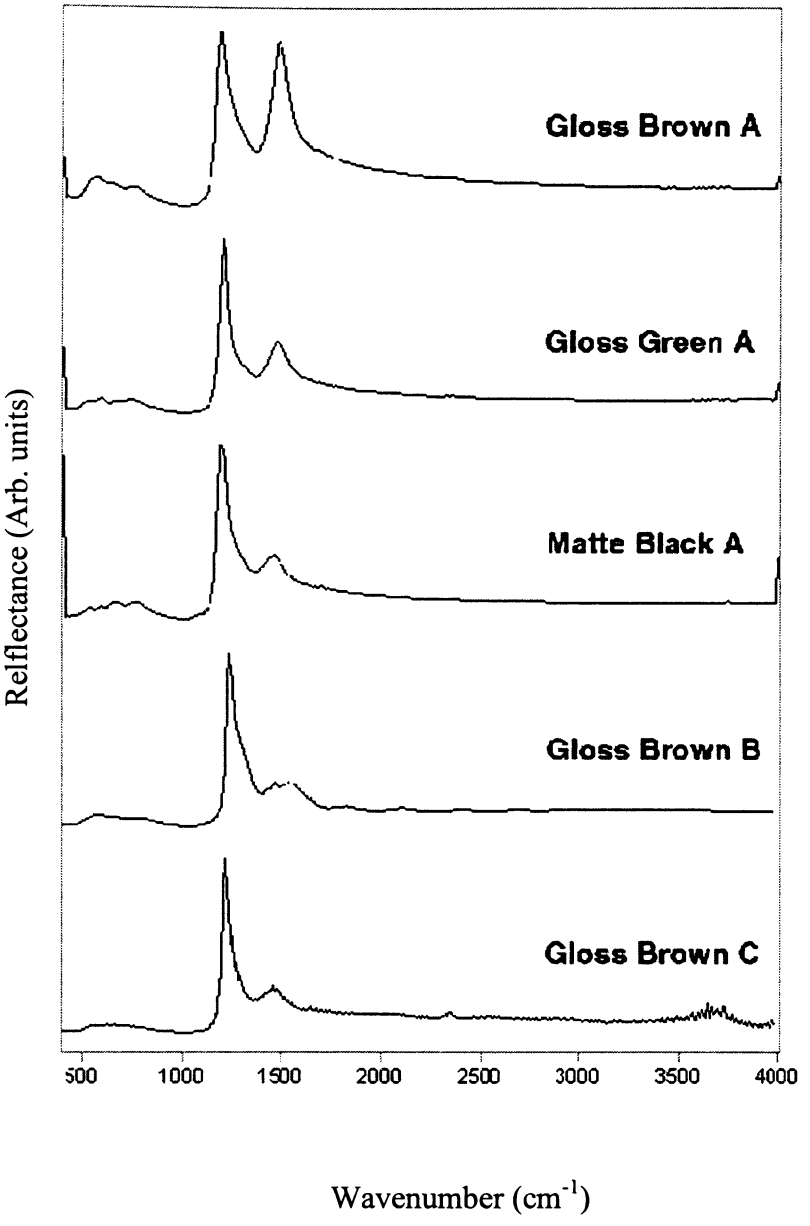

Figure 2 Infrared-reflectance spectra of porcelain enamel coating surfaces.

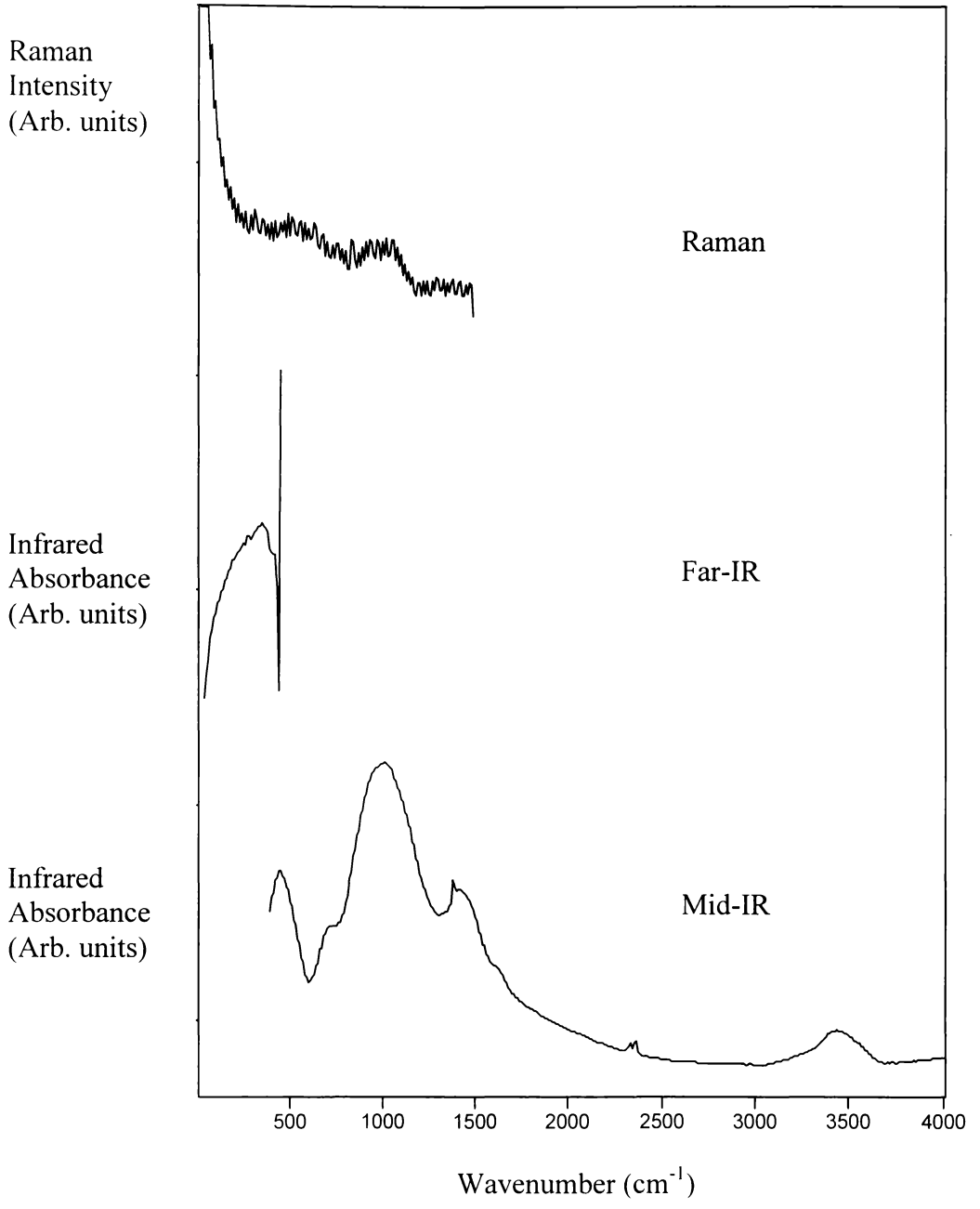

Figure 3 Raman and infrared spectra of frit A.

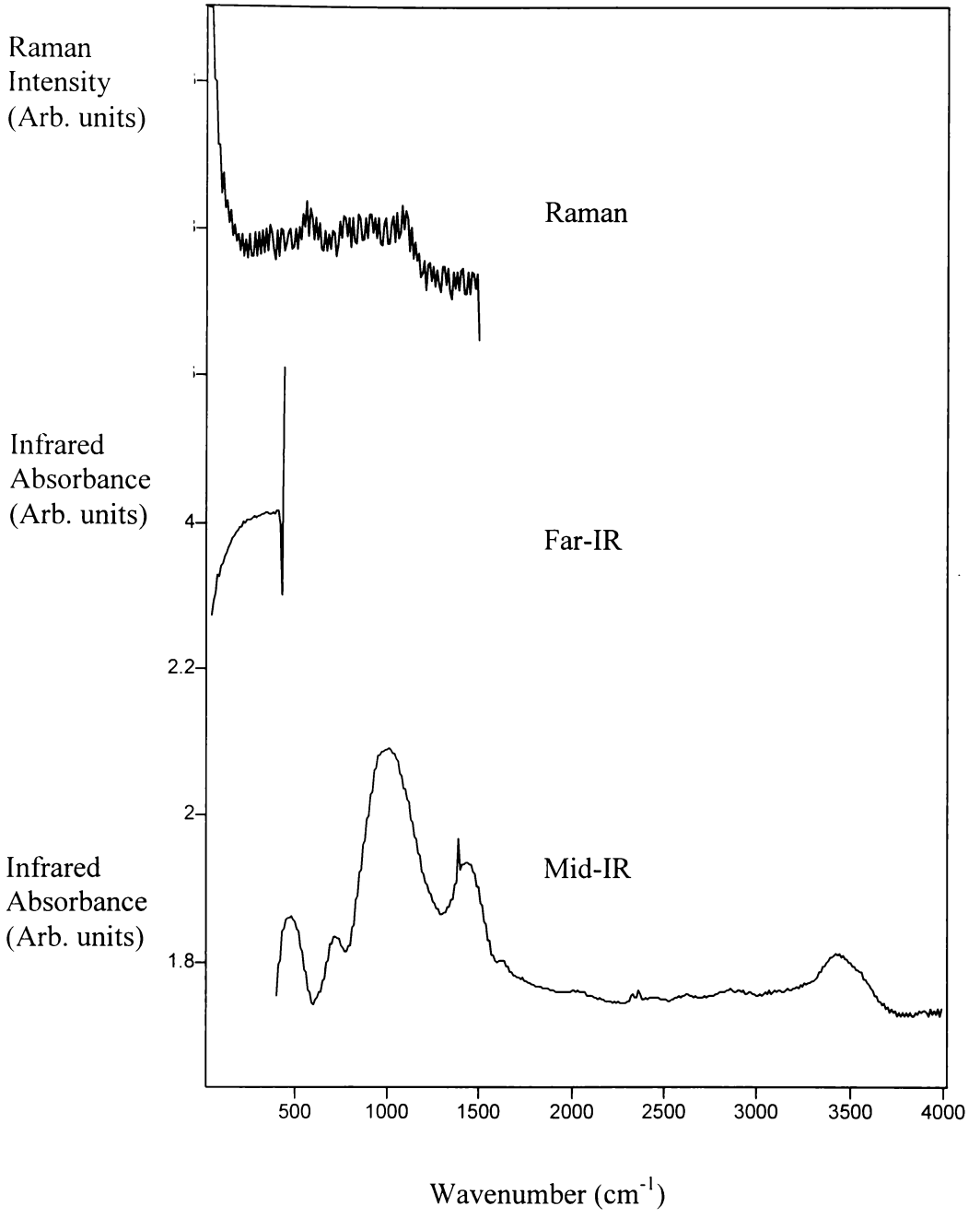

Figure 4 Raman and infrared spectra of frit A2.

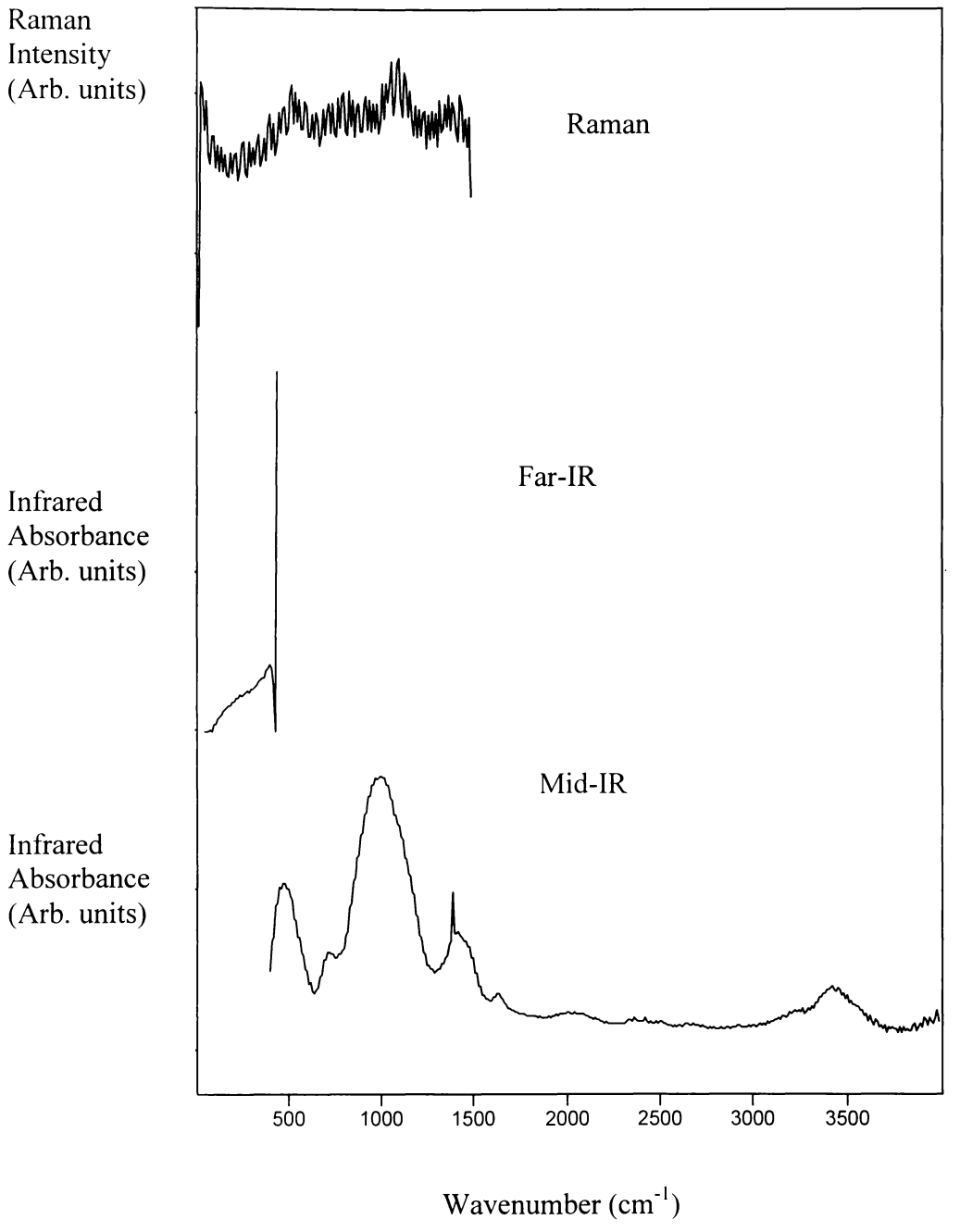

Figure 5 Raman and infrared spectra of frit A3.

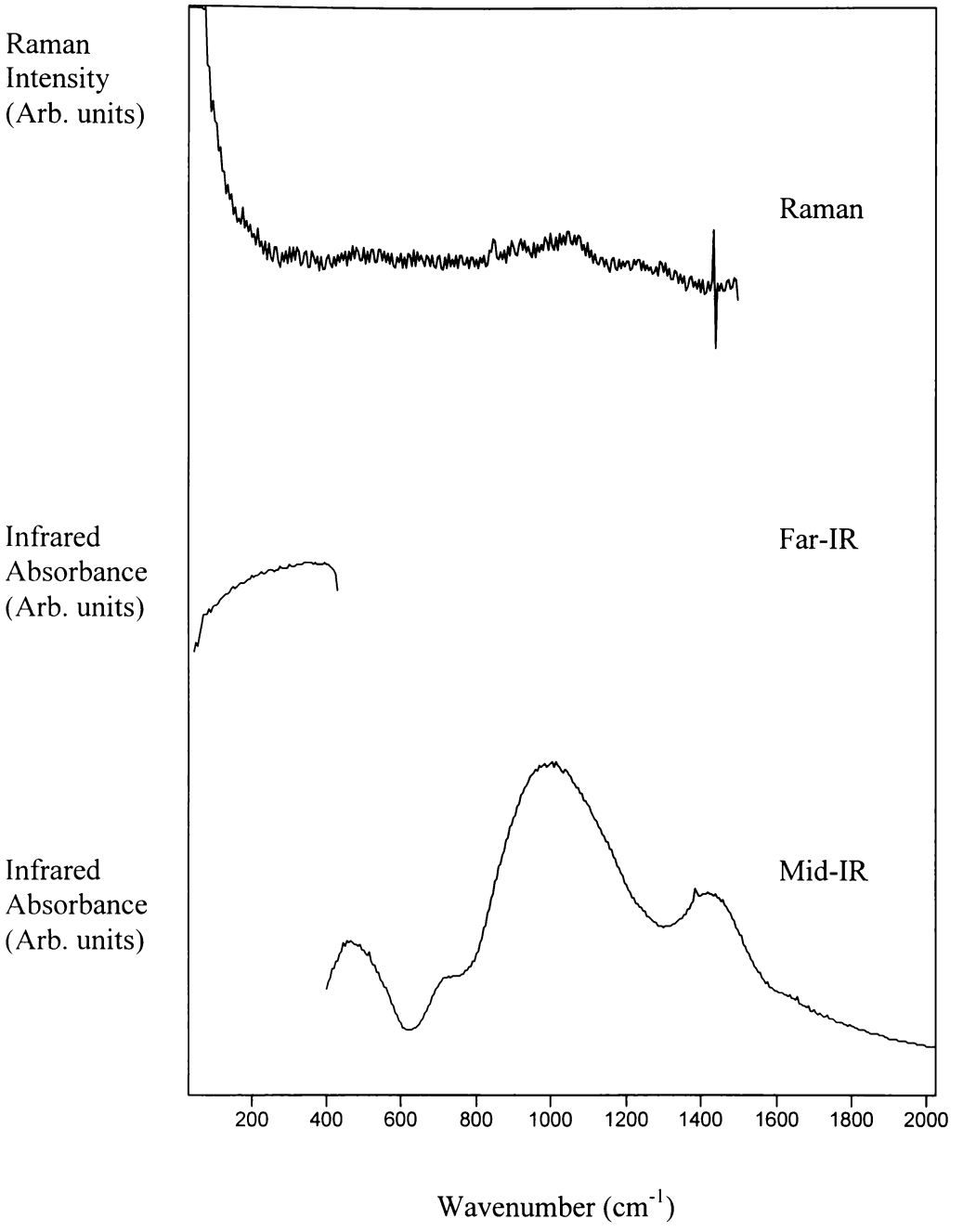

Figure 6 Raman and infrared spectra of frit A4.

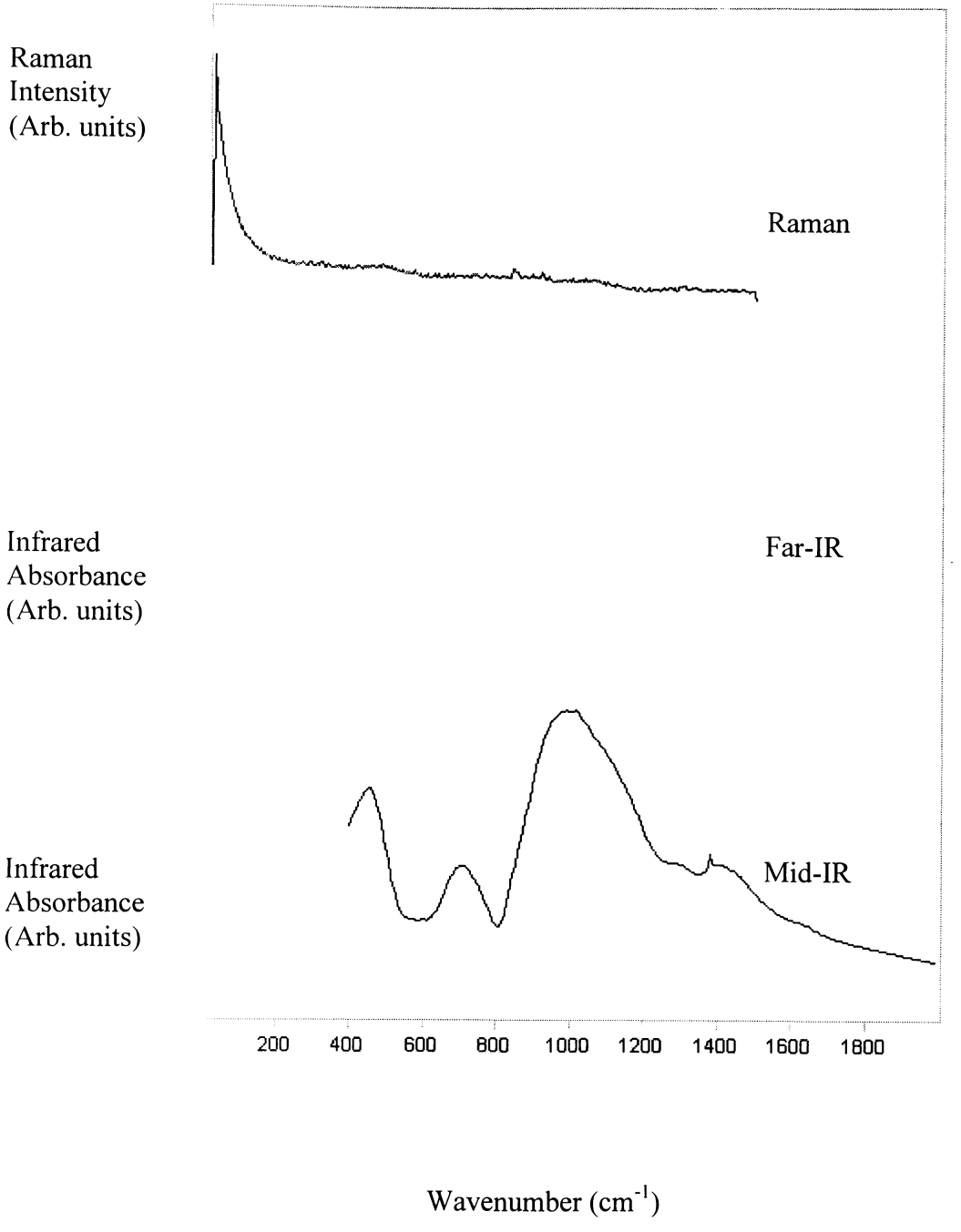

Figure 7 Raman and infrared spectra of frit A5.

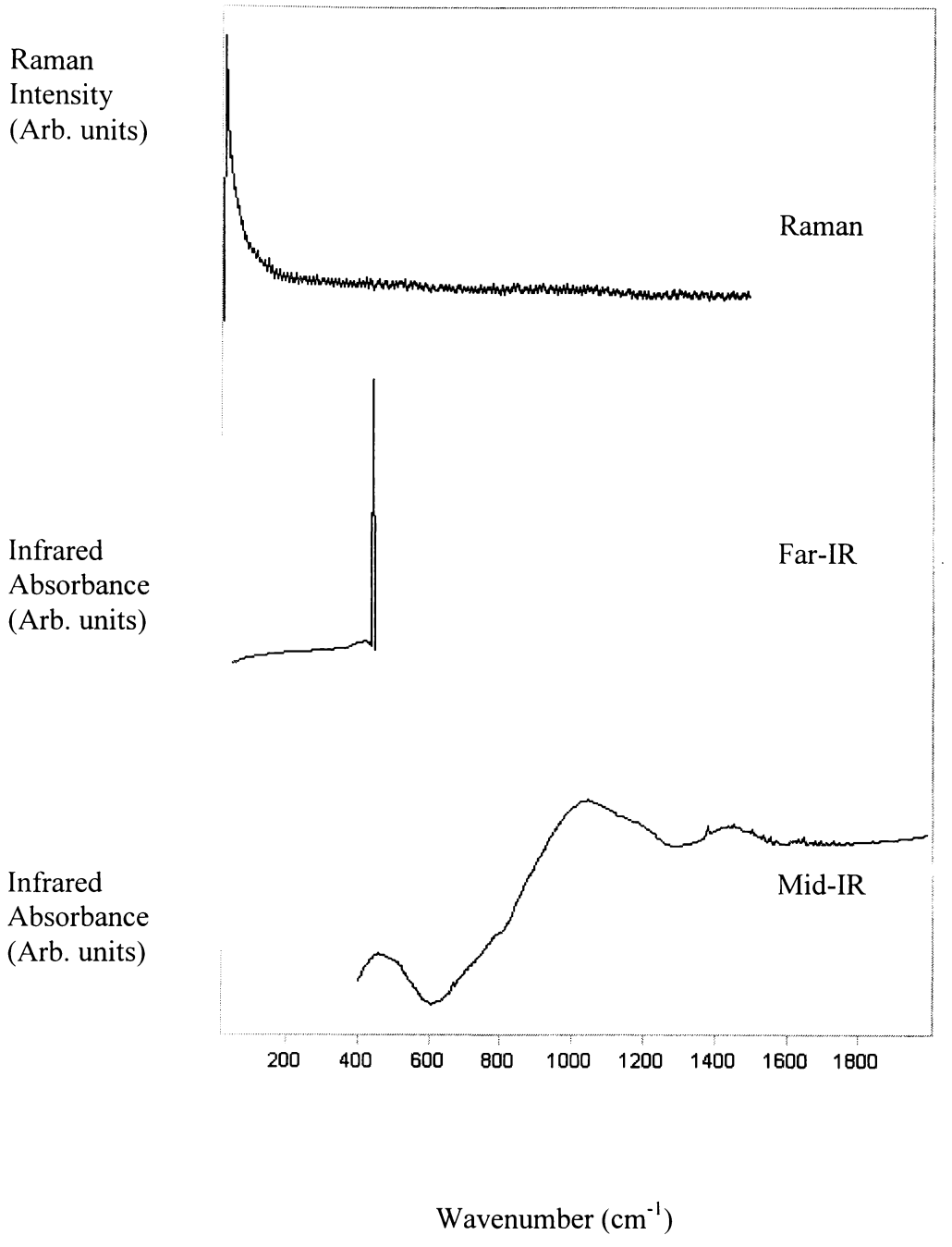

Figure 8 Raman and infrared spectra of frit B1.

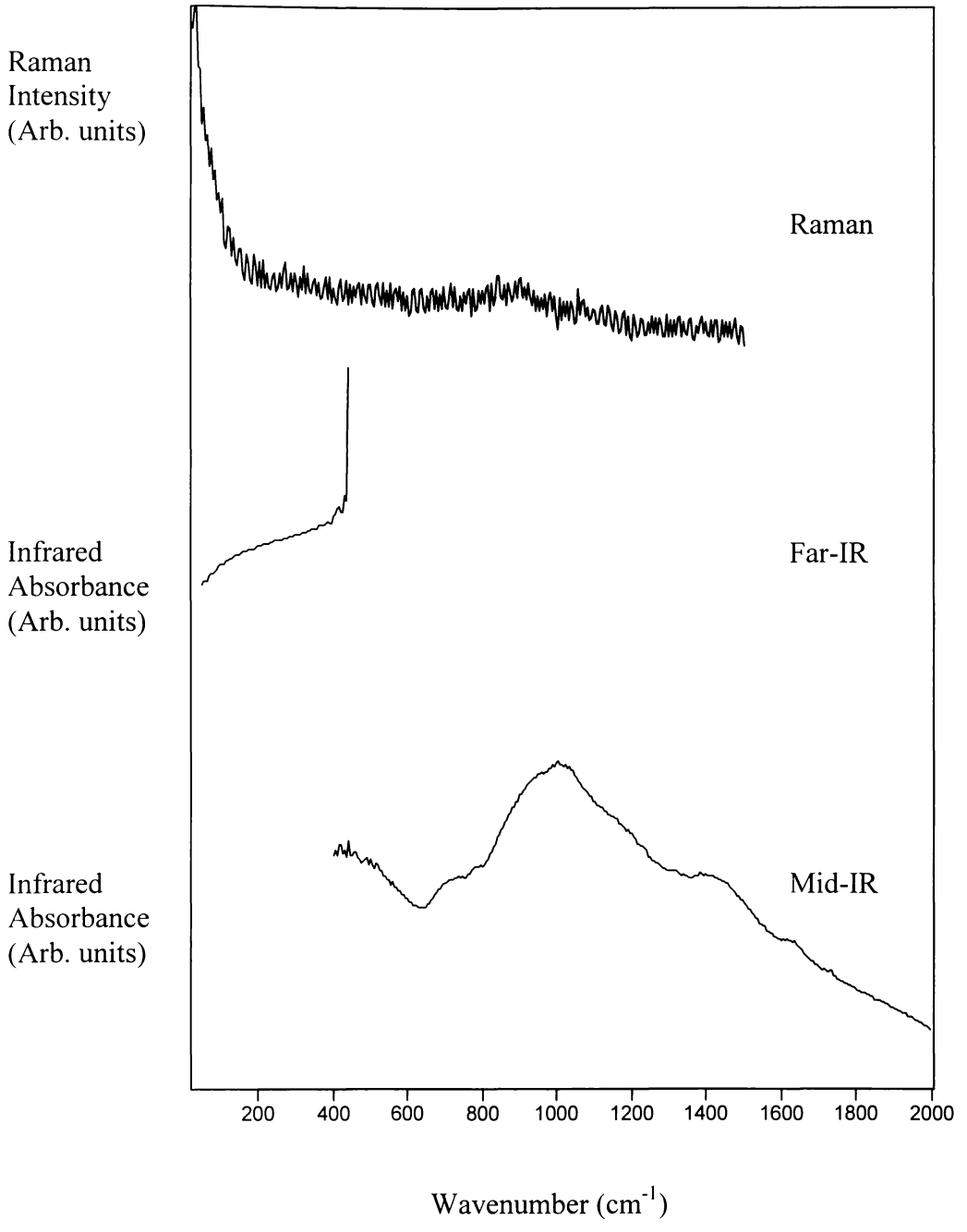

Figure 9 Raman and infrared spectra of frit B2.

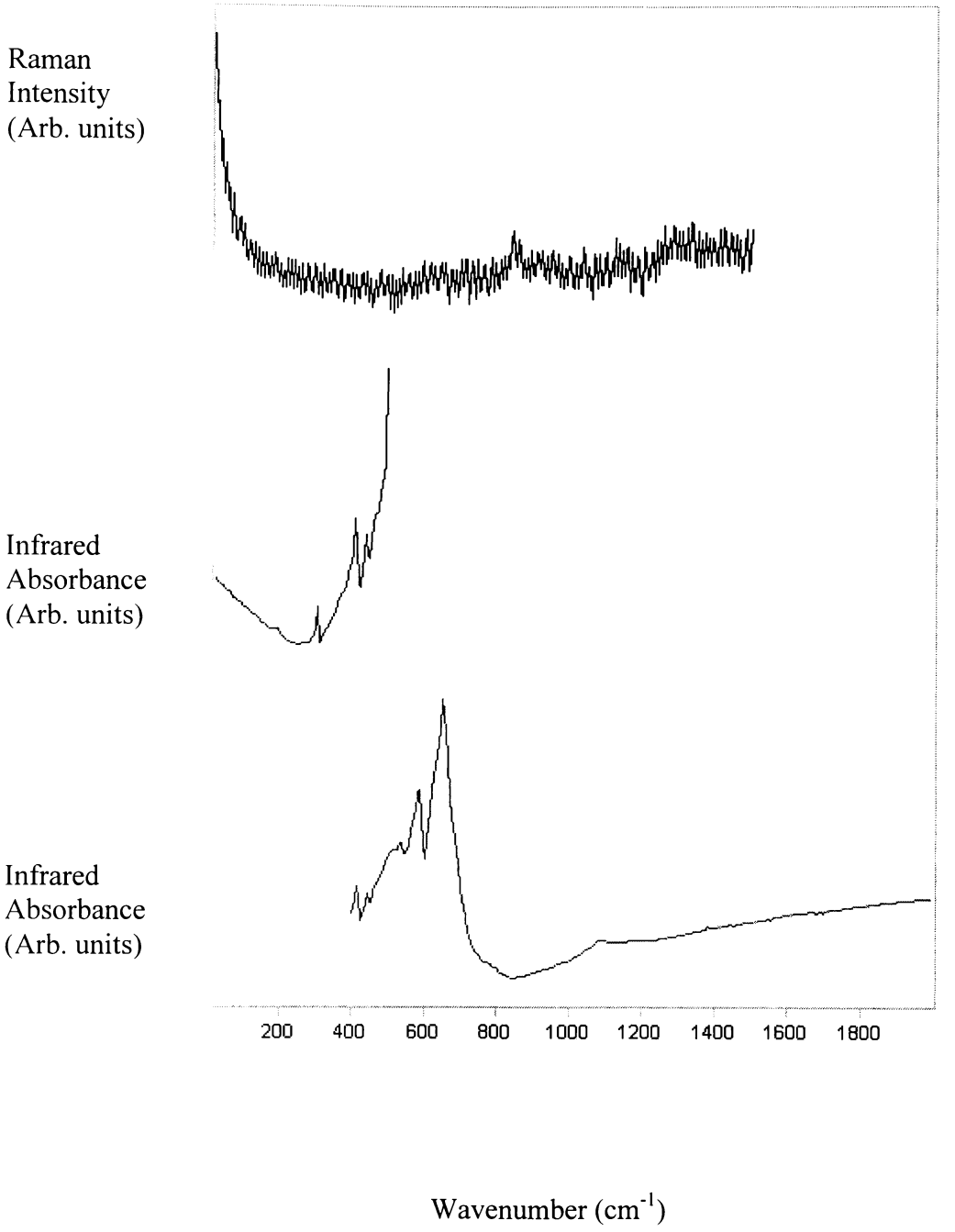

Figure 10 Raman and infrared spectra of GGA colouring pigment (GGA1).

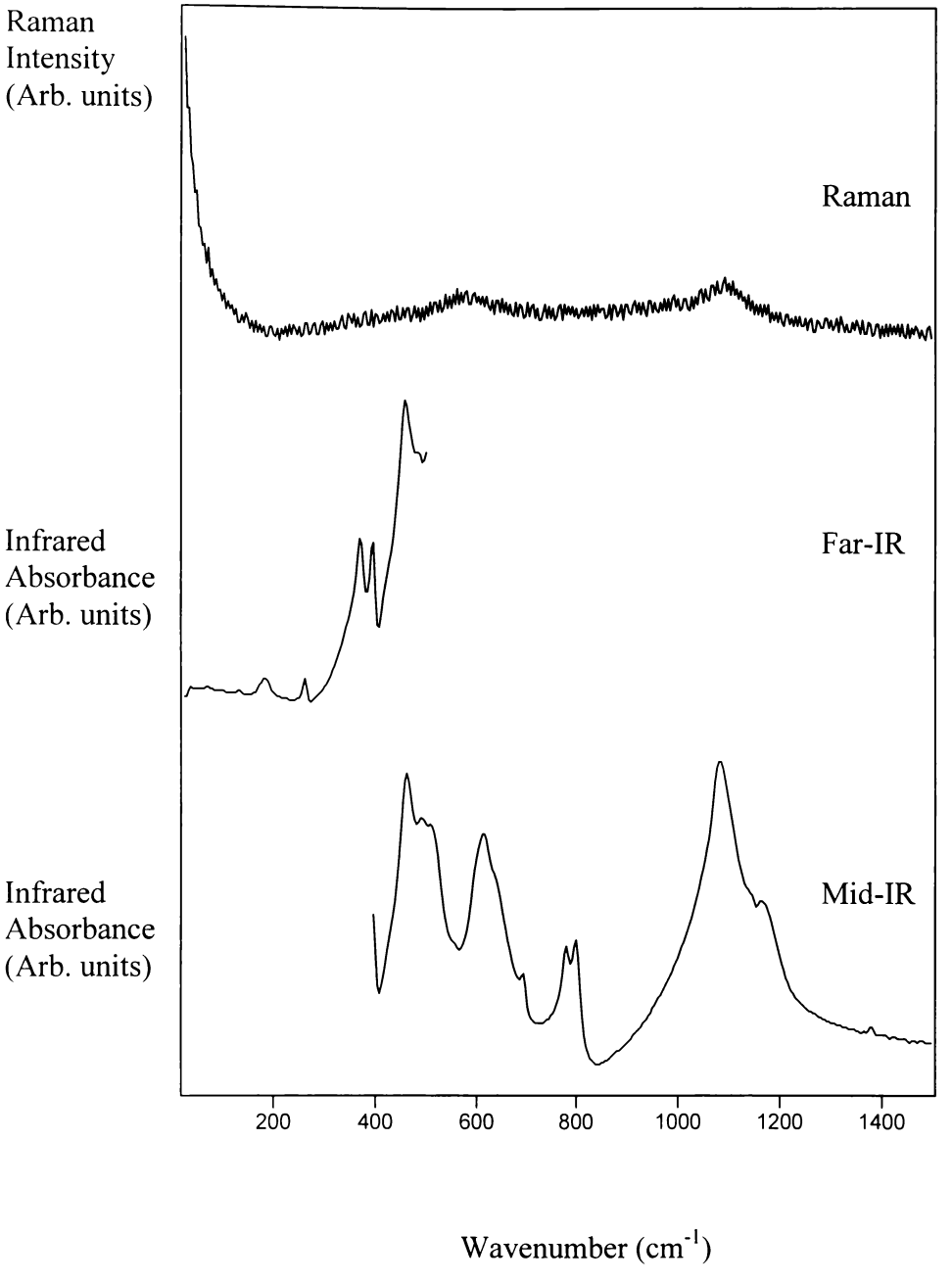

Figure 11 Raman and infrared spectra of GBA colouring pigment (GBA1).

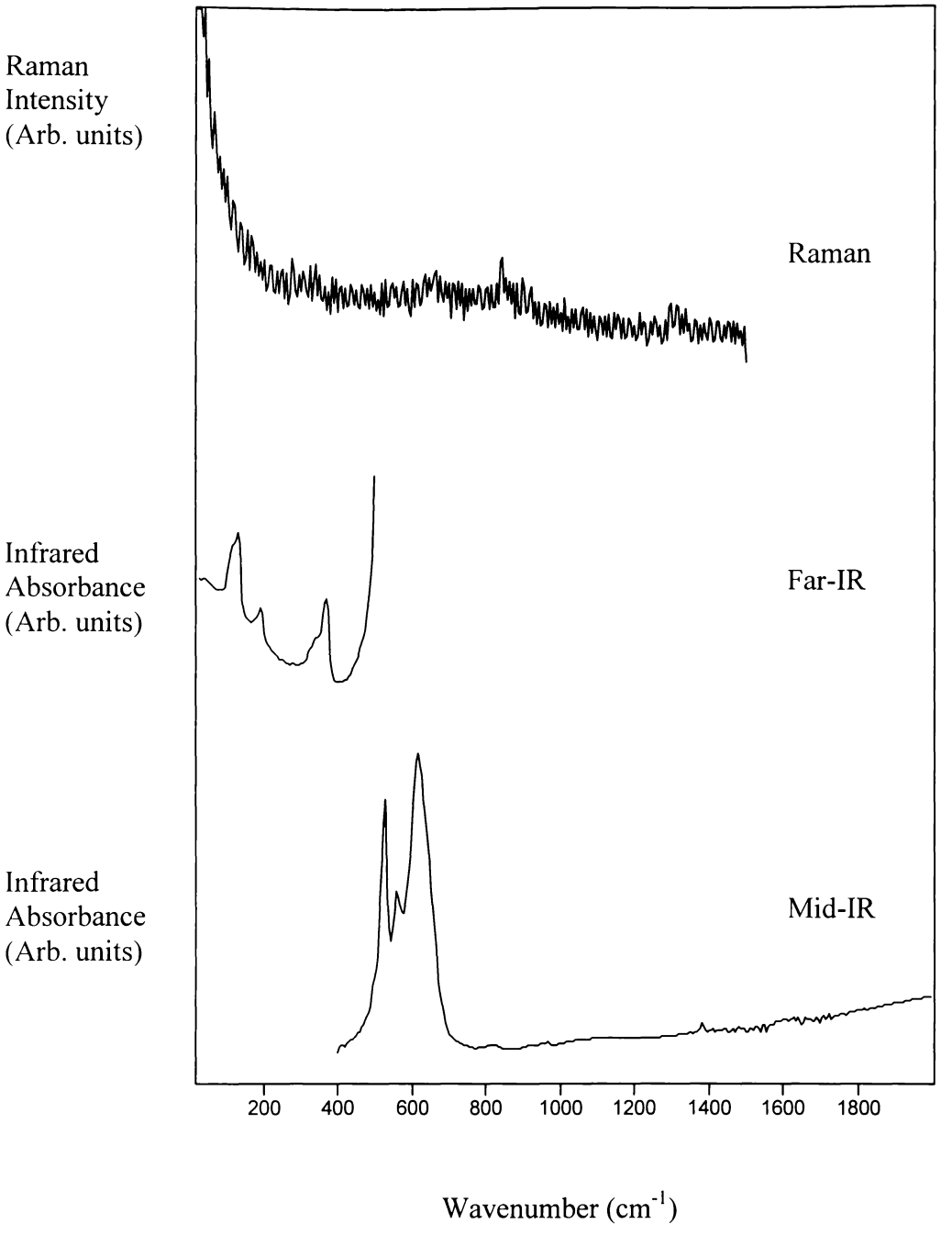

Figure 12 Raman and infrared spectra of MBA colouring pigment (MBA1).

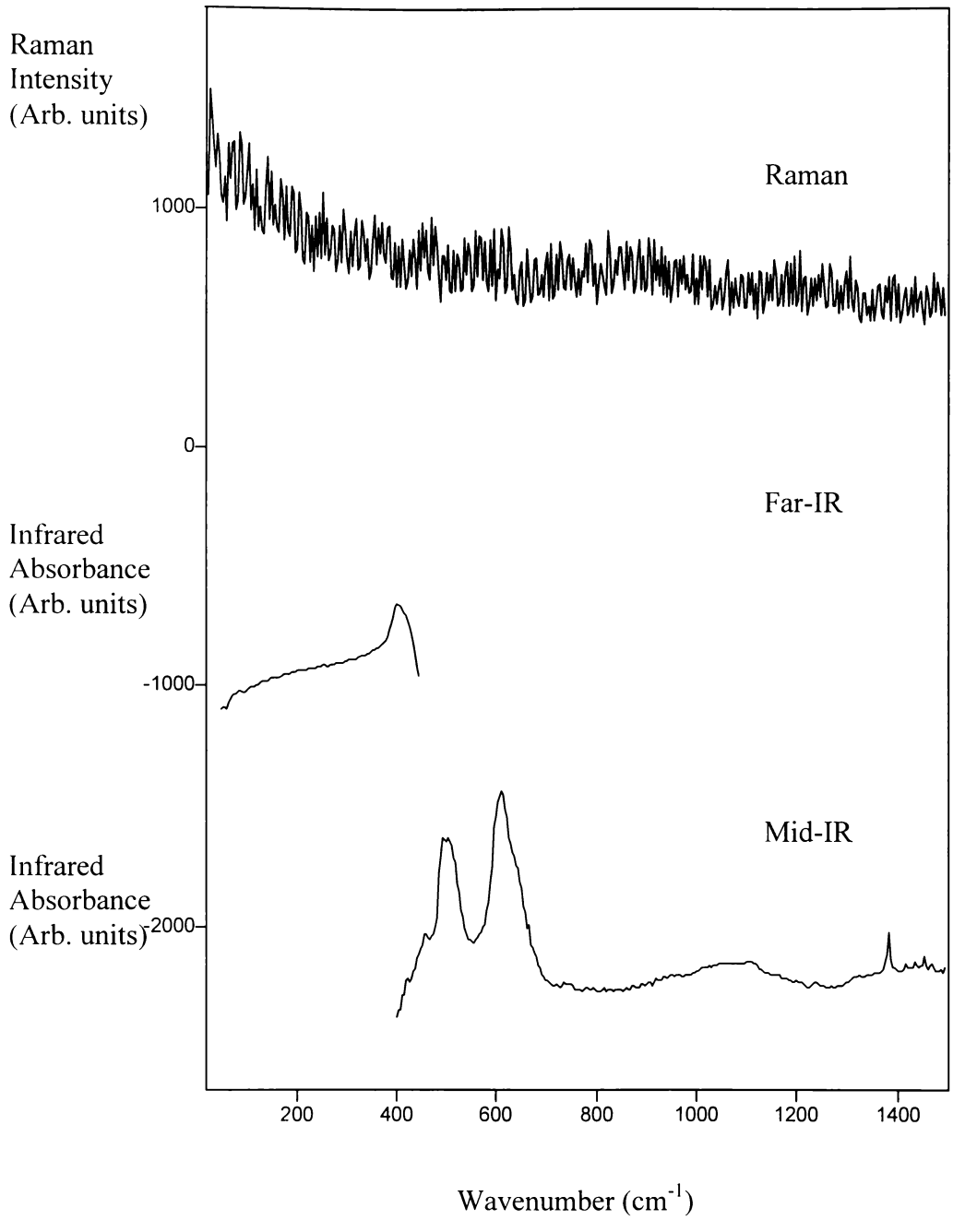

Figure 13 Raman and infrared spectra of GBB colouring pigment 1 (GBB1).

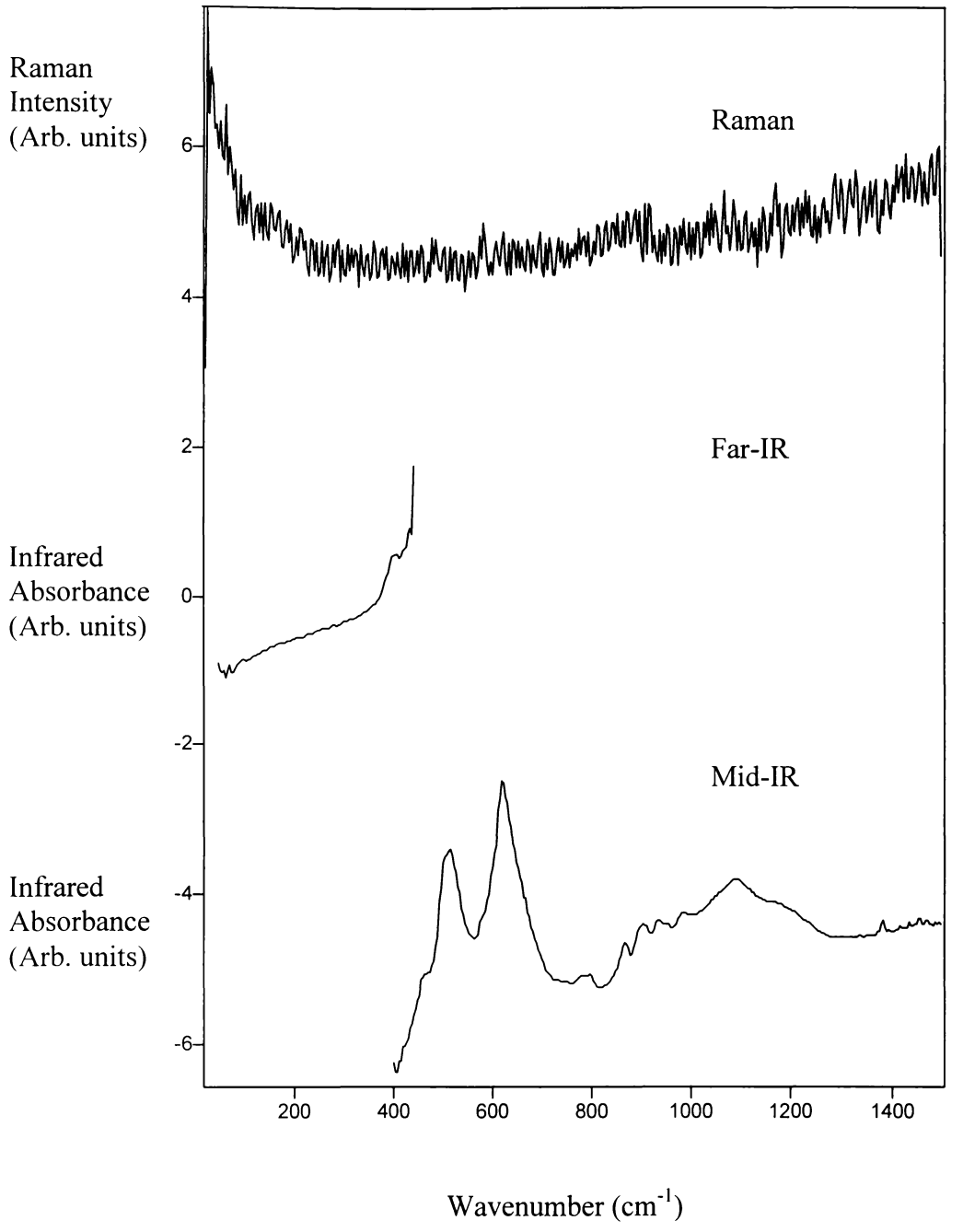

Figure 14 Raman and infrared spectra of GBB colouring pigment 2 (GBB2).

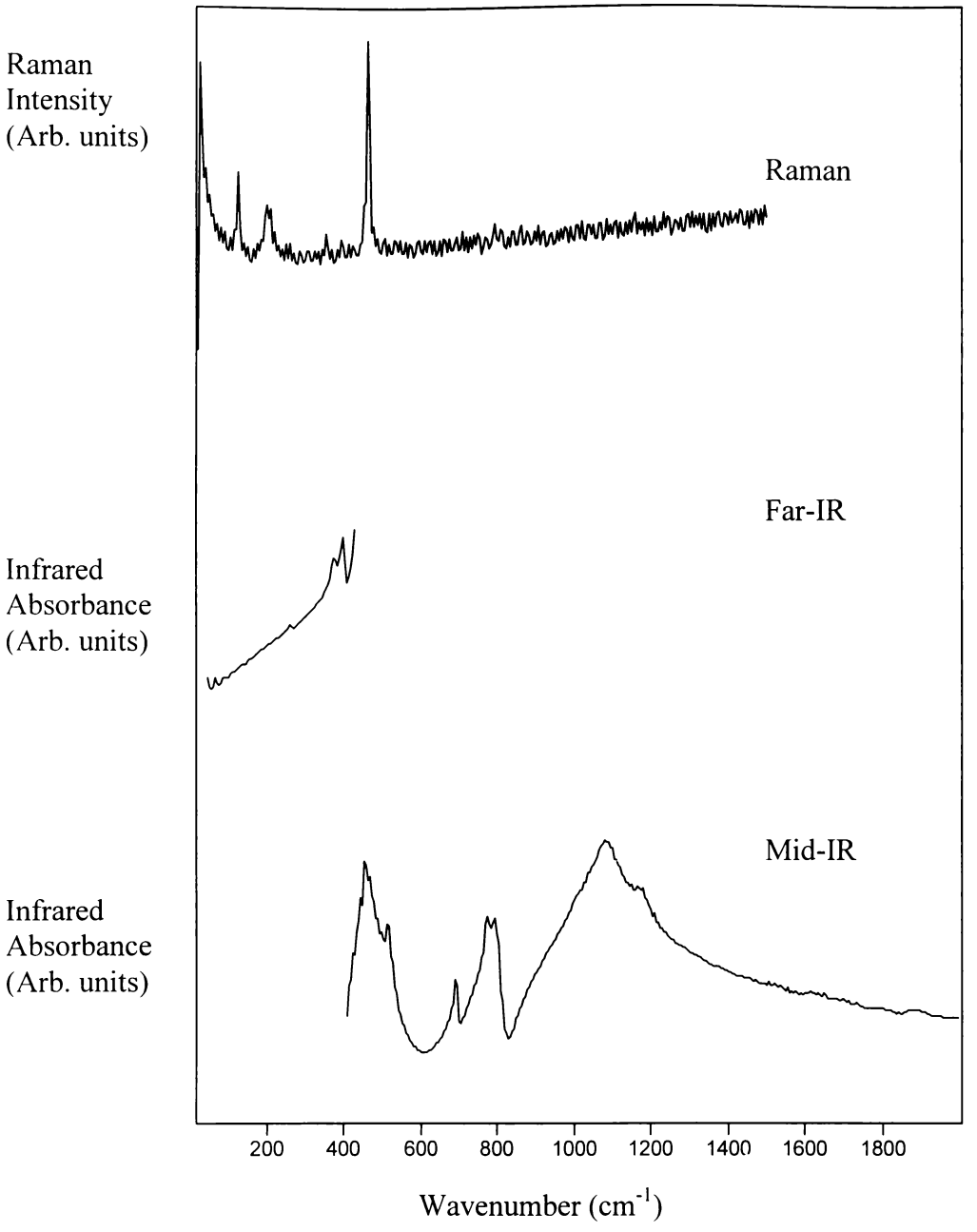

Figure 15 Raman and infrared spectra of silica.

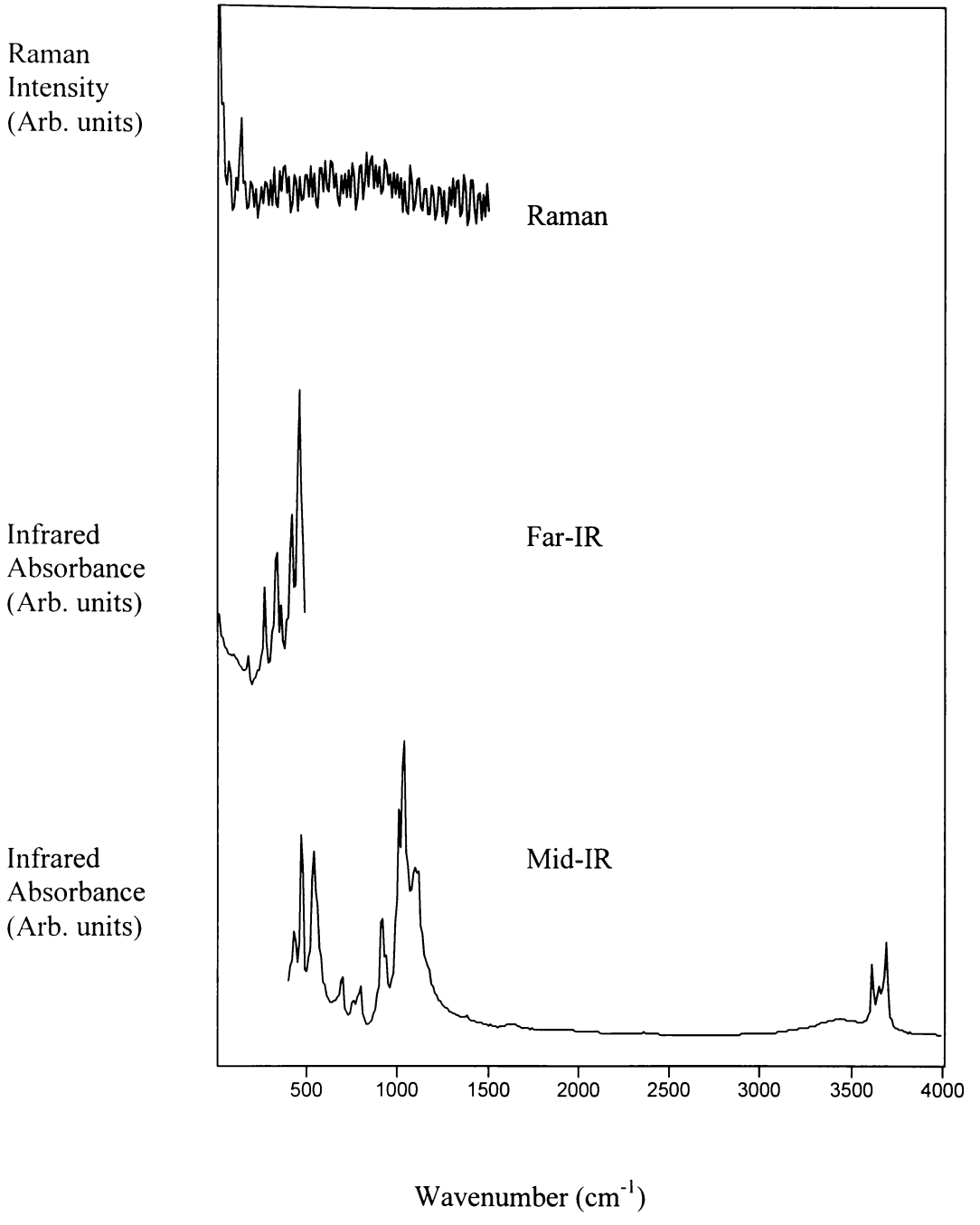

Figure 16 Raman and infrared spectra of HB clay.

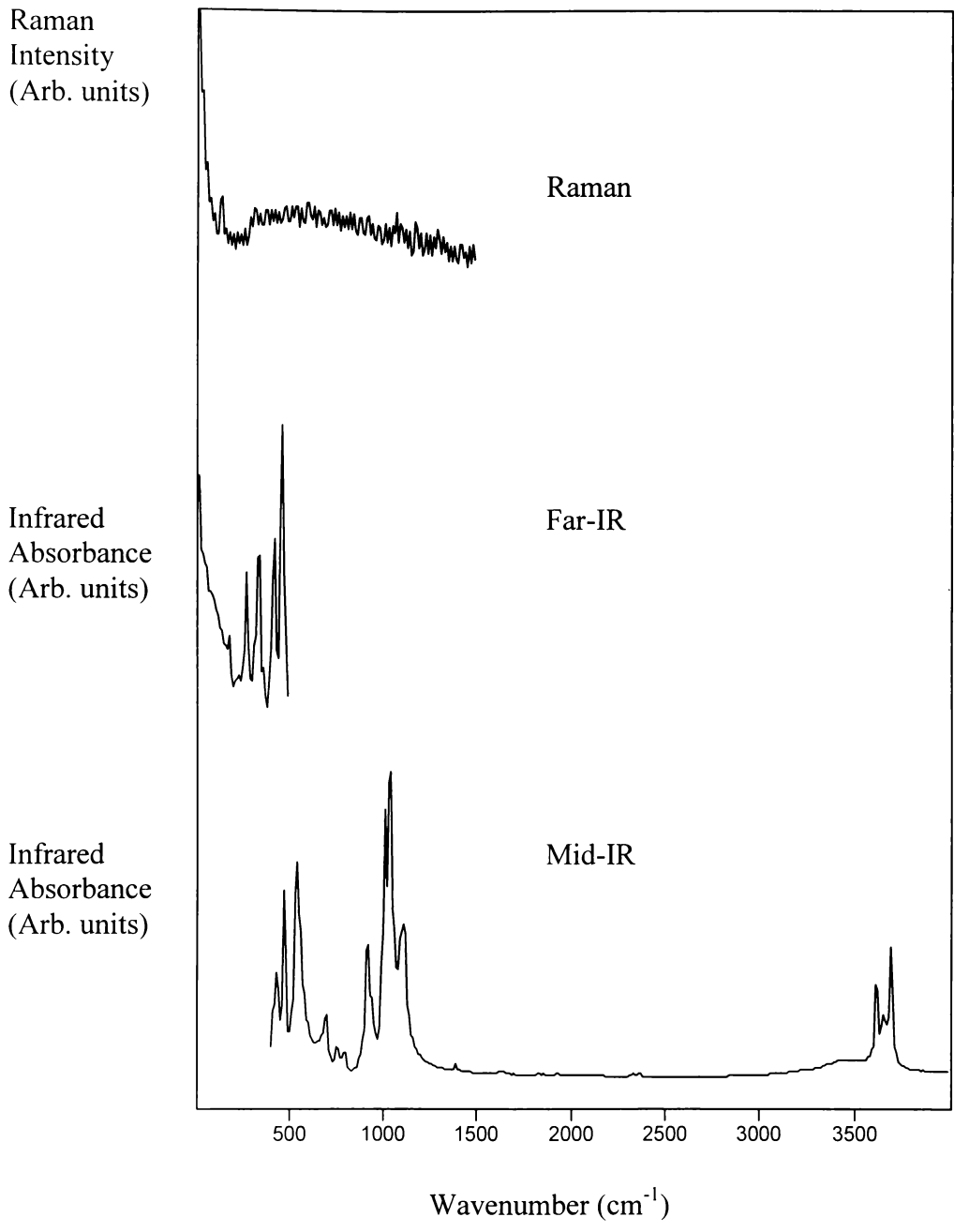

Figure 17 Raman and infrared spectra of Kaolex clay.

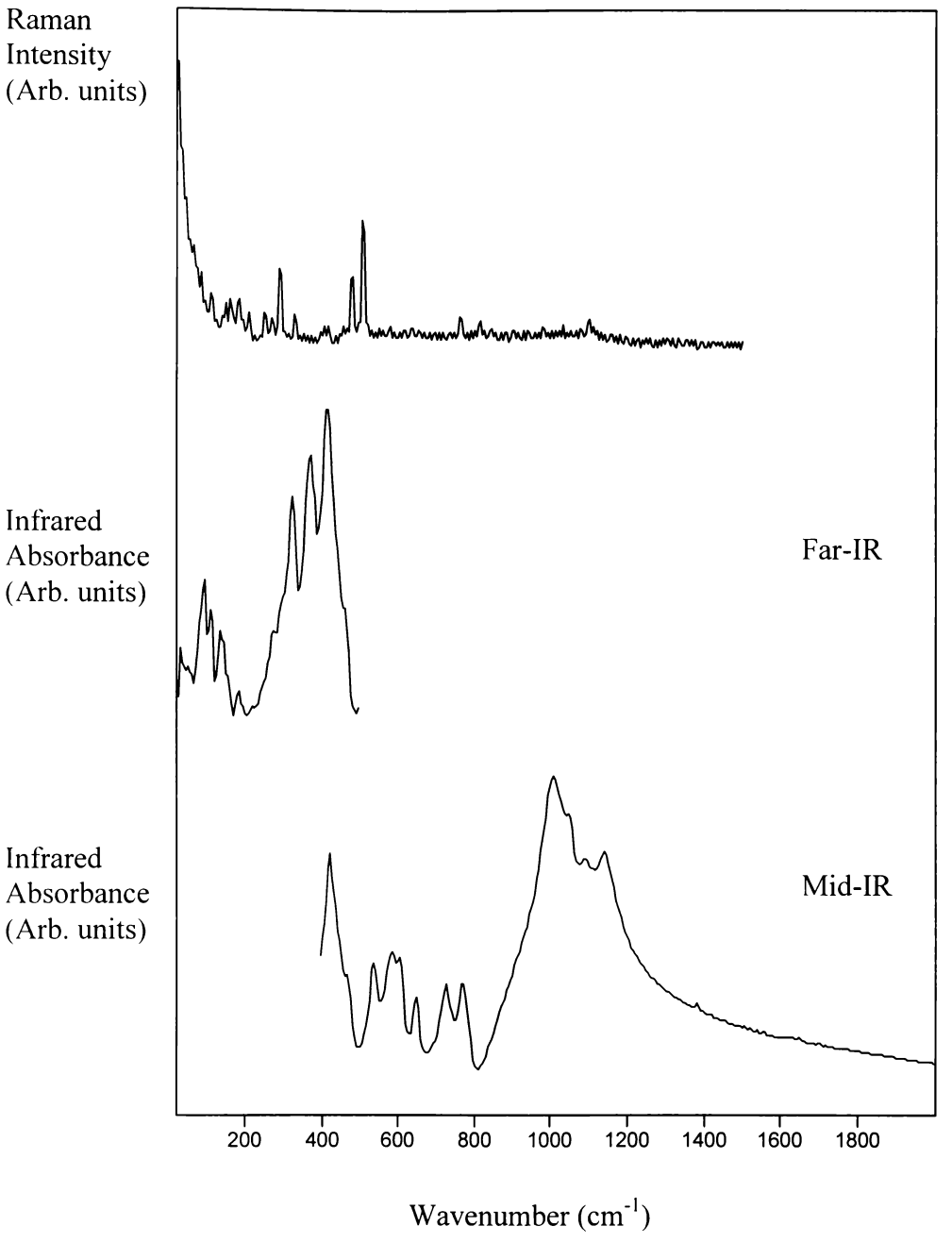

Figure 18 Raman and infrared spectra of feldspar.

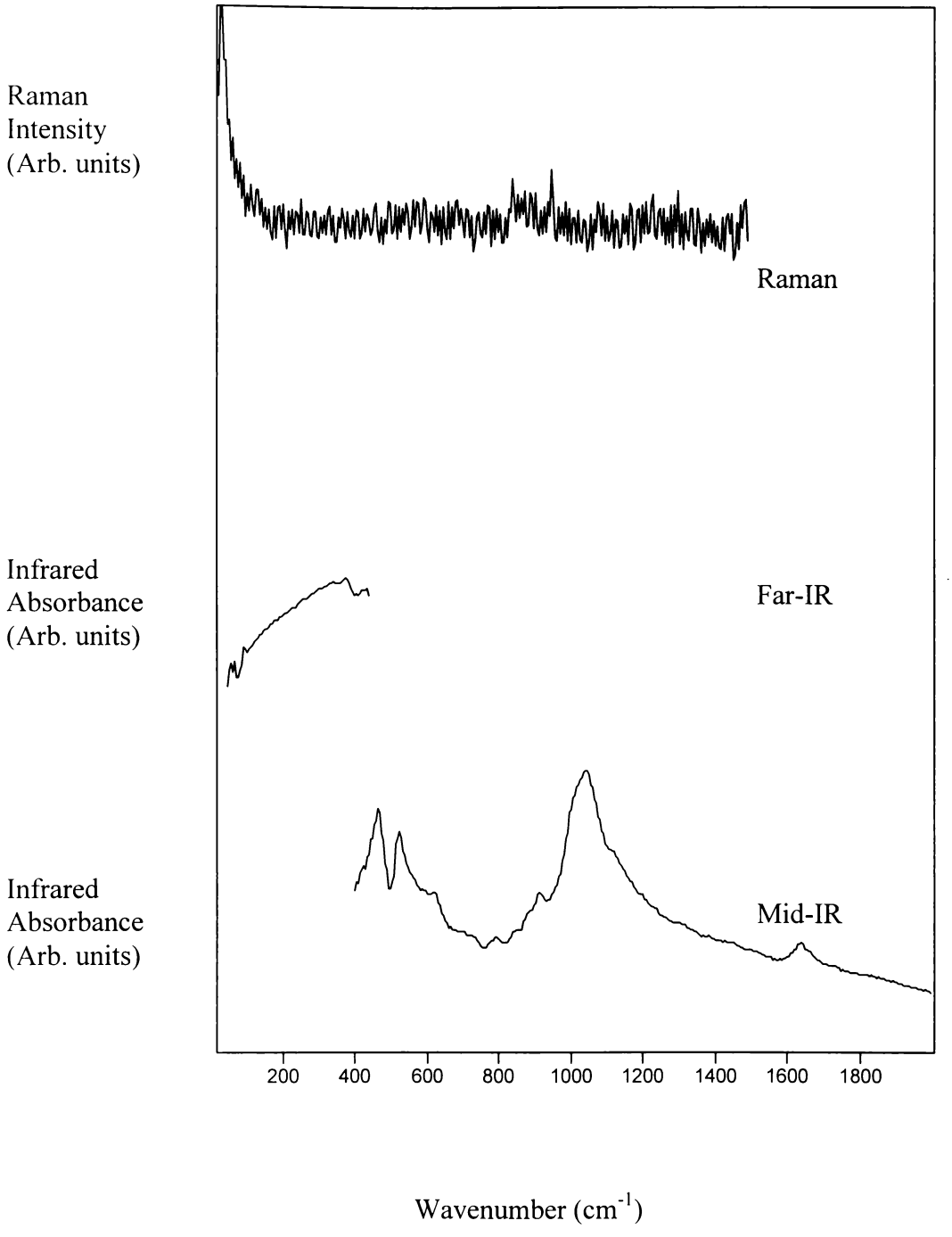

Figure 19 Raman and infrared spectra of bentonite.

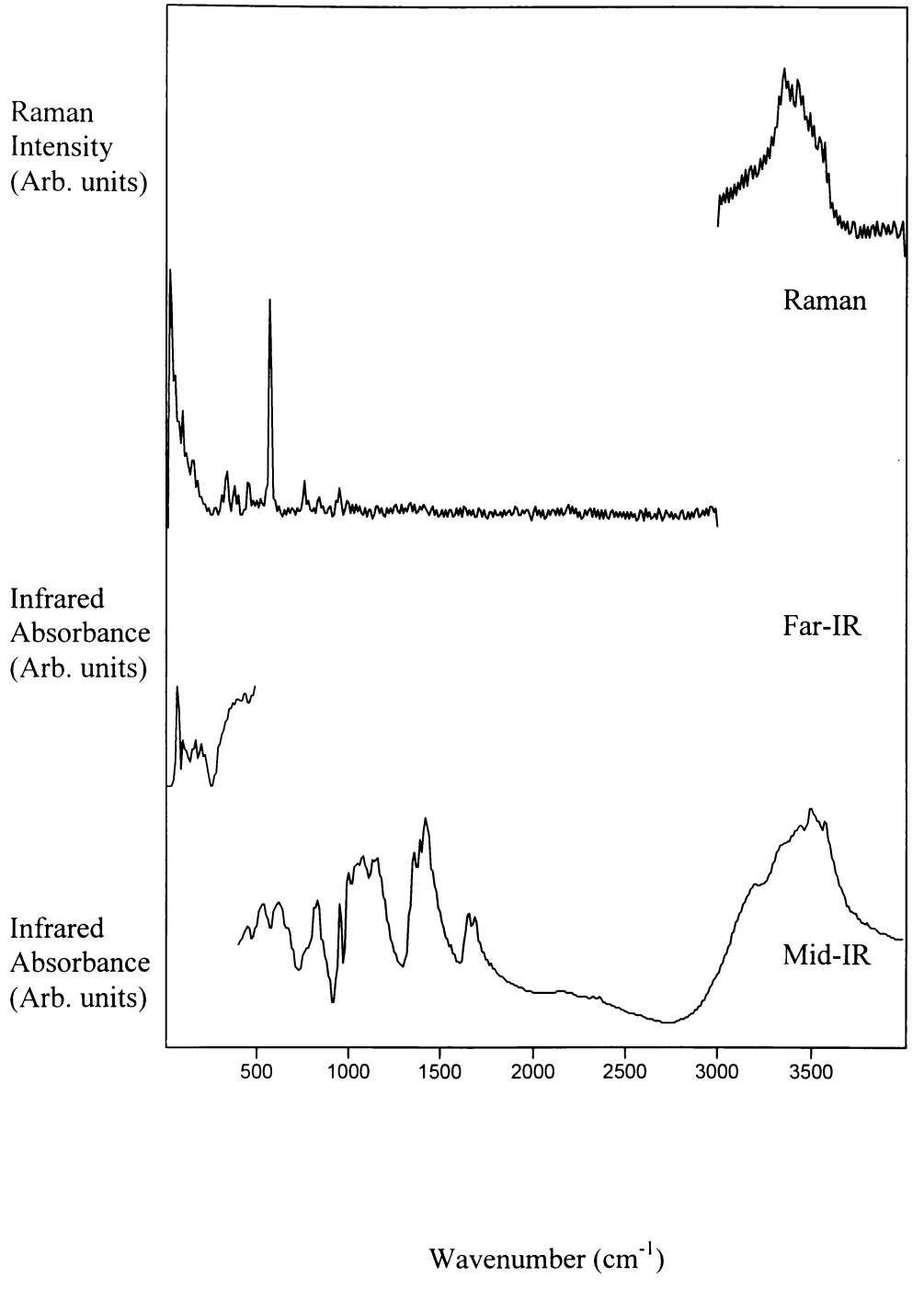

Figure 20 Raman and infrared spectra of borax.

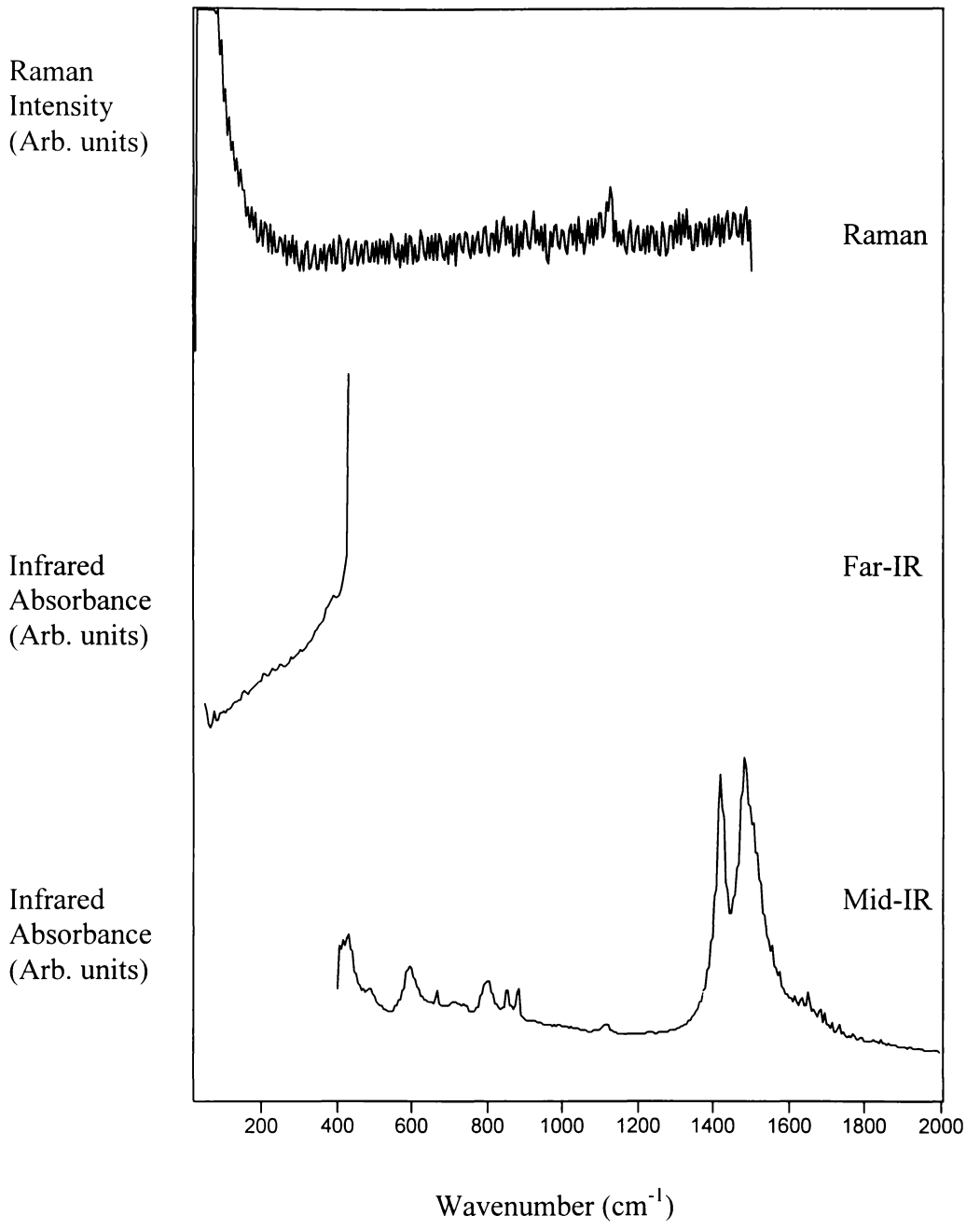

Figure 21 Raman and infrared spectra of magnesium carbonate.

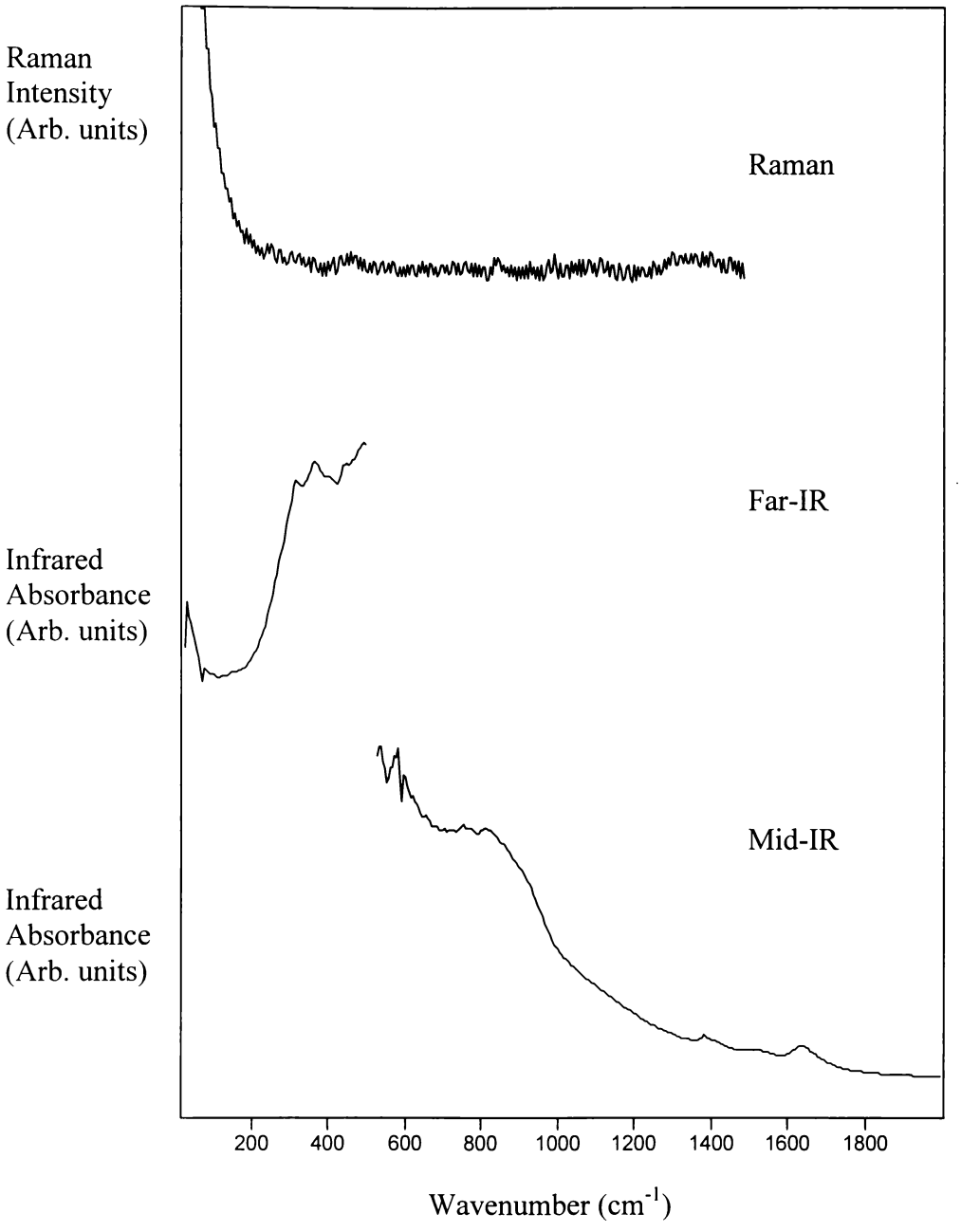

Figure 22 Raman and infrared spectra of calcined alumina.

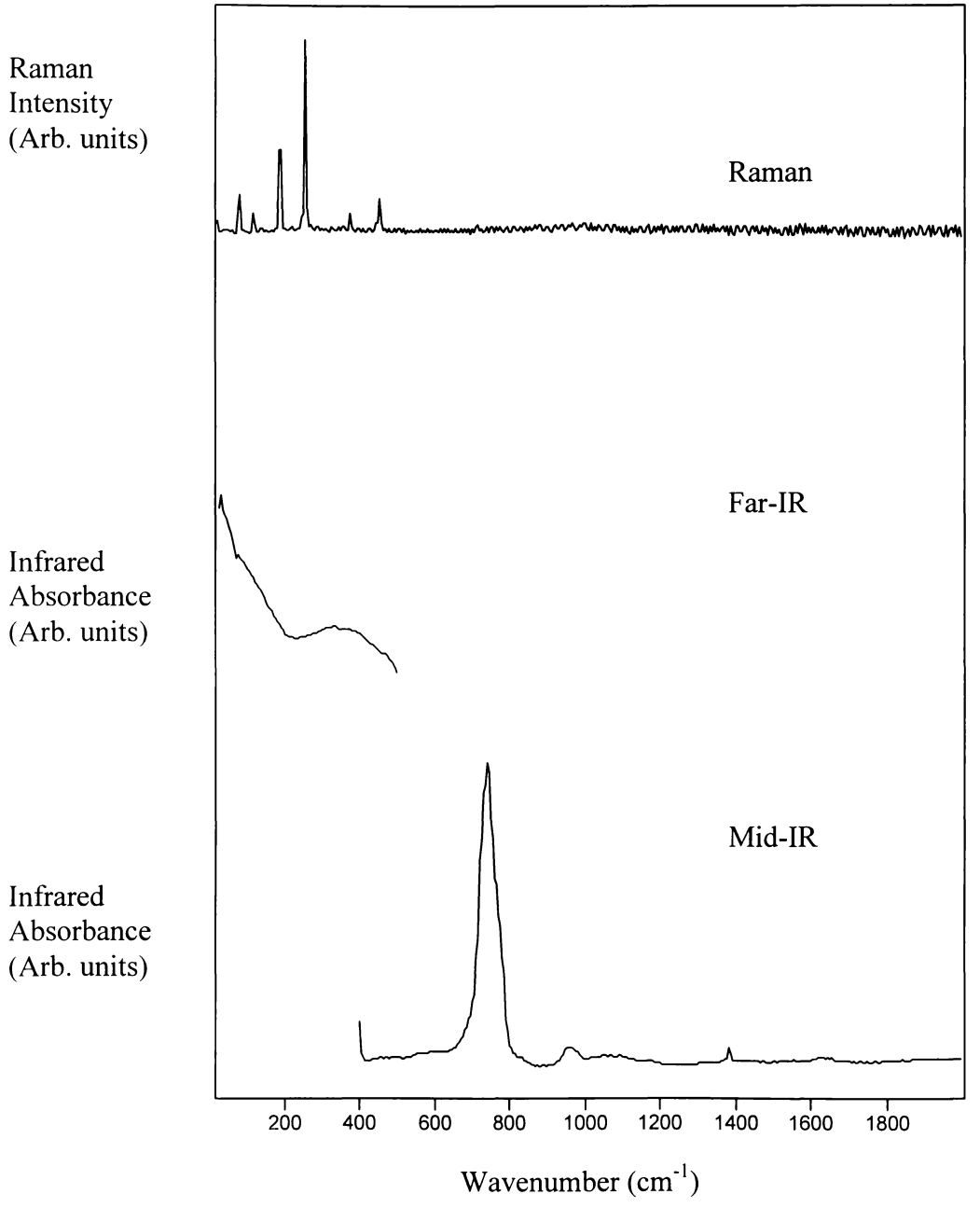

Figure 23 Raman and infrared spectra of antimony oxide.

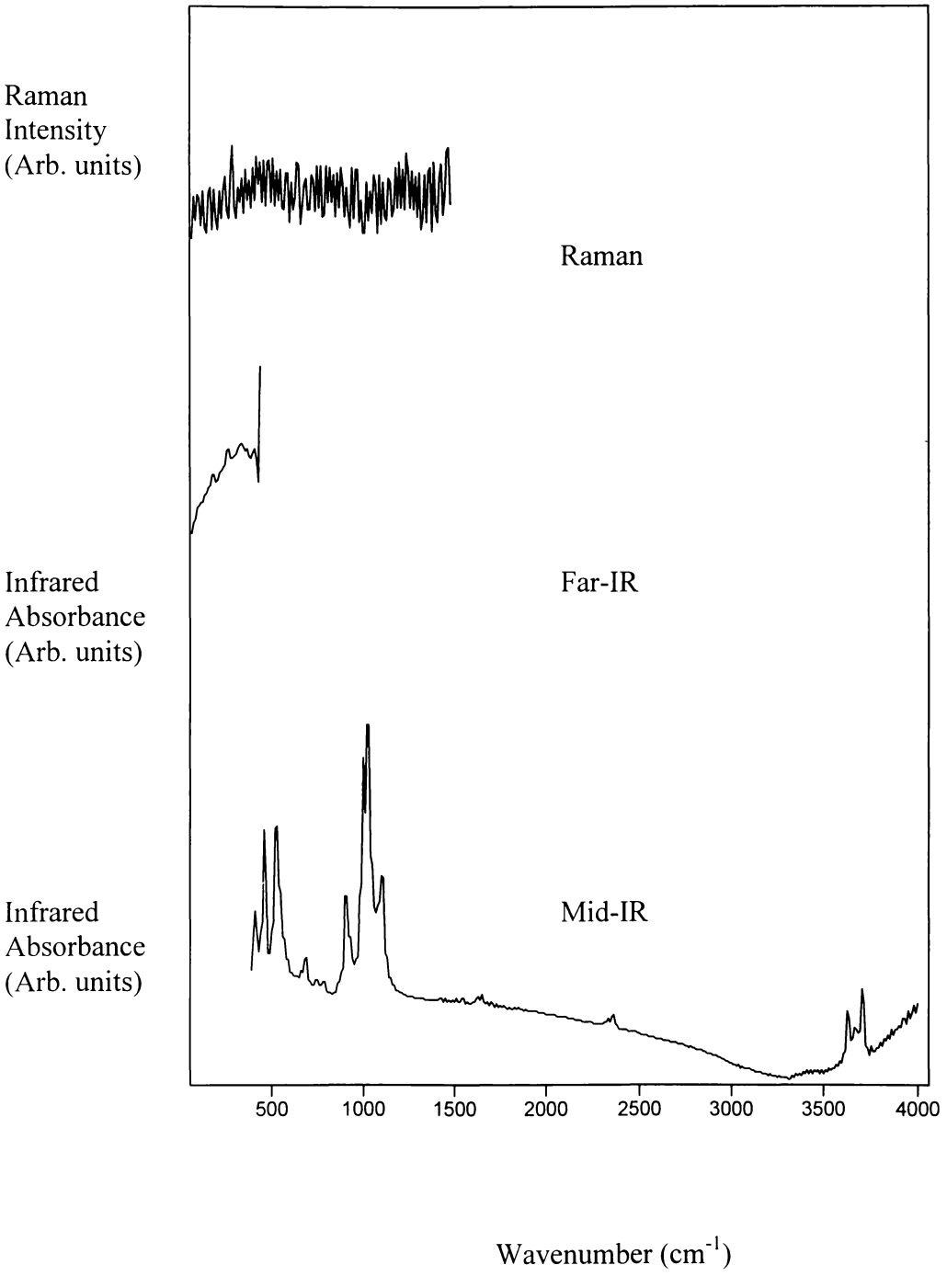

Figure 24 Raman and infrared spectra of clay for GBB.

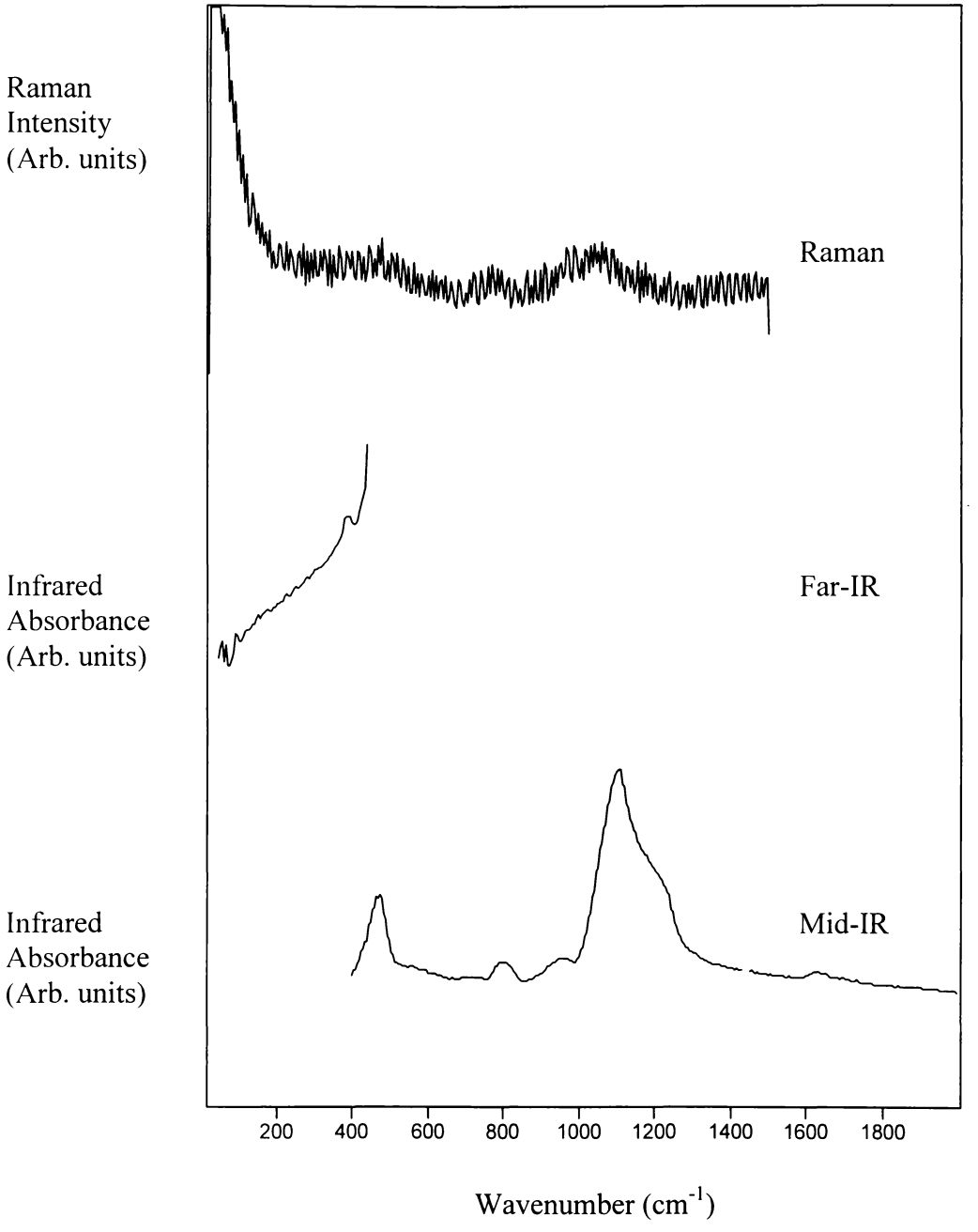

Figure 25 Raman and infrared spectra of mill addition used in GBB.

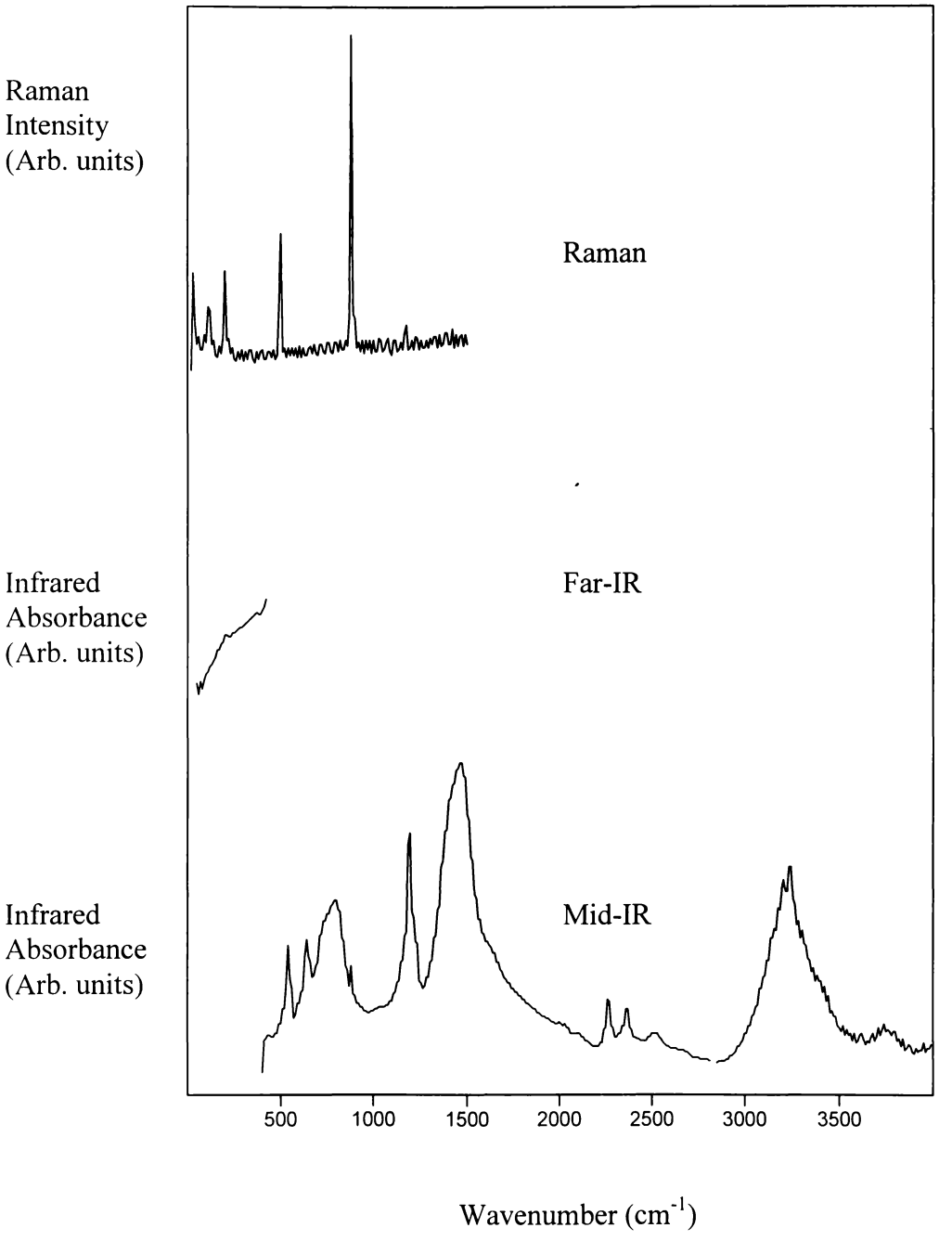

Figure 26 Raman and infrared spectra of boric acid.

1. Visual Examination of Commercial Coatings

Visual (human-eye) examination of the GBA (Figure 1b) surface after exposure to hot sodium hydroxide (48 hours) exhibited some loss of gloss from etching. The citric acid solution tested (2.5 hours) gloss coating surfaces highlighted a total loss of all gloss (Figure 1c). The panel surface exposed to the boiling citric acid vapour (Figure 1d) exhibited a partial loss of gloss and areas of liquid staining from vapour condensation.

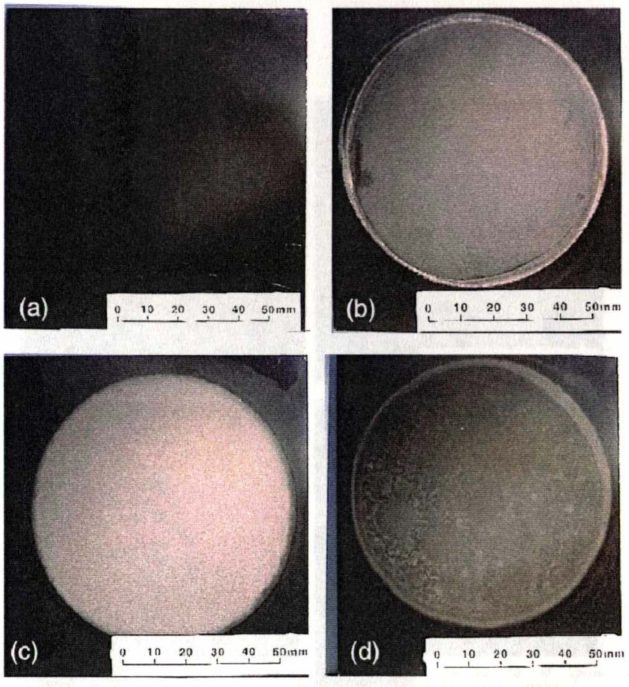

Figure 1 GBA test panels after exposure to hot sodium hydroxide for 48 hours (b), boiling citric acid solution for 2.5 hours (c) and acid vapour for 2.5 hours (d). Control=(a).

After 48 hours of exposure to hot sodium hydroxide, the surfaces of GBB panels (Figure 2b) were etched and there was a total loss of all gloss. However, there was no visible deterioration after the panels had been exposed to citric acid solution and vapour for 2.5 hours. After exposure to boiling citric acid for 6 hours (Figure 2c), the test area was slightly discoloured but there was no weight loss (see Figure 5.1, Chapter 5). There was no visible deterioration on the surface of the test panel after exposure to citric acid vapour for 6 hours (Figure 2d). After 24 hours, the visible change in gloss was greater for citric acid solution (Figure 2e) and vapour (Figure 2f) testing. This was also reflected by the greater weight loss (Figure 5.1-Chapter 5).

The surface of GBC coating, after exposed to hot sodium hydroxide for 48 hours exhibited a high proportion of corrosion (Figure 3b). The surface has a film, which in

places has spalled (or etched) to expose underlying layers. There is some loss of gloss after citric acid solution testing for 2.5 hours (Figure 3c) and slightly more after 24 hours of testing (Figure 3e). The panel exposed to citric acid vapour for 2.5 hours (Figure 3d) shows very little deterioration and only slightly more deterioration when exposed for 24 hours (Figure 3f).

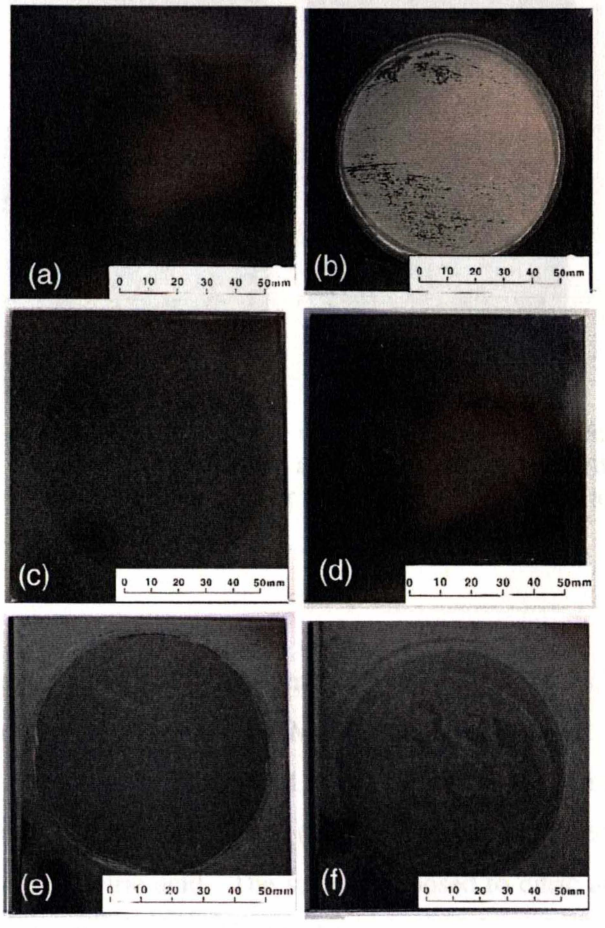

Figure 2 GBB test panels after exposure to hot sodium hydroxide for 48 hours (b), boiling citric acid solution for 6 hours (c), acid vapour for 6 hours (d), boiling citric acid solution for 24 hours (e) and acid vapour for 24 hours (f). Control=(a).

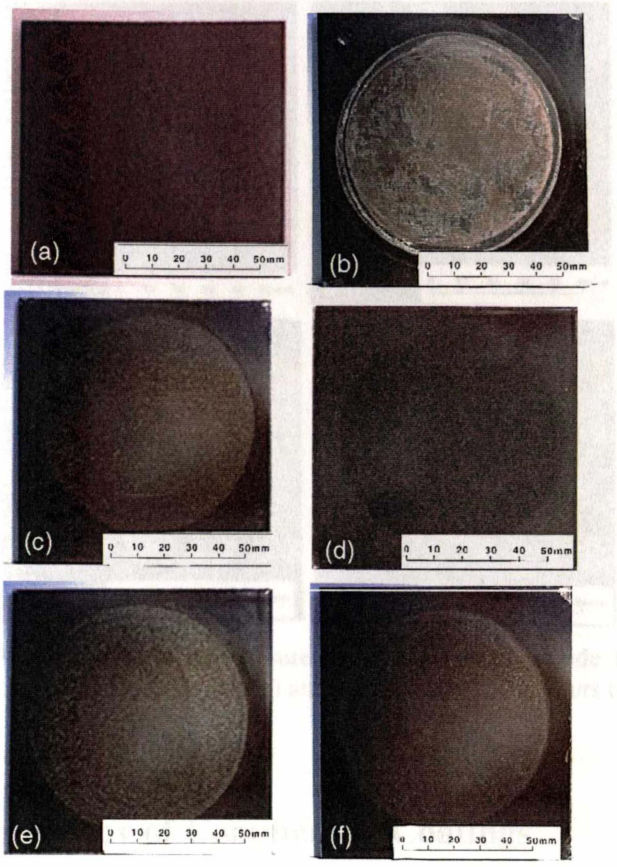

Figure 3 GBC test panels after exposure to hot sodium hydroxide for 48 hours (b), boiling citric acid solution for 2.5 hours (c) acid vapour for 2.5 hours (d), boiling citric acid solution for 24 hours (e) and acid vapour for 24 hours (f). Control=(a).

The MBA surface, exposed to the hot sodium hydroxide, for 48 hours, exhibits etching of the top layer (Figure 4b). Many of the MBA samples examined after 2.5 hours of exposure to boiling citric solution, exhibited a high percentage of the steel substrate, due to large areas of removal of the enamel coat (Figure 4c). The MBA coating therefore has little resistance to boiling citric acid. The surface exposed to citric acid vapour showed some deterioration and water staining (Figure 4d).

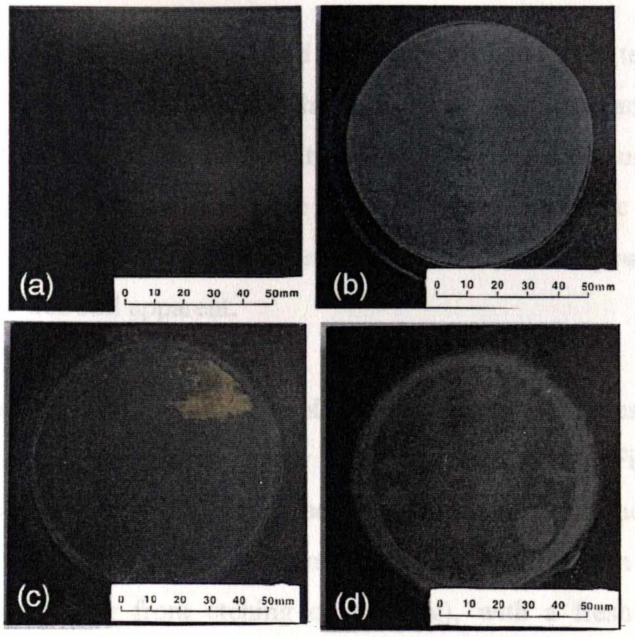

Figure 4 MBA test panels after exposure to hot sodium hydroxide for 48 hours (b), boiling citric acid solution for 2.5 hours (c) and acid vapour for 2.5 hours (d). Control=(a).

2. Optical Microscopy of Commercial Coatings

This section shows optical microscopy examples of surfaces before and after acid and alkali corrosion tests. The surface variations for the coating surfaces, using dark field and bright field illumination, are given in Appendix 4.

Examination of GBA and GGA coating surfaces showed they had undergone similar deterioration. This was expected because they have the same composition other than their colouring oxides. Only GBA micrographs are shown in this appendix (Figure 5).

The GBA coating surface shows a good bubble structure before testing (Figure 5b). After 48 hours of exposure to hot sodium hydroxide, the surface exhibited corrosion and many holes (pores) can be clearly seen (Figure 5h). After 2.5 hours of exposure to boiling citric acid solution there was a lot of deterioration (leaching) of the enamel coating and the surface had a powdered glass (granular film) appearance (Figure 5d). The surface of the GBA sample displayed some micro cracking after it had been exposed to boiling citric acid vapour for 2.5 hours (Figure 5f). This is caused by tension in the coating from thermal expansion mismatch (thermal expansion coefficient much higher than the substrate). There are also regions with a glassy type appearance (presumably silica), as can be seen in the upper centre section of the micrograph.

The surface of the GBB coating shows good bubble dispersion before testing (Figure 6b). After exposure to hot sodium hydroxide, the surfaces of the GBB samples deteriorated substantially (Figure 6h). This deterioration is also illustrated using bright field illumination (Figure 6g). The surface of the GBB sample showed little corrosion after 24 hours of exposure to boiling citric acid solution (Figure 6d) and vapour (Figure 6f), and the bubble structure was still apparent.

The original surface of GBC samples display well-dispersed bubbles (Figure 7b) and lighter brown coloured phase and darker black coloured areas (Figure 7a). After exposure to hot sodium hydroxide, the surface had deteriorated and the bubble structure disappeared (Figure 7h). The centre of the micrograph shows a region of high corrosion (depressed region resulting from etching or spalling), with a fresh surface exposed beneath the top surface layer. Most of the corrosion on GBC samples exposed to citric acid solution (over 24 hours) appears to have occurred where the darker (black coloured) phase exists (Figure 7d). This region shows a glassy appearance and tension cracks (Figure 7c). Corrosion has also occurred after 24 hours exposure to acid vapour (Figure 7f), although this is less pronounced compared to boiling citric acid solution tested samples.

Unlike gloss-type coatings, the surface of unexposed MBA samples is rough (Figure 8b). The bubbles observed are dispersed more intermittently. All MBA samples corroded when exposed to alkali or acid. After exposure to hot sodium hydroxide, the surface became rough and exhibited many holes and pores (Figure 8h). Samples exposed to boiling citric acid solution had the most corrosion, including areas where the enamel had been completely removed to expose the steel substrate (Figure 8d). The sample corrodes when exposed to boiling citric acid vapour but the steel substrate is not exposed (Figure 10f).

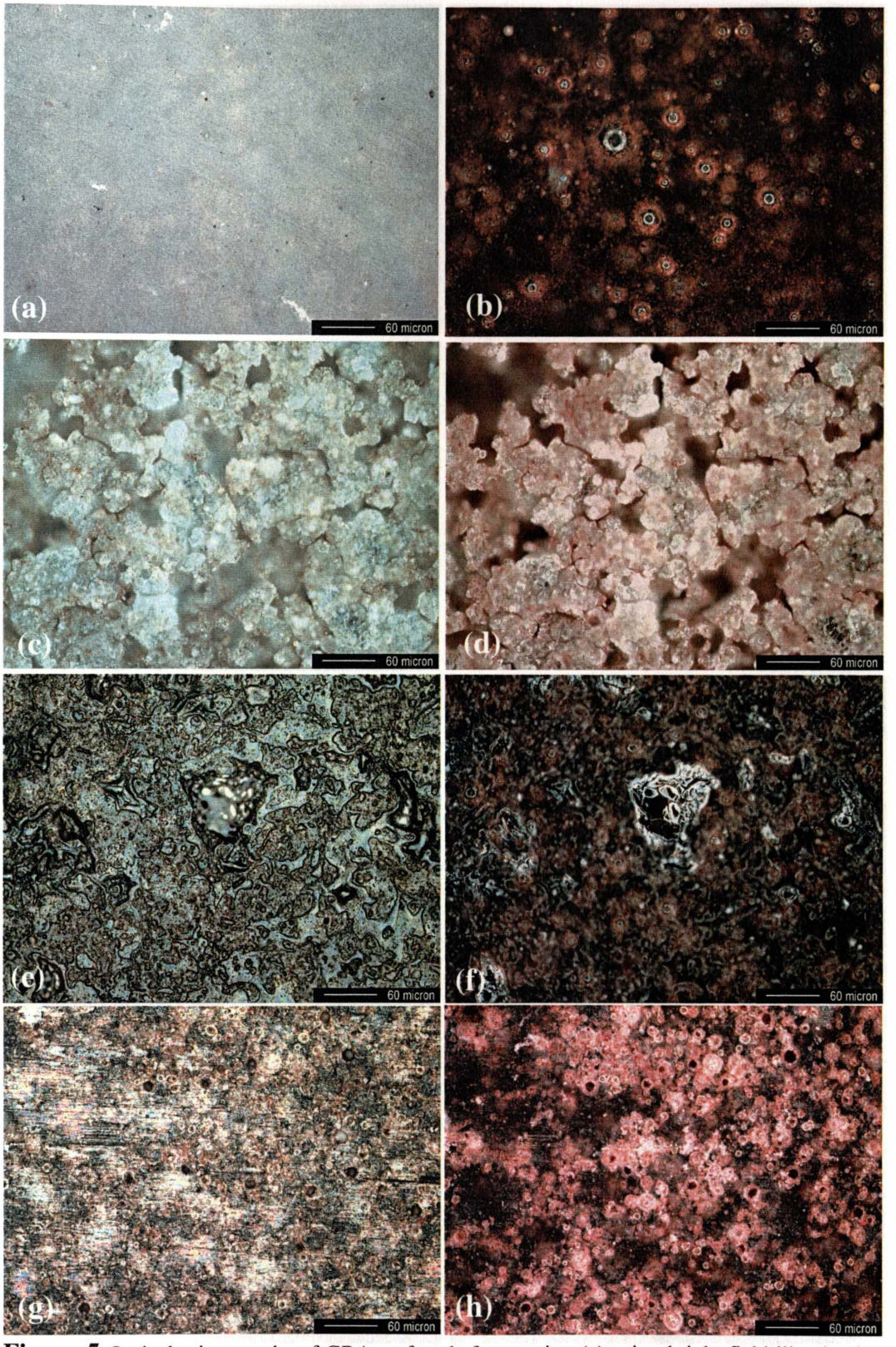

Figure 5 Optical micrographs of GBA surface before testing (a) using bright field illumination (BF) and (b) using dark field illumination (DF). GBA surface after exposure to: (c) boiling citric acid solution for 2.5 hours (BF) and (d) (DF); (e) acid vapour for 2.5 hours (BF) and (f) (DF); (g) hot sodium hydroxide for 48 hours (BF) and (h) (DF)

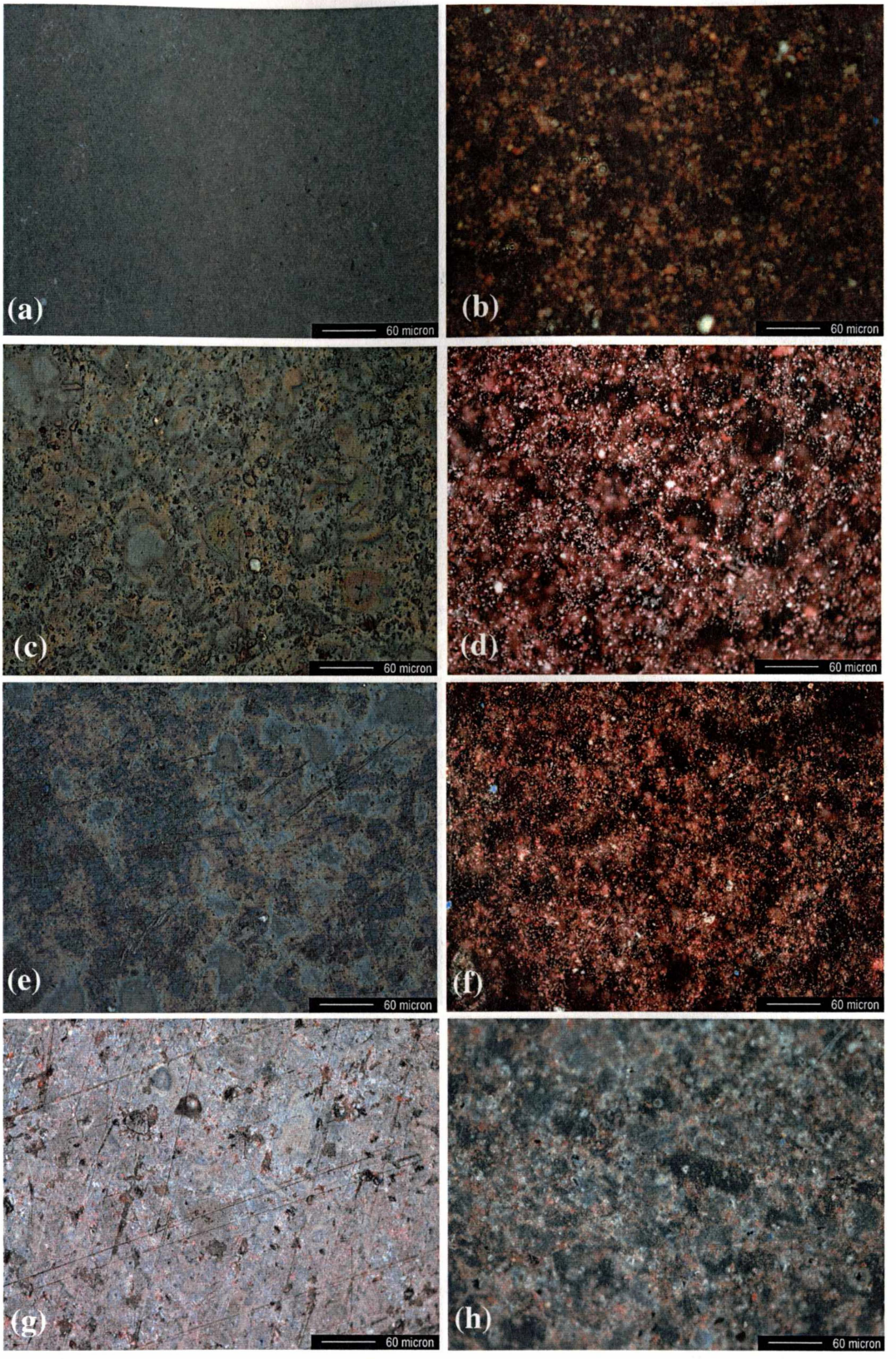

Figure 6 Optical micrographs of GBB surface before testing (a) using bright field illumination (BF) and (b) using dark field illumination (DF). GBB surface after exposure to: (c) boiling citric acid solution for 24 hours (BF) and (d) (DF); (e) acid vapour for 24 hours (BF) and (f) (DF); (g) hot sodium hydroxide for 48 hours (BF) and (h) (DF).

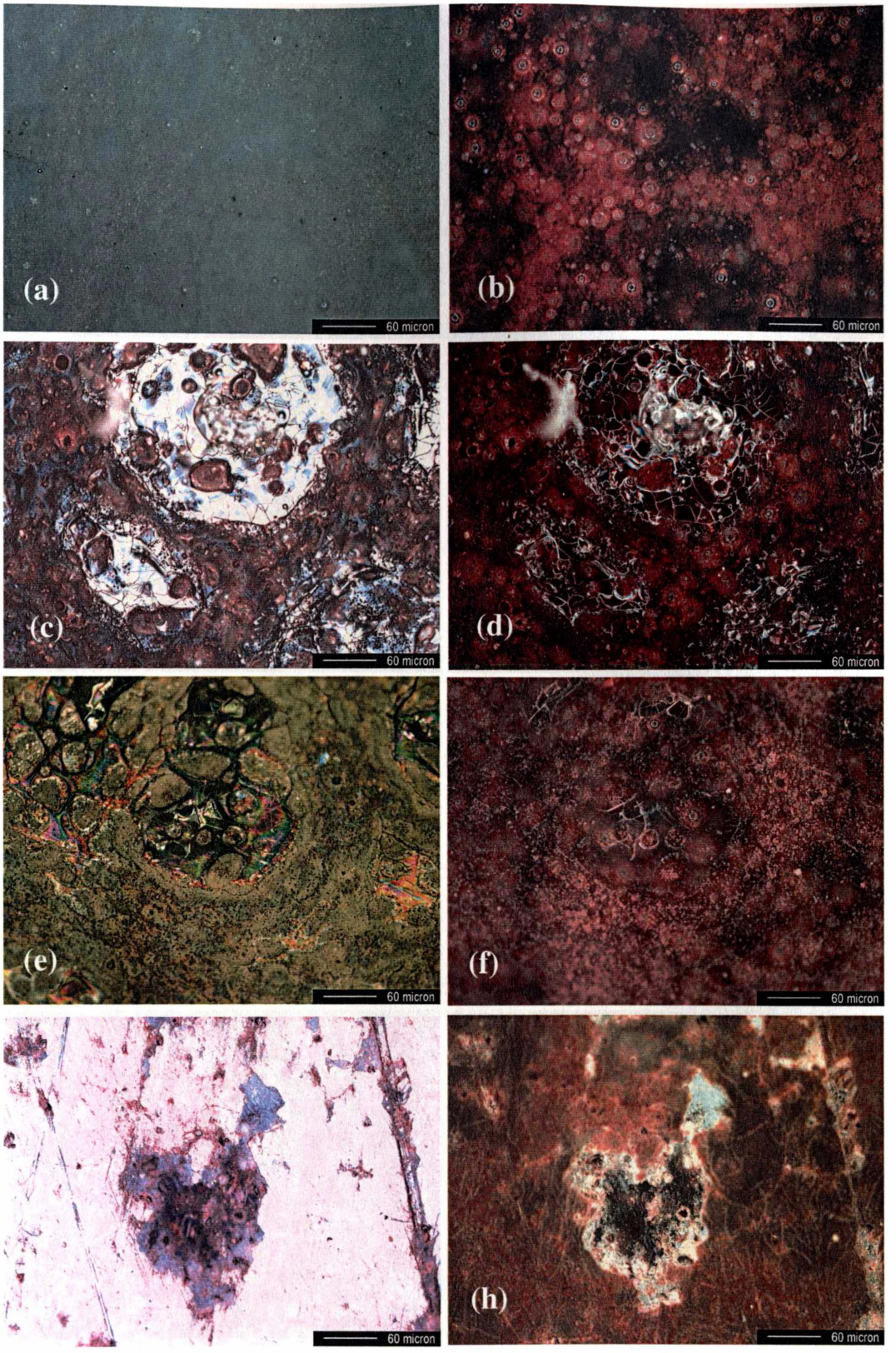

Figure 7 Optical micrographs of GBC surface before testing (a) using bright field illumination (BF) and (b) using dark field illumination (DF). GBC surface after exposure to: (c) boiling citric acid solution for 24 hours (BF) and (d) (DF); (e) acid vapour for 24 hours (BF) and (f) (DF); (g) hot sodium hydroxide for 48 hours (BF) and (h) (DF).

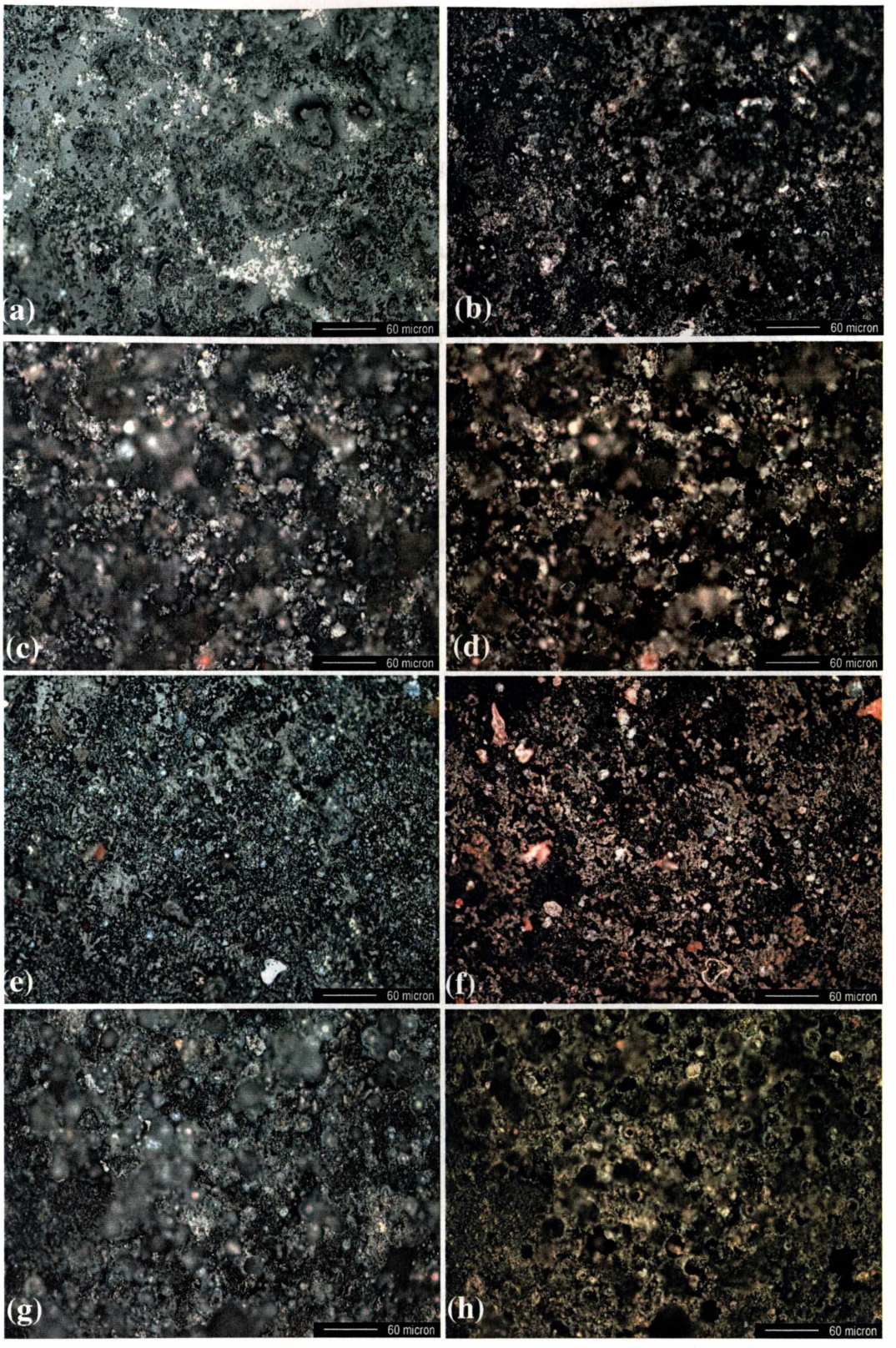

Figure 8 Optical micrographs of MBA surface before testing (a) using bright field illumination (BF) and (b) using dark field illumination (DF). MBA surface after exposure to: (c) boiling citric acid solution for 2.5 hours (BF) and (d) (DF); (e) acid vapour for 2.5 hours (BF) and (f) (DF); (g) hot sodium hydroxide for 48 hours (BF) and (h) (DF).

3. Scanning Electron Microscopy (SEM) and Energy dispersive X-ray analysis (EDS)

The severe reaction when the GBA coating surface was exposed to boiling citric acid solution was examined using EDS in conjunction with SEM. A granular layer was formed (Figure 9a) and tension cracking also occurred. Some of the regions in the micrograph show pores, which possibly were bubbles that were exposed to the reagent hence accelerating the corrosion of the layer in these regions. The micro cracking from these pores appears wider than those in other regions of the micrograph.

A qualitative EDS spectrum of a section of the enamel coating observed in Figure 9(a) is given in 9(b). The spectrum displays mainly Si, therefore elements that were present in the coating surface layer before testing (see Figure 26-Appendix 2) were leached into the solution during the test. A low magnification (approximately 25x) micrograph of the GBA coating surface (Figure 9c) shows the granular film or powdered glass appearance that commonly occurs in severely reacted enamel coatings. Block-like particles due to micro cracking in the layer can be seen at higher (approximately 2500 times) magnification (Figure 10a). The spectrum for the composition from the centre particle (Figure 10a) shows an intense Si peak.

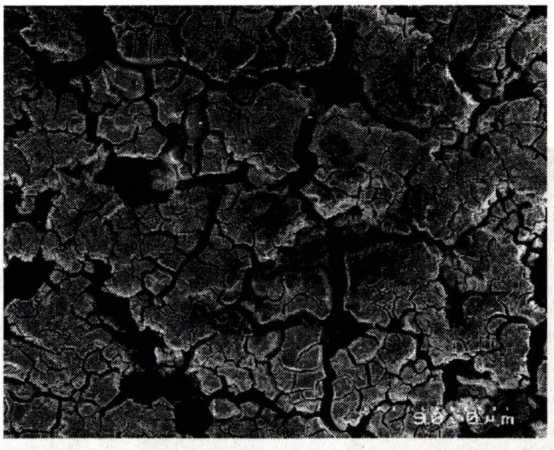

Figure 9(a) SEM micrograph of GBA surface after exposure to boiling citric acid (2.5 hours).

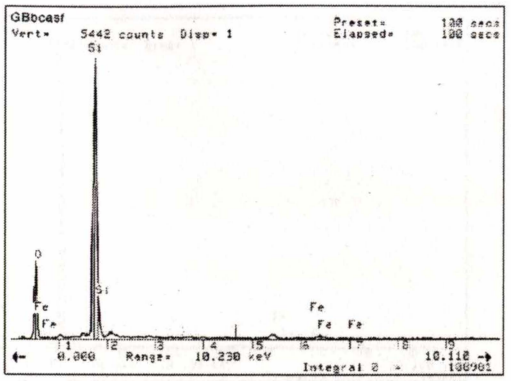

Figure 9(b) EDS spectrum showing composition of region from Figure 9(a).

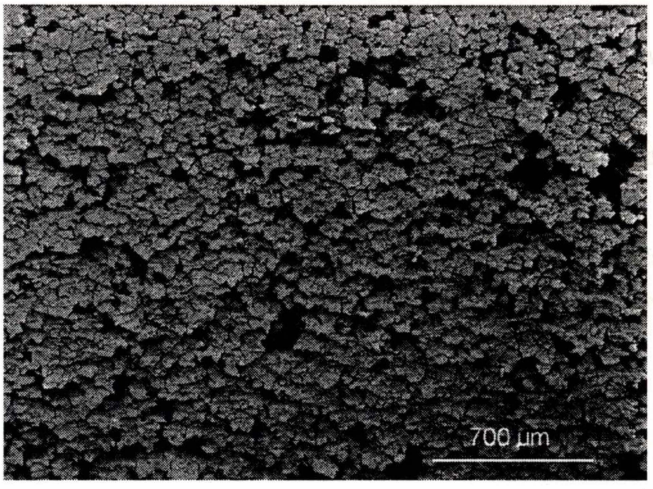

Figure 9(c) EDS micrograph of GBA surface at low magnification (approx. 25x magnification).

Figure 10(a) SEM micrograph of GBA surface after exposure to boiling citric acid for 2.5 hour using high magnification (approx. 2500x).

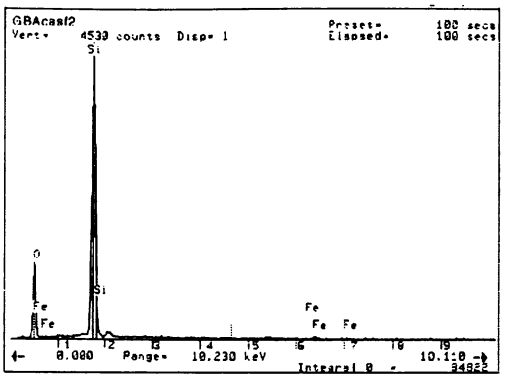

Figure 10(b) EDS spectrum showing composition of region from Figure 10(a).

High magnification (4000x) of a cross-section of the GBA coating, is given in Figure 11a. The EDS spectrum (Figure 12b) indicates that the corroded region from Figure 11a contains mainly Si and some Fe and Zr. Zirconium is used to increase acid resistance, so its occurrence is not unexpected. Particles from an area in the top of the SEM micrograph (7000x magnification) of the surface of the GBA coating (Figure 12a) were analysed using EDS (Figure 12b) and found to be mainly Si with small amount of Fe and Zr.

The surface of the GBA coating developed many micro cracks after being exposed to citric acid vapour (Figure 13a). The deterioration after exposure to acid vapour was much lower than when exposed to acid solution. The hole in the bottom left of the micrograph is likely to be a bubble that was exposed to citric acid vapour.

The EDS spectrum of the surface (Figure 13b) is very similar to that of the melted surface (Figure 26-Appendix 2) and indicates that little leaching of the oxides has occurred, in contrast to the result from surface exposure to the acid solution. The spectrum (Figure 9c) of a sample from within the hole shown in Figure 13a indicates very small silica content, in contrast to the spectrum for the surface, which has a higher silica peak intensity. The other elements in the spectrum of the sample from the melted surface are also present in the sample from the hole, but their concentrations have increased.

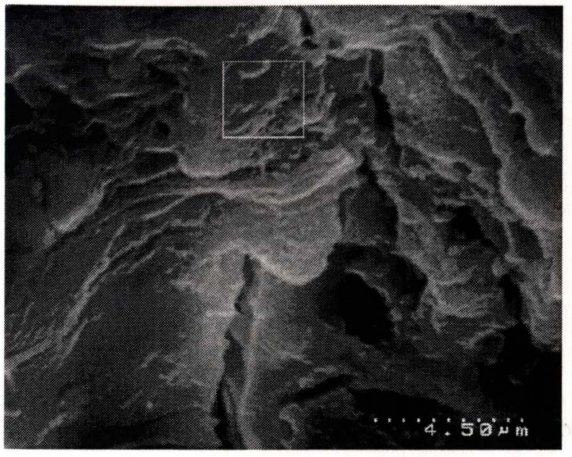

Figure 11(a) SEM micrograph of GBA cross-section near surface after exposure to boiling citric acid for 2.5 hours (approx. 4000X magnification). Square box shows region where EDS spectrum was taken (see Figure 11b).

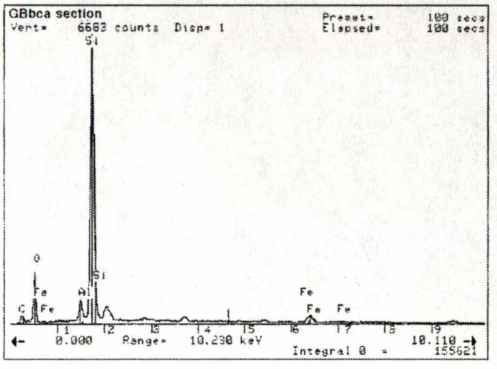

Figure 11(b) EDS spectrum showing composition of region from Figure 12(a).

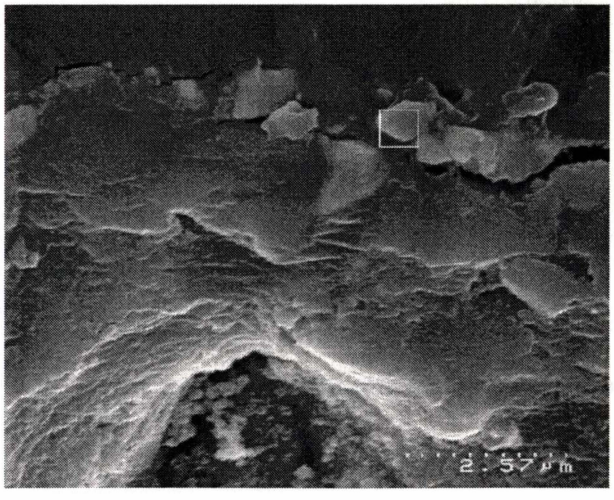

Figure 12(a) SEM micrograph of GBA cross-section displaying particles near surface after exposure to boiling citric acid (2.5 hours) using high magnification (approx. 7000X). Square box shows region where EDS spectrum was taken (see Figure 12b).

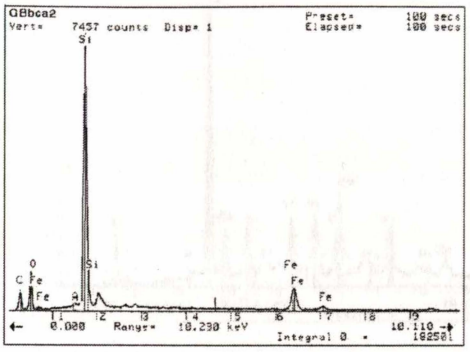

Figure 12(b) EDS spectrum showing composition of particle from Figure 12(a).

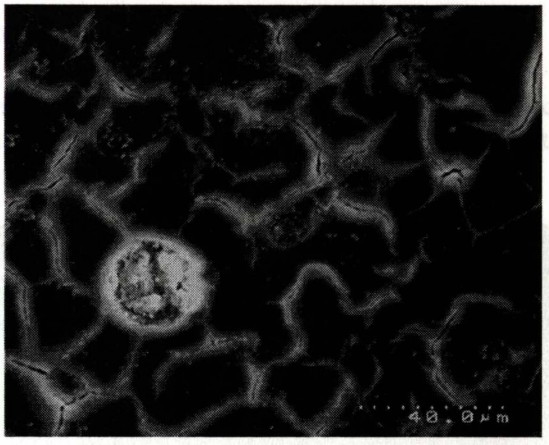

Figure 13(a) SEM micrograph of GBA surface after exposure to boiling citric acid vapour (2.5 hours). Displays micro cracking and hole.

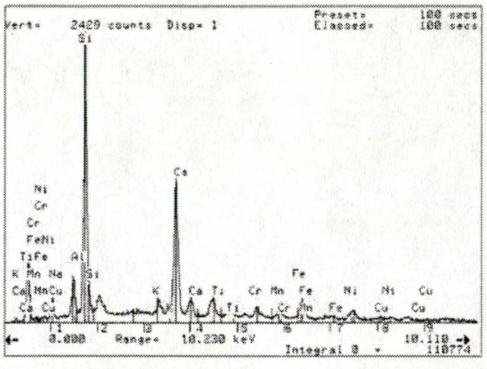

Figure 13(b) EDS spectrum of GBA surface after exposure to citric acid vapour (2.5 hours).

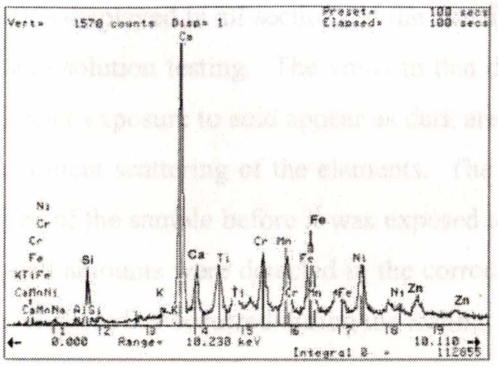

Figure 13(c) EDS spectrum of GBA hole region from surface, after exposure to citric acid vapour (2.5 hours).

4. Elemental Mapping

Elemental distribution mapping of the GBA coating after each corrosive test was performed. The mapped surface, after exposure to boiling citric acid solution (2.5 hours), is displayed in Figure 14.

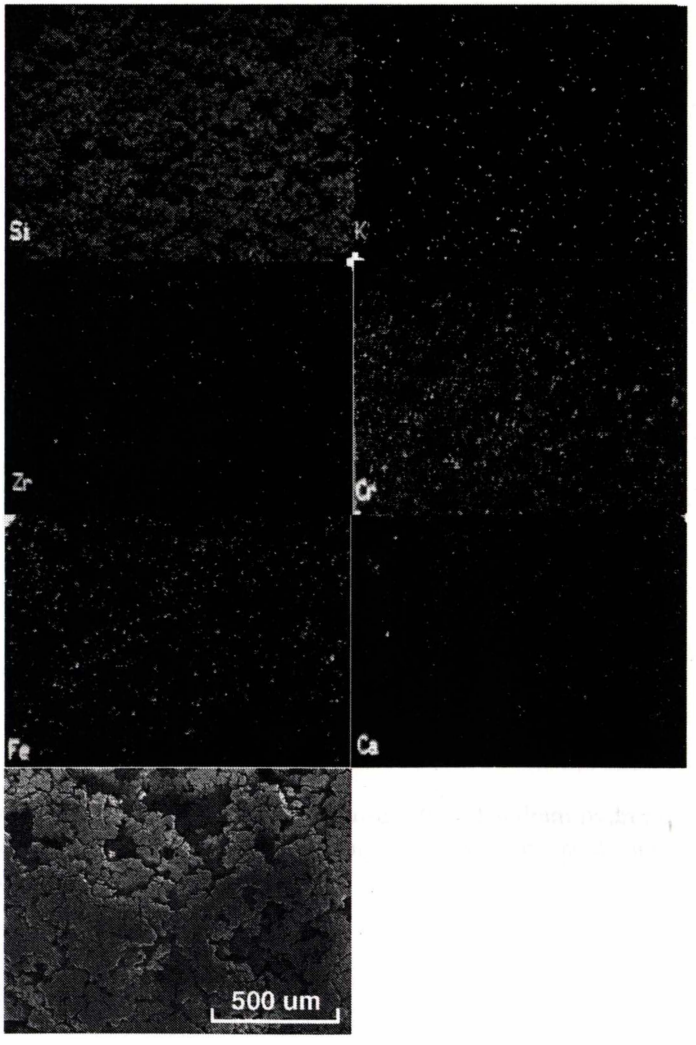

Figure 14 EDS elemental concentration mapping of GBA surface after exposure to boiling citric acid solution (2.5 hours).

The element Si (top right) is displayed in all sections of the remaining coating (that hasn't disseminated) after the acid solution testing. The voids in that developed in the coating surface (see micrograph) after exposure to acid appear as dark areas in the Si map. Many other maps featured intermittent scattering of the elements. The element Ca was widely distributed over the surface of the sample before it was exposed to acid (for example, see Figure 6.16), but only small amounts were detected in the corroded samples (Figure 14), therefore leaching of this element has occurred during the testing.

5. Visual Examination of Trial Coatings

All test panels of variations of GBA (that is, GBI to IV) have a similar appearance (Figures 15-18). There is surface etching and total loss of gloss in the exposed to citric acid solution. Panels exposed to acid vapour show some discoloration and water staining from vapour condensation. Test panels exposed to hot sodium hydroxide also corroded and lost gloss.

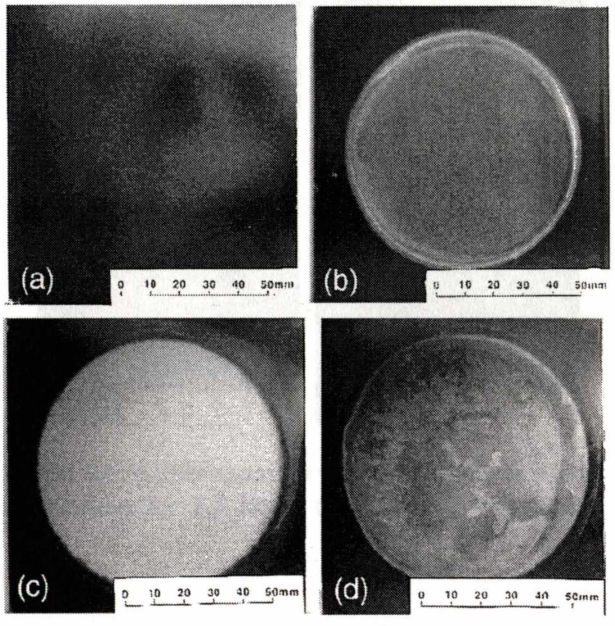

Figure 15 GBI test panels after exposure to hot sodium hydroxide for 48 hours (b), boiling citric acid solution for 2.5 hours (c) and acid vapour for 2.5 hours (d). Control=(a).

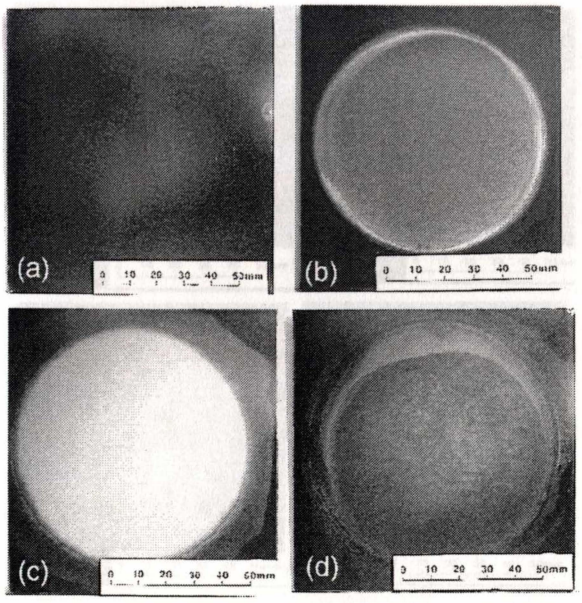

Figure 16 GBII test panels after exposure to hot sodium hydroxide for 48 hours (b), boiling citric acid solution for 2.5 hours (c) and acid vapour for 2.5 hours (d). Control=(a).

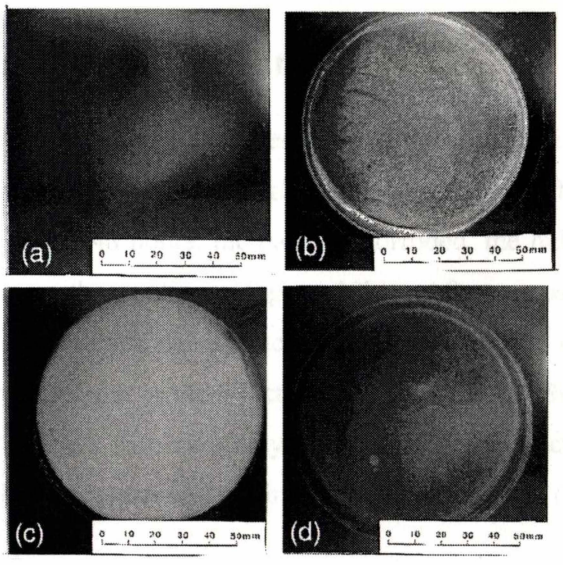

Figure 17 GBIII test panels after exposure to hot sodium hydroxide for 48 hours (b), boiling citric acid solution for 2.5 hours (c) and acid vapour for 2.5 hours (d). Control=(a).

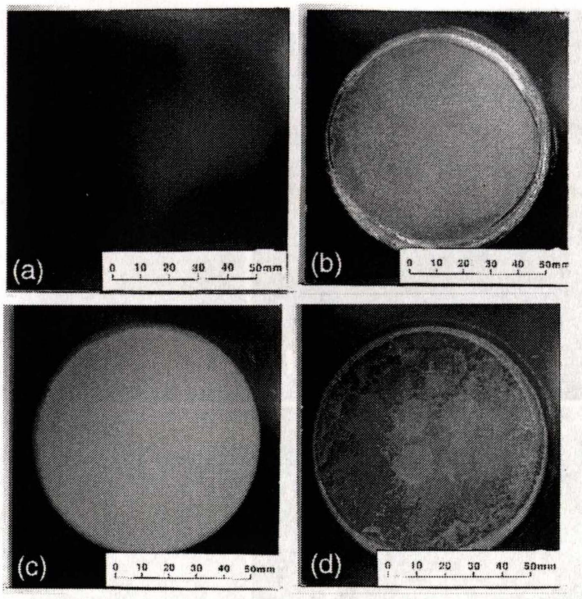

Figure 18 GBIV test panels after exposure to hot sodium hydroxide for 48 hours (b), boiling citric acid solution for 2.5 hours (c) and acid vapour for 2.5 hours (d). Control=(a).

6. Optical Microscopy of Trial Coatings

The surface of GBI enamel coating before testing exhibits a bubble structure (Figure 19b), with a higher density of bubbles in the lighter coloured areas. After exposure to hot sodium hydroxide solution for 48 hours, the panel is corroded, the bubble structure was lost, and there are holes in the coating (Figure 19h). After exposure to citric acid solution for 2.5 hours (Figure 19d), the surface of GBI sample was etched to reveal a powdered glassy substance (similar to the effect observed for GBA). Surfaces exposed to citric acid vapour for 2.5 hours display glassy areas with micro cracking, whilst other areas appear unaffected by the vapour and retain their bubble structure (Figure 19f).

After exposure to hot sodium hydroxide for 48 hours, the surface of GBII samples (Figure 20h) have some holes and there are more light phase regions than on the surface of GBI (which had an even distribution of the light and dark regions (Figure 19h). The surface of GBII after 2.5 hours exposure to citric acid solution (Figure 20d) is similar to that of GBI (Figure 19d), except for the larger voids in the etched surface. The surface exposed to citric acid vapour for 2.5 hours (Figure 20f) has more micro cracking than occurred with GBI (Figure 19f). The surface appearances for GBIII and IV (Figures 21 and 22) after chemical testing are very similar to GBI. The GBIV surface exposed to citric acid solution for 2.5 hours has larger void regions than the other enamel coating surfaces. This is reflected in the higher weight loss (and hence greater corrosion).

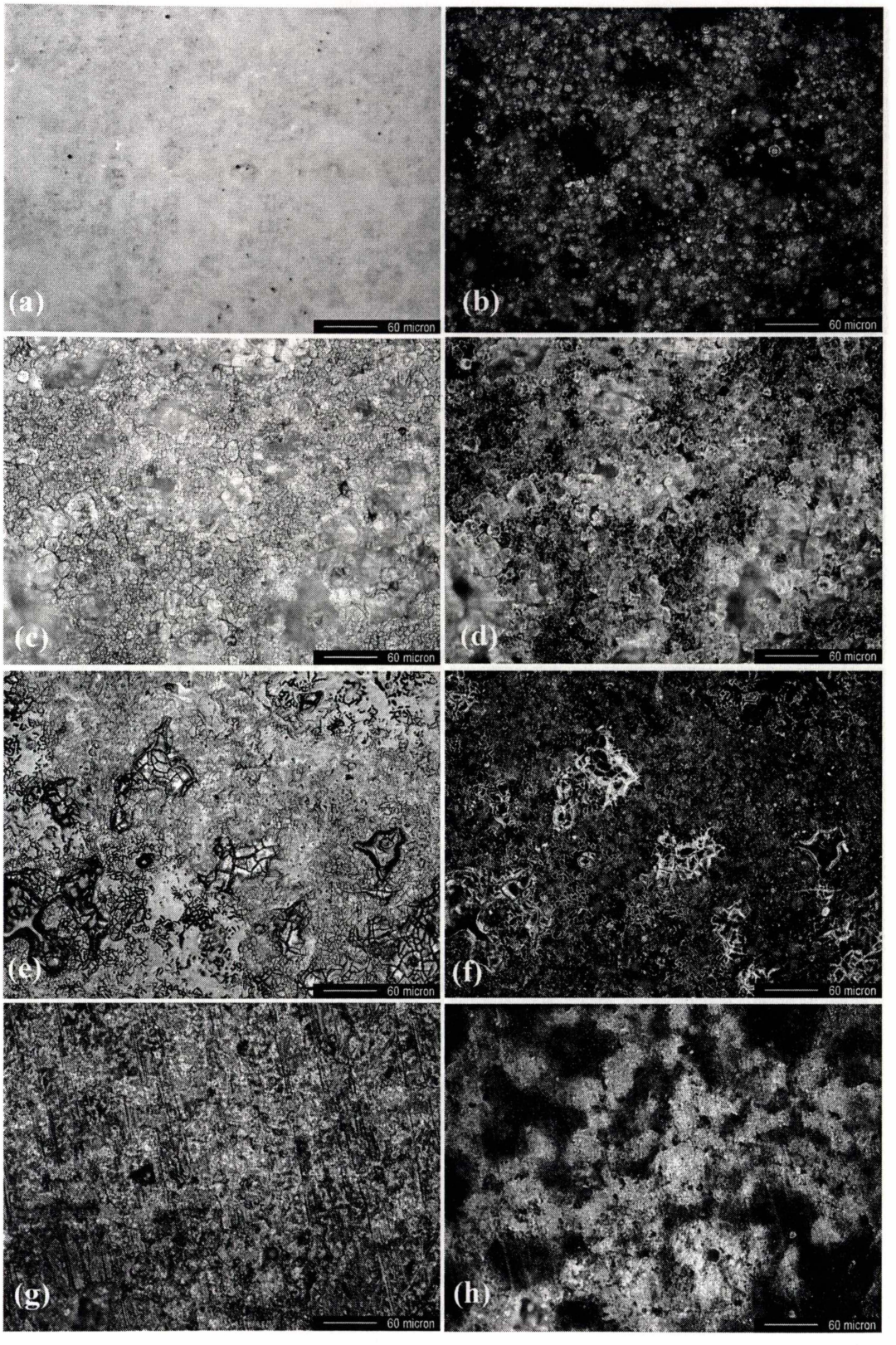

Figure 19 Optical micrographs of gloss brown I surface before testing (a) using bright field illumination (BF) and (b) using dark field illumination (DF). Gloss brown I surface after exposure to: (c) boiling citric acid solution for 2.5 hours (BF) and (d) (DF); (e) acid vapour for 2.5 hours (BF) and (f) (DF); (g) hot sodium hydroxide for 48 hours (BF) and (h) (DF).

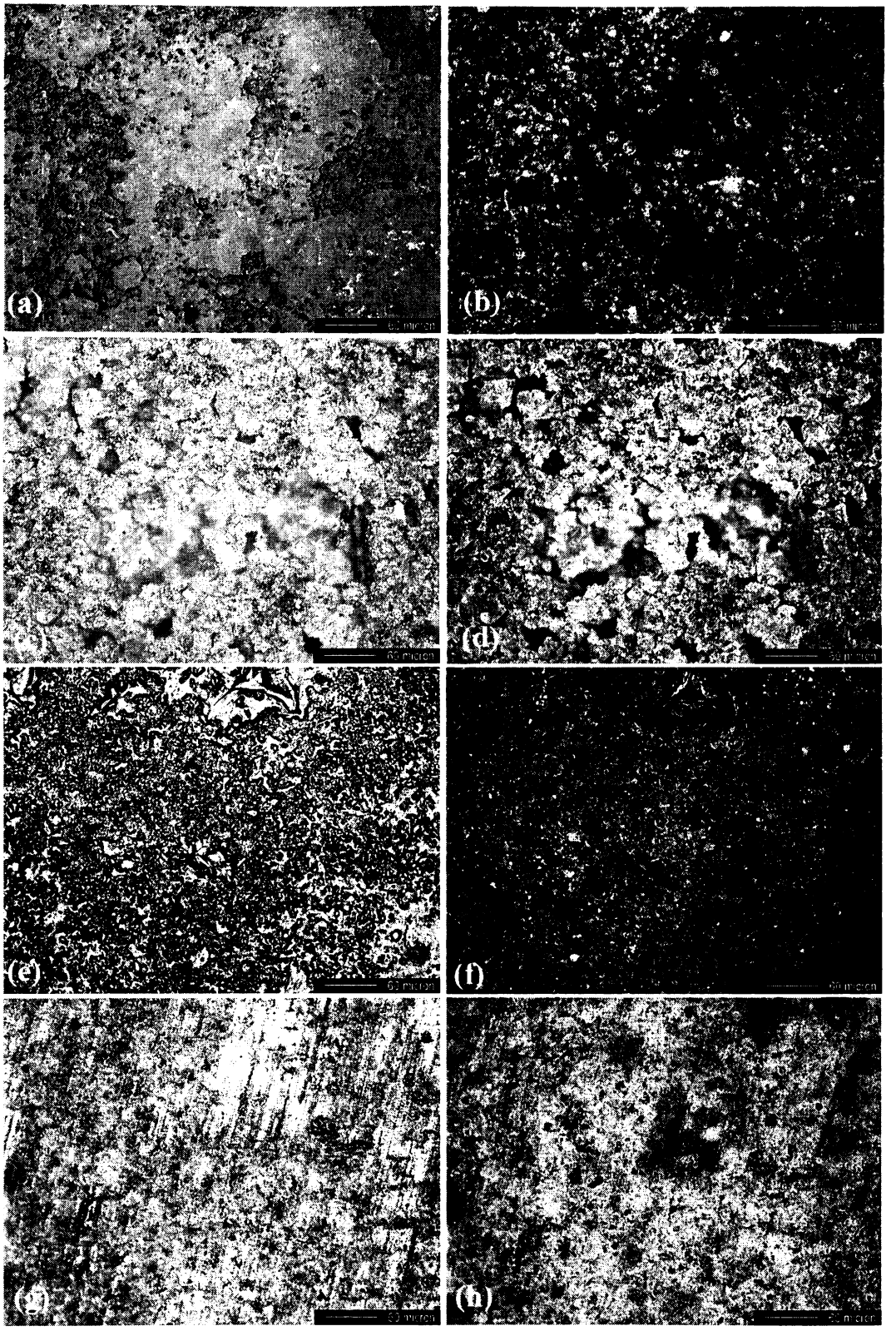

Figure 20 Optical micrographs of gloss brown II surface before testing (a) using bright field illumination (BF) and (b) using dark field illumination (DF). Gloss brown II surface after exposure to: (c) boiling citric acid solution for 2.5 hours (BF) and (d) (DF); (e) acid vapour for 2.5 hours (BF) and (f) (DF); (g) hot sodium hydroxide for 48 hours (BF) and (h) (DF).

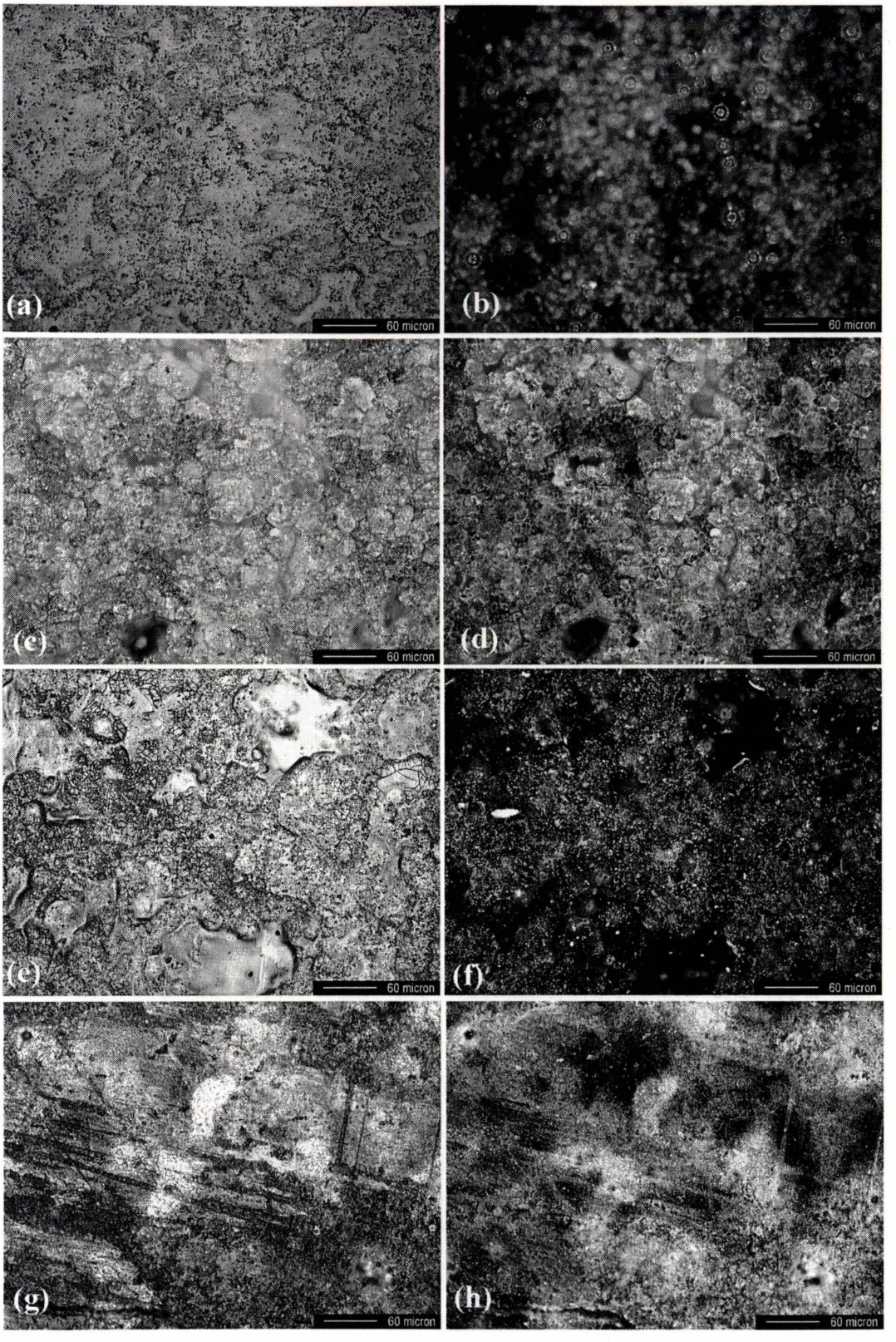

Figure 21 Optical micrographs of gloss brown III surface before testing (a) using bright field illumination (BF) and (b) using dark field illumination (DF). Gloss brown III surface after exposure to: (c) boiling citric acid solution for 2.5 hours (BF) and (d) (DF); (e) acid vapour for 2.5 hours (BF) and (f) (DF); (g) hot sodium hydroxide for 48 hours (BF) and (h) (DF).

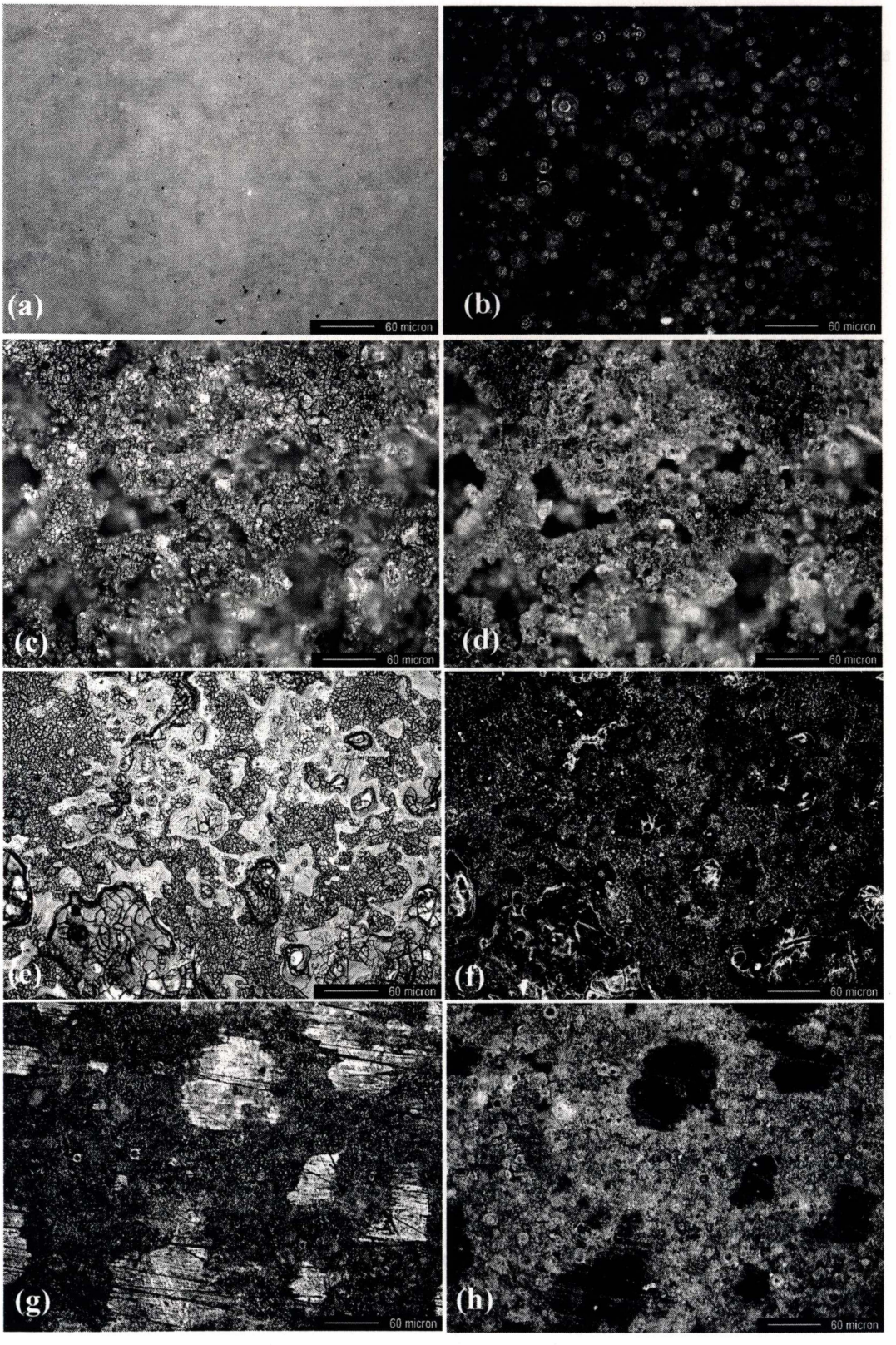

Figure 22 Optical micrographs of gloss brown IV surface before testing (a) using bright field illumination (BF) and (b) using dark field illumination (DF). Gloss brown IV surface after exposure to: (c) boiling citric acid solution for 2.5 hours (BF) and (d) (DF); (e) acid vapour for 2.5 hours (BF) and (f) (DF); (g) hot sodium hydroxide for 48 hours (BF) and (h) (DF).

Table 1 Average weight losses with time for commercial enamel coatings after surface exposure to boiling citric acid solution and vapour. (n=6)

	Weight loss (g/m^2)					
	2.5 hours		6 hours		24 hours	
Coating sample	solution	vapour	solution	vapour	solution	vapour
MBA	366.10 ±112.85	16.93 ± 9.63	–	–	–	–
GGA	67.11 ±13.35	7.07 ±2.41	–	–	–	–
GBA	70.8 ±17.92	5.47 ±2.97	–	–	–	–
GBB	0	0	0	0	3.65 ±0.48	1.24 ±0.64
GBC	0.79 ±1.23	0.67 ±1.11	–	–	9.88 ±4.31	5.72 ±2.41

± = Standard Deviation; - = not tested

Table 2 Average weight loss of commercial enamel coatings after 48 hours of surface exposure to hot sodium hydroxide (n = 6).

Coating sample	Weight loss ($g/m^2/d$)
GGA	6.15 ±1.43
GBA	6.44 ±2.14
MBA	26.55 ±4.07
GBB	10.41 ±0.61
GBC	13.15 ±0.87

± = Standard deviation

Table 3 Effect of adding different mill additions to the average weight loss of enamel coating surfaces exposed to boiling citric acid solution and vapour for 2.5 hours. (n = 6)

	Mill addition increase (wt%)		Weight loss (g/m^2) after 2.5 hours	
Coating specimen	Silcia	HB clay	Solution	vapour
GBA	0	0	70.8 ± 17.92	5.47 ± 2.97
GBI	9	0	40.36 ± 4.26	4.13 ± 0.24
GBII	0	9	64.47 ± 8.69	5.53 ± 0.26
GBIII	3	3	56.74 ± 4.73	5.53 ± 2.01
GBIV	5	0	67.98 ± 4.91	5.02 ± 0.97

± = Standard Deviation

Table 4 Average weight loss of gloss brown A and trial mill addition variation enamels after 48 hours exposure to hot sodium hydroxide (n=6).

Coating specimen	Mill addition increase (wt%)		Weight loss ($g/m^2/d$)
	Silica	HB clay	
GBA	0	0	6.44 ± 1.14
GBI	9	0	5.90 ± 0.16
GBII	0	9	9.50 ± 0.38
GBIII	3	3	6.96 ± 0.15
GBIV	4	0	5.81 ± 0.46

± = Standard Deviation